UNIVERSIDAD POLITÉCNICA DE MADRID

ESCUELA TÉCNICA SUPERIOR DE INGENIEROS DE TELECOMUNICACIÓN

DEPARTAMENTO DE SEÑALES, SISTEMAS Y RADIOCOMUNICACIONES

ANALYSIS OF IMAGE PROCESSING, MACHINE LEARNING AND INFORMATION FUSION TECHNIQUES FOR CONTACT-LESS HAND BIOMETRICS

Belén Ríos Sánchez
Ingeniera en Informática

Directores:

Carmen Sánchez Ávila
Doctora en Ciencias Matemáticas

Hiroshi Ishikawa
Doctor en Informática

Madrid, 2017

TRIBUNAL

Tribunal nombrado por el Magnífico y Excelentísimo Sr. Rector de la Universidad Politécnica de Madrid.

Presidente	Dr.	D.	_____
Vocal	Dr.	D.	_____
Vocal	Dr.	D.	_____
Vocal	Dr.	D.	_____
Secretario	Dr.	D.	_____

Realizado el acto de lectura y defensa de la Tesis el día _____ de Septiembre de 2017 en Madrid.

_____

Calificación

_____	_____
Presidente	Vocal
_____	_____
Vocal	Vocal
_____	
Secretario	

ABSTRACT

In this thesis different techniques of image processing, machine learning and information fusion have been analysed in relation to their applicability to contact-less hand biometrics. To this end, a modular and configurable system that explodes the multimodal nature of the hand to increase its robustness and accuracy have been designed, implemented and evaluated. Given the fact that different applications have different accuracy and time performance needs, the evaluation is aimed to provide a fair comparative of methods under different environmental conditions that helps to adapt the system to the specific requirements of a concrete final application.

A correct hand segmentation is necessary to extract reliable and invariant biometric features. For this reason, a comparative of different segmentation methods that include well-known methods such as global thresholding and graph cuts as well as a novelty flooding-based method which combines different image-based segmentation approaches. These methods have been compared using diverse datasets of images which cover a wide spectrum of capturing conditions.

On the other hand, a comprehensive evaluation of different palmprint feature extraction methods comprising Gabor and Sobel filters, Local Binary Patterns, Local Derivative Patterns and Curvelets has been carried out. Different parameter configurations have also been tested with the aim of finding out which arrangement provides better results for each method. In addition to palmprint, also hand geometry features have been extracted. This evaluation includes also two different feature matching approaches: distance-based and Support Vector Machines.

In addition, it has also been evaluated the feasibility of combining different feature extraction methods to yield into a more precise and robust multimodal solution. Two different levels for fusing the biometric information have been compared: score-level and feature-level.

Finally, an evaluation methodology that allows for a fair comparison between different methods has been proposed. In particular, an evaluation protocol is offered with the aim of not only obtaining an extensive evaluation of the complete system under different environmental conditions, and testing multiple combinations of methods for each module, but also providing a basis against which to compare future research.

Keywords: Accuracy, Biometrics, Computation Requirements, Configurable, Curvelets, Distance, Evaluation, Feature-level fusion, Flooding, Fusion, Gabor, Graph-Cuts, Hand Geometry, Local Binary Patterns, Local Derivative Patterns, Modular, Multimodal, Palmprint, Score-level fusion, Segmentation, Sobel, Support Vector Machines, Thresholding, Varied Environmental Conditions.

RESUMEN

En esta tesis se han analizado diferentes técnicas de procesado de imagen, aprendizaje automático y fusión de la información en relación a su aplicabilidad a la biometría de mano sin contacto. Para ello se ha diseñado, implementado y evaluado un sistema modular y configurable que explota la naturaleza multimodal de la mano para incrementar su robustez y precisión. Dado el hecho de que no todas las aplicaciones tienen las mismas necesidades, el propósito principal de esta evaluación es proporcionar una comparativa objetiva de los distintos métodos bajo diferentes condiciones ambientales que ayude a adaptar el sistema a los requisitos específicos de precisión y tiempos de computación de aplicaciones concretas.

Una segmentación correcta de la mano es necesaria para extraer características biométricas fiables e invariantes. Por este motivo, se ha realizado una comparativa de diferentes métodos de segmentación incluyendo enfoques bien conocidos como la umbralización global o los *graph cuts*, así como una nueva aproximación basada en inundación. Estos métodos han sido comparados utilizando diferentes bases de datos de imágenes que cubren un amplio espectro de condiciones de captura.

Por otro lado, se ha llevado a cabo una completa evaluación de diferentes métodos de extracción de características de la huella palmar incluyendo filtrado de Gabor y Sobel, Patrones Binarios Locales, Patrones Derivativos Locales y *Curvelets*. Junto a las características de palma también se han extraído características de la geometría de la mano. Así mismo, se han probado también diferentes configuraciones de parámetros para cada uno de los métodos con el fin de encontrar la configuración que mejor se ajusta a cada uno de ellos. Además, esta evaluación incluye dos métodos de comparación de características: cómputo de distancias y máquinas de vector soporte.

Adicionalmente, en esta tesis también se ha evaluado la viabilidad de combinar distintos métodos de extracción de características para conseguir una solución multimodal más precisa y robusta. La fusión de la información ha sido realizada a dos niveles diferentes: nivel de puntuaciones y nivel de características, y los resultados de ambos métodos han sido comparados.

Finalmente, se ha propuesto una metodología de evaluación que permite la comparación objetiva entre distintos métodos. En concreto, se ha propuesto un protocolo de evaluación con el objetivo de no solo realizar una amplia evaluación del sistema bajo diferentes condiciones ambientales y probar distintas combinaciones de métodos para cada módulo, si no también proporcionar una base contra la que poder comparar futuras investigaciones.

Palabras clave: Biometría, Condiciones Ambientales, Configurable, Curvelets, Distancia, Evaluación, Fusión, Fusión a nivel de características, Fusión a nivel de puntuación, Gabor, Geometría de Mano, Graph-Cuts, Huella Palmar, Inundacin, Máquinas de Vector Soporte, Modular, Multimodalidad, Patrones Binarios Locales, Patrones Derivativos Locales, Precisión, Segmentación, Sobel, Tiempo de computación, Umbralización.

AGRADECIMIENTOS

Hace ya tiempo comencé este largo y enriquecedor camino que me ha permitido adentrarme en el maravilloso mundo de la investigación, con todas sus cosas buenas y no tan buenas. Durante esta etapa, he crecido tanto en lo profesional como en lo personal, y he podido incluso conocer otros mundos y culturas. Ahora que llega a su fin, me gustaría dar las gracias a todos los que habéis formado parte de él de una u otra manera: enseñanzas, consejos, colaboraciones o palabras de ánimo que tanta falta hacen en determinados momentos.

En primer lugar, me gustaría dar las gracias a Carmen por todo lo aprendido bajo su tutela. Gracias por tus enseñanzas, consejos, esfuerzo y dedicación. Gracias por tu comprensión y ayuda en todo momento, por hacer el camino mucho más fácil y siempre tener palabras de ánimo. Gracias por hacerme creer que era posible.

Igualmente, quisiera agradecer al profesor Ishikawa la oportunidad de formar parte de su equipo y los conocimientos transmitidos, así como los esfuerzos realizados para que mi estancia en Tokio fuera lo mejor posible y estar siempre disponible para cualquier duda o consulta. Gracias Sensei.

Asimismo, quiero dar las gracias de una forma muy especial al CeDInt, porque allí no sólo estoy encantada de ir a trabajar cada día porque me gusta lo que hago y me siento como en casa, sino porque me ha proporcionado algo mucho más valioso: grandes amigos. Gracias a Asun por abrirme la puerta hace ya más de 8 años y darme la oportunidad de dar mis primeros pasos en el mundo de la investigación. Gracias a ReaVi, porque allí empecé esta aventura y en cierto modo siento que nunca me fuí, porque los comienzos siempre marcan el camino y los buenos amigos siempre quedan, estén donde estén. Gracias al gb2s por acogerme, enseñarme y hacer posible esta tesis, especialmente a Gonzalo por su generosidad y ayuda, por estar siempre dispuesto a enseñar; a Javier Guerra, por transmitirme todo lo que sé sobre una buena evaluación biométrica; a Alberto, por su colaboración indirecta; a Javier Andrés por su ayuda con todas esas pequeñas dudas; y a Vainen, por hacer que siempre sean las 15:30. Gracias también al resto de grupos del CeDInt y empresas colindantes por vuestro interés y palabras de ánimo en todo momento, sobre todo en esta recta final. Mención especial a Guille, Milena y Jie por su inestimable ayuda con "la otra tesis".

También quisiera agradecer a todos los que hicieron posible la estancia en Japón, desde los que me animaron a irme hasta los que aportaron la financiaron. Gracias a todo el Ishikawa Lab., especialmente a Oyamada san, Thomas y Mochizuki san, por su ayuda no sólo en el plano académico sino haciendo mi estancia en Tokio mucho más llevadera. Y cómo no podría ser de otra forma si hablamos de Japón, me gustaría dedicar una mención muy especial a Nadia San por entrar en mi vida de una forma tan sigilosa y envolvente para andar este camino en paralelo conmigo, por estar siempre ahí a lo largo de estos cinco años con esa mirada tan positiva. Gambatte Kudasai!!

Además, me gustaría dar las gracias a mis amigos por los ánimos, las risas, los consejos y el cariño. Porque con vosotros todo es mucho más sencillo.

De igual forma, no puedo pasar sin dar las gracias a la persona que ha recorrido a mi lado la etapa final del camino, facilitando cada paso, siempre dispuesto a ayudar, siempre atento. Gracias Manu.

Finalmente, mis mayores gracias son para mi familia por su apoyo en todo momento, especialmente para mis padres y hermano. Gracias por enseñarme el significado de las palabras constancia y perseverancia, que rendirse no es una opción y lo importante del trabajo bien hecho. Porque sin vosotros nada de esto hubiera sido posible.

Me hubiera gustado nombrar y dedicar unas palabras uno por uno a todos los que habéis estado presentes durante todo este tiempo, pero me temo que de hacerlo la longitud de estos agradecimientos competiría con la de la propia tesis. Podría haber puesto una lista de nombres, pero eso mejor lo dejamos para las tareas por hacer o los lugares por visitar. Por ello, no penséis que me he olvidado de ninguno de vosotros, es simplemente una limitación espacial.

Gracias.

CONTENTS

LIST OF FIGURES

LIST OF TABLES

Part I

THESIS STATEMENT

1

INTRODUCTION

The expansion of technology has derived into a great number of applications and services which requires a non-intrusive but reliable verification of the users' identity. Traditional identification methods such as passwords are becoming insecure due to the ease with which they can be stolen or the difficulty to remember a great amount of different complicated keys. Biometrics is an active research field in which considerable efforts have been made during the last decades, and that is increasingly being integrated into current technology as an attractive alternative to conventional identity verification approaches. Accordingly, it is not difficult to find a large proportion of the population which is familiar with some biometric techniques, such as fingerprints, voice or face recognition.

In particular, the increase in the use of mobile devices has caused a growing trend toward touch-less biometrics, where hand-based biometrics have demonstrated to gave a great potential and are considered as comfortable and secure by users [67]. The evolution from contact systems, where hand pose variations were restricted [164, 202, 137, 95], to contact-less systems, where fewer collaboration from the user is required, has led to a wider acceptance but also raised the overall complexity. Since it is an image-based biometric, in addition to typical trials coming from the properties of each hand trait, new challenges derived from contact-less nature of the images have to be addressed. These trials include blurriness, lighting changes, cluttered backgrounds or intra-class variations due to the absence of constraints in hand posing, orientation or openness degree. Accordingly, traditional restrictive approaches have given way to less constraining developments including those where images are captured under controlled background and lighting conditions but there are not pose restrictions [27, 104, 133, 150] and those which are able to deal with real life environments lighting variations or complicated backgrounds [45, 46, 126].

Combining multiple biometric modalities allows to take advantage of the strengths of each single modality, compensating some of the limitations derived from their intrinsic nature, the maturity of the technology and the capturing conditions. The exploitation of the complementarity between biometric modalities increases the overall accuracy, improves the performance, reduces the vulnerability and therefore, results in more robust biometric systems which offer enhanced security against forgeries [52]. Due to different biometric traits can be extracted from hand images such as hand geometry [47, 35], palmprint [97] or hand veins [208, 191], hand can be considered multimodal itself and, thus, it is possible to improve the system performance by exploiting the information provided by its different traits. In this manner, some hand multimodal systems have been developed during the last years combining hand

geometry and palm veins [140], palmprint and palm veins [185, 134], palmprint and hand geometry [103, 137, 56, 158] or hand geometry, palmprint, knuckleprints and veins [135] among others.

A comprehensive collection of works made so far organized according to the capturing conditions and the biometric trait employed is shown in Table 1.

Background	Lighting Conditions	Pose Restrictions	Biometric Trait	References
Controlled	Controlled	Contact, Pegs	Hand Geom.	[78, 80, 160, 163, 164, 118, 183, 54]
			Palmprint	[202, 98, 95, 43, 22, 174, 96, 190, 101, 81, 68, 121, 62, 149, 69, 209, 206, 193, 108, 85, 148, 152, 139, 66, 2, 113]
			Palmprint, Hand Geom.	[110]
			Hand Geom., Dorsal Veins	[140]
			Palmprint, Palm Veins	[185, 25]
			Palmprint, Knuckleprint	[130]
			Palmprint, Hand Geom., Fingerprints	[168]
		Contact, Surface Marks	Hand Geom.	[177]
			Palmprint	[102]
		Contact, Free Placement	Hand Geom.	[189, 65, 51, 72, 11, 195, 194, 5, 200, 58, 55, 54, 128, 3, 39, 87, 6]
			Palmprint	[70, 27, 111, 100, 8, 196, 101, 209, 108, 169, 205, 139]
			Palmprint, Hand Geom.	[153, 137, 141, 56, 147]
			Palmprint, Finger Texture	[154]
			Palmprint, Knuckleprint	[120]
			Finger Geom., Finger Texture	[155]

Background	Lighting Conditions	Pose Restrictions	Biometric Trait	References
Controlled	Controlled	Contact, Free Placement	Palmprint, Hand Geom., Fingerprints	[156, 53, 197]
			Palmprint, Hand Geom., Hand Veins	[7]
		Contact-less	Hand Geom.	[104, 82, 192, 175]
			Palmprint	[133, 125, 126]
			Palmprint, Hand Geom.	[23, 186, 20]
			Palmprint, Palm veins	[136]
			Palmprint, Hand Geom., Finger Surface	[150]
			Palmprint, Hand Geom., Veins	[14]
			Palmprint, Hand Geom., Knuckleprint, Palm veins, Finger veins	[135]
Controlled	Indoor	Contact, Surface Marks	Palmprint, Hand Geom.	[103]
		Contact-less	Palmprint	[121, 89, 170]
			Palmprint, Palm Veins	[182]
			2D Palmprint, 2D Hand Geom., 2D Finger Tex., 3D Palmprint, 3D Finger Tex.	[89]
Uncontrolled	Indoor	Contact-less	Hand Geom.	[124, 123, 41, 40, 35]
			Palmprint	[44, 45, 46, 133, 125, 126, 165]
			Palmprint, Hand Geom.	[157]

Table 1.: Hand biometrics approaches classified according to the nature of the testing images in terms of environmental conditions and pose restrictions and the involved traits.

1.1 THESIS MOTIVATION AND CONTRIBUTIONS

This thesis is aimed to analyse different techniques of image processing, machine learning and information fusion for contact-less hand biometrics. To this end, a contact-less hand biometric system which explodes the multimodal nature of the hand to increase its robustness and accuracy has been designed, implemented and evaluated. The system is oriented to deal with all kinds of scenarios including unconstrained or adverse environments. In addition, given the large amount and variety of applications, a modular and configurable design of the system is proposed which is shown in Figure 1. Accordingly, different methods have been studied for the main modules with the purpose of obtaining an objective comparison between methods which can help to adapt the system to the specific needs of a concrete final application.

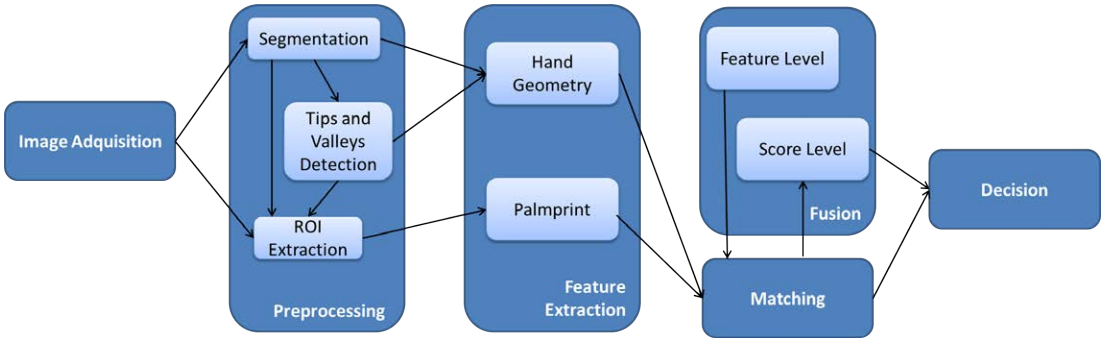

Figure 1.: System structure.

The main contributions of this thesis are stated as follows:

- To conduct a comparative study of different segmentation methods in terms of both, accuracy and computation time, using diverse datasets of images which cover a wide spectrum of capturing conditions. These methods include well-known approaches such as global thresholding and graph cuts as well as a novel method.
- To propose a competitive flooding-based segmentation method which combines different image-based segmentation techniques and is oriented to devices with low-computational resources.
- To provide a comprehensive evaluation of different palmprint feature extraction methods comprising Gabor and Sobel filters, Local Binary Patterns, Local Derivative Patterns and Curvelets. Different parameter configurations have also been tested with the aim of finding out which arrangement provides better results for each method.
- To compare different matching methods including distance-based approaches and Support Vector Machines.
- To analyse the feasibility of combining different feature extraction methods at different levels to yield into a more precise and robust solution.

- To propose an evaluation methodology based on the definitions suggested by the ISO/IDE 19795 that allows for a fair comparison between different methods. An evaluation protocol is offered with the aim of not only obtaining an extensive evaluation of the complete system under different environmental conditions and testing multiple combinations of methods for each module, but also providing a basis against which to compare future research.

1.2 THESIS CONTENTS DESCRIPTION

The remainder of this thesis is organized as follows.

- Part ii describes the image acquisition and preprocessing modules.
  - Chapter 2 outlines the capturing process where the user presents the hand to the camera and the image is recorded. In addition, a description of the databases employed to test the system is provided.
  - Chapter 3 contains the description of the segmentation module, aimed to separate the hand from the background. Here, different segmentation methods are described and a new method is proposed. In addition, they are compared in terms of accuracy and computation time.
  - Chapter 4 shows how to detect the meaningful points and to extract the region of interest which will be subsequently used to extract the biometric features.
- Part iii gives the details about the feature extraction and comparison methods, together with the fusion of biometrics procedure.
  - Chapter 5 details different feature extraction methods for palmprint and hand geometry.
  - Chapter 6 summarises the feature comparison methods included in the system.
  - Chapter 7 outlines the approaches employed for the fusion of biometric information.
- Part iv presents the evaluation of the biometric system.
  - Chapter 8 outlines the evaluation protocol.
  - Chapter 9 provides the evaluation of the different modules using a set of images captured under controlled environmental conditions to provide a fair technology evaluation.
  - Chapter 10 presents the evaluation of the different modules using a set of images captured under realistic conditions.
  - Chapter 11 provides the results obtained when different palmprint and hand geometry feature extraction methods are combined.
- Part v provides the conclusions and future research lines.

Part II

IMAGE ACQUISITION AND PREPROCESSING

2

ACQUISITION

2.1 INTRODUCTION

Image acquisition module is aimed to capture raw data of individuals which will be subsequently processed to extract biometric information. In the case of hand biometrics, the user presents the hand to the sensor (camera) and an image is recorded. A correct acquisition is crucial due to it directly conditions the preprocessing module, particularly the segmentation process. Segmentation, in turn, can influence the feature extraction procedure and thus, the final result.

First approaches in hand biometrics made use of voluminous capturing devices that contain pegs to enforce the user to keep an appropriate position of the hand and guarantee optimum environmental conditions [164, 202]. This way, the posterior processing of the images is eased and the intra-user variability derived from hand pose variations is reduced. Nevertheless, these capturing devices present some drawbacks such as shape distortion, discomfort or unnatural posture of the hands [55].

Thus, these capturing devices evolved into scanners which requires the hand to be in contact with a flat surface but does not restrict the openess degree of the fingers nor the position [137, 141, 154, 127, 106, 87]. Most of contact-based approaches guarantee uniform lighting conditions and well contrasted background with the aim of facilitating the segmentation process. Nevertheless, when they are used in real scenarios hygienic and public-health concerns appear [124], reducing the user acceptability.

Accordingly, contact-less approaches have gained ground in the last years. Some of these works still keep controlled environmental conditions [135, 90], but the natural trend is toward non-constrained captures [44, 41, 157] where varied illumination and backgrounds add extra difficulties.

In order to avoid wrong captures as far as possible, a clearly defined image acquisition procedure is necessary. Section 2.2 presents some recommendations for users that have been found specially relevant for this purpose during the accomplishment of this thesis. In addition, databases used to evaluate the performance of the system and its are described down below (Section 2.3).

2.2 IMAGE ACQUISITION PROCEDURE

To ensure a correct image acquisition the following recommendations should be taken into consideration:

- The hand should be outstretched, with the palm facing the camera and in a plane parallel to the camera plane.

- The whole hand should be contained in the image and as close as possible to the camera in order to get as most texture details as possible.
- The hand should be centred in the image.
- It is required that no other piece of skin or object with a similar color appears in the background of the image. Moreover, a non cluttered and well contrasted background is recommended.
- Constant and neutral illumination is also preferred.
- Most of the rings can cause difficulties to the segmentation algorithms, so users are requested to remove their rings unless they are thin and similar to the skin colour (golden rings).
- No restrictions on the use of bracelets or watches are imposed.

2.3 DATABASES

2.3.1 *Database 1: The Hong Kong Polytechnic University Contact-free 3D/2D Hand Images Database (Ver 1.0)*

First database used in this thesis is the 2D subset of the Hong Kong Polytechnic University Contact-free 3D/2D Hand Images Database (Ver 1.0) [89], called 2DHK database hereafter. Textured 3D and 2D scans of the inner surface (palm-side) of the hand were recorded in order to establish a large scale hand image database using completely contact-free imaging setup. It was made freely available[1] to the researchers with the objective of promoting the development of more user-friendly and reliable hand identification systems.

Images were acquired using a commercially available 3D digitizer Minolta VIVID 910 in a process which spanned over 4 months. 2DHK database contains images from 177 volunteers in the age range of 18-50 years with multiple ethnic backgrounds. Images were recorded in two separated sessions with no fixed lapse between them, from one week to three months. Five images per session and person were captured. Therefore, this database includes 3,540 hand images (of 3D and corresponding 2D) that have a resolution of 640×480 pixels. Together with the 2D and 3D images, the region of interest of every image is also provided, which includes the most representative part of the palmprint, properly aligned and cropped.

All the hand images were recorded in an indoor environment, with no restrictions on the surrounding illumination but controlled constant black background which strongly contrast with the skin colour to facilitate the segmentation process. In fact, the data collection process was carried out at three different locations which had notable variations in surrounding illuminations. During the image acquisition, every user was requested to hold the right hand in front of the scanner at a distance of about 0.7 m, which empirically maximized the relative size of the hand in the acquired image, keeping the palm approximately parallel to the image plane of the scanner and

1 http://www.comp.polyu.edu.hk/~csajaykr/myhome/database_request/3dhand/Hand3D.htm

inside the imaging area. No additional constraints about hand pose were imposed nor the users were instructed to remove hand jewellery that they were wearing. In order to introduce variations in the database, users were asked to change their hand position after the acquisition of every image.

Figure 2 depicts some sample images of 2DHK database together with their associated region of interest.

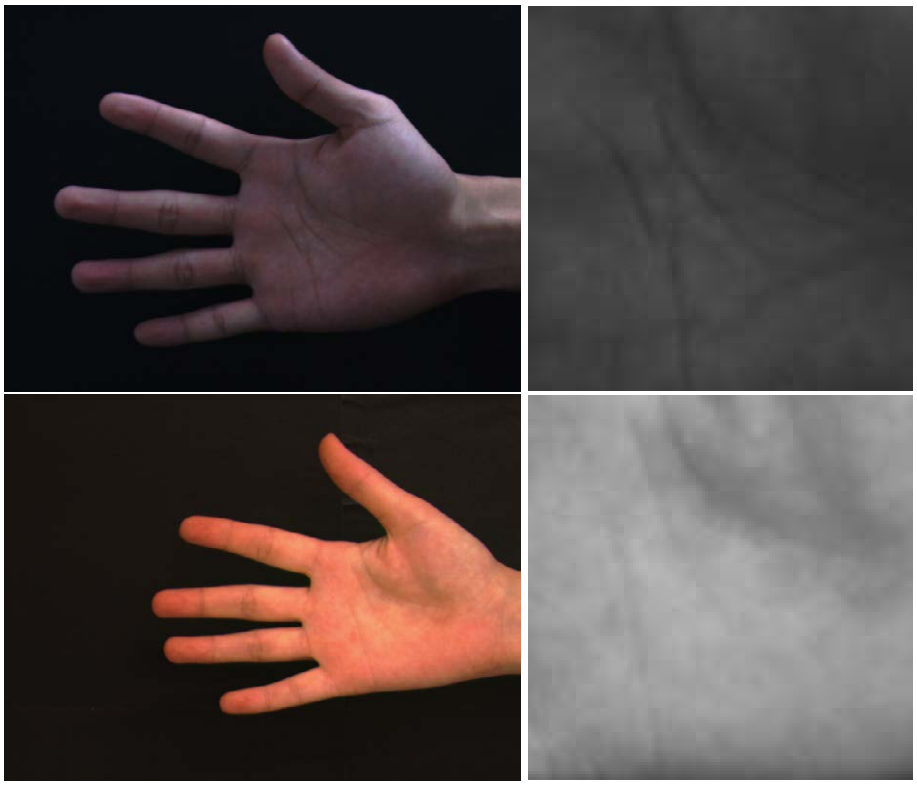

Figure 2.: 2DHK database sample images.

2.3.2 *Database 2: gb2s_ID Database*

Second database used in this thesis is the gb2s_ID Database (ver. 2.0)[2] [36]. It was created with the aim of evaluating hand segmentation methods in contact-less semi-controlled environments and to construct a wider synthetic database.

Images were acquired by the camera of a mobile device, the smartphone HTC Desire S, at a resolution of 2592×1552 pixels. gb2s_ID Database contains hand captures of 107 individuals comprised in an age range from 16 to 60 years old with multiple ethnic backgrounds, and gathering males and females in similar proportion. Images from both hands were captured in two different sessions separated by 10-15 minutes. 10 images per hand, person and session were recorded.

The acquisition procedure was carried out in an indoor environment under natural light. Aimed to facilitate the segmentation process and to ensure a proper feature extraction, well contrasted neutral backgrounds were preferred. Accordingly, the user

2 http://www.gb2s.es

was requested to hold his hand opened naturally with the palm facing to the camera in a plane parallel to the camera plane at a distance around 10-15 cm. This acquisition procedure implies no severe lighting conditions, pose or distance to mobile camera constraints neither requires any removal of rings, bracelets or watches. Consequently, gb2s_ID Database presents a huge variability in terms of size, skin color, orientation, hand openness and illumination conditions as can be seen at Figure 3.

Figure 3.: gb2s_ID Database sample images.

2.3.3 *Database 3: gb2s_Synthetic Database*

The third database used in this thesis is the gb2s_Synthetic Database[3] [36], created with the aim of evaluating to what extent segmentation methods can satisfactory perform a hand isolation from backgrounds of real-life scenarios. In addition, this database provides automatically segmented ground-truth images.

The creation of the gb2s_Synthetic Database considered the hands extracted in former database (gb2s_ID) and a set of textures including carpets, fabrics, glasses, muds, different objects, papers, parquet, pavements, plastics, skins and furs, skys, soils, stones, tiles, trees, walls and woods. In particular, each original image from gb2s_ID database was combined with 91 different textures obtained from the website `http://mayang.com/textures/`, giving as a result more than 270,000 new synthetic images. Figure 4 shows some synthetic sample images for the same hand capture.

3 `http://www.gb2s.es`

Figure 4.: gb2s_Synthetic Database sample images.

2.3.4 *Database 4: gb2sμMOD Hand Dataset*

Finally, the last database used in this thesis is the gb2sμMOD Hand Dataset, which is part of the the gb2sμMOD database [157] and was mainly designed to overcome the absence of hand video databases and the lack of infrared images. In particular, the subset of visual spectrum images corresponding to the palm side of the hand will be employed to evaluate the biometric system here presented.

Visible light videos were captured by an e-CAM51_USB that was mounted in a small electronic board together with one LED. Videos were recorded in ".avi" format at a resolution of 640×480 px. with no constant frame rate between videos. 60 contributors aged between 20 and 60 years old with different ethnic backgrounds participated in the database recording process. gb2sμMOD Hand Dataset contains videos of palm-side and backside of both hands recorded in three separated sessions in order to capture time variability. Separation between sessions was not predefined in order to simulate a realistic use of the biometric system and it can vary between a few days to several weeks. 5 videos per contributor were recorded for sessions 1 and 2 while for session 3 just 4 videos were captured.

gb2sμMOD database was recorded in an indoor environment under varied environmental conditions. Sessions 1 and 2 were recorded under quasi optimum conditions to allow a better evaluation of the algorithms, and session 3 under realistic extreme conditions to test the performance of the system in real-world cases. During the first and second sessions a dark grey shelf was employed as background while for the third session new elements such as fabrics, photographs, clothes and other decorative elements were introduced in the room to provide new dynamic backgrounds that change from one participant to another. In similarity with the backgrounds, lighting conditions were more restricted in the first two sessions in order to obtain samples as controlled as possible to facilitate evaluation of time influence in both, the biometric traits and the user's behaviour when using the biometric system. To this end, all the samples in sessions 1 and 2 were captured with ceiling indirect lights on and without direct natural light. To simulate realistic as well as extreme scenarios, four lighting variations were introduced for the third session: 1) natural illumination, maintaining ceiling lights off and natural light; 2) severe shadows, covering a significant portion of the hand; 3) saturated, lighting hands in excess, and 4) low-light conditions, generated with shutters down and no artificial light elements.

Regarding hand pose, users were requested to hold the hand outstretched and in a plane parallel to the camera plane, entirely within the image and as big as possible. It was also required that no other piece of skin appears in the image. Due to the use of rings can cause difficulties to the segmentation algorithms, participants were also asked to remove their rings in case they wore one. No restrictions on the use of bracelets and watches were imposed.

Figure 5 illustrates some sample images from the same user recorded in different sessions and lighting conditions.

(a) Session 1 (b) Session 2

(c) Session 3 - Natural Lighting (d) Session 3 - Severe Shadows

(e) Session 3 - Saturated (f) Session 3 - Low Intensity Illumination

Figure 5.: gb2sμMOD Hand Dataset sample images.

3

SEGMENTATION

3.1 INTRODUCTION

Image segmentation is considered a classic tough problem in computer vision with a great number of varied applications (from biometrics or security to medical applications), and whose solution tightly depends on the sort and the quality of the input image and the objects to be delineated. In this way, to obtain an accurate and robust result is a challenging task due to low contrast, noise, occlusions, background clutter, similarity of intensity distributions and weak edges between adjacent objects, which could derive in artificial edges, discontinuous contours or overlapping objects. As a result of decades of researching, a big amount of different algorithms have been developed, which are typically divided into image based and model based approaches.

Purely image based methods just take into account information coming directly from the image, deriving into weak results in the presence of noise, poorly distinguishable tissues, background clutter and object occlusions. These methods can in turn be divided into boundary-based approaches, which include edge detectors [64, 17], Active Contours [91], Live wire [49] or Level sets [119, 31] among others, and region-based approaches, comprising methods such as intensity thresholding [138, 167], region growing [19], clustering [77, 143], watershed [10, 159], graph cuts [12, 13] or Fuzzy Connectedness [178].

On the contrary, model based approaches use statistical models previously constructed, which usually contains information about the mean shape of the object of interest and its principal variations and can also encode additional information related to the appearance of the object. Active Shape Models [30], Active Appearance Models[28, 29], m-Reps[144] and Atlas-based methods [151] are embraced in this category. Even though these methods are a really powerful tool capable to obtain accurate and robust solutions in cases that are well covered by the training set, they are very sensitive to initialization and generally fail for new images slightly different to those employed to build the model.

Combination of complementary methods from different categories have recently attracted a growing interest, aimed to enforce their strengths and to reduce their weaknesses. Accordingly, it is possible to combine two or more boundary and/or region methods [129, 50, 26], boundary methods with model-based approaches [114] or region methods with model-based approaches [162, 24] to arrive at a more powerful hybrid strategy that can overcome the weakness of the component methods.

Most of the works in hand image segmentation for biometric applications carried out to the date employ image-based methods. Particularly, global thresholding approach is clearly the most outstanding method, as can be seen in Table 2. This is mainly due to in the majority of the cases the images are captured under controlled environmental conditions [164, 202, 102, 141, 154, 106, 87] to ensure a good contrast between the hand and the background, which greatly facilitates the segmentation. Some of these authors, in addition to environmental restrictions also force the position of the hand during the capture through the use of pegs [164, 202] or other marks [104], while others just require the user to freely place the hand on a flat surface [137, 141, 154, 106, 87] or allow for contactless capturing [104, 150]. When good conditions are guaranteed, simple solutions such as basic clustering [200] or skin colour modelling as a probability distribution [135] also work fine.

Nevertheless, technology expansion has derived into more complex and changing scenarios for biometric applications which present new challenges. These difficulties are mainly related to the capturing conditions, especially uncontrolled backgrounds or lighting conditions, and the use of portable devices which usually offer computational limited resources. To facilitate the segmentation of images recorded in non-controlled environments it is possible to use infrared cameras [124, 123, 140]. However, their use is not widespread yet. In these situations, despite some authors keep using easy methods such as global thresholding [90] or skin colour modelling as a probability distribution [135, 165], more advanced techniques are usually required such as advanced graph-based clustering techniques [61, 40, 42] or neural networks [44, 46]. Although without biometric purposes, other noteworthy methods including Markov Random Fields (MRF)[181], RCE Neural Networks[199, 173], Shape Models[30] and hybrid such as the combination of MRF and shape priors [9] or a set of image-based methods [172] have also been applied for hand image segmentation in non-constrained images.

Table 2 shows a compilation of hand segmentation approaches using visual spectrum images for biometrics purposes classified according to the nature of the testing images in terms of pose restrictions and environmental conditions.

Despite the efforts made up to the moment, segmentation continues to be the weakest point of almost every computer vision application. In the specific case of hand biometrics, it is a critical step due to the quality of the segmentation directly influences the hand geometry features or the procedure to extract and align the region of the palm including the most significative palmprint features (Sec. 4). Therefore, a correct segmentation is mandatory to extract reliable and invariant biometric features. In addition, different fields of application have different requirements and some adjustments in the modules of the biometric system should be made.

For this reason, one of the main contributions of this thesis is a comparative of different segmentation methods in terms of accuracy and computation time aimed to obtain objective data which could be used in the future to decide which kind of segmentation is more suitable for a concrete final application. These methods include global thresholding, which is the easiest but most extended approach as commented above, and more sophisticated and well known methods such as Graph Cuts. Thresholding segmentation is a really simple solution which requires low computational resources but entail very specific capturing conditions to provide a good per-

Pose Restrictions	Background	Lighting Conditions	Segmentation Approach	References
Contact, Pegs	Controlled	Controlled	Thresholding	[164, 98, 202, 118, 22, 183, 62, 149, 110, 169, 85]
Contact, Surface Marks	Controlled	Controlled	Thresholding	[102, 148]
Contact, Free Placement	Controlled	Controlled	Thresholding	[153, 189, 137, 156, 65, 70, 141, 27, 51, 111, 195, 72, 11, 194, 155, 154, 115, 7, 56, 5, 53, 100, 58, 197, 8, 55, 196, 128, 3, 179, 147, 127, 106, 87]
Contact, Free Placement	Controlled	Controlled	Clustering	[200, 166]
Contactless	Controlled	Controlled	Thresholding	[104, 23, 127, 150]
Contactless	Controlled	Controlled	Skin colour modelling	[146, 133, 136, 135]
Contact, Surface Marks	Controlled	Indoor	Thresholding	[103]
Contactless	Controlled	Indoor	Thresholding	[88, 89, 90, 182]
Contactless	Controlled	Indoor	Clustering	[60, 61, 40]
Contactless	Uncontrolled	Indoor	Skin colour modelling	[133, 165]
Contactless	Uncontrolled	Indoor	Clustering	[36, 40, 38, 37, 42, 157]
Contactless	Uncontrolled	Indoor	Neural Networks	[44, 45, 46]

Table 2.: Hand segmentation for biometric applications using visual spectrum images classified according to the nature of the testing images in terms of pose restrictions and environmental conditions.

formance. On the contrary, Graph cuts is able to handle more complicated situations but are computationally expensive and sometimes need user collaboration. Aimed to achieve a compromised solution between accuracy and computational resources, a novel flooding-based approach which is combination of several image-based methods has been developed and analysed. All the methods has been tested using images from the databases described in sec. 2.3 which cover a wide spectrum of capturing conditions.

Although most of the previous works in hand image segmentation employ RGB colour space, it is dependent on the capturing device and present high correlation between the red, green and blue colors [92]. In this thesis CIEL*a*b* (CIE 1976 L*a*b*) colour space [32, 33] has been selected to represent the images. CIEL*a*b* was created to provide a unifying space color reference model which linearly describe color variations including all perceivable colors by the human eye. It isolates in L channel the ligthness of the image while use a and b channels to represent red-green and

yellow-blue colour changes respectively. Previous studies have demonstrated that CIEL*a*b overcomes other colour spaces for satisfactory representing the skin colour of individuals [187, 92, 4]. Given the nature of this colour space, L channel contains higher variation than the remaining two, which provide more distinctive information about the skin [92, 34]. Accordingly, removing L channel from the representation allows to obtain a more accurate model of the hand reducing the influence of lighting variations [92].

The remainder of this chapter is organized as follows. Section 3.2, 3.3 and 3.4 provide a description of thresholding, graph cuts and flooding-based adopted approaches together with theoretical fundamentals when necessary. Section 3.5 shows the results of each segmentation method in terms of quantitative analysis. Section 3.6 describes the segmentation quality control module.

3.2 THRESHOLD BASED SEGMENTATION

Global thresholding segmentation is based on the assumption that the background is uniform and well contrasted with the element of interest. As presented in Section 3.1, it is the most extended method for hand image segmentation due to its speed, simplicity and suitability when the input images are captured under controlled illumination conditions and background is uniform and highly contrast with the hand skin colour.

Accordingly, assuming some cases of use where environmental conditions accomplish these requirements, an easy and fast segmentation method based on thresholding has been integrated in the system. To calculate the threshold value, the method proposed by Otsu[138] has been applied. The binary image is then refined by means of morphological operations and small regions that correspond to noise are eliminated.

3.2.1 *Algorithm Overview*

A description of the algorithm can be found below together to an illustration of the different steps (Figure 6).

1. First, the image is converted from RGB to grayscale CIEL*a*b* space color to separate lighting from color information. In this case, layer L is selected for binarization due to it contains more colour contrasting features when dark neutral with low reflections background is assumed (Figure 6b).
2. Next, the threshold value is calculated by means of Otsu's algorithm [138].
3. Then, the image is thresholded (Figure 6c).
4. Once the image is binarized, opening and closing morphological operations with disk structural elements of size 5 and 3 respectively are applied (Figure 6d).
5. Finally, the region with the biggest area is selected as hand and the remaining ones are deleted (Figure 6e).

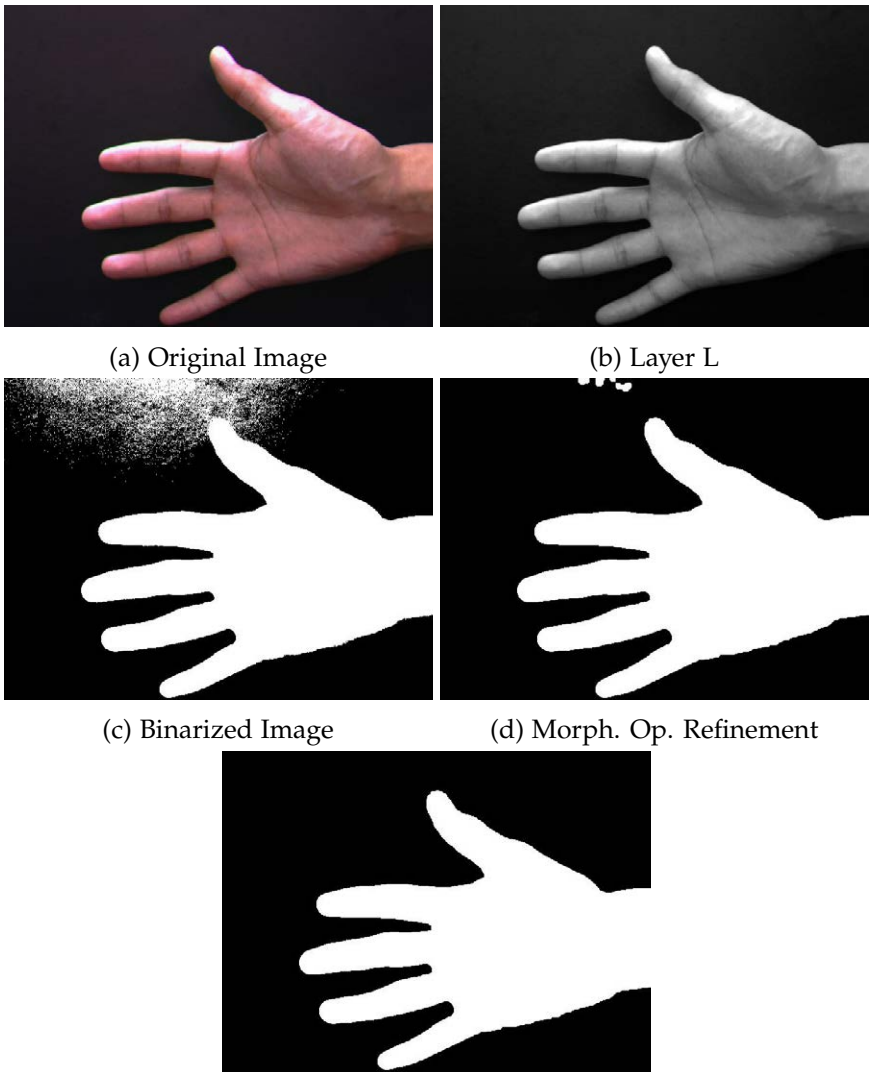

(a) Original Image (b) Layer L

(c) Binarized Image (d) Morph. Op. Refinement

(e) Final result

Figure 6.: Threshold based segmentation algorithm overview.

Implementation of the algorithm has been made in C++ and makes use of openCV library, which contains many useful functionalities for image processing.

3.3 GRAPH CUTS SEGMENTATION

Aimed to provide the system with a less restrictive segmentation tool regarding background and lighting conditions, an algorithm build on graph cuts has been integrated in the system, which is able to deal with certain real life situations. Graph cuts [12, 13] have become popular in the last decade for a variety of applications in computer vision such as image restoring, stereo matching or image segmentation, due to their global performance. This method takes into account both, regional and boundary information and guarantees a globally optimal solution without initialization requirements and allowing interactive guidance when necessary.

3.3.1 *Theoretical Fundamentals*

Despite the fact that an in-depth explanation on Graph Cuts is out of the scope of this thesis, hereafter a briefly description is provided in order to situate the reader and allow him to familiarize with graph cuts formulation for the segmentation problem.

3.3.1.1 *Graph Cuts*

Let $\mathcal{G} = (\mathcal{V}, \mathcal{E})$ be a directed weighted graph consisting of a set of vertices $\mathcal{V}$ and a set of edges $\mathcal{E}$ connecting these vertices. Each edge $e \in \mathcal{E}$ has a non-negative cost w_e. The set $\mathcal{V}$ consists of two types of nodes: neighbourhood nodes $\mathcal{P}$ which correspond to pixels, voxels, or other features and two special vertices called *terminals*: the source, s, and the sink, t, which in case of binary segmentation represent "object" and "background" labels. There are usually two types of edges in the graph: n-links and t-links. n-links connect pairs of neighbouring pixels or voxels, representing a neighbourhood system in the image which can be 4- or 8-connected for 2D images. The cost of n-links corresponds to a penalty for discontinuity between the pixels. t-links connect neighbourhood nodes $\mathcal{P}$ with terminal nodes. The cost of a t-link connecting a pixel and a terminal corresponds to a penalty for assigning the corresponding label to the pixel.

A cut $\mathcal{C} \subset \mathcal{E}$ is a subset of edges, such that if $\mathcal{C}$ is removed from $\mathcal{G}$, then $\mathcal{V}$ is partitioned into two disjoint sets $\mathcal{S}$ and $\mathcal{T} = \mathcal{V} - \mathcal{S}$ such that $p \in \mathcal{S}$ and $q \in \mathcal{T}$. There are no paths from terminal nodes s to terminal nodes t when all edges in the cut are removed. The cost of the cut C is the sum of its edge weights:

$$C = \sum_{e \in \mathcal{C}} w_e \tag{1}$$

The *minimum cut* problem on a graph is to find a cut that has the smallest cost among all cuts, i.e. min-cut. According to Ford and Fulkerson's work [57], min-cut is equivalent to maximum flow and the max-flow/min-cut algorithm can be used to find the minimum cut in polynomial time.

3.3.1.2 *Binary Segmentation using Graph Cuts*

Image segmentation can be regarded as a pixel labelling problem that involves assigning image pixels a set of labels $\mathcal{L}$ [107]. Particularly, segmenting an object from its background can be formulated as a binary labelling problem, i.e. each pixel in the image has to be assigned a label from the label set $\mathcal{L} = \{0, 1\}$, where 0 and 1 stand for background and object respectively. Let $\mathcal{P}$ be the set of all pixels in the image and let $\mathcal{N}$ be the standard 4 or 8-connected neighbourhood system on $\mathcal{P}$, consisting of ordered pixel pairs (p, q) where $p < q$. Let $f_p \in \mathcal{L}$ be the label assigned to pixel p, and $f = \{f_p | p \in \mathcal{P}\}$ be the collection of all label assignments. The set $\mathcal{P}$ is partitioned into two subsets, where pixels in one subset are labelled as background and the ones in the other subset are labelled as object.

The problem can be solved using an energy minimization framework, where the labelling corresponding to the minimum energy is chosen as the solution. The energy function commonly used for image segmentation is defined by eq. 2:

$$E(f) = \sum_{p \in \mathcal{P}} D_p(f_p) + \lambda \sum_{(p,q) \in \mathcal{N}} V_{p,q}(f_p, f_q). \tag{2}$$

In Eq. 2, the first term is called the *regional* or *data* term because it incorporates regional constraints into the segmentation. Specifically, it measures how well pixels fit into the object or background models under the labelling f. $D_p(fp)$ is the penalty for assigning label f_p to pixel p. The more likely f_p is for p, the smaller is $D_p(f_p)$. The object/background models could be known beforehand, or modelled from the seeds provided by the user. In case that interactive segmentation is allowed and the user indicate some seeds, in order to ensure that they are segmented correctly, for any object seed p, one sets $D_p(0) = \infty$, and for any background seed p, one sets $D_p(1) = \infty$. Typically, data penalties $D_p(\cdot)$ indicate individual label-preferences of pixels based on observed intensities and pre-specified likelihood function.

Interaction potentials $V_{p,q}$ encourage spatial coherence by penalizing discontinuities between neighbouring pixels. The second sum in Eq. 2 is called the *boundary, interactive* or *smoothness* term because it incorporates the boundary constraints. A segmentation boundary occurs whenever two neighbouring pixels are assigned different labels. $V_{pq}(f_p, f_q)$ is the penalty for assigning labels f_p and f_q to neighbouring pixels. This term is used to incorporate the prior knowledge about most nearby pixels are expected to have the same label, therefore there is no penalty if neighbouring pixels have the same label and a penalty otherwise. Typically,

$$V_{pq}(f_p, f_q) = w_{pq} \cdot I(f_p \neq f_q), \tag{3}$$

where $I(\cdot)$ is an identity function of a boolean argument defined as

$$I(\cdot) = \begin{cases} 1 & \text{if } f_p \neq f_q, \\ 0 & \text{otherwise.} \end{cases} \tag{4}$$

To align the segmentation boundary with intensity edges, w_{pq} is typically a non-increasing function of $|I_p - I_q|$, where I_i corresponds to the intensity of pixel i. For instance, one of the most extended functions is [12]:

$$w_{pq} = e^{-\frac{(I_p - I_q)^2}{2\sigma^2}}, \tag{5}$$

where σ represents the camera noise.

Parameter $\lambda \geq 0$ in Eq. 2 weights the relative importance between the regional and boundary terms. Smaller λ makes regional term more important compared with the boundary constraint and result in a segmentation which obeys the regional model more. On the contrary, larger values of λ result in a segmentation with higher boundary cost, which usually derives into shorter boundary length. Therefore, this parameter is one of the most important parameters in the graph cut framework, and the hardest parameter to pick beforehand. Typically, different images have different optimal values for this parameter.

Finally, it is possible to optimize the energy function in eq. 2 by graph cut method when V_{pq} is a submodular function [94]. For the particular case of binary segmentation the energy is submodular when $V(0,0) + V(1,1) \leq V(1,0) + V(0,1)$ is satisfied.

3.3.2 *Algorithm Overview*

A description of the algorithm can be found below together to an illustration of the different steps (Figure 7).

1. First, the image is resized for computational efficiency. The new size is provided as an input parameter.
2. Second, the pixel intensities are normalized. Assuming that the hand is placed at the center of the image, a subregion at the center of the image is selected as hand seed. Color distribution of this target is modelled as a Gaussian distribution and the image is normalized in terms of the mean of the distribution to reduce the influence of lighting conditions (Figure 7b).
3. Next, the normalized image is converted from RGB to CIEL*a*b* space color to separate lighting from color information. In addition, layer b is selected for binarization due to it contains the bluish hue missing in the skin (Figure 7c).
4. Then, layer b is thresholded by means of Otsu's algorithm[138](Figure 7d). This binarization is used to model the intensity of background and foreground pixels. Gaussian mean of these distributions are used to define first order terms in equation Eq. 2. In the presented implementation a correction factor has been applied over these terms which is provided as an input parameter.
5. After that, graph cut segmentation is performed using an 8-connected pixels neighbourhood (Figure 7e).
6. Finally, holes are filled and opening and closing mophological operations are applied to refine the result. In addition, in case that more than one region are present in the image, the blob with the biggest area is selected as hand (Figure 7f).

Implementation of the algorithm has been made in C++ and makes use of openCV and opengm libraries, where many useful tools for image processing and graph based applications can be found. Particularly, for graph-cuts optimization the max-flow implementation presented in [13] was used, which was specifically designed for computer vision applications and significantly outperformed the standard techniques because it has linear time performance.

3.4 FLOODING BASED SEGMENTATION

In certain scenarios a low computation time prevails over any other feature of the system. Some cases of use can even sacrifice accuracy to some extent if real-time computation is achieved. Nevertheless, they have often to deal with non-optimal capturing conditions. With the aim of covering these situations, a simple but fast hybrid algorithm is proposed in this thesis, which combine several well-known image-based methods to achieve fair accurate segmentations at daily-life environments and in a reasonable amount of time.

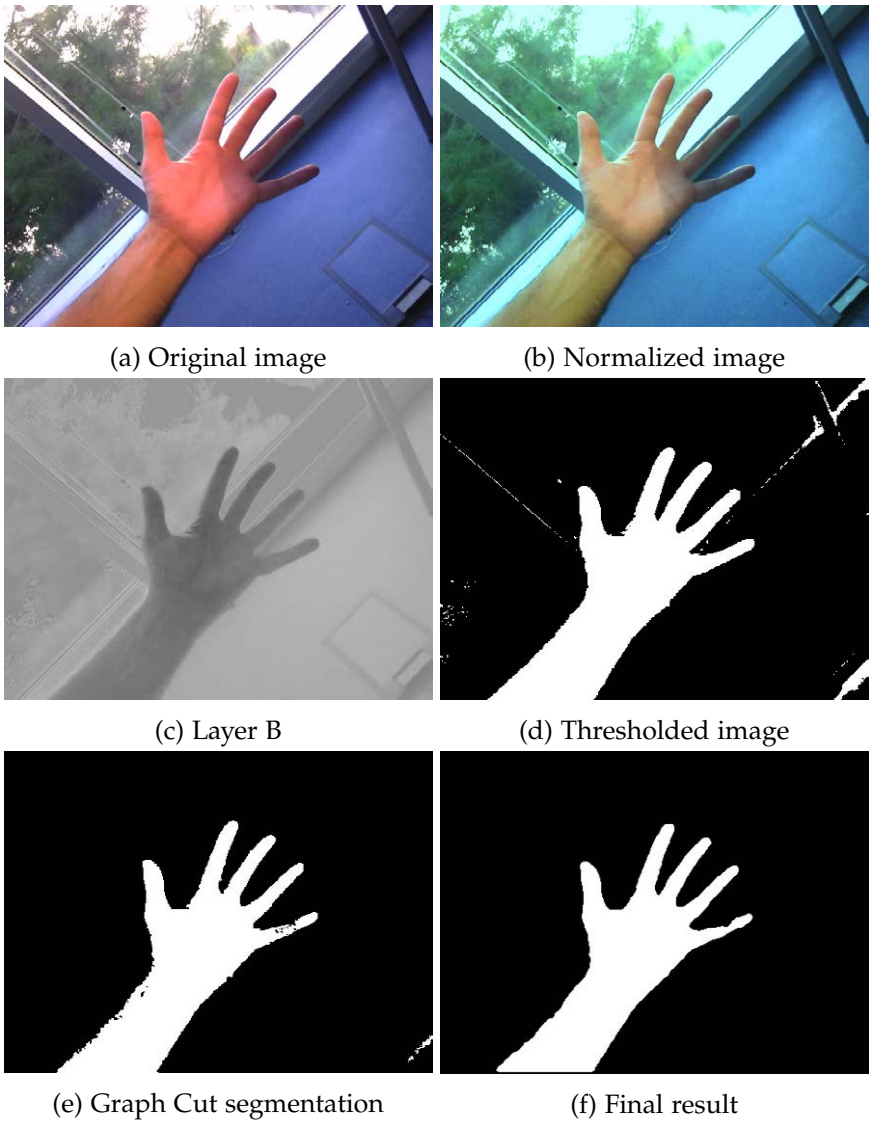

(a) Original image (b) Normalized image

(c) Layer B (d) Thresholded image

(e) Graph Cut segmentation (f) Final result

Figure 7.: Graph cuts based segmentation algorithm overview.

3.4.1 *Algorithm Overview*

The algorithm is described step-by-step under these lines. Main stages of the algorithm are illustrated in Figure 8.

1. First, the pixel intensities are normalized. Assuming that the hand is placed at the center of the image, a subregion at the center of the image is selected as hand seed. Color distribution of this target is modelled as a Gaussian distribution and the image is normalized in terms of the mean of the distribution (Figure 8b) to reduce the influence of lighting conditions.

2. Next, the normalized image is converted from RGB to CIEL*a*b* space color to separate lighting from color information. In addition, layer b is selected for binarization due to it contains the bluish hue missing in the skin (Figure 8c).

(a) Original Image

(b) Normalized image

(c) Layer B

(d) Median Filter over Otsu's binarization result

(e) Canny filter over Layer L

(f) Sum of binarized image, Layer L and Canny filtered image

(g) Flooding based segmentation result

Figure 8.: Flooding based segmentation algorithm overview.

3. Then, layer b is thresholded by means of Otsu's algorithm[138] and a mean filter is applied to attenuate noise (Figure 8d).

4. After that, Canny filter is applied over layer L which contains more enlightening border information (Figure 8e).

5. Layer L, the binarized image and the convolved image resulting from the application of Canny filter are summed to generate a new image which contains well defined border for posterior flooding (Figure 8f).

6. Finally, flooding segmentation is performed from the center of this summed image taking as a connectivity criteria that the intensity difference between pixels does not be higher than the intensity difference between neighbouring pixels in the hand target extracted at the first step. Then, mean filter is applied to attenuate noise. Final result can be seen in Figure 8g.

This algorithm has been implemented in C++ and makes use of openCV library.

3.4.2 *Flooding based segmentation using graph cuts binarization*

A variation of the algorithm aimed to face more extreme situations has been also developed. Main difference between both approaches resides in the method employed to obtain the first rough binarization. In this case Graph Cuts are used instead of simple Otsu's thresholding. Not unexpectedly, runtime is notably increased in relation to flooding based segmentation using thresholding at the initial step, but it can be considered as negligible with regard to Graph Cuts segmentation execution time. Nevertheless, the increase in time is compensated by improved results which outperform all the methods explained beforehand.

The algorithm is described step-by-step down below. Main steps of the algorithm are illustrated in Figure 9.

1. First, the pixel intensities are normalized. Assuming that the hand is placed at the center of the image, a subregion at the center of the image is selected as hand seed. Color distribution of this target is modelled as a Gaussian distribution and the image is normalized in terms of the mean of the distribution (Figure 9b) to reduce the influence of lighting conditions.

2. Next, the normalized image is converted from RGB to CIEL*a*b* space color to separate lighting from color information. In addition, layer b is selected for binarization due to it contains the bluish hue missing in the skin (Figure 9c).

3. Then, layer b is thresholded by means of Otsu's algorithm[138](Figure 9d). This binarization is used to model the intensity of background and foreground pixels. Gaussian mean of these distributions after applying a corrector factor are used to define first order terms in Eq. 2.

4. After that, graph cut segmentation using an 8-connected pixels neighbourhood is performed (Figure 9e).

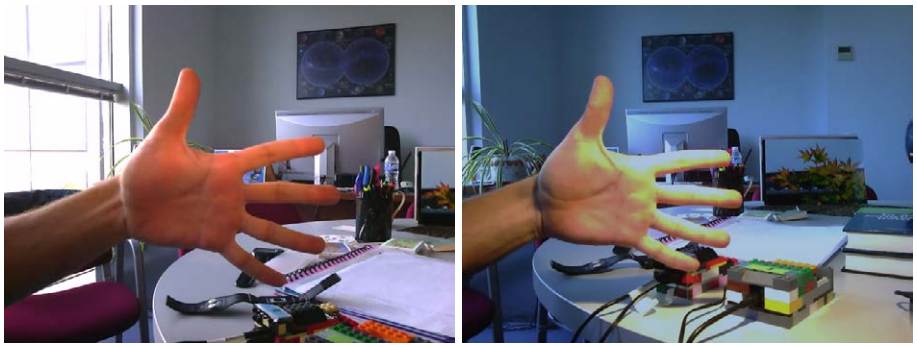

(a) Original Image

(b) Normalized image

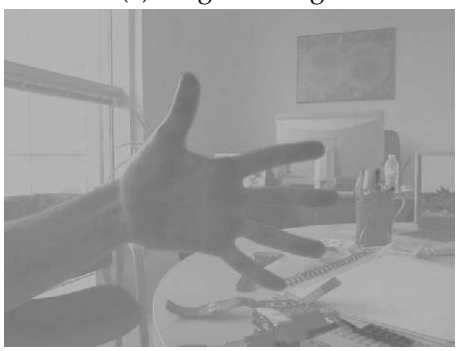

(c) Layer B

(d) Otsu binarization over Layer B

(e) Graph cuts segmentation

(f) Filling holes refinement

(g) Sum of graph cuts segmentation result and layer L

(h) Flooding based segmentation using graph cuts result

Figure 9.: Flooding based segmentation using graph cuts overview

5. Holes are filled in the segmented image (Figure 9f) and its complementary image is summed to layer L in order to generate a new image which contains well defined border for posterior flooding segmentation (Figure 9g).

6. Finally, flooding segmentation is performed from the center of this summed image taking as a connectivity criteria that the intensity difference between pixels does not be higher than the intensity difference between neighbouring pixels in the hand target extracted at the first step. In case that more than one region are present in the image, the blob with a bigger area is selected as hand. Final result is depicted in Figure 9h.

Similarly, this variation of the algorithm has also been implemented in C++ using openCV library.

3.5 SEGMENTATION EVALUATION

This chapter is aimed to provide the reader with a complete evaluation of the segmentation methods explained beforehand.

3.5.1 *Datasets*

To evaluate the methods, images captured under different environmental conditions have been used. Specifically, a subset of images have been selected from each database described in sec. 2.3:

- **Dataset 1** is composed of a subset of 354 images belonging to Database 1 described in sec. 2.3.1, one per user and session. Since these images have a dark neutral background and controlled lighting conditions, they represent the easiest segmentation case.

- **Dataset 2** includes 212 images from Database 2 (sec. 2.3.2), one per user and hand. These images present different almost monochromatic backgrounds and natural controlled lighting conditions, slightly increasing the difficulty of the segmentation process.

- **Dataset 3** comprises 11.011 images included in Database 3 (sec. 2.3.3), one per user, hand and texture. The great variety of backgrounds present in this dataset significantly increases the complexity of the segmentation task.

- **Dataset 4** contains 600 images from Database 4. As described in 2.3.4 these database was captured in three different sessions with different backgrounds and lighting conditions. First and second sessions include images with monochromatic background and controlled artificial lighting conditions while third session presents different real-life backgrounds and varied challenging lighting conditions. To compose this dataset one image per user and hand have been selected from those captured in the first session and one image per user, hand and lighting condition have been chosen from the third session. The uncontrolled

(or even adverse) environmental conditions of most of the images derives in a challenging segmentation dataset.

For every image included in these datasets, a groundtruth image has been manually delineated. It was a tedious, difficult, subjective and time-consuming work, but also important because it allows for a reliable evaluation of the segmentation results.

3.5.2 *Criteria*

A great number of evaluation methods can be found in the literature for image segmentation [74, 122, 180, 203]. Since groundtruth images have been generated for the datasets used in the evaluation, F-score metric has been selected to measure the performance of the algorithms presented beforehand.

F-score is defined as the harmonic mean of precision (also named confidence or positive predictive value) and recall (also named sensitivity or true positive rate):

$$F = 2 \cdot \frac{PR}{P + R} \tag{6}$$

where P and R are given by

$$P = \frac{TP}{TP + FP} \quad R = \frac{TP}{TP + FN} \tag{7}$$

and TP, FP and FN stands for true positive, false positive and false negative, respectively. In binary segmentation true positive are those pixels labelled as object in the segmented image that match with the ground truth image, false positive are those pixels labelled as object but are background indeed, and false negative are those pixels which are wrongly classified as background. Higher values of the F-score correspond to better segmentations.

3.5.3 *Threshold-based Segmentation Evaluation*

Performance of threshold-based segmentation is presented in Table 3 using the datasets described formerly. It can be seen that very competitive results are achieved by this method when the capturing conditions are controlled and the hand is placed over a dark well contrasted background. Nevertheless, performance is drastically decreased as soon as small variations in the environmental conditions are introduced.

Taking advantage of the fact that Dataset4 was recorded under different lighting conditions, a disaggregated evaluation of threshold-based segmentation method using this dataset is presented in table 4 to analyse the influence of illumination. It can be seen that results are similar in the four cases. Nevertheless, it is worth highlighting that better results are obtained when a great amount of light is directed to the hand, saturating it and favouring the segmentation process. On the other hand, contrary to expectations, the worst results are obtained when the scene is illuminated with natural light.

	Image Size (px.)	F-Score	Average time (s)
Dataset1	640x480	0.9860	0.1732
Dataset2	2592x1552	0.3661	1.8567
Dataset2	640x384	0.3664	0.1472
Dataset2	480x287	0.3666	0.0973
Dataset3	2592x1552	0.3659	1.8031
Dataset3	640x384	0.3674	0.1480
Dataset3	480x287	0.3700	0.0970
Dataset4	640x480	0.3641	0.1703

Table 3.: Threshold-based segmentation performance using different datasets.

Lighting Conditions	F-Score
Natural	0.3369
Severe Shadows	0.3610
Saturated	0.3939
Low-Intensity	0.3893

Table 4.: Threshold-based segmentation performance under different lighting conditions with daily-life backgrounds.

3.5.4 *Graph-Cuts Segmentation Evaluation*

Better results of graph-cuts segmentation method are presented in Table 5 for each dataset together with their parameter configuration. A complete study including all the parameters configuration evaluated for each dataset can be found in Appendix A.1. Results show that this method achieve slightly worse performance than threshold-based segmentation in the case that capturing conditions are controlled. However, its response to environmental conditions variations is notably better and performance is gradually decreased in accordance to the increase of the dataset complexity. Regarding the computation time, graph-cuts segmentation is quite more expensive, augmenting the system response in the order of around 10 times. Nevertheless, reducing the image size by a third can halve the computation time without loss of accuracy, which is even increased in some cases.

	Image Size (px.)	Balancing Terms	Lambda	F-Score	Average time (s)
Dataset1	640x480	0	0.15	0.9469	11.2690
Dataset1	480x360	0	0.15	0.9371	6.4866
Dataset2	640x384	0.5	0.5	0.8936	9.5294
Dataset2	480x287	0.5	0.15	0.9013	5.3263
Dataset3	640x384	0.55	0.15	0.7587	9.5423
Dataset3	480x287	0.65	3	0.7621	5.3219
Dataset4	640x480	0.65	0.15	0.6566	11.5392
Dataset4	480x360	0.75	1.5	0.6705	6.4404

Table 5.: Graph Cuts segmentation performance using different datasets.

Taking advantage of the fact that Dataset4 was recorded under different lighting conditions, a disaggregated evaluation of threshold-based segmentation method using this dataset is presented in table 6 to analyse the influence of illumination. It can be seen that better results are achieved under natural lighting conditions as well as low intensity illumination, which present quite similar performance. The worst result is obtained when a great amount of light is directed to the hand. It can be explained by the adopted colour space, which isolates the lightness component in a channel which is removed in order to make the algorithm more robust against the influence of lighting variations.

Lighting Conditions	Image Size (px.)	Balancing Terms	Lambda	F-Score
Natural	640x480	0.65	0.15	0.7342
Natural	480x360	0.65	10	0.7563
Severe Shadows	640x480	0.75	1.5	0.6733
Severe Shadows	480x360	0.75	10	0.6701
Saturated	640x480	1	1	0.5922
Saturated	480x360	0.85	0.5	0.5930
Low-Intensity	640x480	0.75	0.5	0.7227
Low-Intensity	480x360	0.75	3	0.7517

Table 6.: Graph Cuts segmentation performance under different lighting conditions with daily-life backgrounds.

3.5.5 *Flooding-based Segmentation Evaluation*

Performance of flooding-based segmentation using thresholding as initial binarization method is presented in Table 7 for each dataset. It can be seen that competitive results are achieved by this method, which not only present similar performance to Graph-Cuts but also clearly overcomes it in relation to the computation time. In addition, obtained results show that image resolution does not influence the accuracy neither the efficiency of the method.

	Image Size (px.)	F-Score	Average time (s)
Dataset1	640x480	0.9392	1.1408
Dataset2	2592x1552	0.9399	0.4340
Dataset2	640x384	0.8885	0.3057
Dataset2	480x287	0.8774	0.3154
Dataset3	2592x1552	0.7296	0.7197
Dataset3	640x384	0.6827	0.5908
Dataset3	480x287	0.6608	0.5313
Dataset4	640x480	0.6053	0.81684

Table 7.: Flooding-based segmentation performance using different datasets.

Table 8 shows the result of the algorithm variation described in 3.4.2 which uses Graph Cuts as initial segmentation method. Different parameter configurations have

been tested, but only the best arrangement for each dataset is presented in Table 8. For a complete relation of the evaluated configurations and the obtained results the reader is referred to Appendix A.2. It can be derived from the results that even when accuracy is improved for some datasets and the best results for Datasets 3 and 4 are obtained among all the methods, this increase is not large enough to compensate the computation efficiency decrease introduced by the application of graph-cuts as initial segmentation method.

	Image Size (px.)	Balancing Terms	Lambda	F-Score	Average time (s)
Dataset1	640x480	0	0.15	0.9000	9.4472
Dataset1	480x360	0	0.15	0.8969	5.4141
Dataset2	640x384	0.5	3	0.9122	9.8199
Dataset2	480x287	0.55	3	0.9111	5.6760
Dataset3	640x384	0.5	1.5	0.8151	15.0869
Dataset3	480x287	0.5	3	0.8120	5.1747
Dataset4	640x480	0.75	15	0.6047	12.5385
Dataset4	480x360	0.75	10	0.6151	7.4561

Table 8.: Flooding based segmentation performance for different datasets when graph cuts are used as initial binarization method.

Taking advantage of the fact that Dataset4 was recorded under different lighting conditions, disaggregated evaluations of flooding based segmentation have been carried out to analyse the influence of illumination. Table 9 presents the results when thresholding is used as initial binarization while Table 10 shows the results when graph cuts are applied in this first stage. It can be noted that natural light provides the better results in the case of thresholding initial binarization, followed closely by severe shadows and low-intensity lighting conditions, while in the case of applying graph-cuts as initial binarization, best performance is obtained under low-intensity and natural lighting conditions. The worst result in both cases is produced when a great amount of light is directed to the hand. Similarly to graph-cuts approach, it can be explained by the adopted colour space, which isolates the lightness component in a channel which is removed in order to make the algorithm more robust against the influence of lighting variations.

Lighting Conditions	F-Score
Natural	0.6567
Severe Shadows	0.6207
Saturated	0.4185
Low-Intensity	0.6171

Table 9.: Flooding-based segmentation performance under different lighting conditions with daily-life backgrounds.

Lighting Conditions	Image Size (px.)	Balancing Terms	Lambda	F-Score
Natural	640x480	0.65	15	0.6505
Natural	480x360	0.65	10	0.6658
Severe Shadows	640x480	0.85	15	0.6157
Severe Shadows	480x360	0.85	10	0.6302
Saturated	640x480	0.85	30	0.5193
Saturated	480x360	1	30	0.6007
Low-Intensity	640x480	0.75	0.75	0.6617
Low-Intensity	480x360	0.75	1.5	0.6818

Table 10.: Flooding-based segmentation performance under different lighting conditions with daily-life backgrounds when graph cuts are used as initial binarization method.

3.6 SEGMENTATION QUALITY CONTROL

As mentioned at the beginning of this chapter (Sec. 3.1), when images present some characteristics such as cluttered background, blurriness or difficult lighting conditions the segmentation process became specially challenging. In other cases, difficulties are produced because the user does not follow the recommendations provided at Section 2.2. Most common errors produced by user's behaviour are non stretched and non separated fingers which often lead into segmented hands which only contain four fingers. The four-fingers error is also produced by the use of rings, specially when rings contrast with the skin colour. In these cases the finger wearing the ring does not appear in the segmented image. Figure 10 shows some examples of incorrect segmentations.

A quality control module is necessary to ensure that the segmented image contains a hand and that it has enough quality to success the complete recognition process. This way the transfer of segmentation errors to final rates is avoided. When the algorithms fail due to environmental conditions providing a binary image which is almost totally black or almost totally white, these images are automatically discarded and a new sample would be required. Those segmentations that do not contain a hand will raise an error during the Fingers Extraction or Inter-Finger Valleys detection procedures. These procedures will be explained in Sections 4.2 and 4.3. Finally, those images in which fingers are not separated enough or the use of rings derives into the absence of one or more fingers will also be automatically detected during the Fingers Extraction process.

There are other cases which are more difficult to detect, such as those cases where shadows are detected as a part of the hand distorting its silhouette. They are not taken into account by current segmentation quality module and usually produce errors in subsequent steps. Nevertheless, the implementation of a more robust segmentation quality module is out of the scope of this thesis, but it will be recommended in case a prototype will be put into practice.

Figure 10.: Images incorrectly segmented.

4

MEANINGFUL POINTS DETECTION AND REGION OF INTEREST EXTRACTION

4.1 INTRODUCTION

To extract biometric information of the hand, it is necessary to detect some meaningful points which allows to detect those parts of the hand which contains most characteristic information of the user, such as finger geometry and palm-print features. In particular, fingertips and valleys between fingers are detected together with the central part of the palm, which concentrates the most relevant palm-print information. This sub-image is commonly named Region of Interest (ROI). Given the contact-less nature of this trait, to obtain robust and invariant features it is also necessary to align the ROIs into a common coordinate system to avoid problems related to rotation and translation movements among hands in different images.

4.2 FINGERS EXTRACTION AND CLASSIFICATION

First, starting from the binary image resulting from the segmentation process (B), fingers are isolated by means of morphological operations. Applying an opening operator with disk structural element, fingers are removed from the segmented image giving as a result a new image B_p which contains those regions corresponding to the palm and the arm in case it appears in the segmented image. Given B and B_p the regions corresponding to the fingers (B_f) are straightforwardly calculated by a simple operation as defined in eq. 8:

$$B_f = B \cdot \overline{B}_p \tag{8}$$

where $\cdot$ is an operator which indicates a logical AND operation between B and the complementary of B_p. Fingers isolation process is illustrated in Figure 11.

Then, a refinement process is applied in cases that more than 5 regions result from the previous operations. Small regions, regions in contact with the image borders and regions that are more separated from the other regions and the center of the image are removed during this process.

Finally, fingers are identified according to the euclidean distances between their centroids. Those fingers whose centroids are separated by the biggest distance are thumb and little fingers. From these two, the one that present a bigger distance to the remaining fingers is the thumb. Index and ring fingers are identified by proximity to thumb and little fingers respectively. Middle finger identification is straightforward.

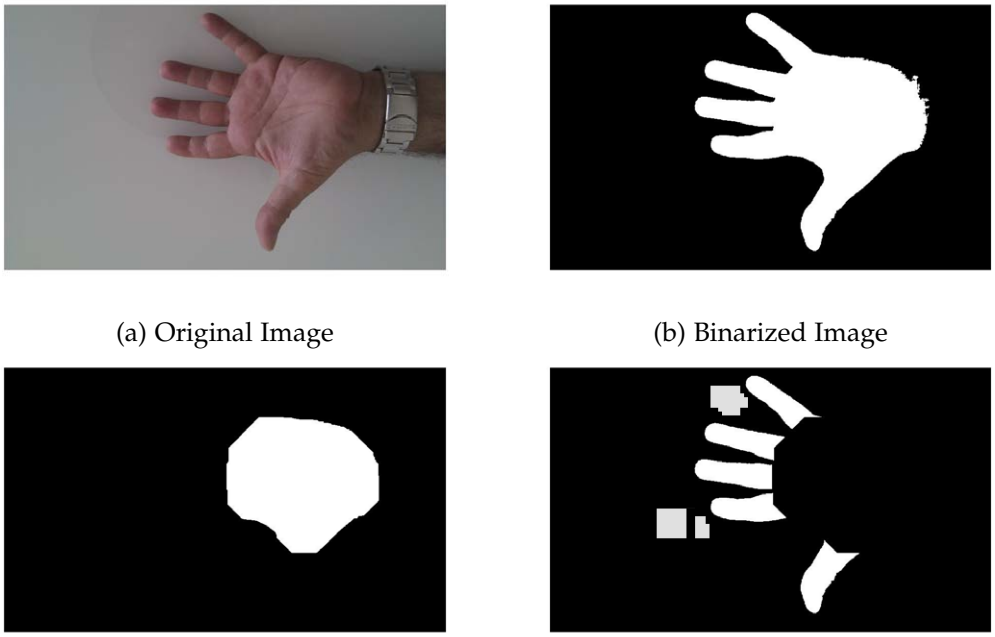

(a) Original Image (b) Binarized Image

(c) Palm region (d) Fingers

Figure 11.: Fingers isolation process.

4.3 INTER-FINGERS VALLEYS DETECTION

To calculate the inter-finger valleys, the contour and the centroid of the hand are detected (Fig. 12a). Then, euclidean distances between each contour point and the centroid of the hand are calculated (Fig. 12b). Those points which are farther from the centroid corresponds to fingertips and wrist, while those points between tips and wrist which are closer to the centroid corresponds to interfinger valleys and the exterior basis of thumb and little fingers. From these six valleys (Fig. 12c), index-middle ($v_{i,m}$), middle-ring ($v_{m,r}$), and ring-little $v_{r,l}$ valleys are selected as those which are closer to the centroid of the corresponding fingers.

4.4 PALM REGION EXTRACTION

As mentioned formerly, to obtain the palmprint features it is necessary to remove those areas that do not contain relevant information, providing as a result a subimage commonly named Region of Interest (ROI) which needs to be properly aligned. To this end, starting from the binary image resulting from the segmentation process and the inter-finger valleys, the ROI is extracted using a similar method to that proposed in [27].

Using inter-finger valleys as reference points, two vertex of the ROI (v_1 and v_2) are detected. A straight line is traced between $v_{m,r}$ and $v_{i,m}$ and it is extended towards index finger outer side. v_1 corresponds to the middpoint between $v_{i,m}$ and the cut off point between this line and the hand contour farthest to the $v_{i,m}$. The same actions are

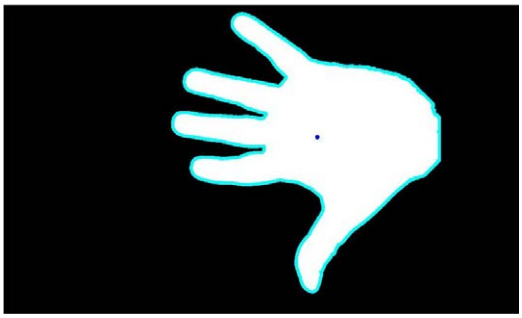

(a) Hand contour and centroid

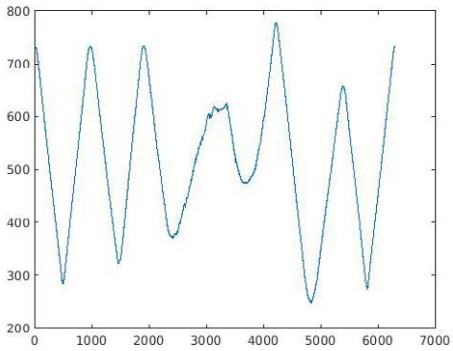

(b) Hand Contour-Centroid Distances

(c) Inter-finger Valleys

Figure 12.: Inter-finger Valleys detection process.

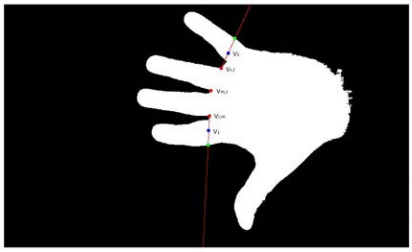

(a) Vertex

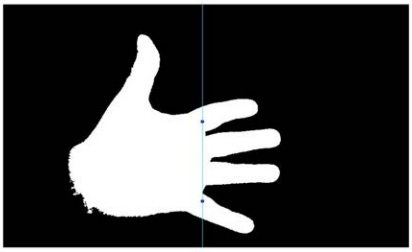

(b) Alignment

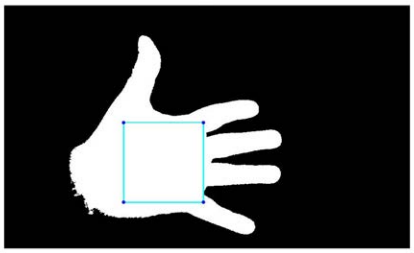

(c) Region of Interest

(d) Cropped and Enhanced ROI

Figure 13.: ROI extraction, alignment and enhancement procedure.

repeated between $v_{m,r}$, $v_{r,l}$, and little finger to obtain v_2. This procedure is illustrated in Figure 13a. Then, these new points are aligned in the vertical axis with the thumb finger upwards (Figure 13b).

Then, taking as region size (s) the euclidean distance between v_1 and v_2, the two segments of size s that are perpendicular to the segment $\overline{v_1 v_2}$, start at v_1 and v_2, and are closer to the hand centroid, are extracted. The end points of these segments corresponds to the remaining two vertex of the ROI (Fig. 13c).

Finally, the ROI is enhanced by means of histogram equalization and resized to a common size of 128×128 px.

ROI detection and alignment process is strongly dependant on the accuracy of the segmentation, which also affects the valley detection procedure. When the segmentation is not precise enough and this lack of accuracy is not detected automatically by the segmentation quality control module (Sec. 3.6), it can derive into the extraction of incorrect ROIs. Figure 14 depicts some examples of incorrect ROIs together with their original and segmented images. Detection of incorrect ROIs is an important step in order to avoid unexpected behaviour of posterior feature extraction and comparison modules. The implementation of a ROI quality control module is out of the scope of this thesis, so a visual supervision has been carried out discard incorrect ROIs but some ideas will be provided as future lines (Sec. 12.3).

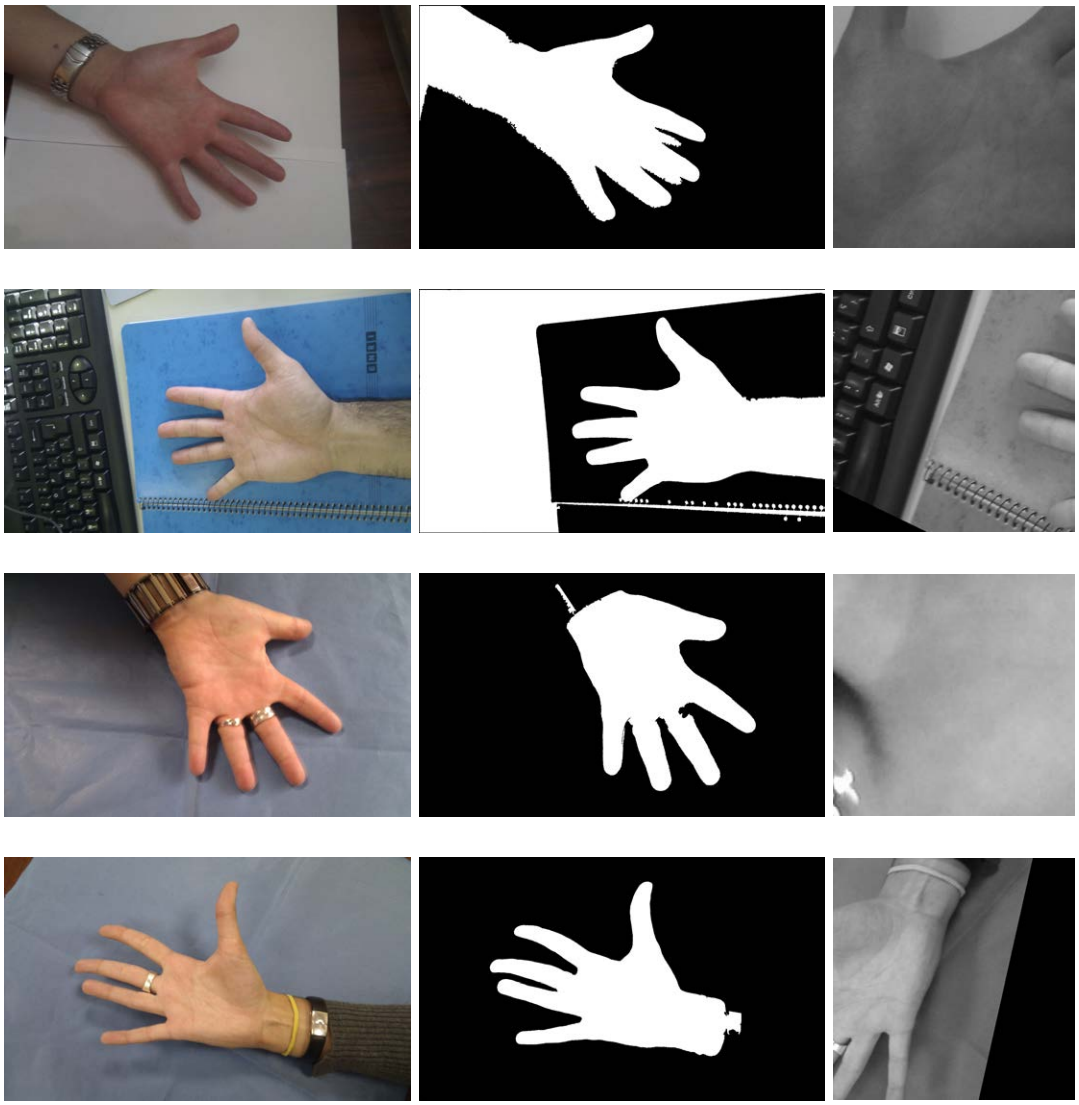

Figure 14.: Regions of Interest incorrectly detected and aligned together with their corresponding original images and segmentations.

Part III

MULTIMODAL HAND BIOMETRICS

5

FEATURE EXTRACTION

5.1 INTRODUCTION

Hand images contain features related to different biometric traits including palmprint, hand geometry, fingerprints, palm veins or knuckleprint among others. This thesis is focused in two of the most widely extended hand traits: palmprint and hand geometry. Interest on palmprint and hand geometry biometrics has experimented a strong growth in the last decades due to its useful characteristics as uniqueness, permanence, reliability, user-friendliness, acceptability, non-intrusiveness, and low cost of the acquisition devices, which make them attractive for civil and commercial applications.

Palmprint is composed of numerous and stable line features: principal lines, wrinkles and ridges. Although the principal lines are genetically dependent, most of the wrinkles and ridges are not, deriving in a reliable identifier which is exclusive even in monozygotic twins [99]. Using an image or video stream of their palms, users can be authenticated by detecting the principal lines and wrinkles, even when the capture device is a low resolution camera as those integrated in mobile phones.

Palmprint feature extraction methods can be classified into two principal groups: minutiae-based, that requires high-quality images to locate minutiae points, singular points and analyse ridges [207, 21, 176, 18, 112, 205], and texture-based, that are able to deal with low-quality images and are the methods preferred in this thesis. These methods can also be divided into line-based, subspace and statistical approaches [97]. The line-based group includes those approaches which take into account the structural information of the image as morphological operators or edge detectors like Sobel filter [133], OLOF [126] or Harris corner detector [139]. Those methods which are based on the appearance of the image (PCA, LDA, FCA) are enclosed in the subspace group [27, 116]. Finally, the statistical group contains feature descriptors as Fourier transform [109], Gabor filters [202, 95, 96, 45], Local Binary Patterns [133] or Local Derivative Patterns [170].

A comprehensive literature review about texture-based palmprint biometric verification is detailed in Table 11, where previous works are classified according to the nature of testing images in terms of environmental conditions and pose restrictions. In addition, the specific features and the matching method are detailed in each case, together with the obtained results.

Background	Lighting Conditions	Pose Restric.	Features	Matching	Crew Size	Results (%)	Ref.
Controlled	Controlled	Contact, pegs	Gabor filter	Hamming Distance	120	5.5 EER	[98]
			Gabor filter	Normalized Hamming distance	193	0.6 EER	[202]
			Competitive Code (gabor filter)	Angular distance	193	3×10^{-6} FAR, 1.6 FRR	[95]
			Curvelets	Euclidean Distance	100	6.25 EER	[43]
			PalmCode Competitive Code Ordinal Code	Hamming Distance, Cohort information	193	0.15 EER 0.17 EER 0.13 EER	[101]
			Ordinal Code (Gabor, OLOF)	Hamming Distance	283	0.22 EER	[174]
			SAX	MINDIST	100	1.33 EER	[22]
			Fusion Code (ellip.gabor)	Hamming Distance	284	1.2×10^{-5} FAR, 7.7 FRR	[96]
			RLOC, FRAT	Pixel-Area Matching	193	0.16 EER	[81]
			Laplacian Palm	Nearest Neighbour	120	0.3 EER	[185]
			Gabor filter	Hamming Distance	50	0.47 EER	[121]
			Circular Gabor	Normalized Hamming distance	193	1.2 FRR, 0 FAR	[62]
			BOCV (gabor filter)	Hamming distance	193	0.0189 EER	[68]
			LBP multiscale	χ^2 distance	100	99.67 RA	[69]
			Gabor filter	Normalized Hamming Distance	200	0.92 EER	[149]
			SMCC, sDoG fil.	Angular distance	193	0.014 EER	[209]
			Curvelets	RBF-NN	48	0 FAR 7.6 FRR	[193]
			MFRAT, LBP MFRAT, LTP	χ^2 distance	193	99.56 Ac. 99.82 Ac.	[206]

Background	Lighting Conditions	Pose Restric.	Features	Matching	Crew Size	Results (%)	Ref.
Controlled	Controlled	Contact, pegs	ICP, Compet. Code ICP, RLOC	Angular distance	193	0.0201 EER 0.0571 EER	[108]
			Directional mask	DTW	50	49 Err.	[110]
			Curvelets	Nearest Neighbour	100	99.9 ARR	[113]
			Wavelet Ridgelet Bandlet	BP-NN	190	93.3 Ac. 95.8 Ac. 96.5 Ac.	[2]
Controlled	Controlled	Contact, Surface Marks	PalmCode (gray-level variations)	Similarity meassure	40	3.03 EER	[102]
Controlled	Controlled	Contact, Free Place.	Sobel filter Morphol. Features	Multi-template Matching BP-NN Multi-template Matching BP-NN	50	4.5 FRR, 6.7 FAR 0.6 FRR, 1.79 FAR 3.3 FRR, 6.6 FAR 0.5 FRR, 0.96 FAR	[70]
			FDA	Euclidean distance	50	5.98 FAR, 6 FRR	[137]
			Gaussian mask, Sobel filter	Euclidean distance	130	3.80 FAR, 1.40 FRR	[156]
			Wavelets, PCA Wavelets, FDA Wavelets, ICA	Euclidean distance Euclidean distance Cosine distance	75	2.98 EER 1.4 EER 1.9 EER	[27]
			Gabor filter	Hamming distance	109	0.22 EER	[56]
			Gabor filter	Hamming distance	109	0.18 EER	[53]
			Wavelet	Euclidean distance	98	16 EER	[197, 117]
			Wavelets, Zernike moments	Clustering, BP-NN	100	2.74 EER	[100]
			SMCC, sDoG filters	Angular distance	301	0.48 EER	[209]

Background	Lighting Conditions	Pose Restric.	Features	Matching	Crew Size	Results (%)	Ref.
Controlled	Controlled	Contact, Free Place.	OLOF	Normalized Hamming distance	80	0.01 EER	[63]
			ICP, Compet. Code ICP, RLOC	Angular distance	312	0.794 EER 0.814 EER	[108]
			DCT, HMM	Viterbi recognizer	165	1.299 EER	[120]
			SLG, KLT operator	LK traking	312	0.29 EER	[130]
Controlled	Controlled	Contactless	Directional Code (Wavelet, Sobel)	Hamming distance	136	1.97 EER	[136]
			Competitive Code	Angular distance	180	0.0738 EER	[14]
			OLOF	Normalized Hamming distance	235	0.61 EER	[125, 126]
			OLOF	Normalized Hamming distance	80	1.07 EER	[63]
			Directional Code	Hamming distance	136	1.97 EER	[135]
Controlled	Indoor	Contact, Surface Marks	Directional Mask	Similarity meassure	100	4.49 FAR, 2.04 FRR	[103]
Controlled	Indoor	Contactless	Sobel, LBP	χ^2 distance PNN	320	1.52 EER 0.74 EER	[133]
			Gabor filter	Hamming distance	50	8.71 EER	[121]
			Competitive code	Hamming distance	177	1.22 EER	[89]
			Entropy	Canberra distance Manhattan distance Lorentzian distance Euclidean distance	-	15.17 FAR 35 FRR 14.01 FAR 36 FRR 15.12 FAR 35.5 FRR 17.41 FAR 36.5 FRR	[182]
Uncontrolled	Indoor	Contactless	Gabor filter	Hamming distance	16	2.25 EER	[44]
			Gabor filters bank	HDE based on SVMs	49	1.7 EER	[45]
			Normalized Sub-images	HDE based on SVMs	49	1.5 EER	[46]

Background	Lighting Conditions	Pose Restric.	Features	Matching	Crew Size	Results (%)	Ref.
Uncontrolled	Indoor	Contact-less	OLOF	Normalized Hamming distance	110 100	2.25 EER 0.98 EER	[125] [126]
			LBP	χ^2 distance	20	3.77 EER	[165]
			LCDP	Histogram Intersection	200	1.08 EER	[170]

Table 11.: Texture-based palmprint Biometric Verification techniques classified according to the nature of testing images in terms of environmental conditions and pose restrictions. The specific features and the matching method are detailed in each case, together with the obtained results.

On the other side, hand also includes geometric characteristics such as palm and finger length and widths, inter-finger areas and angles or contour silhouette curvatures. These features are easily extractable from the binary image obtained from the segmentation process and are highly compatible with other features present in the hand images such as palmprint.

Hand geometry feature extraction methods can be separated into two main streams: contour-based approaches and distance-based approaches. Former methods analyse the information about the hand shape extracted from the hand contour and include approaches such as contour alignment [78, 195, 194], contour angles [11], b-spline curves [118], zernike moments [5], eigenhands [177], independent component analysis [200], radon transform [128] or contour curvature and distance to the centroid [36]. Later methods extract geometrical information about the hand included in the palm and fingers and are more widespread mainly due to its simplicity. Most simple feature vectors are composed by grayscale profiles [160, 80] or finger widths [40, 35, 58, 35], finger widths and lengths [124, 123, 55, 54] or finger widths and lengths together with fingertips information [41, 189]. Other works also add hand and palm information about size or angles together with finger meassurements [164, 72, 183, 188, 82, 192, 48]. Surface and perimeter information [52, 3] or even 3D information [175] have also been added to basic measurements to construct more complex feature vectors. A totally different approach is presented in [6], where a connected graph is constructed to model the distances between finger tips and inter-finger valleys. Finally, a hybrid approach is presented in [65] which merge contour-based information with geometric features.

A comprehensive literature review about hand geometry biometrics is detailed in Tables 12 and 13, which show contour-based and geometric features-based approaches for biometric verification purposes respectively. In this tables previous works are classified according to the nature of testing images in terms of environmental conditions and pose restrictions. In addition, the specific features and the matching method are detailed in each case, together with the obtained results.

Background	Lighting Conditions	Pose Restric.	Features	Matching	Crew Size	Results (%)	Ref.
Controlled	Controlled	Contact, Pegs	Contour Points	MAE	6	4.17 EER	[78]
			B-Spline curves	Curve fitting	20	5.00 VE	[118]
			Chain Code	DTW	50	31 Err	[110]
		Contact, Surface Marks	Eigen Hand	Euclidean distance	5	5 FMR	[177]
		Contact, Free Place.	Control Points	Contour Alignment	108	2.41 EER	[194, 195]
			Zernike Moments	Euclidean distance	40	2 EER	[5]
			Contour Points	ICA	458	1.79 EER	[200]
			Radon Transform	Euclidean distance	18	5.1 EER	[128]
Uncontrolled	Indoor	Contact-less	Parametric curves, Cent-Cont distances	Fuzzy Alignment	45	3.70 EER	[36]

Table 12.: Contour-based approaches for Hand Geometry Biometric Verification classified according to the nature of testing images in terms of environmental conditions and pose restrictions. The specific features and the matching method are detailed in each case, together with the obtained results.

Background	Lighting Conditions	Pose Restric.	Features	Matching	Crew Size	Results (%)	Ref.
Controlled	Controlled	Contact, Pegs	FW, FD, PW, PH, IFP, An	Euclidean distance Hamming distance Gaussian Mixture Models	20	23 FAR, 19 FRR 16 FAR, 9 FRR 6.6 FAR, 9 FRR	[163]
			FL, FW, PW	Absolute distance	50	0 FAR, 5 FRR	[160]
			FL, FW, PW	Weighted Euclidean distance	50	12 EER	[80]
			FW, FH, FD, PW, An	Euclidean distance Hamming distance Gaussian Mixture Models	20	12 EER 8 EER 6 EER	[164]

Background	Lighting Conditions	Pose Restric.	Features	Matching	Crew Size	Results (%)	Ref.
Controlled	Controlled	Contact, Pegs	FH, FW, PW	Euclidean distance	24	2.1 EER	[183]
			FC, FL, FW, An, IFPD	Euclidean distance	100	1.81 EER	[140]
		Contact, Surface Marks	HG, A, FW, FW, PW, PL	Similarity meassure	100	5.29 FAR 8.24 FRR	[103]
		Contact, Free Place.	FL, FW, FTRP	GMM and Euclidean distance	29	89 HIT, 2.2 FAR	[189]
			FL, FW, PW	Euclidean distance	50	4.28 FAR, 4.00 FRR	[137]
			FL, FW, PW, IFPD	Euclidean distance	130	15.30 FAR, 13.00 FRR	[156]
			FL, FW	distance	80	2 EER	[11]
			FL, FW, P	MLP	22	4.70 DCF	[52]
			FL, FW	SVMs	109	0.22 EER	[56]
			FL, FW, PW, WVD	SVMs	18	92 Ac.	[82]
			FW	Kullback-Leiber distance	750	4.19 EER	[58]
			FL, FW, IFPD	Euclidean distance	98	21 EER	[197, 117]
			FL, FW	SVMs	109 550 85	0.92 EER 0.65 EER 99.85 RR	[53] [55] [54]
			FW, FP, FA	Euclidean distance Absolute distance	50	0.41 EER 0.32 EER	[3]
			FW	LS-SVMs	80	0.25 EER	[63, 127]
			FL, FW, PW, FR	k-NN	35	5.08 FRR, 4.87 FAR	[188]
			Interfinger Points and Fingertips distances Graph	SVMs	144	0.69 FAR, 2.08 FRR	[6]
Controlled	Controlled	Contact-less	FL, FW, PL, PW, A, HL, P, S, E, CA, Ex, CP	k-NN Naïve Bayes SVMs FFN	100	93.8 Ac. 94.6 Ac. 95 Ac. 94 Ac.	[105]
			FL, FW, PW, FD, IFVD, An	Euclidean distance	100	2.04 EER	[192]

Background	Lighting Conditions	Pose Restric.	Features	Matching	Crew Size	Results (%)	Ref.
Controlled	Controlled	Contact-less	FL, FW, FD, An, A	Euclidean distance	180	2.41 EER	[14]
			FW	LS-SVMs	80	0.83 EER	[63, 127]
			PW, PL, FW, FL, CIFPD, An	Euclidean distance	136	3.61 EER	[135]
			FL, FW	Euclidean distance	100	95.84 Ac.	[84]
			FL, FW, WVD, 3DFW, ASD,	Mahalanobis distance	17	1.61 EER	[175]
Controlled	Indoor	Contact-less	FL, FW, FA, P	Euclidean	177	6.3 EER	[88]
			FL, FW, PW, FP	Euclidean distance	177	6.3 EER	[89]
Uncontrolled	Indoor	Contact-less	FW	SVMs	20	6.3 EER	[123]
			FW, FL, FTC	SVMs	50	6 EER	[41]
			FW	SVMs	120	3.8 EER	[40]
			FW	Statistical Matching	287	1.4 EER	[35]
	Infrared	Contact-less	FW	SVMs	30 20	4.2 EER 3.4 EER	[123] [124]

Table 13.: Geometry-based approaches for Hand Geometry Biometric Verification classified according to the nature of testing images in terms of environmental conditions and pose restrictions. The specific features and the matching method are detailed in each case, together with the obtained results. FL, FW, FH, FD, FP, FA, FR, FC, PL, PH, PW, HL, IFP, IFPD, CIFPD, FTRP, CP, WVD, An, A, P, S, E, CA, Ex and ASD stands for fingers length, fingers widht(s), fingers height, fingers deviation, fingers perimeter, fingers area, fingers curvature, ratio between fingers, palm lenght, palm height, palm width(s), hand length, inter finger points location, inter finger points distances, centroid - inter finger points distances, fingertips region points, centroid position, wrist-valleys distance, angles, area, perimeter, solidity, extent, convex area, excentricity and axis to surface distances respectively.

5.2 PALMPRINT

5.2.1 *Sobel filter*

Considering the fact that palmprint features are mainly lines, edge detectors can be used to describe its texture as demonstrated in [133]. The Sobel operator [171] is a derivative mask that applied to an image emphasizes the regions which contains borders by measuring the spatial gradient with respect to a threshold in the appropriate direction.

In this case, due to the fact that palmprint lines appear in several directions, four different convolution kernels have been separately applied to measure the response of the gradient component in orientations 0, 45, 90 and 135 degrees, as shown in Figure 15.

The feature vector which describes the texture of the palmprint is just a concatenation row by row of the binarized image(s) one after the other. In order to generate a feature vector having a tractable size in terms of computation efficiency, the original images are reduced in size before the application of the Sobel filter.

Implementation has been codified in MATLAB.

5.2.2 *Zero DC Circular Gabor filter*

The Circular Gabor filter is a variation of the traditional Gabor filter which was proposed for rotation invariant texture segmentation [204]. It has been previously applied to palmprint identification at controlled environments [202, 62].

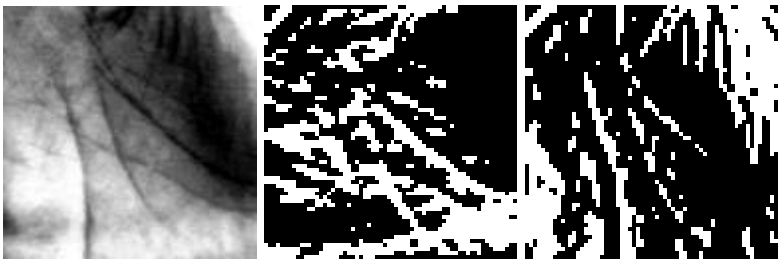

(a) Palmprint ROI (b) 0° response (c) 45° response

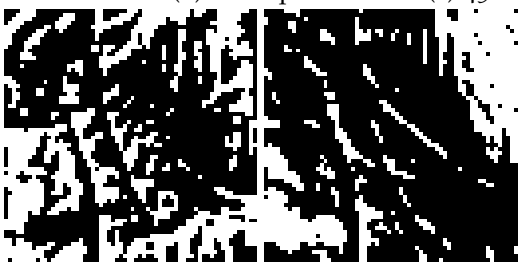

(d) 90° response (e) 135° response

Figure 15.: Original and filtered images using Sobel operator at four different directions when threshold parameter is set to 0.25.

The Circular Gabor filter is mathematically defined by the following expression:

$$G(x,y,\sigma,F) = \frac{1}{2\pi\sigma^2} e^{\left(-\frac{x^2+y^2}{2\sigma^2}\right)} e^{\left(2\pi i F\left(\sqrt{x^2+y^2}\right)\right)} \tag{9}$$

where σ is the standard deviation of the gaussian envelope and F is the central frequency of the Circular Gabor filter.

In the same way that the authors in [202], we removed the DC (direct current) component from the discrete Circular Gabor Filter to make it more robust against brightness variability applying the next formula:

$$\widetilde{G}(x,y,\sigma,F) = G(x,y,\sigma,F) - \frac{\sum_{i=-n}^{n}\sum_{j=-n}^{n} G(i,j,\sigma,F)}{2(n+1)^2} \tag{10}$$

where $2(n+1)^2$ is the size of the filter.

Choosing the appropriate value of the Gabor filter parameters is crucial to obtain a descriptive enough result when analysing the texture of the palmprint. To this end, different values for the central frequency of the Circular Gabor filter, the standard deviation of the gaussian envelope and the filter size will be tested in Chapter 9 to decide the best parameter arrangement.

The image containing the preprocessed ROI is convolved with the Zero DC Circular Gabor filter. The resulting image has two components, the real and the imaginary parts from which we extract two binary images by thresholding (Figure 16). If the bit in the imaginary part is major or equal to zero, then a value equal to 1 is assigned to the corresponding pixel in the binary image associated to the imaginary part, otherwise it is set to 0 value. We proceed in the same way for the real part.

Similarly to the Sobel operator approach, the final feature vector is composed by concatenating row by row the binary images corresponding to the real and the imaginary parts of the convolved image.

Implementation has been codified in MATLAB.

5.2.3 *Local Binary Pattern*

Local Binary Pattern (LBP) operator is a popular texture descriptor presented in [131] whose robustness, simplicity and good performance in both, accuracy and computa-

(a) Palmprint ROI (b) Real Part (c) Imaginary Part

Figure 16.: Original and filtered images corresponding to the real and imaginary parts of the convolved image using the Zero DC Circular Gabor filter.

tion efficiency, make it suitable for many computer vision and image processing applications, including palmprint recognition using contactless images acquired under controlled environmental conditions, as demonstrated in [133].

First of all, the LBP code is calculated for every pixel in the image employing the intensities corresponding to that pixel and its neighbours. In the original LBP operator a 3×3 neighbourhood is established. To obtain gray-scale invariance, the intensity of the evaluated pixel (the central pixel) is substracted from the gray value of the neighbours giving as a result a Local Binary Pattern. Then, this pattern is weighted, and the obtained values are added up to obtain the LBP code which contains information about the local features of the texture of the image. This process is graphically shown in Figure 17 and is formally described as:

$$LBP_{code} = \sum_{p=0}^{P-1} S(g_p - g_c)2^p \tag{11}$$

where g_p corresponds to the intensity value of the neighboor pixels $(p_0, ..., p_{P-1})$, g_c is the gray value of the central pixel and S is the threshold function defined in equation 12:

$$S(x) = \begin{cases} 1, & \text{if } x \geq 0 \\ 0, & \text{if } x < 0 \end{cases} \tag{12}$$

Then, the texture of the image is commonly represented by the histogram of the calculated LBP codes.

In 2002, Ojala et al. extended LBP operator definition to neighbourhood of different sizes [132]. The original operator is derived to a general case based on circular symmetry in a region of P neighbour pixels inside a circle of radius R. Following this principle, the operator is denoted as $LBP_{P,R}$. This way, LBP operator is defined by two parameters: P and R, where P represents the number of neighbour pixels and control the angular space quantification and R corresponds to the radius of the circle and determines the operator spatial resolution.

In that work Ojala et al. also observed that there are some binary patterns which occur more frequently in the texture description: the Uniform Binary Patterns [132]. These patterns contains very few spatial transitions, there are no more than two bitwise 0/1 changes in the pattern when it is traversed circularly: 0000000, 1111111,

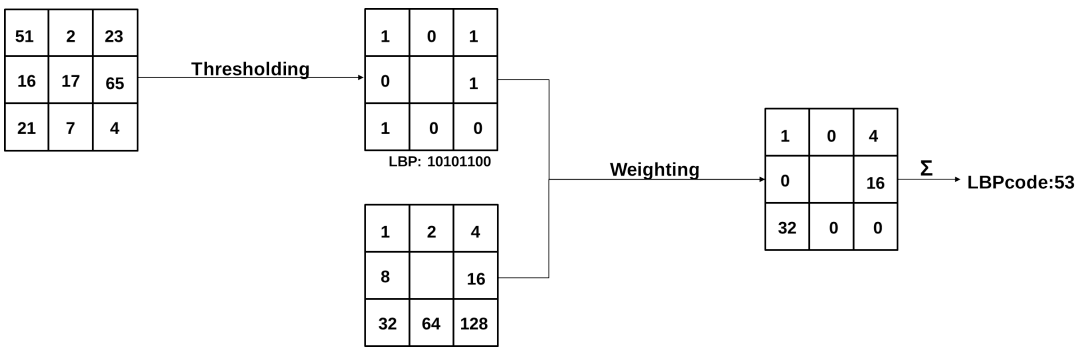

Figure 17.: LBP code computation.

(a) Palmprint ROI (b) LBP features (c) LBPU features

Figure 18.: Features extracted using Local Binary Patterns and Uniform Binary Patterns.

00000111 or 0001100 are examples of uniform binary patterns while 00100110 is not uniform. In this case, to compute the histogram of the image, a different label is given to each uniform binary pattern and another one is assigned to the rest of binary patterns. This way, a shorter texture descriptor is obtained without loosing of relevant information, and therefore it is representative enough of the distribution of the local features of the image. Formally:

$$LBPU_{code} = \begin{cases} \sum_{p=0}^{P-1} S(g_p - g_c)2^p, & \text{if } uniform \\ P+1 & \text{otherwise} \end{cases} \tag{13}$$

Texture features extracted using LBP and LBPU can be seen in be Figure 18.

Although texture histograms could be directly used as the feature vector corresponding to the user of the biometric system, aimed to add some global information, the image is divided in various regions and a histogram is calculated for each subimage. Finally, histograms are concatenated to compose the final biometric feature vector which describes the palm.

Implementation has been codified in MATLAB and is based on Marko Heikkilä and Timo Ahonen original implementation[1].

5.2.4 *Local Derivative Pattern*

Local Derivative Pattern (LDP) is a high-order texture descriptor originally proposed for face recognition with the aim to capture more detailed discriminative information. LDP encodes directional pattern features based on local $(n-1)^{th}$-order derivative variations based on a binary coding function. As they are high-order local patterns, they provide a stronger discriminative capability in describing detailed texture information than first order local patterns as used in LBP.

1 www.cse.oulu.fi/CMV/Downloads/LBPMatlab

Z1	Z2	Z3
Z8	Z0	Z4
Z7	Z6	Z5

Figure 19.: 8-neighbourhood around Z_0 [201].

Given an image $I(Z)$, let Z_0 be a point in $I(Z)$, and $Z_i, i = 1,..,8$ be the neighbouring point around Z_0 as depicted in Figure 19. The n^{th}-order directional LDP in direction α at $Z = Z_0$ is defined by equation 14:

$$\begin{aligned} LDP^n_\alpha(Z_0) = \{&f(I^{n-1}_\alpha(Z_0), I^{n-1}_\alpha(Z_1)), f(I^{n-1}_\alpha(Z_0), I^{n-1}_\alpha(Z_2)), \\ &..., f(I^{n-1}_\alpha(Z_0), I^{n-1}_\alpha(Z_8))\} \end{aligned} \tag{14}$$

where $f(\cdot,\cdot)$ is a binary coding function determining the types of local pattern transitions and $I^{n-1}_\alpha(Z_j)$ is the $(n-1)^{th}$-order derivative in direction α at $Z = Z_j$ being $j = 0,..,8$, and $\alpha = 0°, 45°, 90° and 135°$.

$f(I^{n-1}_\alpha(Z_0), I^{n-1}_\alpha(Z_i))$ encodes the $(n-1)^{th}$-order gradient transitions into binary patterns and is defined as follows:

$$f(I^{n-1}_\alpha(Z_0), I^{n-1}_\alpha(Z_i)) = \begin{cases} 0, if I^{n-1}_\alpha(Z_i)) \cdot I^{n-1}_\alpha(Z_0)) > 0 \\ 1, if I^{n-1}_\alpha(Z_i)) \cdot I^{n-1}_\alpha(Z_0)) \leq 0 \end{cases}, \quad i = 1,..,8. \tag{15}$$

The n^{th}-order LDP is a concatenation of directional LDPs in four directions with a 45 representation resolution defined according to equation 16:

$$LDP^n(Z) = LDP^n_\alpha(Z) | \alpha = 0°, 45°, 90° and 135°. \tag{16}$$

In particular, 2nd-derivative patterns have been used for palmprint features representation. In this case, equations 14, 15 and 16 are particularized as follows:

$$\begin{aligned} LDP^2_\alpha(Z_0) = \{&f(I'_\alpha(Z_0), I'_\alpha(Z_1)), f(I'_\alpha(Z_0), I'_\alpha(Z_2)), \\ &..., f(I'_\alpha(Z_0), I'_\alpha(Z_8))\} \end{aligned} \tag{17}$$

$$f(I'_\alpha(Z_0), I'_\alpha(Z_i)) = \begin{cases} 0, if I'_\alpha(Z_i)) \cdot I'_\alpha(Z_0)) > 0 \\ 1, if I'_\alpha(Z_i)) \cdot I'_\alpha(Z_0)) \leq 0 \end{cases}, i = 1,..,8. \tag{18}$$

$$LDP^2(Z) = LDP^2_\alpha(Z) | \alpha = 0°, 45°, 90° and 135° \tag{19}$$

and the first derivatives in the mentioned four directions at $Z = Z_0$ are written according to equation 20:

$$\begin{aligned} I'_{0°}(Z_0) &= I(Z_0) - I(Z_4) \\ I'_{45°}(Z_0) &= I(Z_0) - I(Z_3) \\ I'_{90°}(Z_0) &= I(Z_0) - I(Z_2) \\ I'_{135°}(Z_0) &= I(Z_0) - I(Z_1). \end{aligned} \tag{20}$$

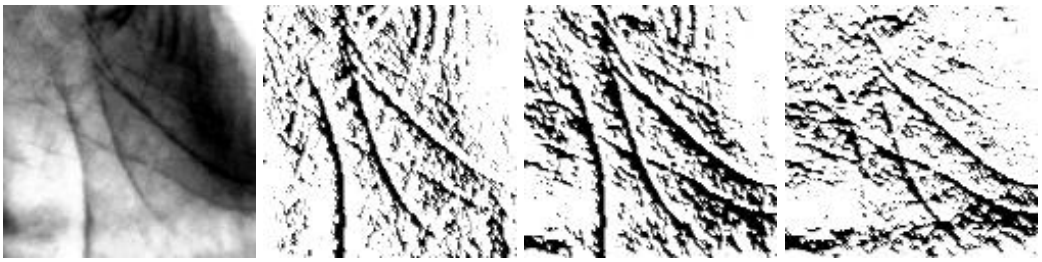

(a) Palmprint ROI (b) LDP features in 0° direction (c) LDP features in 45° direction (d) LDP features in 90° direction

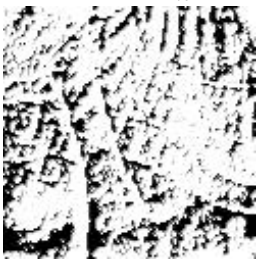

(e) LDP features in 135° direction

Figure 20.: Original ROI and LDP features extracted at four different directions.

Figure 20 depicts the 2nd-order LDP features extracted at 0°, 45° , 90° and 135° directions from a Palmprint ROI, and an example about how to compute the 2nd-order LDP is shown in Figure 21.

Once the patterns are computed, the algorithm works in the same way than LBP approach and the texture of the image is represented by the histogram of the LDP codes. Similarly, aimed to add some global information, the image is divided in various regions and the histogram is calculated for each sub-image. Finally, histograms are concatenated to compose the final biometric feature vector which describes the palm.

In addition, aimed to evaluate if some direction (or combination of directions) is more representative of the palmprint texture, a variant of the algorithm has also been implemented. In this implementation it is possible to specify the direction(s) which are involved in the feature extraction process and the biometric feature vector is computed from the second-order directional LDP in the specified direction(s).

Implementation has been codified in MATLAB based on Marko Heikkilä and Timo Ahonen original implementation for LBP[2].

2 www.cse.oulu.fi/CMV/Downloads/LBPMatlab

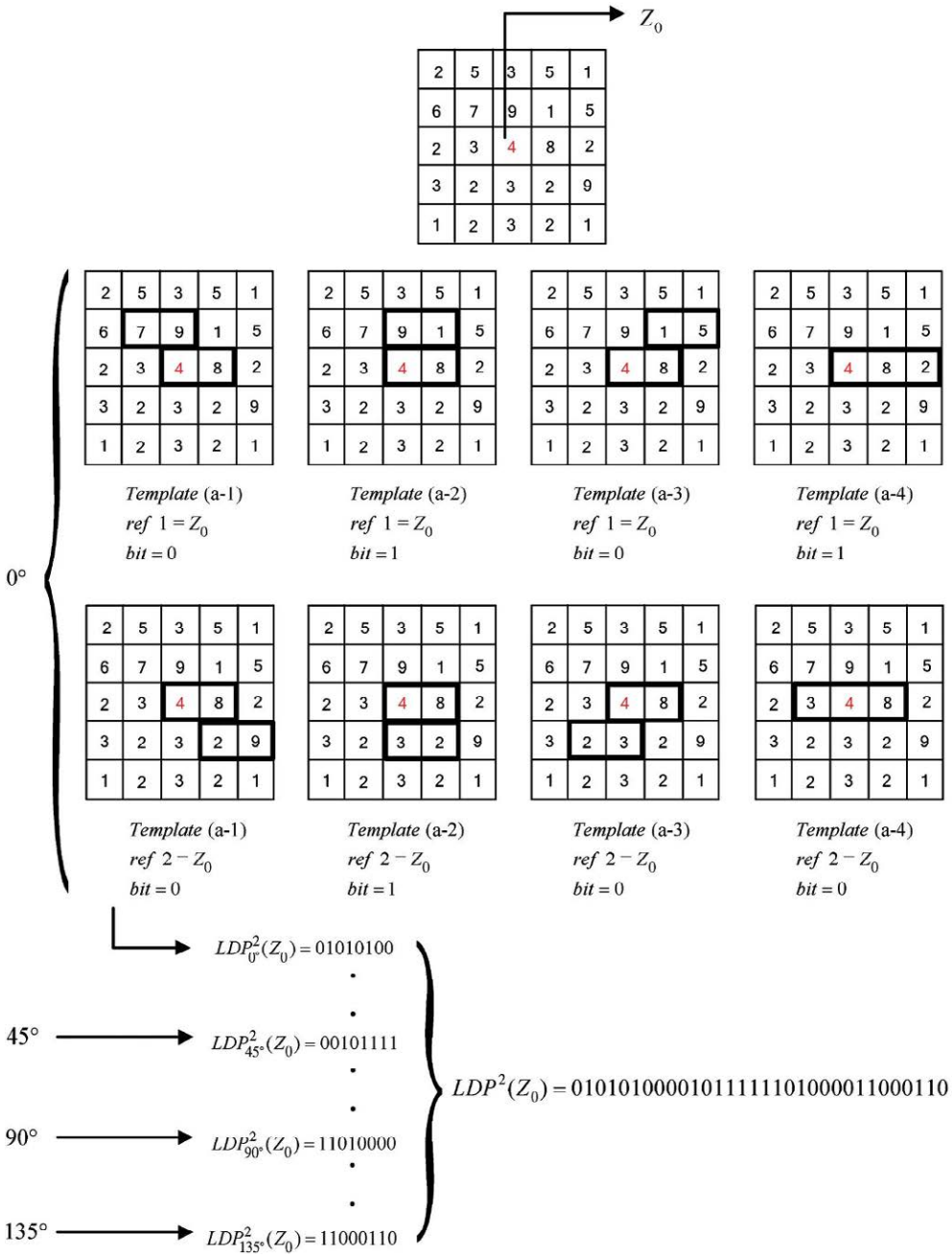

Figure 21.: Example to obtain the second-order LDP micropatterns [201].

5.2.5 *Curvelet*

Curvelet is a mathematical transform proposed by Candes and Donoho [16] to represent edges and other singularities along curves more efficiently than traditional transforms. Conceptually, the curvelet transform is a multiscale pyramid with many directions and positions at each length scale, and needle-shaped elements at fine scales [15]. In this sense, Curvelet transform can be seen as a generalization of the Wavelet transform that permits to represent images at different scales and different

angles, providing rich feature information when applied to image processing. Accordingly, it is a multi-scale, directionally sensitive and highly anisotropic method that can well approximate curved singularities with very few coefficients in a non-adaptive manner.

Given the curved nature of the lines which compose the palmprint, Curvelet transform can be applied to extract palmprint feature information at different scales [43, 113].

The first generation of Curvelet transform[16] is a combination of two-dimension wavelet transform and the ridgelet transform. Wavelet transform decomposes the image into scales and blocks in such a way that curved edges are subdivided into approximate straight lines. Then, each block is analysed by a local ridgelet transform. It is a complex transform that also present wide data redundancy.

Aimed to make it more understandable as well as to reduce data redundancy, curvelet transform was redesigned [15]. The second generation of curvelets was reintroduced as Fast Digital Curvelet Transform and takes on features of faster computation and less redundancy. In particular two new discrete transformations were proposed: Digital Curvelet Transform via USFFT, and Digital Curvelet Transform via Wrapping.

These digital transformations are linear and take as input Cartesian arrays of the form $f[t_1, t_2], 0 \leq t_1, t_2 < n$, providing as output a collection of coefficients $c^D(j, l, k)$ according to equation 21:

$$c^D(j, l, k) := \sum_{0 \leq t_1, t_2 < n} f[t_1, t_2] \overline{\varphi^D_{j,l,k}[t_1, t_2]}, \tag{21}$$

where each $\varphi^D_{j,l,k}$ is a digital curvelet waveform.

To provide a detailed mathematical formulation of the transformations and the computation of coefficients is considered to be beyond the scope of this thesis. The reader is referred to [15] for a complete description of both implementations of the Fast Digital Curvelet Transform.

These two implementations essentially differ by the choice of the spatial grid used to translate curvelets at each scale and angle. In this thesis, Digital Curvelet Transform via Wrapping, that assume a rectangular grid, has been evaluated. As a result of the transformation, a table of digital curvelets coefficients indexed by a scale parameter, an orientation parameter, and a spatial location parameter, is obtained. An example of coefficients extracted from a palmprint image can be seen in Figure 22.

The biometric feature vector is composed by a concatenation of the computed coefficients. In the composition of the feature vector one or more frequency bands can be involved.

Implementation has been implemented in MATLAB and makes use of the code provided at `http://www.curvelet.org/`.

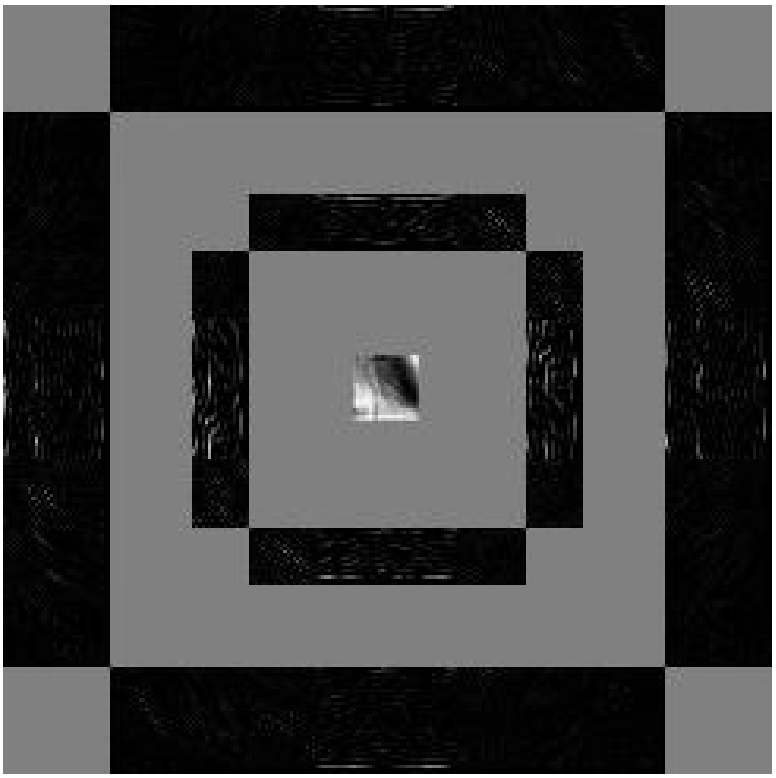

Figure 22.: Digital Curvelet Transform via Wrapping coefficients from a Palmprint image.

5.3 HAND GEOMETRY

Given the five regions corresponding to the fingers, the hand contour, the fingertips and the inter-finger valley points, the hand geometry features are obtained by means of a fingers width-based approach.

For each finger, its geometrical features are obtained as follows:

1. First, the middle point between the valleys corresponding to the finger is computed. It is named basis point and marked as a pink square in Figure 23.
2. Then the line between fingertip and the basis point is calculated and represents the finger length.
3. Next, this segment is divided into the number of features per finger specified as a parameter (green dots in Figure 23).
4. Formerly, a perpendicular line to the finger length line that passes through each division point is computed and the points where this line cut the contour are extracted (blue and red dots in Figure 23). Then, the distance between these points is stored as finger width.
5. Finally, to make the features invariant to changes in scale or size derived from restriction-free capturing processes, the features are normalized by the length of the corresponding finger.

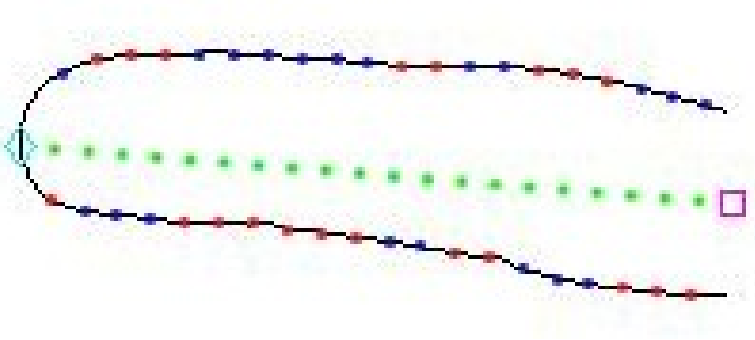

Figure 23.: Finger Geometry Features.

The biometric feature vector is composed by a concatenation of the widths of every finger.

Implementation has been codified in MATLAB.

6

FEATURE MATCHING AND DECISION

6.1 INTRODUCTION

Feature matching (or comparison) and decision are the stages of a biometric system where a new sample is compared against a biometric template previously stored in the system in order to evaluate if they belong to the same person or not. Feature comparison provides the degree of similarity or dissimilarity degree between the biometric features contained in the new sample and the template stored in the system during the enrolment stage. Then, based on a decision policy and this similarity value, the system determines if there is a correspondence between the sample provider and proprietor of the template.

A wide number of different comparison methods have been applied for feature matching in biometrics, including well-known pattern recognition and classification techniques such as minimum distance, decision trees, k-nearest neighbours, naïve Bayes or neural networks. The comparison method is closely related to the feature extraction approach. Accordingly, the comparison method is selected in such a way that its compatibility with the extracted features is guaranteed. A comprehensive literature review of feature matching methods for palmprint and hand geometry biometric verification can be found in Tables 11, 12 and 13, together with the feature extraction method applied in each case.

In this thesis two different methods have been applied in order to obtain comparative results: distance-based and Support Vector Machines (SVMs), detailed in Sections 6.2 and 6.3 respectively.

6.2 DISTANCE-BASED

Distance-based approach is one of the most extended methods for biometric features comparison because of its simplicity and low computational requirements. As a result, it provides a numeric value which represents the difference between two feature vectors. Accordingly, the decision policy established in the system is to consider the compared vectors as belonging to the same person if the computed distance is lower than a previously established threshold.

In particular, three different distances have been included in the system: Euclidean, χ^2 and Histogram Intersection. The former can be applied to all the feature extraction methods described in Chapter 5, while the latter distances are recommended for histogram comparison and thus, applied along with LBP and LDP descriptors.

Finally, as the biometric template is composed by different feature vectors, the new sample is compared against every feature vector in the template and the smaller score is selected.

6.2.1 *Euclidean Distance*

Euclidean distance is defined by equation 22:

$$ED(S,M) = \sqrt{\sum_{i=1}^{n}(S_i - M_i)^2}, \tag{22}$$

where S and M are the feature vectors to compare and n is the length of the vector.

6.2.2 χ^2 *Distance*

χ^2 distance is defined by equation 23:

$$\chi^2(S,M) = \sum_{i=1}^{n}\frac{(S_i - M_i)^2}{S_i + M_i}, \tag{23}$$

where S and M are the feature vectors to compare and n is the length of the vector.

6.2.3 *Histogram Intersection*

Histogram intersection distance is defined by equation 24:

$$HI(S,M) = \sum_{i=1}^{n} min(S_i, M_i), \tag{24}$$

where S and M are the feature vectors to compare and n is the length of the vector.

6.3 SUPPORT VECTOR MACHINES

Support Vector Machines (SVMs in advance) are binary classifiers that are able to analyse the biometric features provided during the training phase to learn a model. In this case, the classification process is based on the search of the hyperplanes which better differentiate the biometric features belonging to an individual from those corresponding to other people. Two strategies can be followed for the hyperplanes search: one-against-all or one-against one. Former strategy creates q SVMs with the aim to differentiate each individual from the remaining, while later creates $q(q-1)/2$ SVMs that separate each pair of classes, being q the number of classes or individuals in the system. In this thesis one-against-all strategy is preferred because of the lineal complexity in regarding to the number of classes and thus, the lower computational effort.

Let be $x_1, x_2, ..., x_n$ the training data used to create the SVMs, where each x_i corresponds to a biometric feature vector. Each input x_i is assigned an output $y_i \in \{-1, 1\}$ where 1 means that the instance belongs to the same user that the trained SVM and

-1 indicates that the sample belongs to any other person. Assuming that every training data satisfies the following conditions:

$$\begin{aligned} x_i \cdot w + b \geq +1, \forall y_i = +1 \\ x_i \cdot w + b \leq -1, \forall y_i = -1 \end{aligned} \tag{25}$$

the equation of the hyperplane is defined as follows:

$$w \cdot x + b = 0 \tag{26}$$

where w is normal to the hyperplane.

In the case the data are linearly separable, it is possible to find the optimal hyperplane which maximizes the margin $m = d_+ + d_-$, where d_+ is the shortest distance between the hyperplane and the closest positive sample and d_- is de shortest distance between the hyperplane and the closest negative sample, by minimizing $\|w\|^2$. Taking into account the constraint defined in equation 27, which is generated by combining the conditions presented in Equation 25:

$$y_i(x_i \cdot w + b) \geq 1, \forall i \tag{27}$$

the problem is equivalent to minimize the quadratic problem defined in equation 28:

$$\frac{1}{2}\|w\|^2 - \sum_{i=1}^{l} \alpha_i y_i (x_i \cdot w + b) + \sum_{i=1}^{l} \alpha_i \tag{28}$$

where α_i are the nonnegative Lagrange multipliers.

Once the equations that characterize the elements of each class are defined, and the surfaces that correspond to each class are delimited, it is possible to classify a new vector z by evaluating the function defined as:

$$f(x) = w \cdot z + b = \sum_{i=1}^{s} \alpha_i y_i (s_i \cdot z) + b, \tag{29}$$

where s is the number of support vectors. In case the sign of Equation 29 is positive, z belongs to class 1, on the contrary it belongs to class 2.

Nevertheless, data are not always linearly separable and a hyperplane able to separate the vectors of each class does not exist. In this case, it is necessary to transform data from the current space to a higher dimensional space, where input data become separable and the optimal hyperplane can be found. The transformation $\phi(x_i)$ applied to every x_i is a vectorial product between support vectors and x_i. In practice, to compute this vectorial product given the high dimension of z could be highly expensive. For this reason, taken into account that if data are previously mapped to an Euclidean space E by a mapping function Φ, the training would only depend on functions of the form $\Phi(x_i) \cdot \Phi(x_j)$, *kernel functions* $K(x_i, x_j) = \Phi(x_i) \cdot \Phi(x_j)$ that do not require knowledge on Φ are introduced.

In this case equation 29 is redefined as follows:

$$f(x) = w \cdot \Phi(z) + b = \sum_{i=1}^{s} \alpha_i y_i (\Phi(s_i) \cdot \Phi(z)) + b = \sum_{i=1}^{s} \alpha_i y_i K(s_i, z) + b. \qquad (30)$$

In the same way, if the sign of Equation 29 is positive, z belongs to class 1, on the contrary it belongs to class 2.

7

BIOMETRICS FUSION

7.1 INTRODUCTION

In general, the term Biometrics Fusion is considered a synonym of Multimodal Biometrics but, according to [145], it includes two general techniques: Multimodal Fusion, where the biometric information is obtained from different physical or behavioural traits, and Intramodal Fusion where the biometric information is obtained from the same trait, but using different features, classifiers or sensors. In the particular case of hand-related biometrics, it is also possible to find to obtain information related to different traits using the same sensor.

Attending to the module of the system in which the biometric information is combined, it could be distinguished between four data fusion levels [52]: sensor or data, feature, matching or score and decision. If the sensor signals are comparable then the raw data can be directly merged. The input signal is the result of sensing the same biometric characteristic with two or more sensors [1]. The feature level provides fusion of data obtained from different features of a single biometric trait, or from different biometric traits [198, 83]. At score level, the fusion system normalizes the scores coming from each biometric modality matcher and combine them into a global score [145, 93, 73, 86]. In the decision level approach the decisions about the user identity obtained from each trait separately are combined to obtain a final decision [184].

The effectiveness of a multimodal biometric system generally depends on the level where the biometric fusion takes place: usually, the earlier the stage the more effective the system is, because the information about the biometrics of the subject to be identified decreases significantly with the processing at the different levels [161]. Therefore, although fusion at the feature level is expected to provide better recognition results, integration at this level is difficult to achieve in practice because the feature sets of the various biometric modalities may not be compatible; for instance, eigencoefficients of face and air-signature characterization are in both qualitative and quantitative different spaces (regarding definition intervals, statistical distribution, etc.). On the other hand, fusion at the decision level is considered to be rigid due to the extremely limited information available at this stage. Thus, fusion at score level is usually preferred, as it is relatively easy to obtain and combine the scores presented by the different modalities. Nonetheless, despite the evidence of this claim provided by the literature, the authors in [103] describe a hand-based verification sys-

tem that combines the geometric features of the hand with palmprints at the feature and matching score levels, resulting in better performance the latter.

In the last decade some works which exploit the information coming from different hand-related biometrics have been developed. These hand multibiometric approaches include hand geometry and palmveins [140], palmprint and palmveins [185, 136, 59, 182], palmprint and hand geometry [153, 103, 137, 141, 56, 110, 20], hand veins, hand geometry and fingerprints [168], palmprint, hand geometry and fingerprints [7, 53, 197], palmprint, hand geometry and hand veins [71, 14], palmprint and knuckleprint [120, 130] or hand geometry, palmprint, knuckleprint, palm veins and finger veins [135].

From the point of view of the capturing conditions, even when some of these works employ contactless images captured by fix devices [134, 23, 135] and/or under semi-controlled lighting conditions and background [134, 103, 135], most of them work with images recorded in controlled environments.

Table 14 gathers multimodal hand biometric approaches classified according to the involved traits, the nature of the testing images in terms of environmental conditions and pose restrictions, and the level in which the information is fused.

In this thesis the multibiometric nature of the hands will be exploited to improve the system performance. In particular intramodal fusion will be carried out by fusing palmprint information coming from different algorithms as well as multimodal fusion, involving hand geometry and palmprint biometrics traits. Fusion will be performed at feature and score levels, in order to provide a fair comparison.

Biometric Traits	Background	Lighting Conditions	Pose Restrictions	Fusion Level	References
Hand Geom., Palmprint	Controlled	Controlled	Contact, Pegs	Score level	[25]
				-	[110]
	Controlled	Indoor	Contact, Surface Marks	Score level	[103]
	Controlled	Controlled	Contact, Free Placement	Feature level	[147]
				Score level	[153, 137, 141, 56]
	Controlled	Controlled	Contact-less	Feature level	[23]
				Score level	[20]
				Decision level	[186]
	Uncontrolled	Indoor	Contact-less	Feature level	[44]
	-	-	-	Decision level	[84]

Biometric Traits	Background	Lighting Conditions	Pose Restrictions	Fusion Level	References
Hand Geom., Dorsal Veins	Controlled	Controlled	Contact, Pegs	Score level	[140]
Palmprint, Fingerprints	Controlled	Controlled	Contact, Free Placement	Feature level	[117]
Palmprint, Finger Geom.	Controlled	Controlled	Contact, Free Placement	Score level	[155]
Palmprint, Palm Veins	Controlled	Controlled	Contact, Pegs	Sensor level	[185]
	Controlled	Indoor	Contact-less	Feature level	[182]
	Controlled	Controlled	Contact-less	Score level	[136]
Palmprint, Knuckleprint	Controlled	Controlled	Contact, Pegs	Score level	[130]
	Controlled	Controlled	Contact, Free Placement	Score level	[120]
Palmprint, Finger Texture	Controlled	Controlled	Contact, Free Placement	Score level	[154]
Palmprint, Finger Surface	Controlled	Controlled	Contact-less	Feature level	[150]
Hand Geom., Palmprint, Fingerprints	Controlled	Controlled	Contact, Free Placement	Feature level	[53]
	Controlled	Controlled	Contact, Free Placement	Score level	[53, 197, 117]
	Controlled	Controlled	Contact, Free Placement	Decision level	[53]
Hand Geom., Palmprint, Veins	Controlled	Controlled	Contact, Free Placement	Decision level	[7]
	Controlled	Controlled	Contact-less	Score level	[14]
	-	Controlled	-	Score level	[71]
Hand Geom., Palmprint, Finger Geom.	Controlled	Controlled	Contact, Free Placement	Score level	[156]

Biometric Traits	Background	Lighting Conditions	Pose Restrictions	Fusion Level	References
Palmprint., Hand Geom., Finger Geom.	Controlled	Controlled	Contact-less	Score Level	[63, 127]
Hand Geom., Palmprint, Knuckleprint, Palm Veins, Finger Veins	Controlled	Controlled	Contact-less	Score Level	[135]
2D Palmprint, 2D Hand Geom., 2D finger texture, 3D Palmprint, 3D Finger Texture	Controlled	Indoor	Contact-less	Score level	[89]

Table 14.: Multimodal hand biometric approaches classified according to the involved traits, the nature of the testing images in terms of environmental conditions and pose restrictions and the level in which the information is fused.

7.2 NORMALIZATION

Differences between feature spaces can be reflected in the statistical distributions of the feature vectors in the case of fusion at feature level as well as the statistical distributions of the distances among features when fusion is performed at score level. For this reason, both approaches require a normalization step before the fusion.

Normalization involves to change the location and scale parameters of the original distribution in such a way that data is transformed into a common domain. Normalization can be fixed or adaptive in regarding to the data used to obtain the normalization parameters. In the first case a set of training data is analysed to extract a model that will be used to estimate the normalization parameters, while in the second case parameters are estimated based on the test sample, presenting a higher capacity to adapt to variations in the input data such as variable-length feature vectors. In this thesis fixed approach have been selected given the availability of training data and the fix length of the feature vectors.

There exist many possible normalization procedures including min-max, decimal scaling, z-score, median and median absolute deviation, double sigmoid, tanh-estimator or Biweight estimators. In [79] an analysis of these techniques is presented in terms of performance as well as two statistical properties that should be required for a correct normalization: robustness and efficiency. Robustness refers to insensitivity to the presence of extreme values, i.e. values at a significant distance from the set bounds, whereas efficiency is related to the proximity of the obtained estimates to the optimal estimates when the distribution of the data is known.

In this thesis min-max normalization and z-score have been selected because of their simplicity, good performance, efficiency and widespread use.

7.2.0.1 *Min-Max Normalization*

Min-max normalization is the best suited for the case where the bounds (maximum and minimum values) are known. In this case, it is possible to easily transform the minimum and maximum scores to 0 and 1, respectively. Unfortunately, it is not possible in real cases since the amount of data is limited and the distributions not always are bounded. Nevertheless, it is possible to estimate the minimum and maximum values from the available data and then apply the min-max normalization. In this sense, let be the data set provided by a certain biometric modality denoted by S_i, where $i = 1, ..., N$, and N is the number of biometric modalities. Then, the normalization obeys equation 31:

$$\tilde{S}_i = \frac{S_i - min(S_{i i=1}^{N})}{max(S_{i i=1}^{N}) - min(S_{i i=1}^{N})} \tag{31}$$

It should be noted that, from the mathematical definition of the min-max normalization, it retains the original distribution except for a scaling factor, transforming the initial data into a common domain [0, 1].

As mentioned above, the min-max normalization is one of the most used normalization procedures due to its simplicity, good performance and efficiency. However, its major inconvenient is that when the minimum and maximum values are estimated from the training data, this normalization procedure could not be robust and it is sensitive to the presence of extreme values. Therefore, the employed database should be exhaustive enough to get a reliable estimation of the scores distribution and thereby to obtain stable bound values.

7.2.0.2 *z-score Normalization*

Another commonly used normalization procedure is the z-score normalization, which uses the mean and standard deviation of the data to shift and scale the initial distribution of scores into a common domain. When the average and variance of the score distribution are accessible, the z-score normalization performs properly. However, this situation is not usual and these parameters must be estimated from the available data. These estimations of mean and variance are optimal for normal distributions while when the original distribution is not Gaussian, the z-score transformation could not preserve the initial distribution. In addition, both parameters mean and std are sensitive to outliers. Accordingly, an extensive enough database of normal distributed data is required to obtain a reliable z-score normalization.

Given data set provided by the different biometric modalities denoted by S_i, where $i = 1, ..., N$, and N is the number of biometric modalities, z-score normalization is defined by equation 32:

$$\tilde{S}_i = \frac{S_i - \mu_i}{\sigma_i} \tag{32}$$

where μ_i and σ_i are the arithmetic mean and the standard deviation of the data provided by the $i - th$ bimoetric modality.

7.3 SCORE LEVEL FUSION

Most commonly used approach for biometric fusion is Score-Level fusion due to its good performance, simplicity and the relative easy access and combination of the scores provided by different biometric modalities. In this approach after normalization, the scores provided by the different biometric techniques are fused to get a unique score that will be used to reach the final decision about the identity of the user.

In mathematical terms this means that the scores s_i, with $i = 1, ..., N$ and N the number of biometric modalities, are mapped from $\mathbb{R}^N \rightarrow \mathbb{R}$ by a function f to get a single score S (Eq. 33):

$$S = f(w_1 s_1, ..., w_N s_N) \tag{33}$$

where the factors w_i weight the influence of each score in the final fusion. These weighting factors are optimized by means of a genetic algorithm which starts with an initial population of 300 individuals and compute 20 generations. This genetic algorithm also allows to decide which fusion rule has a better performance in case that more than one rule is used. In this thesis four weighted rules have been tested: minimum, maximum, sum and product.

7.4 FEATURE LEVEL FUSION

Fusion of biometric information at feature level can involve features extracted by the same method from the same biometric trait, typically used to improve or update the biometric template, features extracted by different methods and belonging to the same trait or features that correspond to different traits. In the latter cases, the fusion can present difficulties derived from the lack of knowledge about the relationship between feature spaces, incompatibility of features or curse-of dimensionality problem, where increasing the number of features might degrade the system performance in cases that the number of training samples is small.

Given the normalized feature vectors $X = \{x_1, x_2, ..., x_m\} \in I\!R^m$ and $Y = \{y_1, y_2, ..., y_n\} \in I\!R^n$ provided by two different biometric sources, the objective of feature level fusion is to find a new feature vector $Z \in I\!R^k$, with $k \leq m + n$, that better represent the user. This new vector Z is typically generated by the concatenation of the two original feature vectors X and Y (Eq. 34) followed by a feature selection process.

$$Z = \{x_1, x_2, ..., x_m, y_1, y_2, ..., y_n\} \in I\!R^{m+n} \tag{34}$$

Feature selection is commonly carried out by means of dimensionality reduction techniques or feature transformation methods. In this case, Principal Component Analysis (PCA) is applied.

Part IV

EVALUATION OF THE BIOMETRIC SYSTEM

8

EVALUATION PROTOCOL

8.1 INTRO

A well defined evaluation methodology allows for a fair comparison between methods as well as to measure real progress achieved with new research and to pinpoint unsolved problems [142]. Nevertheless, hand biometrics literature shows a wide variety of evaluation protocols and metrics for results presentation, even when many authors use the same database.

For this reason, an evaluation protocol is proposed in this thesis to test the performance of different biometric solutions under different environmental conditions, enabling fair comparison and reproducibility of the results. This evaluation protocol is based on the definitions suggested by the ISO/IDE 19795 [75, 76], which presents the requirements and best scientific practices for conducting technical performance testing, as well as the guidelines provided in [142].

Accordingly, one of the contributions of this thesis is a fair comparison of different hand biometrics methods using this unified test framework. Particularly, results of different palmprint and hand geometry recognition monomodal approaches under different capturing conditions will be provided in terms of accuracy and computation time. In addition, multimodal results obtained from their fusion will be also presented.

8.2 ISO/IDE 19795 DEFINITIONS

Most important definitions regarding to biometric applications, data, system interaction and evaluation included in the ISO/IDE 19795 norm [75] are provided hereafter.

8.2.1 *Biometric applications*

- Verification: application in which the user makes a positive claim to an identity and present the biometric sample to the system. Features derived from the submitted sample biometric measure are compared to the enrolled template for the claimed identity, and an accept or reject decision regarding the identity claim is returned. The claimed identity might be in the form of a name, personal identification number (PIN), swipe card, or other unique identifier provided to the system.

- Identification: application in which the user presents the biometric trait to the system and a search of the enrolled database is performed. A candidate list of 0, 1 or more identifiers is returned as a result.
- Closed-set identification: identification for which all potential users are enrolled in the system.
- Open-set identification: identification for which some potential users are not enrolled in the system.

8.2.2 *Biometric data*

- Sample: user's biometric measures as output by the data capture subsystem. In complex systems the sample may consist of multiple presented characteristics.
- Features: digital representation of the information extracted from a sample (by the signal processing subsystem) that will be used to construct or compare against enrolment templates.
- Template or model: user's stored reference measure based on features extracted from enrolment samples. The reference measure is often a template comprising the biometric features for an ideal sample presented by the user. More generally, the stored reference will be a model representing the potential range of biometric features for that user.
- Matching score or similarity score: measure of the similarity between features derived from a sample and a stored template, or a measure of how well these features fit a user's reference model. As features derived from a presented sample become closer to the stored template, similarity scores will increase. A match or non-match decision may be made according to whether this score exceeds a decision threshold.
- Verification decision: determination of the probable validity of a user's claim to identity in the system.
- Candidate list: set of potential enrolled identifiers for a subject produced by an identification attempt (or by a pre-selection algorithm).

8.2.3 *User interaction with a biometric system*

- Presentation: submission of a single biometric sample on the part of a user.
- Attempt: submission of one (or a sequence of) biometric samples to the system.
- Transaction: sequence of attempts on the part of a user for the purpose of biometric transaction. There are three types of transaction: enrolment sequence, resulting in an enrolment or a failure-to-enrol; a verification sequence resulting in a verification decision; or identification sequence, resulting in an identification decision.

- Genuine attempt: single good-faith attempt by a user to match their own stored template.
- Zero-effort impostor attempt: attempt in which an individual submits his/her own biometric characteristics as if he/she were attempting successful verification against his/her own template, but the comparison is made against the template of another user.
- Active impostor attempt: attempt in which an individual tries to match the stored template of a different individual by presenting a simulated or reproduced biometric sample, or by intentionally modifying his/her own characteristics.
- Presentation effects: broad category of variables affecting the way in which the user's inherent biometric characteristics are displayed to the sensor.
- Channel effects: changes imposed on the presented signal in the transduction or transmission process due to the sampling, noise and frequency response characteristics of the sensor and transmission channel.

8.2.4 *Personal involved in the evaluation*

- User: person presenting biometric sample to the system.
- Test subject: user whose biometric data is intended to be enrolled or compared as part of the evaluation.
- Crew: set of test subjects gathered for an evaluation.
- Target population: set of users of the application for which performance is being evaluated.
- Administrator: person performing the testing or enrolment.
- Operator: individual with function in the actual system. Staff conducting enrolment or overseeing verification or identification transactions.
- Observer: test staff member recording test data or monitoring the crew.
- Experimenter: person responsible for defining, designing and analysing the test.
- Test organization: functional entity under whose auspices the test is conducted.

8.2.5 *Types of performance evaluation*

Testing a biometric system will involve the collection of input data, which are used to generate user's templates during the enrolment and for calculation of matching scores for verification or identification attempts.

- Technology evaluation: offline evaluation of one or more algorithms for the same biometric modality using a pre-existing or specially-collected corpus of samples, ideally collected by a universal sensor. Nonetheless, performance against this corpus will depend on both, the environmental conditions and the population. As the corpus is fixed, the results of technology tests are repeatable.
- Scenario evaluation: evaluation in which the end-to-end system performance is determined in a prototype or simulated application of a complete system in an environment that models a real-world target application of interest. Each tested system will have its own acquisition sensor and so will receive slightly different data. Consequently, if multiple systems are being compared, care will be required that data collection across all tested systems is in the same environment with the same population. Test results will be repeatable only to the extent that the modelled scenario can be carefully controlled.
- Operational evaluation: evaluation in which the performance of a complete biometric system is determined in a specific application environment with a specific target population. In general, operational tests results will not be repeatable because of unknown and undocumented differences between operational environments. Furthermore, "ground truth" about the authenticity of the biometric attempt can be difficult to ascertain, particularly if an operational evaluation is performed under unsupervised conditions without an administrator, operator or observer present.
- Online: pertaining to execution of enrolment and matching at the time of image or signal submission. Online testing has the advantage that the biometric sample can be immediately discarded, saving the need for storage and for the system to operate in a manner different from usual. However, it is recommended that images or signals are collected if possible.
- Offline: pertaining to execution of enrolment and matching separately from image or signal submission. Collecting a database of images or signals for offline enrolment and calculation of matching scores allows greater control over which attempts and template images are to be used in any transaction. Technology testing will always involve data storage for later, offline processing. However, with scenario and operational testing, online transactions might be simpler for the tester.

8.2.6 *Performance measures*

- Failure-to-enrol rate (FTE): proportion of the population for whom the system fails to complete the enrolment process. The observed FTE is measured on test crew enrolments. The predicted/expected FTE will apply to the entire target population.
- Failure-to-acquire rate (FTA): proportion of verification or identification attempts for which the system fails to capture or locate an image or signal of sufficient quality.

- False non-match rate (FNMR): proportion of genuine attempt samples falsely declared not to match the template of the same characteristic from the same user supplying the same trait.
- False match rate (FMR): proportion of zero-effort impostor attempt samples falsely declared to match the compared non-self template.
- False reject rate (FRR): proportion of verification transaction with truthful claims of identity that are incorrectly denied.
- False accept rate (FAR): proportion of verification transaction with wrongful claims of identity that are incorrectly confirmed.
- (True-positive) identification rate: proportion of identification transactions by users enrolled in the system in which the user's correct identifier is among those returned. This identification rate is dependent on the size of the enrolment database and a decision threshold for matching scores and/or the number of matching identifiers returned.
- False-negative identification-error rate (FNIR): proportion of identification transactions by users enrolled in the system in which the user's correct identifier is not among those returned.
- False-positive identification-error rate (FPIR): proportion of identification transactions by users not enrolled in the system, where an identifier is returned. So, with closed-set identification FPIR is not possible, as all users are enrolled. The FPIR is dependent on the size of the enrolment database and a decision threshold for matching scores and/or the number of matching identifiers returned.
- Pre-selection error: error that occurs when the corresponding enrolment template is not in the pre-selected subset of candidates when a sample from the same biometric characteristic on the same user is given. In binning pre-selection, pre-selection errors happen when the enrolment template and a subsequent sample from the same biometric characteristic on the same user are placed in different partitions.
- Penetration rate: measure of the average number of pre-selected templates as a fraction of the total number of templates.
- Identification rank: smallest value k for which a user's correct identifier is in the top k identifiers returned by an identification system.

8.3 EVALUATION PROTOCOL

In this thesis, a protocol for technology evaluation of different algorithms have been designed. According to the ISO/IDE 19795 norm [76] technology evaluation presents the following benefits:

- Ability to conduct full cross-comparison tests: technology evaluation affords the possibility to use the entire testing population as claimants to the identities of all other members.

- Ability to conduct exploratory testing: technology evaluation can be run with no real-time output demands and is thus well suited to research and development. It allows the measurement of the effects of algorithmic improvements, parameter changes or the use of different image databases.

- Ability to conduct multi-instance and multi-algorithmic testing. By using common test procedures, interfaces and metrics, technology evaluation affords the possibility to conduct repeatable evaluations of multi-instance systems and multi-algoritmic performance, or any combination thereof.

- When the corpus contains appropriate sample data, technology testing is capable of testing separately all modules subsequent to the human-sensor interface, including: quality control and feedback module(s), signal processing module(s), image fusion module(s), feature extraction and normalization module(s), feature-level fusion module(s), comparison score computation and fusion module(s), and score normalization module(s).

- Elimination of human-sensor interaction from performance measurement allows for repeatable testing.

- If sample data are available, performance can be measured over large target populations, utilizing samples acquired over a period of years.

When designing the technology evaluation protocol for biometric verification systems, some aspects related to evaluation databases as well as biometrics systems benchmarking have been considered:

- Databases. Different databases will be used to test the algorithms. Their characteristics related not only to the capturing conditions but also to the number of users, sessions, or the number of images per user and session can vary, so the evaluation protocol must be flexible enough. An evaluation will be performed separately for each database.

- Development and test datasets. To ensure non-biased and representative results, images of every user are divided into two groups: development and test. The development dataset is used to train and validate the system, adjusting certain parameters such as the acceptance threshold, while the test dataset is employed to simulate real accesses into the system which provides a realistic estimation of its performance.

- Enrolment. To be recognised by the system, a user must be previously registered. To this end, a subset of each user's development images is dedicated to obtain the biometric template required to be enrolled into the system.

- System accesses. During the access stages it is differentiated between genuine users and impostors to evaluate the response of the system in different scenarios. This way, when a user is considered to be a genuine user, the other users represent zero-effort impostors.

The proposed evaluation protocol is composed of three parts. First of all it is necessary to separate the original datasets to allow development and evaluation tasks as previously considered. Next, scores are computed by comparing the biometric features extracted from enrol samples against those coming from access samples. Finally, performance metrics are calculated.

8.3.1 *Dataset Organization*

Accordingly, for each database the images of each user are divided into the following datasets:

- Development subset, which is in turn divided into training, enrolment and access samples. First group of samples is used to train those algorithms that need it, such as PCA or SVMs. Enrolment samples are used to generate the biometric reference template of each user that allows the registration of the user into the system. Finally, access samples are employed to simulate the entrance of the users into the system, which allow to validate the system as well as to adjust certain parameters like the acceptance threshold.
- Test subset, which contains samples employed to simulate new accesses into the previously configured system. These accesses allow for the calculation of more realistic performance rates. According to [142] it is recommendable that development and evaluation subsets will be disjoints subsets, but because of the limited number of users and images in some databases it has been decided that they share the enrolment samples.This approach is justified for verification applications and identification scenarios in which the number of subjects is limited and they are always known, such as office-access control systems [75, 76].

8.3.2 *Computation of Scores*

Once the training, enrolment, and access datasets have been defined, the latter are divided into genuine and impostor samples corresponding to authentic and forger users respectively. Then, the following sequence of actions is executed to test or evaluate the system:

1. The biometric template of each authentic user is created through their enrolment samples.
2. Genuine samples are used to measure whether the algorithm is able to recognize authentic users. In verification processes, these samples of each user will be compared against their own biometric template, providing a list of scores of these attempts.
3. Impostor samples are employed to estimate if the algorithm is able to reject impostors. In verification processes, these samples will be compared against the biometric template of the users trying to be forced, in this case all the other users, providing a list of scores.

4. Both scores are used to obtain certain metrics that provide information about the performance of the system. The acceptance threshold of the biometric system will be selected from the results obtained using the development subset and remain fixed for the test accesses.

8.3.3 *Evaluation*

According to the ISO/IDE 19795 - Part1 [75], it is proposed to calculate several metrics to evaluate the performance of the biometric methods:

- Failure-to-enrol rate (FTE): Proportion of the population for whom the system fails to complete the enrolment process.
- Failure-to-acquire rate (FTA): Proportion of verification or identification attempts for which the system fails to capture or locate an image or signal of acceptable quality.
- False non-match rate (FNMR): Proportion of genuine attempts falsely declared not to match the template of the same characteristic from the same user supplying the sample.
- False match rate (FMR): Proportion of zero-effort impostor attempt samples falsely declared to match the compared non-self template.

In addition, for verification systems, the following rates are also proposed:

- False Rejection Rate (FRR): The false rejection rate is the proportion of genuine verification transactions that will be incorrectly denied. A transaction may consist of one or more genuine attempts depending on the decision policy.

$$FRR = FTA + FNMR \times (1 - FTA)$$

- False Acceptance Rate (FAR): The false acceptance rate is the expected proportion of zero-effort non-genuine transactions that will be incorrectly accepted.

$$FAR = FMR \times (1 - FTA)$$

FTE can be considered as a quality measure about how good is the performance of an algorithm working with a certain sort of images. The False Acceptance Rate and the False Rejection Rate depend on the acceptance threshold of the biometric system that is fixed according to a security policy. A very common policy in biometric systems is to locate the acceptance threshold in the value where FAR and FRR are equal. This value is usually named as Equal Error Rate (EER) and it is an accepted metric to quantify and compare the performance of a biometric algorithm.

This way, validation results will be provided in terms of FTA, FTE and EER. Test results will be provided in terms of FMR and FNMR, keeping as acceptance threshold the value calculated during the validation stage.

9

MONOMODAL EVALUATION UNDER CONTROLLED CONDITIONS

9.1 INTRODUCTION

A complete evaluation of the different monomodal palmprint and hand geometry feature extraction methods presented in Chapter 5 has been conducted in this thesis with the aim to provide a fair comparison between them in terms of accuracy and execution time. In addition, different matching approaches described in Chapter 6 and the influence of the employment of a dimensionality reduction technique have also been evaluated. Moreover, different parameter configurations for each feature extraction method has been tested with the aim to find the best arrangement in each case.

Since the objective is to provide a wide evaluation of different methods, 2DHK database has been used to this end. As detailed in Section 2.3.1, it provides images captured under controlled conditions together with the most representative part of the palmprint properly aligned and cropped, which makes it suitable for a fair analysis of different feature extraction methods. Provided ground truth palms have been used for palmprint evaluation. In the case of hand geometry evaluation threshold based segmentation has been applied to obtain the silhouette of the hands, due to it provides the best results for 2DHK database.

According to the protocol described in Section 8.3, images of each user are divided in two subsets: validation and test. Validation samples, in turn, are divided in three groups: training, enrolment and access. Particularly, as database contains 10 images per user, training, enrolment, access and test subsets are composed by three, three, two and two samples respectively. The images intended for each group have been selected alternatively in such a way that training subset includes samples number 1, 5 and 9, enrolment subset includes samples number 2, 6 and validation access and test subsets include samples 3 and 7 and 4 and 8 respectively. This division has been decided to maximize the variability within each subset in order to simulate the best possible scenario and, consequently, to obtain the best possible results for each combination of feature extraction and matching methods.

Controlled monomodal evaluation results ordered according to the employed trait and feature extraction method are presented down below.

9.2 PALMPRINT

9.2.1 *Sobel filter*

Different configurations of threshold, image size and angles have been tested for Sobel filter. When the configuration involves four angles, results applying principal component analysis (PCA) to reduce the dimensionality of the feature vector are also included. Euclidean distance and Support Vector Machines (SVMs) have been used for feature vector comparison.

The analysis of the results show that the image size can notably vary the accuracy of this feature extraction method. The increase of the image size negatively affects the results. The influence of threshold parameter is not so strong and no pattern can be easy derived from the results. When looking to the angles involved in the feature extraction process, it can be seen that in general 45^o and 135^o provide better results and that the combination of the four angles also improves the accuracy of the system. Finally, dimensionality reduction also helps to improve the results.

Regarding to the comparison methods, it can be seen that the use of SVMs clearly outperforms the use of Euclidean distance for template matching.

Because of the volume of tests made, only the best parameter configuration is shown in table 15 together with its results, but the entire assortment of test is gathered in Appendix B.1. The threshold and image size values which provides better results are 32x32 and 0.1 respectively.

Figure 24 depicts a comparison between the best validation results obtained when Sobel filter is applied as feature extraction method under controlled conditions. Figures 24a and 24b compare the results obtained using Euclidean distance while Figures 24c and 24d compare the results obtained employing SVMs. Each graphic compares

Test Configuration			Results		
			Validation	Test	
Angles (^{o})	PCA	Comparison Method	EER (%)	FMR (%)	FNMR (%)
0	No	Euclidean Distance	1.98	1.91	2.26
45	No	Euclidean Distance	1.38	1.39	2.54
90	No	Euclidean Distance	0.56	0.57	2.54
135	No	Euclidean Distance	0.85	0.82	1.41
0,45,90,135	No	Euclidean Distance	0.56	0.55	1.41
0,45,90,135	Yes	Euclidean Distance	0.56	0.39	0.85
0	No	SVMs	0.28	0.56	0.34
45	No	SVMs	0.0063	0.28	0.011
90	No	SVMs	0.067	0.29	0.10
135	No	SVMs	0.28	0.28	0.35
0,45,90,135	No	SVMs	0.0048	0.046	0.0096
0,45,90,135	Yes	SVMs	0	0.28	0

Table 15.: Best palmprint results using Sobel filter as feature extraction method under controlled conditions. Image size and threshold parameters of feature extraction algorithm have been set to 32x32 and 0.1 respectively.

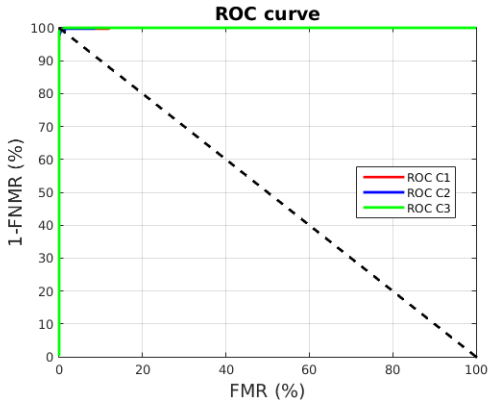

(a) Euclidean Distance. C1: 90^o. C2: 0^o, 45^o, 90^o and 135^o. C3: 0^o, 45^o, 90^o and 135^o + PCA.

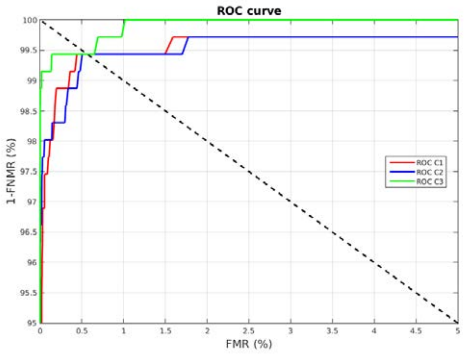

(b) Euclidean Distance (zoomed). C1: 90^o. C2: 0^o, 45^o, 90^o and 135^o. C3: 0^o, 45^o, 90^o and 135^o + PCA.

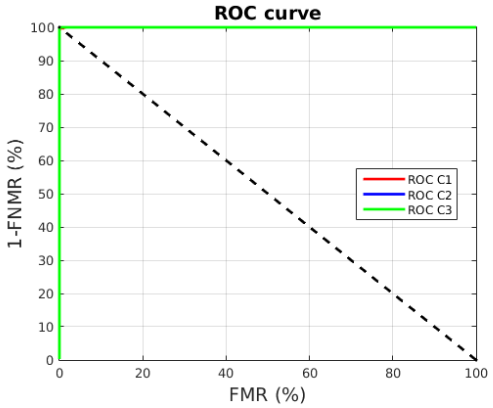

(c) SVMs. C1: 45^o. C2: 0^o, 45^o, 90^o and 135^o. C3: 0^o, 45^o, 90^o and 135^o + PCA.

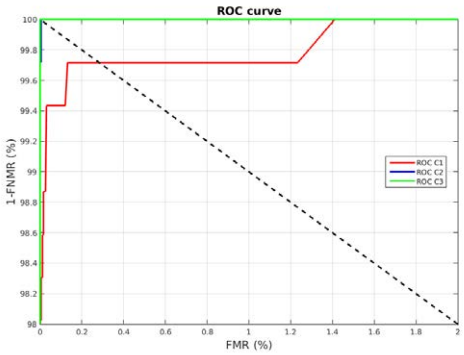

(d) SVMs (zoomed). C1: 45^o. C2: 0^o, 45^o, 90^o and 135^o. C3: 0^o, 45^o, 90^o and 135^o + PCA.

Figure 24.: Comparison of best palmprint results using Sobel filter as feature extraction method and different matching approaches under controlled conditions. Each graphic compares different angles configurations and the application of PCA. Image size and threshold parameters of feature extraction algorithm have been set to 32x32 and 0.1 respectively in all the cases.

the results obtained when different angles are involved in the feature extraction process as well as the use of PCA in the case that the four angles are employed. Image size and threshold parameters have been set to 32x32 and 0.1 respectively in all the cases. Validation and Test results of the best case, which corresponds to image size equal to 32x32, threshold equal to 0.1 and angles 0^o, 45^o, 90^o and 135^o, PCA and SVMs, are compared in Figure 25.

Table 16 shows the feature vector size and recognition time for Sobel filter feature extraction using different combinations of parameters and comparison methods with and without dimensionality reduction. Regarding to the computation time there is not a significant difference between Euclidean distance and SVMs during the recognition. However, SVMs need to be trained, increasing the training time per user in 15.597890 seconds when 1 angle is used, 69.929933 seconds when 4 angles are em-

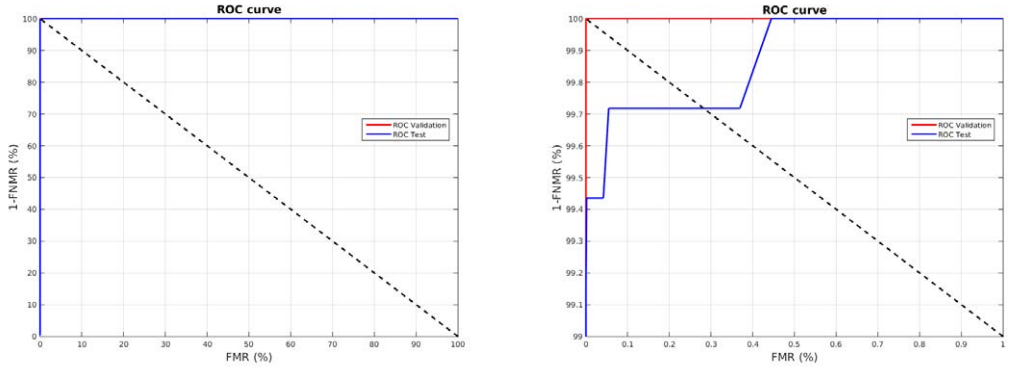

(a) ROC (b) ROC (zoomed)

Figure 25.: Validation and Test results obtained when features are extracted using Sobel filter and compared by SVMs and dimensionality reduction is applied under controlled conditions. Image size, threshold and directions parameters are set to 32x32, 0.1 and 0^o, 45^o, 90^o and 135^o.

# Angles	PCA	Comparison Method	Feature Vector Length	Time (s)
1	No	Euclidean Distance	16384	0.160392
4	No	Euclidean Distance	65536	1.843417
4	Yes	Euclidean Distance	531	1.849234
1	No	SVMs	16384	0.017295
4	No	SVMs	65536	1.69685
4	Yes	SVMs	531	1.692222

Table 16.: Feature vector length and execution time using Sobel filter as feature extraction method under controlled conditions.

ployed and 12.1226727 seconds when the initial feature vector includes 4 angles but PCA is applied to reduce de dimensionality of the template. In turn, PCA also requires 1.423896 extra seconds for training but in this case the training involves the whole crew. Nevertheless, training is made only once so this increasing of time is not really relevant and does not affect the recognition tasks.

In this line, training of PCA and SVMs not only requires additional computation time but also a training database and it can be more problematic. As mentioned in Sec. 8.3, results depends on both, the environmental conditions and the population in which the database is collected. For this reason, a representative enough database is necessary during the training phase but it is not always easy to obtain. Accordingly, these methods are more suitable for closed-set applications where all the users are known and an appropriate training can be made.

9.2.2 *Gabor filter*

Different configurations of filter size, frequency and standard deviation of the gaussian envelope (σ) have been tested for Gabor filter with and without applying principal component analysis (PCA) to reduce the dimensionality of the feature vector.

Test Configuration		Results		
		Validation	Test	
PCA	Comparison Method	EER (%)	FMR (%)	FNMR (%)
No	Euclidean Distance	0.56	0.55	1.41
Yes	Euclidean Distance	0.56	0.39	0.56
No	SVMs	0.27	0.31	0.28
Yes	SVMs	0.054	0.059	0.56

Table 17.: Best palmprint results using Gabor filter as feature extraction method under controlled conditions. Filter size, frequency and σ parameters have been set to 17x17, 0.0916 and 5.16179 respectively.

Euclidean Distance and Support Vector Machines (SVMs) have been used for feature vectors comparison.

The analysis of the results show that there is not a clear influence of any parameter and that results depend on the combination of all of them and the comparison method. Comparing the matching approaches evaluated, it can be seen that the use of SVMs outperforms a little bit the use of Euclidean distance for template matching and that the improvement is higher as worst are the results obtained with Euclidean distance. Finally, dimensionality reduction also helps to slightly improve the results.

Because of the volume of tests made, only the best parameter configuration is shown in table 17 together with its results, but the entire assortment of test is gathered in Appendix B.2. The values for filter size, frequency and σ parameters which provides better results are 17x17, 0.9616 and 6.6179 respectively.

Figure 26 depicts a comparison between the best validation results obtained when Gabor filter is applied as feature extraction method under controlled conditions. Figures 26a and 26b compare the results obtained using Euclidean distance while Figures 26c and 26d compare the results obtained employing SVMs. Each graphic compares the results obtained with and without dimensionality reduction when filter size, frequency and σ parameters are set to 17x17, 0.0916 and 5.16179 respectively. Validation and Test results of the best case, which are provided by SVMs when PCA is applied, are compared in Figure 27.

Table 18 shows the feature vector size and recognition time for Gabor filter feature extraction using different comparison methods with and without dimensionality reduction. Regarding to the computation time there is a small difference between Euclidean distance and SVMs during the recognition, being smaller the recognition time when SVMs are used. However, SVMs need to be trained, increasing the training time per user in 3.710576 seconds over the original templates and 0.076657 when PCA is applied for dimensionality reduction. In turn, PCA also requires 3.326385 extra seconds for training but in this case the training involves the whole crew. Nevertheless, training is made only once so this increasing of time is not really relevant and does not affect the recognition tasks.

In this line, as detailed in Section 9.2.1, PCA and SVMs not only requires additional computation time but also a training database that makes these methods more suitable for closed-set applications.

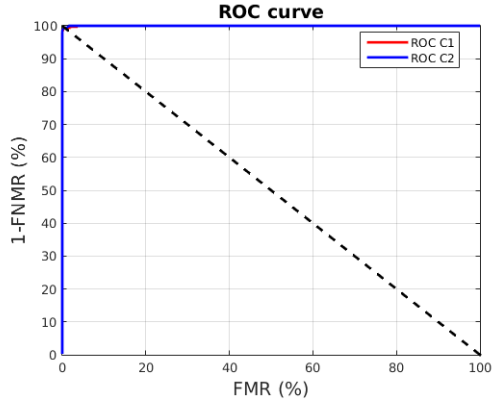

(a) Euclidean distance with (C2) and without(C1) PCA.

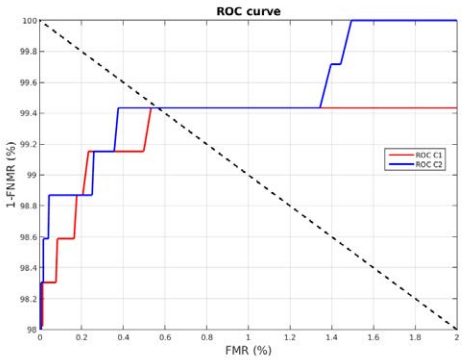

(b) Euclidean distance with (C2) and without(C1) PCA (zoomed).

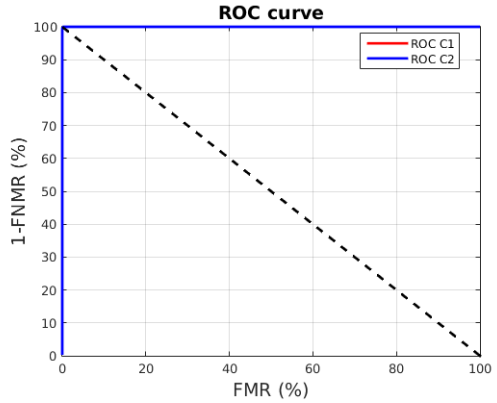

(c) SVMs with (C2) and without(C1) PCA.

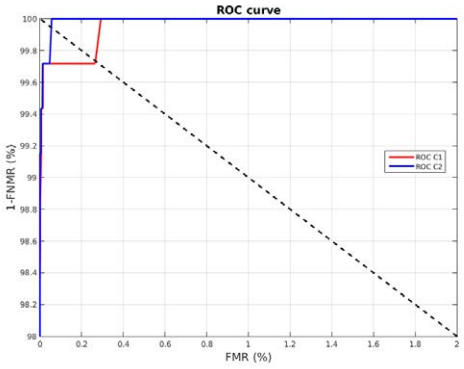

(d) SVMs with (C2) and without(C1) (zoomed).

Figure 26.: Best palmprint results using Gabor filter as feature extraction method under controlled conditions. Filter size, frequency and σ parameters have been set to 17x17, 0.0916 and 5.16179 respectively.

PCA	Comparison Method	Feature Vector Length	Time (s)
No	Euclidean Distance	32768	0.188407
Yes	Euclidean Distance	531	0.188083
No	SVMs	32768	0.07244
Yes	SVMs	531	0.052031

Table 18.: Feature vector length and execution time using Gabor filter as feature extraction method under controlled conditions.

9.2.3 *Local Binary Patterns*

Different configurations of region size, radio, number of neighbours and uniform/non-uniform patterns parameters have been tested for LBP feature extraction. Results applying principal component analysis (PCA) to reduce the dimensionality of the feature vectors are also included. Euclidean distance, χ^2 distance, histogram intersection and Support Vector Machines (SVMs) have been used for feature vectors comparison.

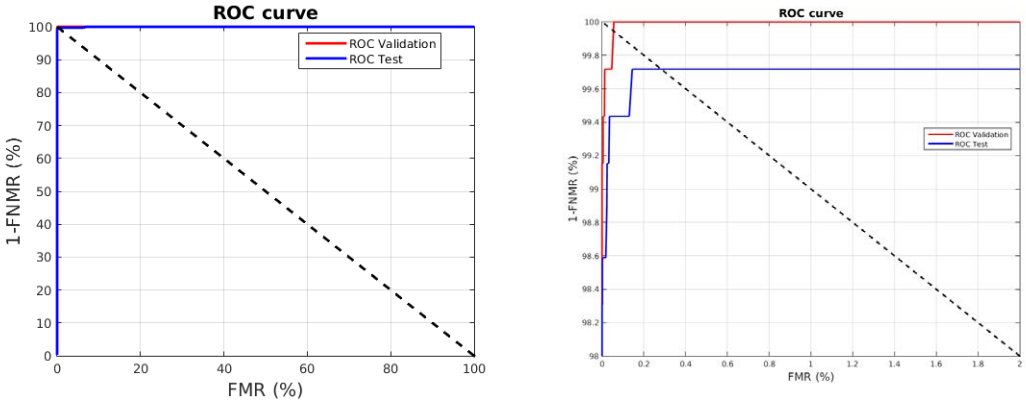

(a) ROC (b) ROC (zoomed)

Figure 27.: Validation and Test results obtained when features are extracted using Gabor filter and compared by SVMs and dimensionality reduction (PCA) is applied under controlled conditions. Filter size, frequency and σ parameters have been set to 17x17, 0.0916 and 5.16179 respectively.

The analysis of the results show that the region size can notably vary the accuracy of this feature extraction method. The increase of the image size negatively affects the results. The influence of radio parameter is not so strong and no pattern can be easy derived from the results. If number of neighbours parameter is examined, it can be seen that 16-neighbourhood provides worst results than 8-neighbourhood. Looking to uniform/non-uniform patterns parameter it can be seen that there is not a great difference between them. Generally, non-uniform patterns provide better results for bigger region sizes, probably because in those cases feature vector dimension is smaller and it contains little global information and thus it is not descriptive enough.

Regarding to the comparison methods, it can be seen that the use of methods oriented to histogram comparison (χ^2 Distance or Histogram Intersection) clearly outperforms the use of Euclidean distance for template matching. Moreover, results show that SVMs certainly provide the best results. Finally, it can be seen that dimensionality reduction also helps to improve the results.

Because of the volume of tests made, only the best parameter configuration is shown in table 19 together with its results, but the entire assortment of test is gathered in Appendix B.3. Although the best result for Euclidean distance is obtained using 8x8 region size, radio 1, 8-neighbourhood and uniform patterns, when methods oriented to histogram comparison or more complex approaches are applied the best parameter configuration is 16x16, 3 and 8 for region size, radio and # of neighbours respectively.

Figure 28 depicts a comparison between the best validation results obtained when LBP is applied as feature extraction method under controlled conditions. Figures 28a and 28b compare the results obtained using Euclidean distance, Figures 28c and 28d compare the results obtained employing χ^2 distance, Figures 28e and 28f compare the results obtained using histogram intersection and Figures 28g and 28h compare the results obtained employing SVMs. Each graphic compares the results obtained

by different values of region size and radio parameters. When features are compared by means of Euclidean distance or SVMs PCA dimensionality reduction is applied. Validation and Test results of the best case, which corresponds to region size equal to 16x16, radio equal to 3 and SVMs matching, are compared in Figure 29.

Table 20 shows the feature vector size and recognition time for LBP filter feature extraction using different combinations of parameters and comparison methods with and without dimensionality reduction. Regarding to the computation time there is a small difference between Euclidean distance and the remaining methods during the recognition, needing more time the former. However, SVMs need to be trained, increasing the training time per user in 1.532363 and 0.436725 seconds for the original vectors computed with 8x8 and 16x16 region sizes respectively, or 0.095569 and 0.07963 seconds for 8x8 an 16x16 region sizes when PCA is applied to reduce de dimensionality of the template. In turn, PCA also requires 1.749102 and 0.365671 extra seconds for training vectors with 8x8 and 16x16 values for the region size, but in this case the training involves the whole crew. Nevertheless, training is made only once so this increasing of time is not really relevant and does not affect the recognition tasks.

Test Configuration				Results		
				Validation	Test	
Region Size	Radio	PCA	Comparison Method	EER (%)	FMR (%)	FNMR (%)
8x8	1	No	Euclidean Distance	2.54	2.50	1.98
8x8	3	No	Euclidean Distance	2.91	2.90	2.54
16x16	1	No	Euclidean Distance	2.64	2.56	1.98
16x16	3	No	Euclidean Distance	2.92	2.78	2.26
8x8	1	Yes	Euclidean Distance	1.61	1.32	1.41
8x8	3	Yes	Euclidean Distance	4.24	2.79	5.65
16x16	1	Yes	Euclidean Distance	2.54	2.41	1.98
16x16	3	Yes	Euclidean Distance	2.68	2.25	2.26
8x8	1	No	χ^2 Distance	0.34	0.32	0.85
8x8	3	No	χ^2 Distance	1.07	0.98	0.85
16x16	1	No	χ^2 Distance	0.64	0.62	1.41
16x16	3	No	χ^2 Distance	0.21	0.20	0.85
8x8	1	No	Histogram Intersection	0.51	0.47	0.85
8x8	3	No	Histogram Intersection	1.11	1.03	0.85
16x16	1	No	Histogram Intersection	0.64	0.61	1.41
16x16	3	No	Histogram Intersection	0.28	0.23	0.85
8x8	1	No	SVMs	0.0048	0.0048	0.28
8x8	3	No	SVMs	0.40	0.45	0.56
16x16	1	No	SVMs	0	0.0016	0.85
16x16	3	No	SVMs	0	0.0016	0.56
8x8	1	Yes	SVMs	0.0032	0.0048	0.56
8x8	3	Yes	SVMs	0.56	0.73	0.85
16x16	1	Yes	SVMs	0	0.0016	0.85
16x16	3	Yes	SVMs	0	0.0032	0.56

Table 19.: Best palmprint results using Local Binary Patterns as feature extraction method under controlled conditions. Patterns are uniform and #Neighboors parameter is set to 8.

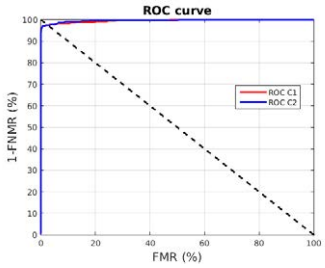

(a) Euclidean distance. C1: 8x8 r.s. and ra. 1. C2: 16x16 r.s. and ra. 1.

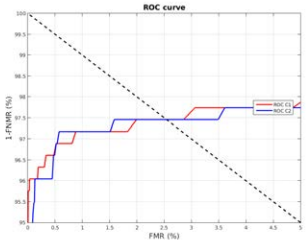

(b) Euclidean distance (zoom). C1: 8x8 r.s. and ra. 1. C2: 16x16 r.s. and ra. 1.

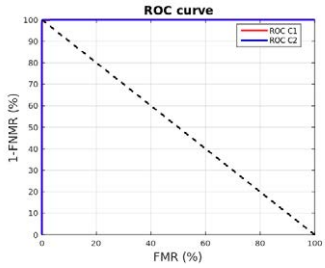

(c) χ^2 distance. C1: 8x8 r.s. and ra. 1. C2: 16x16 r.s. and ra. 3.

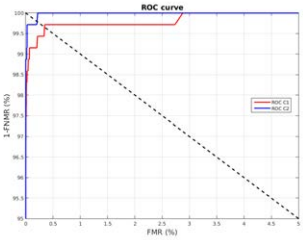

(d) χ^2 distance (zoom). C1: 8x8 r.s. and ra. 1. C2: 16x16 r.s. and ra. 3.

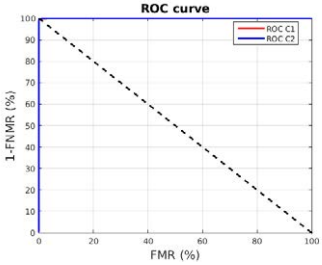

(e) Histogram intersection. C1: 8x8 r.s. and ra. 1. C2: 16x16 r.s. and ra. 3.

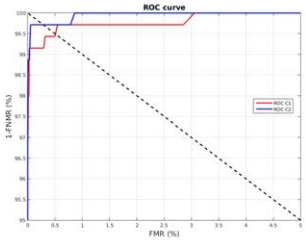

(f) Histogram intersection (zoom). C1: 8x8 r.s. and ra. 1. C2: 16x16 r.s. and ra. 3.

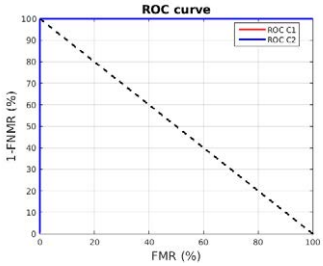

(g) SVMs. C1: 8x8 r.s. and ra. 1. C2: 16x16 r.s. and ra. 3.

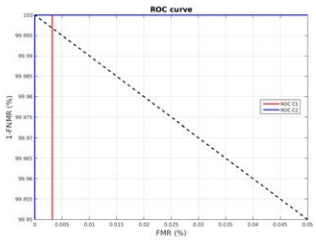

(h) SVMs (zoom). C1: 8x8 r.s. and ra. 1. C2: 16x16 r.s. and ra. 3.

Figure 28.: Best palmprint results using LBP as feature extraction method under controlled conditions. Each graphic compares different region size (r.s.) and radio(ra) configurations. Patterns are uniform and #Neighboors parameter is set to 8 in all the cases.

In this line, as detailed in Section 9.2.1, PCA and SVMs not only requires additional computation time but also a training database that makes these methods more suitable for closed-set applications.

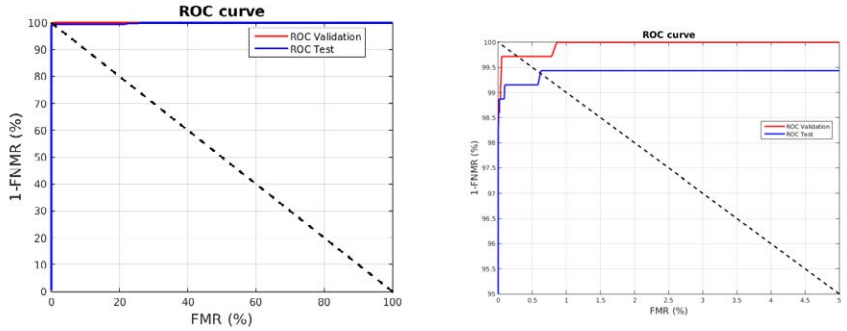

(a) ROC (b) ROC (zoomed)

Figure 29.: Validation and Test results obtained when features are extracted using LBP and compared by SVMs and dimensionality reduction is applied under controlled conditions. Patterns are uniform and parameters #Neighboors, region size and radio have been set to 8, 16x16 and 3 respectively.

Region size	PCA	Comparison Method	Feature Vector Length	Time (s)
8x8	No	Euclidean Distance	14104	0.320847
8x8	Yes	Euclidean Distance	531	0.234214
8x8	No	χ^2 Distance	14104	0.166363
8x8	No	Histogram Intersection	14104	0.165858
8x8	No	SVMs	14104	0.1979
8x8	Yes	SVMs	531	0.175108
16x16	No	Euclidean Distance	3776	0.184008
16x16	Yes	Euclidean Distance	531	0.191659
16x16	No	χ^2 Distance	3776	0.053587
16x16	No	Histogram Intersection	3776	0.053428
16x16	No	SVMs	3776	0.056401
16x16	Yes	SVMs	531	0.057513

Table 20.: Feature vector length and execution time using LBP as feature extraction method under controlled conditions.

9.2.4 *Local Derivative Patterns*

Different configurations of region size and directions have been tested for LDP filter with and without applying principal component analysis (PCA) to reduce the dimensionality of the feature vector. Euclidean distance, χ^2 distance, histogram intersection and Support Vector Machines (SVMs) have been used for feature vectors comparison.

The analysis of the results show that even when the best result is obtained with a region size value of 32x32, in general regions of 16x16 pixels provides better results and that the increasing of the region sizes negatively influences the results, probably because of the loss of global information. It can also be seen that when Euclidean distance is used 8x8 is the best choice for region size parameter but when methods oriented to histogram comparison (χ^2 distance or histogram intersection) or more complex approaches (SVMs) are used, the region size which provides better results is 16x16. Looking to the number of directions involved in the feature extraction process it can be seen that as more directions are used better are the results, but that using

all the directions introduces some noise and the results are slightly worst than in the three-directions case.

Regarding to the comparison methods, it can be seen that the use of SVMs clearly outperforms the use of distance based and histogram intersection approaches for template matching. Finally, dimensionality reduction also helps to improve the results.

Because of the volume of tests made, only the best parameter configuration is shown in table 21 together with its results, but the entire assortment of test is gathered in Appendix B.4.

Algorithm Parameters				Results		
				Valid.	Test	
Region Size	Directions (^{o})	PCA	Comparison Method	EER (%)	FMR (%)	FNMR (%)
8x8	0	No	Euclidean Distance	2.23	2.04	3.11
8x8	45	No	Euclidean Distance	2.54	2.55	1.41
8x8	90	No	Euclidean Distance	1.69	1.86	2.26
8x8	135	No	Euclidean Distance	1.69	1.38	1.69
8x8	0, 45	No	Euclidean Distance	1.59	1.51	1.41
8x8	0, 90	No	Euclidean Distance	1.69	1.56	1.13
8x8	0, 135	No	Euclidean Distance	1.72	1.61	1.98
8x8	45, 90	No	Euclidean Distance	1.93	2.03	1.13
8x8	45, 135	No	Euclidean Distance	1.13	1.15	1.13
8x8	90, 135	No	Euclidean Distance	1.13	1.15	3.11
8x8	0, 45, 90	No	Euclidean Distance	1.41	1.34	1.69
8x8	0, 45, 135	No	Euclidean Distance	1.41	1.33	1.13
8x8	0, 90, 135	No	Euclidean Distance	1.41	1.38	1.69
8x8	45, 90, 135	No	Euclidean Distance	1.13	1.17	1.13
8x8	0, 45, 90, 135	No	Euclidean Distance	1.13	1.14	0.85
8x8	0	Yes	Euclidean Distance	1.98	1.71	1.69
8x8	45	Yes	Euclidean Distance	1.98	1.81	1.98
8x8	90	Yes	Euclidean Distance	1.69	1.72	1.41
8x8	135	Yes	Euclidean Distance	1.69	1.66	3.11
8x8	0, 45	Yes	Euclidean Distance	1.69	1.38	1.69
8x8	0, 90	Yes	Euclidean Distance	1.67	1.39	0.85
8x8	0, 135	Yes	Euclidean Distance	1.41	1.07	1.13
8x8	45, 90	Yes	Euclidean Distance	1.40	1.29	1.13
8x8	45, 135	Yes	Euclidean Distance	1.13	0.90	0.28
8x8	90, 135	Yes	Euclidean Distance	0.97	0.85	1.41
8x8	0, 45, 90	Yes	Euclidean Distance	1.43	1.16	1.41
8x8	0, 45, 135	Yes	Euclidean Distance	1.41	1.07	0.85
8x8	0, 90, 135	Yes	Euclidean Distance	1.13	0.93	0.85
8x8	45, 90, 135	Yes	Euclidean Distance	1.00	0.83	0.56
8x8	0, 45, 90, 135	Yes	Euclidean Distance	1.38	1.12	0.56
16x16	0	No	χ^2 Distance	2.26	2.26	3.11
16x16	45	No	χ^2 Distance	2.26	2.26	1.69
16x16	90	No	χ^2 Distance	6.34	6.10	7.34
16x16	135	No	χ^2 Distance	3.95	3.73	5.93
16x16	0, 45	No	χ^2 Distance	1.30	1.29	0.85
16x16	0, 90	No	χ^2 Distance	2.20	2.11	1.13
16x16	0, 135	No	χ^2 Distance	1.02	0.95	0.85
16x16	45, 90	No	χ^2 Distance	3.22	3.16	2.54
16x16	45, 135	No	χ^2 Distance	1.95	1.83	1.69
16x16	90, 135	No	χ^2 Distance	4.24	4.05	5.93
16x16	0, 45, 90	No	χ^2 Distance	1.98	1.91	1.13
16x16	0, 45, 135	No	χ^2 Distance	0.99	0.99	0.85

Algorithm Parameters				Results		
				Valid.	Test	
Region Size	Directions (^{o})	PCA	Comparison Method	EER (%)	FMR (%)	FNMR (%)
16x16	0, 90, 135	No	χ^2 Distance	1.66	1.56	1.69
16x16	45, 90, 135	No	χ^2 Distance	2.82	2.68	2.82
16x16	0, 45, 90, 135	No	χ^2 Distance	1.69	1.62	1.13
16x16	0	No	Histogram Intersection	1.24	1.23	1.98
16x16	45	No	Histogram Intersection	1.41	1.42	1.13
16x16	90	No	Histogram Intersection	2.26	2.13	2.54
16x16	135	No	Histogram Intersection	1.69	1.61	3.95
16x16	0, 45	No	Histogram Intersection	1.17	1.22	0.85
16x16	0, 90	No	Histogram Intersection	1.13	1.17	0.85
16x16	0, 135	No	Histogram Intersection	0.63	0.62	1.13
16x16	45, 90	No	Histogram Intersection	1.41	1.41	1.13
16x16	45, 135	No	Histogram Intersection	1.34	1.27	1.13
16x16	90, 135	No	Histogram Intersection	1.69	1.60	3.11
16x16	0, 45, 90	No	Histogram Intersection	1.41	1.41	0.85
16x16	0, 45, 135	No	Histogram Intersection	0.80	0.80	1.13
16x16	0, 90, 135	No	Histogram Intersection	0.85	0.85	1.13
16x16	45, 90, 135	No	Histogram Intersection	1.69	1.58	0.85
16x16	0, 45, 90, 135	No	Histogram Intersection	1.16	1.15	0.85
16x16	0	No	SVMs	0.57	0.70	0
16x16	45	No	SVMs	0.25	0.34	0.56
16x16	90	No	SVMs	0.56	0.62	0.56
16x16	135	No	SVMs	0.28	0.38	0
16x16	0, 45	No	SVMs	0.10	0.13	0.56
16x16	0, 90	No	SVMs	0.019	0.022	0.56
16x16	0, 135	No	SVMs	0.016	0.0096	0.85
16x16	45, 90	No	SVMs	0.16	0.18	0.56
16x16	45, 135	No	SVMs	0.16	0.20	0.28
16x16	90, 135	No	SVMs	0.28	0.32	0
16x16	0, 45, 90	No	SVMs	0.035	0.048	0.56
16x16	0, 45, 135	No	SVMs	0.0096	0.011	0.28
16x16	0, 90, 135	No	SVMs	0.025	0.021	0.28
16x16	45, 90, 135	No	SVMs	0.13	0.19	0.28
16x16	0, 45, 90, 135	No	SVMs	0.019	0.024	0.28
16x16	0	Yes	SVMs	0.56	0.69	0
16x16	45	Yes	SVMs	0.28	0.36	0.56
16x16	90	Yes	SVMs	0.50	0.57	0.56
16x16	135	Yes	SVMs	0.28	0.37	0.28
16x16	0, 45	Yes	SVMs	0.18	0.22	0.56
16x16	0, 90	Yes	SVMs	0.027	0.035	0.56
16x16	0, 135	Yes	SVMs	0.013	0.013	0.85
16x16	45, 90	Yes	SVMs	0.16	0.19	0.56
16x16	45, 135	Yes	SVMs	0.19	0.22	0.28
16x16	90, 135	Yes	SVMs	0.28	0.34	0
16x16	0, 45, 90	Yes	SVMs	0.057	0.066	0.56
16x16	0, 45, 135	Yes	SVMs	0.011	0.0096	0.28
16x16	0, 90, 135	Yes	SVMs	0.033	0.030	0.28
16x16	45, 90, 135	Yes	SVMs	0.20	0.27	0.28
16x16	0, 45, 90, 135	Yes	SVMs	0.027	0.032	0.28

Table 21.: Best palmprint results using Local Derivative Patterns as feature extraction method under controlled conditions.

Figure 30 depicts a comparison between the best validation results obtained when LDP is applied as feature extraction method under controlled conditions. Figures 30a and 30b compare the results obtained using Euclidean distance, Figures 30c and 30d compare the results obtained employing χ^2 distance, Figures 30e and 30f compare the results obtained using histogram intersection and Figures 30g and 30h compare the results obtained employing SVMs. Each graphic compares the results obtained by different configurations of region size and directions parameters. Validation and Test results of the best case, which corresponds to region size equal to 16x16 and directions 0^o, 45^o, 90^o and 135^o, are compared in Figure 31.

Table 22 shows the feature vector size and recognition time for LDP feature extraction using different combinations of parameters and comparison methods with and without dimensionality reduction. Regarding to the computation time there is a small difference between Euclidean distance and the remaining methods during the recognition, being Euclidean distance more expensive. However, SVMs need to be trained, increasing the training time per user. Also, PCA requires extra time for training, but in this case this time involver the whole crew. Nevertheless, training is made only once so this increasing of time is not really relevant and does not affect the recognition tasks. Training times are shown in table 23.

In this line, as detailed in Section 9.2.1, PCA and SVMs not only requires additional computation time but also a training database that makes these methods more suitable for closed-set applications.

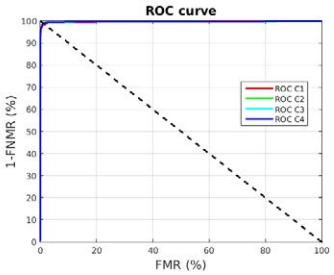

(a) Euclidean distance. C1: 8x8 r.s. and dir. 135. C2: 8x8 r.s. and dirs. 45, 135. C3: 8x8 r.s. and dirs. 45, 90, 135. C4: 8x8 r.s. and dirs. 0, 45, 90, 135.

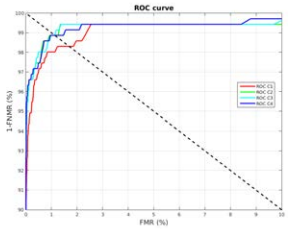

(b) Euclidean distance (zoomed). C1: 8x8 r.s. and dir. 135. C2: 8x8 r.s. and dirs. 45, 135. C3: 8x8 r.s. and dirs. 45, 90, 135. C4: 8x8 r.s. and dirs. 0, 45, 90, 135.

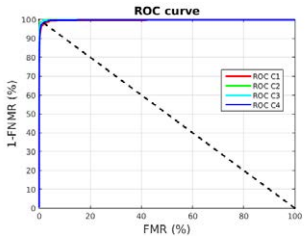

(c) χ^2 distance. C1: 16x16 r.s. and dir. 45. C2: 16x16 r.s. and dirs. 0, 135. C3: 16x16 r.s. and dirs. 0, 45, 135. C4: 16x16 r.s. and dirs. 0, 45, 90, 135.

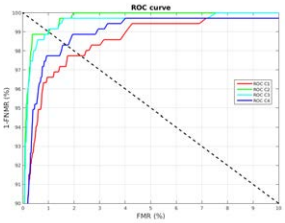

(d) χ^2 distance (zoomed). C1: 16x16 r.s. and dir. 45. C2: 16x16 r.s. and dirs. 0, 135. C3: 16x16 r.s. and dirs. 0, 45, 135. C4: 16x16 r.s. and dirs. 0, 45, 90, 135.

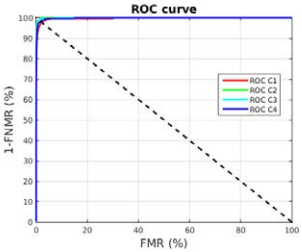

(e) Histogram intersection. C1: 16x16 r.s. and dir. 0. C2: 16x16 r.s. and dirs. 0,135. C3: 16x16 r.s. and dirs. 0, 45, 135. C4: 16x16 r.s. and dirs. 0, 45, 90, 135.

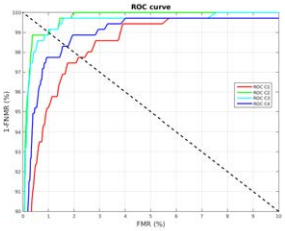

(f) Histogram intersection (zoomed). C1: 16x16 r.s. and dir. 0. C2: 16x16 r.s. and dirs. 0,135. C3: 16x16 r.s. and dirs. 0, 45, 135. C4: 16x16 r.s. and dirs. 0, 45, 90, 135.

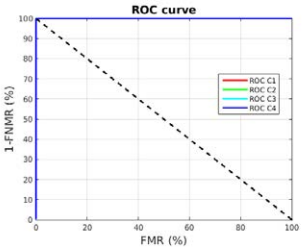

(g) SVMs. C1: 16x16 r.s. and dir. 45. C2: 16x16 r.s. and dirs. 0,135. C3: 16x16 r.s. and dirs. 0, 45, 135. C4: 16x16 r.s. and dirs. 0, 45, 90, 135.

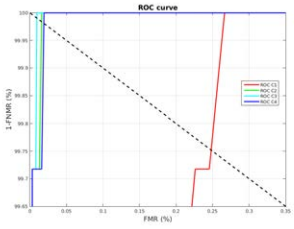

(h) SVMs (zoomed). C1: 16x16 r.s. and dir. 45. C2: 16x16 r.s. and dirs. 0,135. C3: 16x16 r.s. and dirs. 0, 45, 135. C4: 16x16 r.s. and dirs. 0, 45, 90, 135.

Figure 30.: Best palmprint results using LDP as feature extraction method under controlled conditions. Each graphic compares different configurations of region size (r.s) and directions (dir).

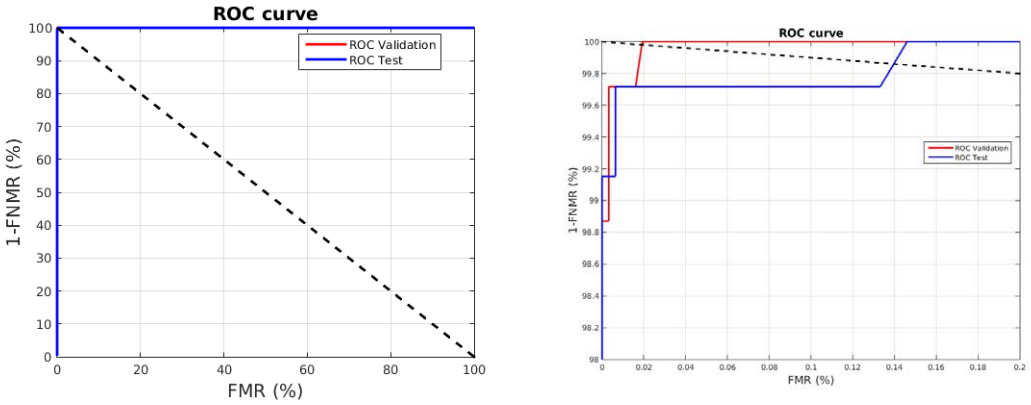

(a) ROC (b) ROC (zoomed)

Figure 31.: Validation and Test results obtained when features are extracted using LDP and compared by SVMs under controlled conditions. Region size is set to 16x16 and the involved directions are 0^o, 45^o, 90^o and 135^o.

Region size	# Directions	PCA	Comparison Method	Feature Vector Length	Time (s)
8x8	1	No	Euclidean Distance	65536	0.837353
8x8	1	Yes	Euclidean Distance	531	0.212729
8x8	2	No	Euclidean Distance	131072	0.232084
8x8	2	Yes	Euclidean Distance	531	0.244636
8x8	3	No	Euclidean Distance	196608	0.2715
8x8	4	Yes	Euclidean Distance	531	0.277218
8x8	4	No	Euclidean Distance	262144	0.425601
8x8	4	Yes	Euclidean Distance	531	0.414895
8x8	1	No	χ^2 Distance	65536	0.078132
8x8	2	No	χ^2 Distance	131072	0.103332
8x8	3	No	χ^2 Distance	196608	0.138133
8x8	4	No	χ^2 Distance	262144	0.277661
8x8	1	No	Histogram Intersection	65536	0.076423
8x8	2	No	Histogram Intersection	131072	0.100286
8x8	3	No	Histogram Intersection	196608	0.134765
8x8	4	No	Histogram Intersection	131072	0.272357
8x8	1	No	SVMs	65536	0.102957
8x8	1	Yes	SVMs	531	0.083338
8x8	2	No	SVMs	262144	0.122016
8x8	2	Yes	SVMs	531	0.105701
8x8	3	No	SVMs	196608	0.292952
8x8	3	Yes	SVMs	531	0.140601
8x8	4	No	SVMs	262144	0.46951
8x8	4	Yes	SVMs	531	0.27958
16x16	1	No	Euclidean Distance	16384	0.16742
16x16	1	Yes	Euclidean Distance	531	0.169078
16x16	2	No	Euclidean Distance	32768	0.166064
16x16	2	Yes	Euclidean Distance	531	0.170412
16x16	3	No	Euclidean Distance	49152	0.20289
16x16	4	Yes	Euclidean Distance	531	0.190765
16x16	4	No	Euclidean Distance	65536	0.208205
16x16	4	Yes	Euclidean Distance	531	0.199956

Region size	# Directions	PCA	Comparison Method	Feature Vector Length	Time (s)
16x16	1	No	χ^2 Distance	16384	0.025788
16x16	2	No	χ^2 Distance	32768	0.04575
16x16	3	No	χ^2 Distance	49152	0.047749
16x16	4	No	χ^2 Distance	65536	0.055594
16x16	1	No	Histogram Intersection	16384	0.025271
16x16	2	No	Histogram Intersection	32768	0.034189
16x16	3	No	Histogram Intersection	49152	0.046025
16x16	4	No	Histogram Intersection	65536	0.053861
16x16	1	No	SVMs	16384	0.032136
16x16	1	Yes	SVMs	531	0.027747
16x16	2	No	SVMs	32768	0.056516
16x16	2	Yes	SVMs	531	0.037356
16x16	3	No	SVMs	49152	0.07844
16x16	3	Yes	SVMs	531	0.049583
16x16	4	No	SVMs	65536	0.09944
16x16	4	Yes	SVMs	531	0.058014

Table 22.: Feature vector length and execution time using LDP as feature extraction method under controlled conditions.

Region size	# Directions	Method	Training Time (s)
8x8	1	PCA	0.376238
8x8	1	SVMs	3.576165
8x8	1	SVMs+PCA	0.077189
8x8	2	PCA	0.764877
8x8	2	SVMs	9.576692
8x8	2	SVMs+PCA	0.074949
8x8	3	PCA	1.142341
8x8	3	SVMs	13.935649
8x8	3	SVMs+PCA	0.081284
8x8	4	PCA	1.465100
8x8	4	SVMs	20.537271
8x8	4	SVMs+PCA	0.073776
16x16	1	PCA	0.188522
16x16	1	SVMs	1.013252
16x16	1	SVMs+PCA	0.077971
16x16	2	PCA	0.221302
16x16	2	SVMs	2.315133
16x16	2	SVMs+PCA	0.075475
16x16	3	PCA	0.316140
16x16	3	SVMs	3.542661
16x16	3	SVMs+PCA	0.076675
16x16	4	PCA	0.492621
16x16	4	SVMs	4.160861
16x16	4	SVMs+PCA	0.074345

Table 23.: PCA and SVMs training time for LDP feature extraction using different region sizes and number of directions to compose the template. PCA is made once over the entire population while SVMs training time provided is the average time per user. SVMs + PCA indicates that PCA is applied to the extracted features previously to the SVM training.

9.2.5 *Curvelet*

Different combinations of Curvelet bands have been tested with and without applying principal component analysis (PCA) to reduce the dimensionality of the templates. Euclidean distance and Support Vector Machines (SVMs) have been used for feature vector comparison. Table 24 and Table 25 shows the obtained results for Euclidean distance and SVMs comparison respectively.

It can be seen that the use of SVMs clearly outperforms the use of Euclidean distance for template matching and that dimensionality reduction also helps to improve the results. Nevertheless, no pattern can be easy derived about the influence of the number of bands involved in the template creation neither about which band are included on it.

Algorithm Parameters		Results		
		Validation	Test	
Bands	PCA	EER (%)	FMR (%)	FNMR (%)
1	No	8.10	8.11	8.19
2	No	7.67	7.73	11.30
3	No	14.52	14.66	17.80
4	No	13.51	13.63	16.10
1, 2	No	8.13	8.16	8.19
1, 3	No	8.20	8.20	8.19
1, 4	No	8.12	8.13	8.19
2, 3	No	9.32	9.42	12.99
2, 4	No	7.63	7.73	11.30
3, 4	No	14.69	14.76	18.08
1, 2, 3	No	8.14	8.19	8.19
1, 2, 4	No	8.06	8.09	8.19
1, 3, 4	No	8.26	8.26	8.19
2, 3, 4	No	9.11	9.24	13.56
1, 2, 3, 4	No	8.14	8.19	8.47
1	Yes	8.10	8.11	8.19
2	Yes	7.34	7.26	10.73
3	Yes	11.02	10.25	12.71
4	Yes	9.04	8.94	11.02
1, 2	Yes	8.03	8.04	8.19
1, 3	Yes	8.05	8.05	8.19
1, 4	Yes	8.08	8.08	8.19
2, 3	Yes	7.06	6.68	9.60
2, 4	Yes	6.79	6.67	10.17
3, 4	Yes	9.44	8.85	11.30
1, 2, 3	Yes	8.13	8.11	8.19
1, 2, 4	Yes	8.01	8.02	8.47
1, 3, 4	Yes	8.02	7.99	8.19
2, 3, 4	Yes	6.86	6.52	9.04
1, 2, 3, 4	Yes	8.11	8.07	8.47

Table 24.: Palmprint Results using Curvelets to extract features and Euclidean distance to compare under controlled conditions.

Figure 32 depicts a comparison between the best validation results obtained when Curvelet is applied as feature extraction method under controlled conditions. Figures 32a and 32b compare the results obtained using Euclidean distance while Figures 32c and 32d compare the results obtained employing SVMs. Each graphic compares the results obtained by different configurations of parameter *bands*. PCA is applied for dimensionality reduction. Validation and Test results of the best case, which corresponds to bands 1, 2, 3 and 4, are compared in Figure 33.

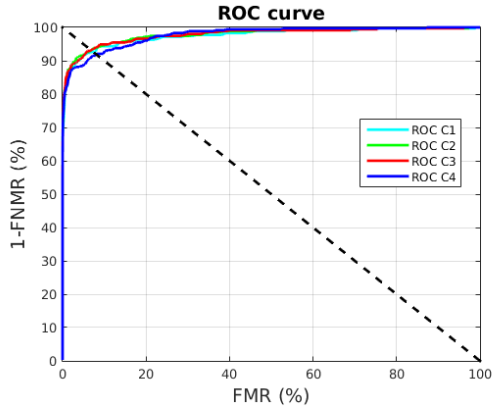

(a) Euclidean distance. C1: band 2. C2: bands 2 and 4. C3: bands 2, 3 and 4. C4: bands 1, 2, 3 and 4.

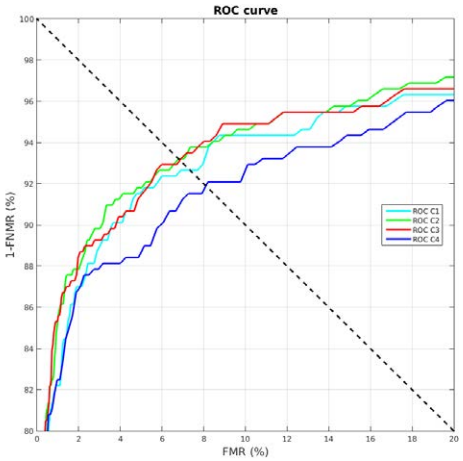

(b) Euclidean distance (zoomed). C1: band 2. C2: bands 2 and 4. C3: bands 2, 3 and 4. C4: bands 1, 2, 3 and 4.

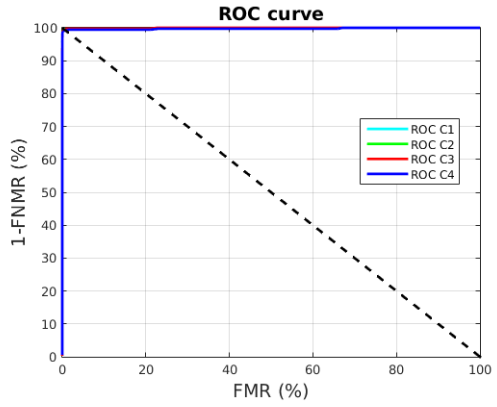

(c) SVMs. C1: band 1. C2: bands 1 and 2. C3: bands 1, 2 and 4. C4: bands 1, 2, 3 and 4.

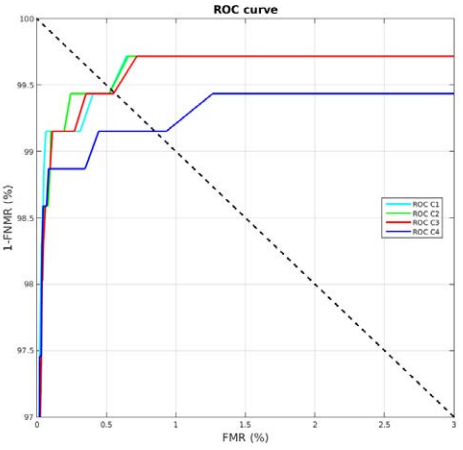

(d) SVMs (zoomed). C1: band 1. C2: bands 1 and 2. C3: bands 1, 2 and 4. C4: bands 1, 2, 3 and 4.

Figure 32.: Best palmprint results using Curvelet as feature extraction method and PCA under controlled conditions. Each graphic compares different configurations of parameter *bands*.

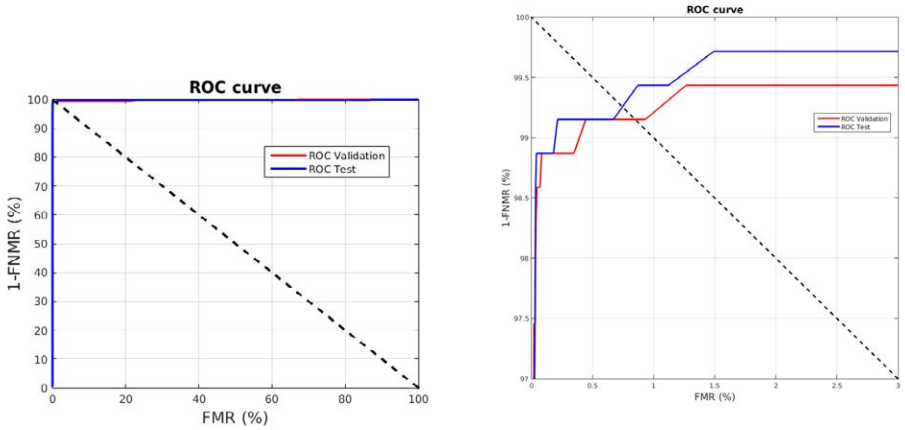

(a) ROC (b) ROC (zoomed)

Figure 33.: Validation and Test results obtained when features are extracted using Curvelet and compared by SVMs under controlled conditions. PCA is applied and 1, 2, 3 and 4 bands are involved in the feature extraction process.

Table 26 shows the feature vector size and recognition time for each individual Curvelet band feature extraction. Time and feature vector size values of the different combinations of bands is directly proportional to the values of the bands which are involved in the combination. Regarding to the computation time there is no significant difference between using Euclidean distance or SVMs to compare feature vectors. However, SVMs need to be trained, increasing the training time per user as shown in Table 27. The use of PCA for dimensionality reduction over the initial feature vector, notably decreases these training times as can be seen in Table 27. In addition, PCA also requires extra time for training, but in this case the training involves the whole crew. Nevertheless, training is made only once so this increasing of time is not really relevant and does not affect the recognition tasks.

Algorithm Parameters		Results		
		Validation	Test	
Bands	PCA	EER (%)	FMR (%)	FNMR (%)
1	No	0.53	0.60	0.56
2	No	1.98	2.17	2.54
3	No	5.93	6.21	7.91
4	No	3.23	3.43	4.80
1, 2	No	0.85	0.90	0.28
1, 3	No	0.56	0.63	0.85
1, 4	No	0.56	0.65	0.56
2, 3	No	2.26	2.43	2.26
2, 4	No	1.69	1.82	1.98
3, 4	No	5.05	5.40	6.21
1, 2, 3	No	0.85	0.87	0.28
1, 2, 4	No	0.56	0.60	0.28
1, 3, 4	No	0.56	0.60	0.85
2, 3, 4	No	1.92	2.07	2.26

Algorithm Parameters		Results		
		Validation	Test	
Bands	PCA	EER (%)	FMR (%)	FNMR (%)
1, 2, 3, 4	No	0.56	0.54	0.56
1	Yes	0.53	0.59	0.56
2	Yes	1.98	2.18	2.26
3	Yes	5.34	5.57	7.63
4	Yes	3.45	3.59	3.11
1, 2	Yes	0.53	0.56	0.85
1, 3	Yes	0.56	0.60	0.56
1, 4	Yes	0.56	0.63	0.56
2, 3	Yes	2.13	2.40	2.54
2, 4	Yes	1.69	1.93	2.26
3, 4	Yes	4.52	4.81	6.50
1, 2, 3	Yes	0.74	0.78	0.28
1, 2, 4	Yes	0.56	0.58	0.85
1, 3, 4	Yes	0.63	0.70	0.56
2, 3, 4	Yes	2.00	2.26	2.54
1, 2, 3, 4	Yes	0.85	0.90	0.56

Table 25.: Palmprint Results using Curvelets to extract features and SVMs to compare under controlled conditions.

In this line, as detailed in Section 9.2.1, PCA and SVMs requires additional computation time but also a training database that makes these methods more suitable for closed-set applications.

Band	PCA	Comparison Method	Feature Vector Length	Time (s)
1	No	Euclidean Distance	441	0.000501
1	Yes	Euclidean Distance	441	0.000512
2	No	Euclidean Distance	5985	0.002523
2	Yes	Euclidean Distance	531	0.004260
3	No	Euclidean Distance	22881	0.012851
3	Yes	Euclidean Distance	531	0.019089
4	No	Euclidean Distance	90145	0.100121
4	Yes	Euclidean Distance	531	0.123185
1	No	SVMs	441	0.003377
1	Yes	SVMs	441	0.008258
2	No	SVMs	5985	0.007813
2	Yes	SVMs	531	0.011654
3	No	SVMs	22881	0.024563
3	Yes	SVMs	531	0.026040
4	No	SVMs	90145	0.146564
4	Yes	SVMs	531	0.130335

Table 26.: Feature vector length and execution time using Curvelets as feature extraction method under controlled conditions.

Band	Method	Training Time (s)
1	PCA	0.215955
1	SVMs	0.22164
1	SVMs+PCA	0.028736
2	PCA	1.054606
2	SVMs	0.142791
2	SVMs+PCA	0.028627
3	PCA	3.320489
3	SVMs	0.784237
3	SVMs+PCA	0.027416
4	PCA	14.579065
4	SVMs	4.247650
4	SVMs+PCA	0.028291

Table 27.: PCA and SVMs training time for Curvelets feature extraction using different bands to compose the template. PCA is made once over the entire population while SVMs training time provided is the average time per user. SVMs + PCA indicates that PCA is applied to the extracted features previously to the SVM training.

9.3 HAND GEOMETRY

Different number of features per finger and the inclusion or not of thumb in the template have been tested for Hand Geometry. Euclidean Distance and Support Vector Machines (SVMs) have been used for feature vectors comparison. Results are presented in table 28 and table 29.

It can be seen that the inclusion of thumb in the template influences negatively the results. It can be a direct consequence of it great mobility, that introduces a high variability in the template. Looking to the number of features per finger it can be seen that this parameter does not present a high influence on the results. Finally, regarding to the comparison methods, it can be seen that the use of SVMs outperforms the use of Euclidean distance for template matching.

Algorithm Parameters		Results		
		Validation	Test	
♯Features	Thumb	EER (%)	FMR (%)	FNMR (%)
20	No	3.95	3.94	3.95
20	Yes	4.24	4.37	3.95
30	No	3.67	3.65	3.95
30	Yes	4.02	4.02	4.24
40	No	3.67	3.64	3.39
40	Yes	3.96	4.05	4.24
50	No	3.77	3.78	3.95
50	Yes	4.07	4.16	4.24

Table 28.: Hand Geometry Results under controlled conditions using Euclidean Distance to compare.

Algorithm Parameters		Results		
		Validation	Test	
♯Features	Thumb	EER (%)	FMR (%)	FNMR (%)
20	No	1.13	0.98	0.85
20	Yes	1.41	1.29	0.85
30	No	1.11	1.02	0.85
30	Yes	1.13	1.02	0.85
40	No	1.13	1.03	0.85
40	Yes	1.46	1.34	0.85
50	No	1.41	1.24	0.56
50	Yes	1.13	1.07	0.85

Table 29.: Hand Geometry Results under controlled conditions using SVMs to compare.

Figure 34 depicts a comparison between the best validation results obtained when hand geometry features are extracted under controlled conditions. Figures 34a and 34b compare the results obtained using Euclidean distance while Figures 34c and 34d compare the results obtained employing SVMs. Each graphic compares the results obtained by different number of features per finger when thumb is not included in the template. Validation and Test results of the best case, which corresponds to 20 features per finger, are compared in Figure 35.

Concerning template size, when 20, 30, 40 or 50 features per finger are employed, feature vectors contains 80, 120, 160 or 200 elements respectively in the case that thumb is excluded of the pattern.

In respect to the execution time, there is not appreciable difference between different number of features per finger. Recognition time is on around 1.008704 seconds for Euclidean distance comparison and 0.045358 for SVMs. SVMs require 1.010324 additional seconds per user for training. Nevertheless, training is made only once so this increasing of time is not really relevant and does not affect the recognition tasks.

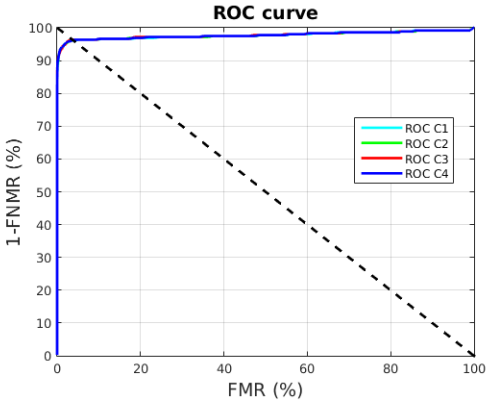

(a) Euclidean distance. C1: 20 features. C2: 30 features. C3: 40 features. C4: 50 features.

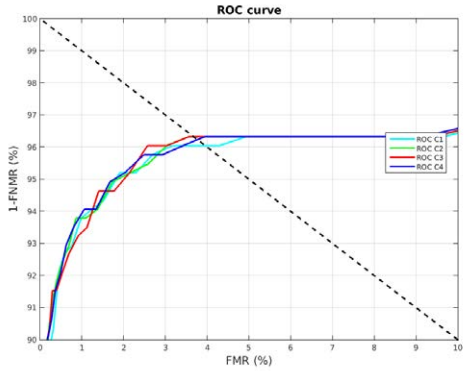

(b) Euclidean distance (zoomed). C1: 20 features. C2: 30 features. C3: 40 features. C4: 50 features.

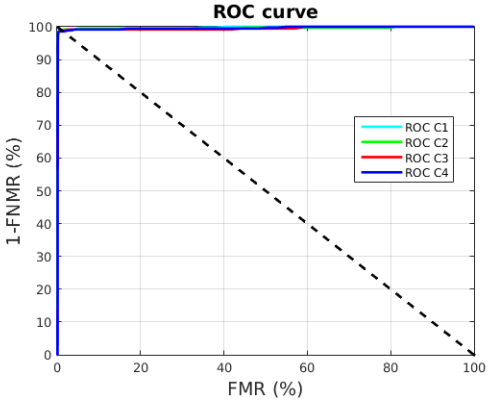

(c) SVMs. C1: 20 features. C2: 30 features. C3: 40 features. C4: 50 features.

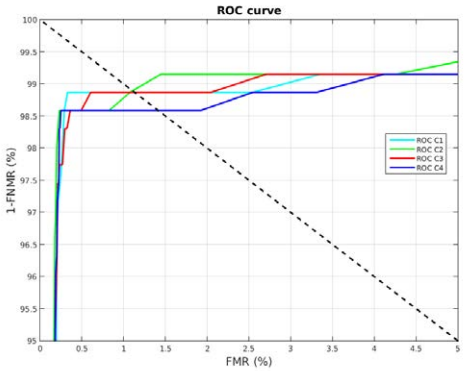

(d) SVMs (zoomed). C1: 20 features. C2: 30 features. C3: 40 features. C4: 50 features.

Figure 34.: Best hand geometry results under controlled conditions. Each graphic compares different number of features per finger when thumb is excluded.

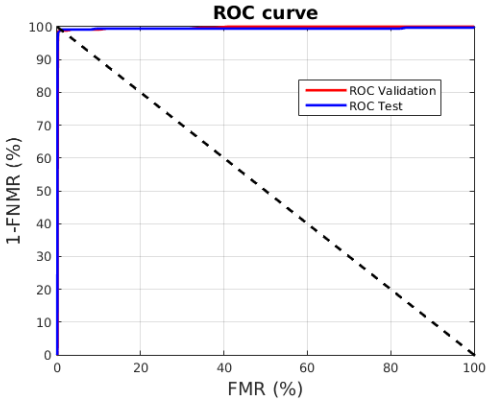

(a) ROC

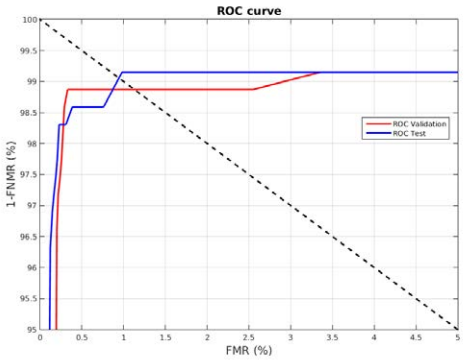

(b) ROC (zoomed)

Figure 35.: Validation and Test results obtained when hand geometry features are extracted using 20 features per finger, thumb is excluded, and compared by SVMs under controlled conditions.

10

MONOMODAL EVALUATION UNDER REALISTIC CONDITIONS

10.1 INTRODUCTION

This chapter presents an evaluation of the different monomodal palmprint and hand geometry feature extraction methods described in Chapter 5 under realistic conditions. The aim of this evaluation is to introduce some variability with regard to environmental conditions and hand pose in order to obtain more realistic results. Similarly to the evaluation under controlled conditions presented in Chapter 9, different matching approaches described in Chapter 6 and the influence of the employment of a dimensionality reduction technique have also been evaluated. Considering the results obtained for the different parameter configurations tested for each feature extraction method, those configurations which presents better results have been selected to repeat the experiments under more complex situations.

To this end, gb2s_ID database have been selected due to the contact-less pose constraint-free nature of its images and background restrictions. Well contrasted neutral backgrounds ease the segmentation task, which has already been thoroughly evaluated in Chapter 3 and it then is not considered crucial at this point. As described in Section 2.3.2, gb2s_ID database provides indoor images captured by the camera of a mobile device under natural lighting conditions, which present present huge variability in terms of size, skin color, orientation, hand openness and illumination conditions which make it suitable for this evaluation. Flooding based segmentation using thresholding as initial binarization have been applied to separate the hand from the background because this method provides results that are comparable to more complex approaches but consuming considerably less resources.

Although gb2s_ID database contains images of both hands, in order to make equitable comparisons with the monomodal evaluation under controlled conditions only one hand is included in this experiments, the left hand. In the same way, a higher number of images per hand and user are provided by gb2s_ID database, but only 10 are randomly selected for the experiments. According to the protocol described in Section 8.3, these 10 images of each user are divided in two subsets: validation and test. Validation samples, in turn, are divided in three groups: training, enrolment and access. Equally to monomodal controlled experiments training, enrolment, access and test subsets are composed by three, three, two and two samples respectively. In this case the images intended for each group have been randomly selected.

Even when well contrasted neutral backgrounds in general ease the segmentation procedure, some images in gb2s_ID database still present challenging characteristics such as pink background, light reflections or the use of rings that difficult the extrac-

tion of a precise silhouette of the hand or the palmprint ROI detection. As explained in Chapter 3, these images are discarded by segmentation quality control module or by visual supervision of the extracted and aligned palmprint ROIs. Those users for whom there are not enough images for training and enrollment after the supervision are considered as FTE. In particular, a FTE equal to 6.79 % has been obtained. In addition, FTA has been calculated over the entire database getting a rate of 18.42 %. It is more elevated than expected, mainly due to there are some users for whom all the images are discarded. Nevertheless, as the number of images per user is quite higher than 10, those users which are not included in the FTE maintain at least 10 images so these FTA rate has not been included in the FMR and FNMR computation.

Monomodal evaluation results under realistic conditions ordered according to the employed trait and feature extraction method are presented down below followed by their joint analysis.

10.2 PALMPRINT

10.2.1 *Sobel filter*

Table 30 presents the results of the evaluation under realistic conditions for Sobel filter feature extraction.

Figure 36 depicts a comparison between the best validation results obtained when Sobel filter is applied as feature extraction method under realistic conditions. Figures 36a and 36b compare the results obtained using Euclidean distance while Figures 36c and 36d compare the results obtained employing SVMs. Each graphic compares the results obtained when different angles are involved in the feature extraction process

Test Configuration			Results		
			Validation	Test	
Angles	PCA	Comparison Method	EER (%)	FMR (%)	FNMR (%)
0	No	Euclidean Distance	2.90	2.88	3.65
45	No	Euclidean Distance	3.38	3.28	5.73
90	No	Euclidean Distance	4.17	3.84	6.25
135	No	Euclidean Distance	2.60	2.73	4.69
0,45,90,135	No	Euclidean Distance	2.08	1.97	4.69
0,45,90,135	Yes	Euclidean Distance	1.22	1.24	5.73
0	No	SVMs	2.08	2.28	3.65
45	No	SVMs	1.28	1.42	5.73
90	No	SVMs	1.56	1.57	4.69
135	No	SVMs	1.04	1.11	5.21
0,45,90,135	No	SVMs	1.04	1.21	3.13
0,45,90,135	Yes	SVMs	1.04	1.04	4.17

Table 30.: Palmprint results using Sobel filter as feature extraction method under realistic conditions. Image size and threshold parameters of feature extraction algorithm have been set to 32x32 and 0.1 respectively.

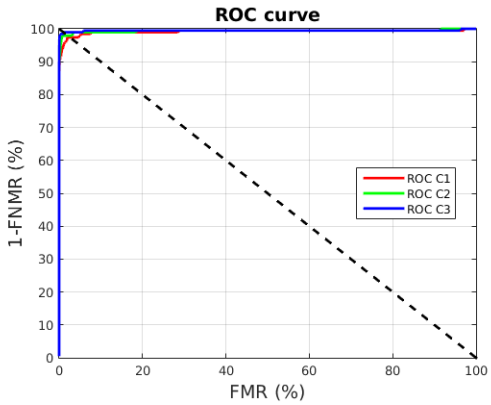

(a) Euclidean Distance. C1: 135^o. C2: 0^o, 45^o, 90^o and 135^o. C3: and 0^o, 45^o, 90^o and 135^o + PCA.

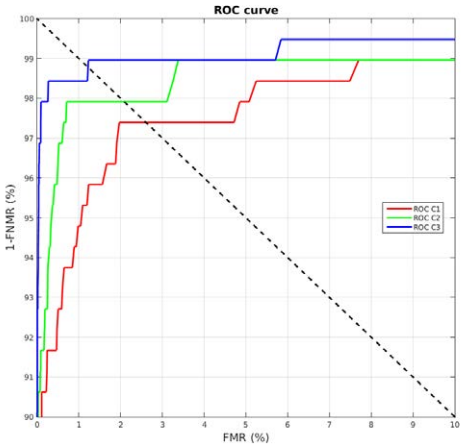

(b) Euclidean Distance (zoomed). C1: 135^o. C2: 0^o, 45^o, 90^o and 135^o. C3: and 0^o, 45^o, 90^o and 135^o + PCA.

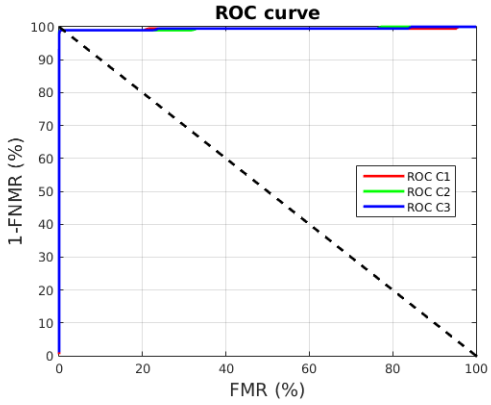

(c) SVMs. C1: 135^o. C2: 0^o, 45^o, 90^o and 135^o. C3: and 0^o, 45^o, 90^o and 135^o + PCA.

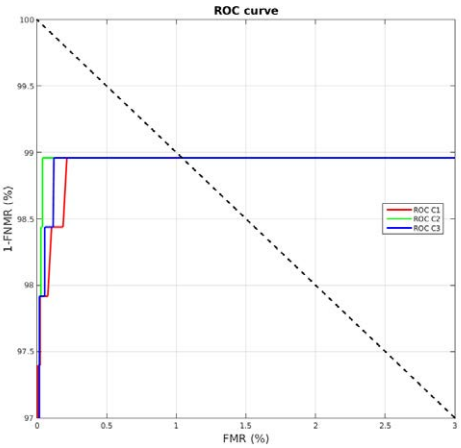

(d) SVMs (zoomed). C1: 135^o. C2: 0^o, 45^o, 90^o and 135^o. C3: and 0^o, 45^o, 90^o and 135^o + PCA.

Figure 36.: Comparison of best palmprint results using Sobel filter as feature extraction method and different matching approaches under realistic conditions. Each graphic compares different angles configurations and the application of PCA. Image size and threshold parameters of feature extraction algorithm have been set to 32x32 and 0.1 respectively in all the cases.

as well as the use of PCA in the case that the four angles are employed. Image size and threshold parameters have been set to 32x32 and 0.1 respectively in all the cases. Validation and Test results of the best case, which corresponds to image size equal to 32x32, threshold equal to 0.1 and angles 0^o, 45^o, 90^o and 135^o, PCA and SVMs, are compared in Figure 37.

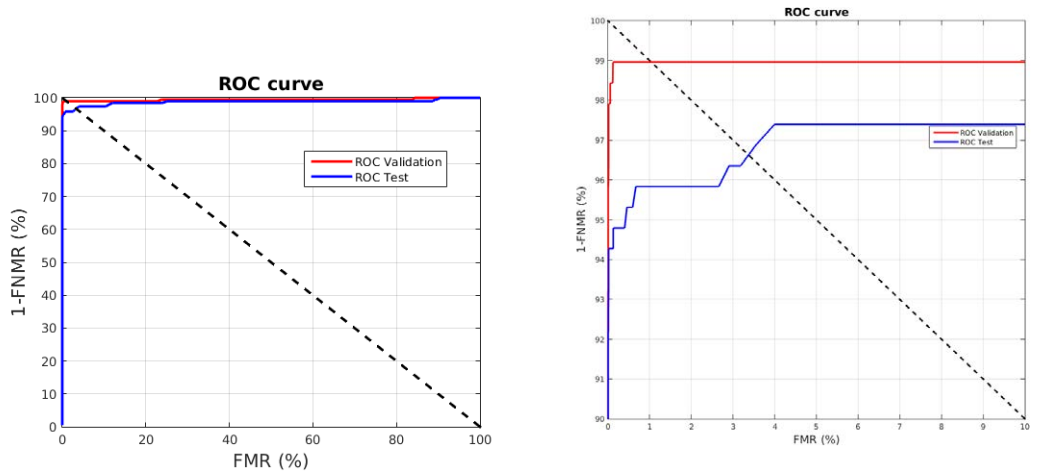

(a) ROC (b) ROC (zoomed)

Figure 37.: Validation and Test results obtained when features are extracted under realistic conditions using Sobel filter and compared by SVMs and dimensionality reduction is applied. Image size, threshold and directions parameters are set to 32x32, 0.1 and 0^o, 45^o, 90^o and 135^o respectively.

10.2.2 *Gabor filter*

Table 31 presents the results of the evaluation under realistic conditions for Gabor filter feature extraction.

Figure 38 depicts a comparison between the best validation results obtained when Gabor filter is applied as feature extraction method under realistic conditions. Figures 38a and 38b compare the results obtained using Euclidean distance while Figures 38c and 38d compare the results obtained employing SVMs. Each graphic compares the results obtained with and without dimensionality reduction when filter size, frequency and σ parameters are set to 17x17, 0.0916 and 5.16179 respectively. Validation and Test results of the best case, which are provided by SVMs when PCA is applied, are compared in Figure 39.

Test Configuration		Results		
		Validation	Test	
PCA	Comparison Method	EER (%)	FMR (%)	FNMR (%)
No	Euclidean Distance	2.08	2.02	5.73
Yes	Euclidean Distance	1.56	1.47	6.25
No	SVMs	1.04	1.13	2.60
Yes	SVMs	1.56	1.68	4.17

Table 31.: Palmprint results using Gabor filter as feature extraction method under realistic conditions. Filter size, frequency and σ parameters have been set to 17x17, 0.0916 and 5.16179 respectively.

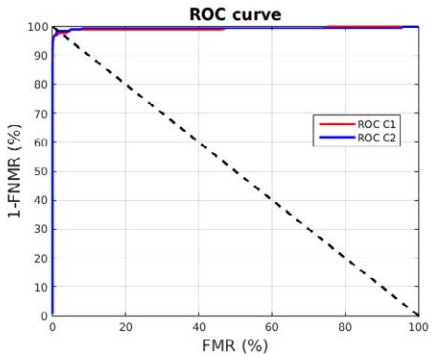

(a) Euclidean distance with (C2) and without(C1) PCA.

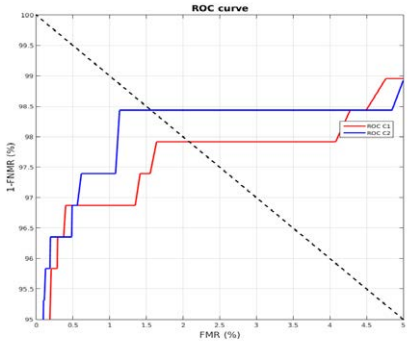

(b) Euclidean distance with (C2) and without(C1) PCA (zoomed).

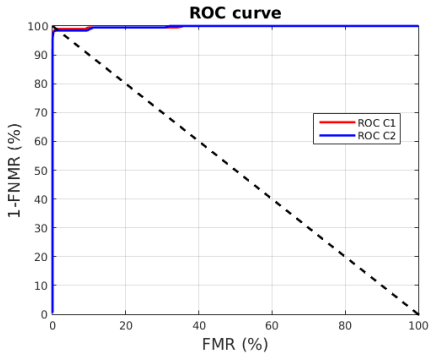

(c) SVMs with (C2) and without(C1) PCA.

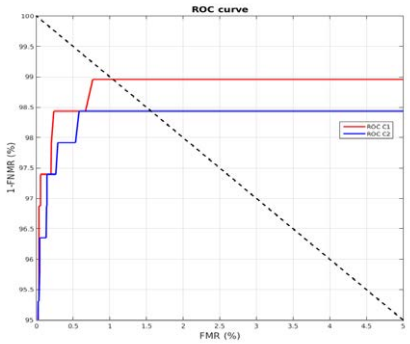

(d) SVMs with (C2) and without(C1) (zoomed).

Figure 38.: Best palmprint results using Gabor filter as feature extraction method under realistic conditions. Filter size, frequency and σ parameters have been set to 17x17, 0.0916 and 5.16179 respectively.

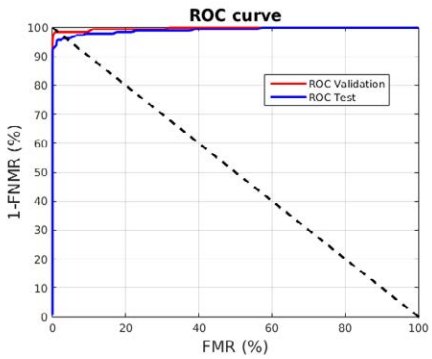

(a) ROC

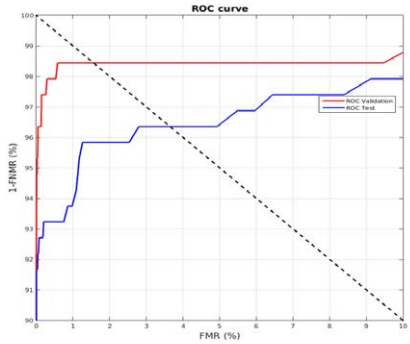

(b) ROC (zoomed)

Figure 39.: Validation and Test results obtained when features are extracted using Gabor filter and compared by SVMs and dimensionality reduction (PCA) is applied under realistic conditions. Filter size, frequency and σ parameters have been set to 17x17, 0.0916 and 5.16179 respectively.

10.2.3 *Local Binary Patterns*

Table 32 presents the results of the evaluation under realistic conditions for LBP feature extraction.

Test Configuration				Results		
				Validation	Test	
Region Size	Uniform	PCA	Comparison Method	EER (%)	FMR (%)	FNMR (%)
8x8	1	No	Euclidean Distance	6.14	6.32	8.33
8x8	3	No	Euclidean Distance	8.70	9.34	14.58
16x16	1	No	Euclidean Distance	4.69	5.10	7.29
16x16	3	No	Euclidean Distance	5.73	5.74	9.38
8x8	1	Yes	Euclidean Distance	2.12	2.61	5.73
8x8	3	Yes	Euclidean Distance	6.81	8.10	8.33
16x16	1	Yes	Euclidean Distance	3.13	3.60	6.77
16x16	3	Yes	Euclidean Distance	2.19	2.79	5.73
8x8	1	No	χ^2 Distance	2.18	2.01	3.13
8x8	3	No	χ^2 Distance	5.21	5.04	6.77
16x16	1	No	χ^2 Distance	2.08	2.08	4.69
16x16	3	No	χ^2 Distance	2.60	2.68	5.73
8x8	1	No	SVMs	0.73	0.68	3.13
8x8	3	No	SVMs	2.60	2.90	3.65
16x16	1	No	SVMs	0.52	0.41	3.13
16x16	3	No	SVMs	1.04	0.97	2.08
8x8	1	Yes	SVMs	1.04	1.08	3.13
8x8	3	Yes	SVMs	3.13	3.18	4.17
16x16	1	Yes	SVMs	0.52	0.42	3.13
16x16	3	Yes	SVMs	1.04	1.16	2.60

Table 32.: Palmprint results using Local Binary Patterns as feature extraction method under realistic conditions. Patterns are uniform and #Neighboors parameter is set to 8.

Figure 40 depicts a comparison between the best validation results obtained when LBP is applied as feature extraction method under realistic conditions. Figures 40a and 40b compare the results obtained using Euclidean distance, Figures 40c and 40d compare the results obtained employing χ^2 distance, and 40f compare the results obtained using SVMs. Each graphic compares the results obtained by different values of region size when patterns are uniform and parameters #Neighboors and radio are set to 8 and 1 respectively. Validation and Test results of the best case, which corresponds to region size equal to 16x16and SVMs matching, are compared in Figure 41.

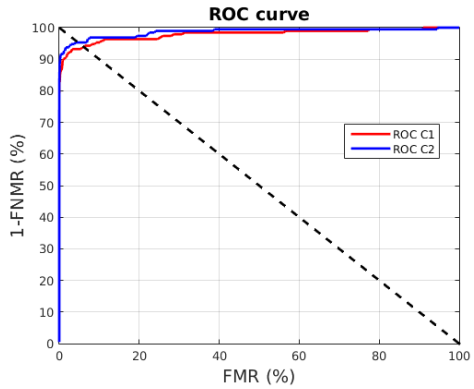

(a) Euclidean distance. C1: 8x8 reg. size. C2: 16x16 reg.size

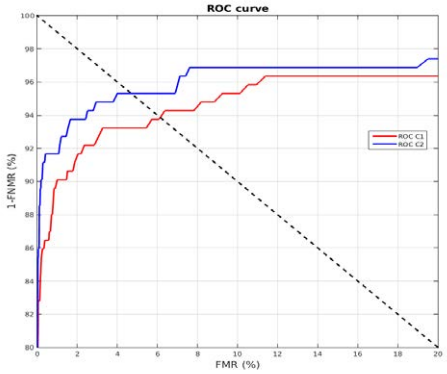

(b) Euclidean distance (zoom). C1: 8x8 reg. size. C2: 16x16 reg. size.

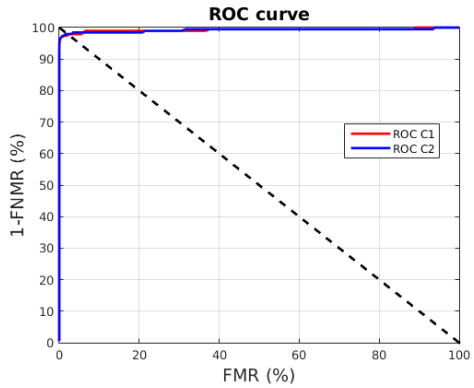

(c) χ^2 distance. C1: 8x8 reg. size. C2: 16x16 reg. size.

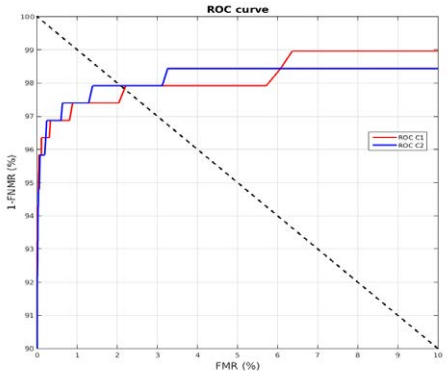

(d) χ^2 distance (zoom). C1: 8x8 reg. size. C2: 16x16 reg. size.

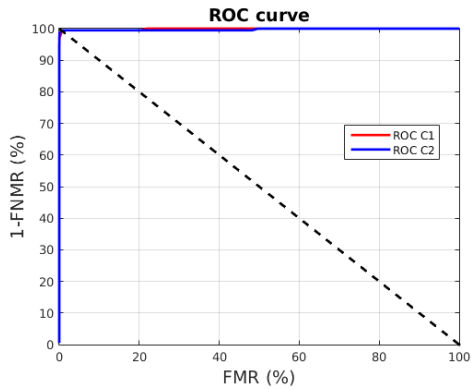

(e) SVMs. C1: 8x8 reg. size. C2: 16x16 reg. size.

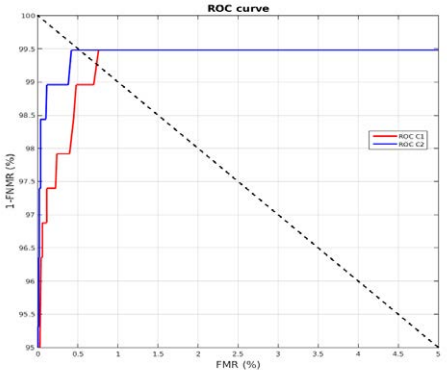

(f) SVMs (zoom). C1: 8x8 reg. size. C2: 16x16 reg. size.

Figure 40.: Best palmprint results using LBP as feature extraction method under realistic conditions. Each graphic compares different region sizes. Patterns are uniform and parameters #Neighboors and radio are set to 8 and 1 respectively in all the cases.

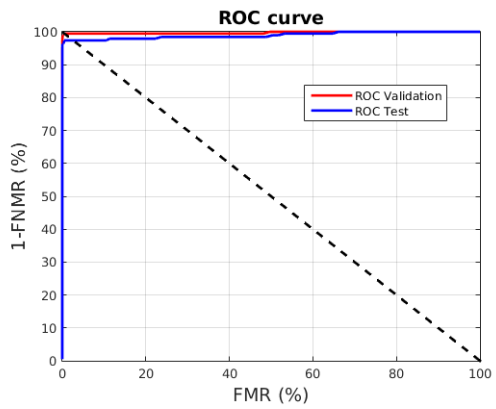

(a) ROC

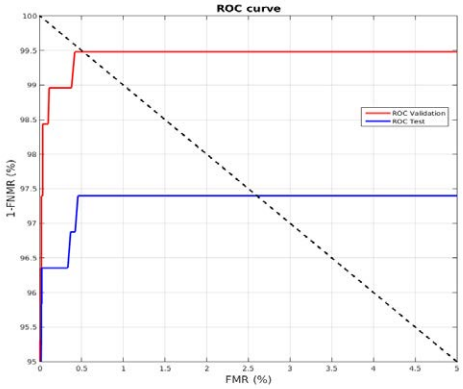

(b) ROC (zoomed)

Figure 41.: Validation and Test results obtained when features are extracted using LBP and compared by SVMs under realistic conditions. Patterns are uniform and parameters #Neighboors, region size and radio have been set to 8, 16x16 and 1 respectively.

10.2.4 *Local Derivative Patterns*

Table 33 presents the results of the evaluation under realistic conditions for LDP feature extraction.

Algorithm Parameters				Results		
				Valid.	Test	
Region Size	Directions	PCA	Comparison Method	EER (%)	FMR (%)	FNMR (%)
16x16	0	No	Euclidean Distance	4.06	4.40	5.73
16x16	45	No	Euclidean Distance	3.65	3.74	5.73
16x16	90	No	Euclidean Distance	5.07	5.32	7.29
16x16	135	No	Euclidean Distance	4.69	5.19	7.81
16x16	0, 45	No	Euclidean Distance	3.65	4.16	5.73
16x16	0, 90	No	Euclidean Distance	3.85	4.08	5.73
16x16	0, 135	No	Euclidean Distance	4.17	4.59	7.29
16x16	45, 90	No	Euclidean Distance	4.15	4.30	5.73
16x16	45, 135	No	Euclidean Distance	4.69	4.90	6.77
16x16	90, 135	No	Euclidean Distance	4.35	4.53	7.29
16x16	0, 45, 90	No	Euclidean Distance	4.08	4.35	5.21
16x16	0, 45, 135	No	Euclidean Distance	4.17	4.51	6.77
16x16	0, 90, 135	No	Euclidean Distance	4.17	4.29	6.77
16x16	45, 90, 135	No	Euclidean Distance	4.69	4.96	6.25
16x16	0, 45, 90, 135	No	Euclidean Distance	4.42	4.62	6.25
16x16	0	Yes	Euclidean Distance	4.09	4.47	5.73
16x16	45	Yes	Euclidean Distance	4.17	4.32	5.21
16x16	90	Yes	Euclidean Distance	4.76	5.06	7.29
16x16	135	Yes	Euclidean Distance	4.69	5.12	7.81

Algorithm Parameters				Results		
				Valid.	Test	
Region Size	Directions	PCA	Comparison Method	EER (%)	FMR (%)	FNMR (%)
16x16	0, 45	Yes	Euclidean Distance	3.28	3.70	5.73
16x16	0, 90	Yes	Euclidean Distance	3.13	3.41	6.77
16x16	0, 135	Yes	Euclidean Distance	4.17	4.58	7.29
16x16	45, 90	Yes	Euclidean Distance	3.13	3.23	6.77
16x16	45, 135	Yes	Euclidean Distance	4.17	4.24	6.77
16x16	90, 135	Yes	Euclidean Distance	4.17	4.38	6.77
16x16	0, 45, 90	Yes	Euclidean Distance	3.13	3.31	5.73
16x16	0, 45, 135	Yes	Euclidean Distance	3.13	3.50	6.25
16x16	0, 90, 135	Yes	Euclidean Distance	3.65	3.85	6.77
16x16	45, 90, 135	Yes	Euclidean Distance	3.65	3.78	7.29
16x16	0, 45, 90, 135	Yes	Euclidean Distance	3.64	3.93	6.25
16x16	0	No	χ^2 Distance	10.79	11.04	9.38
16x16	45	No	χ^2 Distance	5.17	5.30	5.73
16x16	90	No	χ^2 Distance	6.29	6.21	9.38
16x16	135	No	χ^2 Distance	4.43	4.17	7.81
16x16	0, 45	No	χ^2 Distance	6.25	6.32	6.77
16x16	0, 90	No	χ^2 Distance	5.41	5.64	4.69
16x16	0, 135	No	χ^2 Distance	2.93	2.66	6.25
16x16	45, 90	No	χ^2 Distance	4.17	4.33	5.73
16x16	45, 135	No	χ^2 Distance	2.60	2.51	3.13
16x16	90, 135	No	χ^2 Distance	4.30	4.13	8.33
16x16	0, 45, 90	No	χ^2 Distance	5.25	5.58	5.21
16x16	0, 45, 135	No	χ^2 Distance	2.60	2.45	5.73
16x16	0, 90, 135	No	χ^2 Distance	3.13	3.00	4.69
16x16	45, 90, 135	No	χ^2 Distance	2.84	2.87	3.65
16x16	0, 45, 90, 135	No	χ^2 Distance	2.94	2.81	4.69
16x16	0	No	SVMs	1.56	1.58	3.13
16x16	45	No	SVMs	1.56	1.51	3.13
16x16	90	No	SVMs	1.56	1.45	5.21
16x16	135	No	SVMs	2.27	2.30	5.73
16x16	0, 45	No	SVMs	1.04	0.83	3.65
16x16	0, 90	No	SVMs	1.04	0.91	3.13
16x16	0, 135	No	SVMs	1.56	1.51	3.13
16x16	45, 90	No	SVMs	1.04	0.87	3.13
16x16	45, 135	No	SVMs	1.04	0.97	3.65
16x16	90, 135	No	SVMs	1.60	1.44	5.73
16x16	0, 45, 90	No	SVMs	1.04	0.93	3.13
16x16	0, 45, 135	No	SVMs	1.04	0.94	3.13
16x16	0, 90, 135	No	SVMs	1.04	0.82	3.13
16x16	45, 90, 135	No	SVMs	1.04	0.90	3.65
16x16	0, 45, 90, 135	No	SVMs	1.04	0.88	3.13

Algorithm Parameters				Results		
				Valid.	Test	
Region Size	Directions	PCA	Comparison Method	EER (%)	FMR (%)	FNMR (%)
16x16	0	Yes	SVMs	2.05	2.08	4.17
16x16	45	Yes	SVMs	1.56	1.39	3.13
16x16	90	Yes	SVMs	2.00	1.79	5.21
16x16	135	Yes	SVMs	2.24	2.23	5.73
16x16	0, 45	Yes	SVMs	1.04	0.89	3.65
16x16	0, 90	Yes	SVMs	0.82	0.67	3.13
16x16	0, 135	Yes	SVMs	1.56	1.43	4.17
16x16	45, 90	Yes	SVMs	1.04	0.88	3.65
16x16	45, 135	Yes	SVMs	1.04	0.91	3.65
16x16	90, 135	Yes	SVMs	1.86	1.72	5.73
16x16	0, 45, 90	Yes	SVMs	0.80	0.57	3.13
16x16	0, 45, 135	Yes	SVMs	1.04	0.95	3.13
16x16	0, 90, 135	Yes	SVMs	1.04	0.90	3.65
16x16	45, 90, 135	Yes	SVMs	1.04	0.98	4.17
16x16	0, 45, 90, 135	Yes	SVMs	1.04	0.92	3.13

Table 33.: Palmprint results using Local Derivative Patterns as feature extraction method under realistic conditions.

Figure 42 depicts a comparison between the best validation results obtained when LDP is applied as feature extraction method under realistic conditions. Figures 42a and 42b compare the results obtained using Euclidean distance, Figures 42c and 42d compare the results obtained employing χ^2 distance and Figures 42e and 42f compare the results obtained by means of SVMs. Each graphic compares the results obtained by different configurations of directions parameter when region size is set to 16x16. In the cases of Euclidean distance and SVMs comparison PCA is applied for dimensionality reduction. Validation and Test results of the best case, which corresponds to region size equal to 16x16, directions 0^o, 45^o, 90^o and 135^o, and SVMs, are compared in Figure 43.

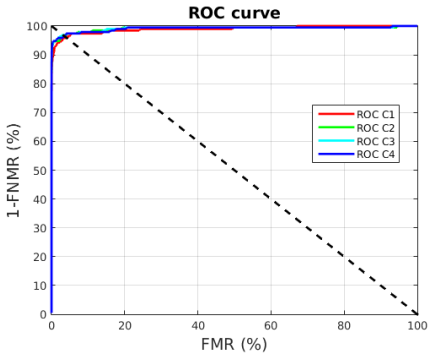

(a) Euclidean distance. C1: dir. 0. C2: dirs. 0,90. C3: dirs. 0, 45, 90. C4: dirs. 0, 45, 90, 135.

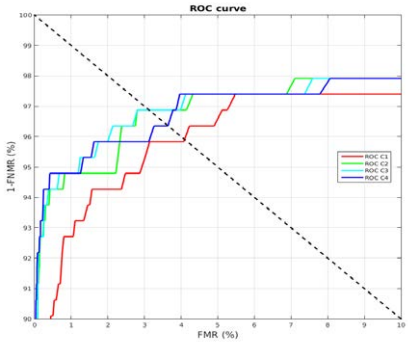

(b) Euclidean distance (zoomed). C1: dir. 0. C2: dirs. 0,90. C3: dirs. 0, 45, 90. C4: dirs. 0, 45, 90, 135.

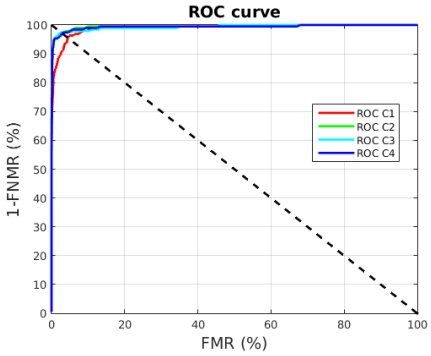

(c) χ^2 distance. C1: dir. 135. C2: dirs. 45, 135. C3: dirs. 0, 45, 135. C4: 16x16 r.s. and dirs. 0, 45, 90, 135.

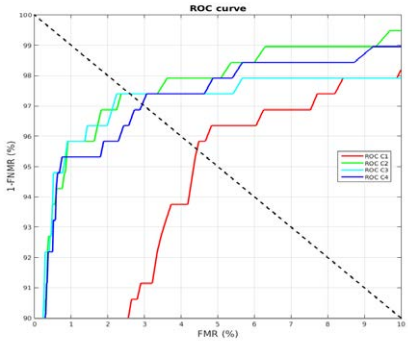

(d) χ^2 distance (zoomed). C1: dir. 135. C2: dirs. 45, 135. C3: dirs. 0, 45, 135. C4: 16x16 r.s. and dirs. 0, 45, 90, 135.

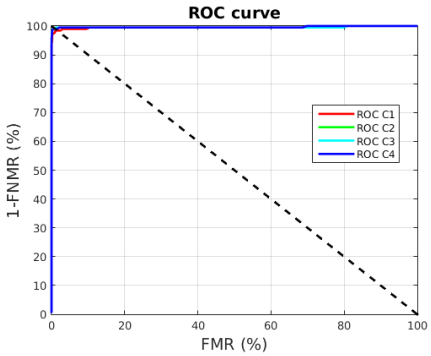

(e) SVMs. C1: dir. 45. C2: dirs. 0,90. C3: 16x16 r.s. and dirs. 0, 45, 90. C4: dirs. 0, 45, 90, 135.

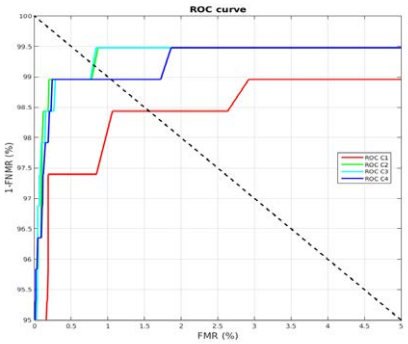

(f) SVMs (zoomed). C1: dir. 45. C2: dirs. 0,90. C3: 16x16 r.s. and dirs. 0, 45, 90. C4: dirs. 0, 45, 90, 135.

Figure 42.: Best palmprint results using LDP as feature extraction method under realistic conditions. Each graphic compares different configurations of directions (dir) when region size is set to 16x16.

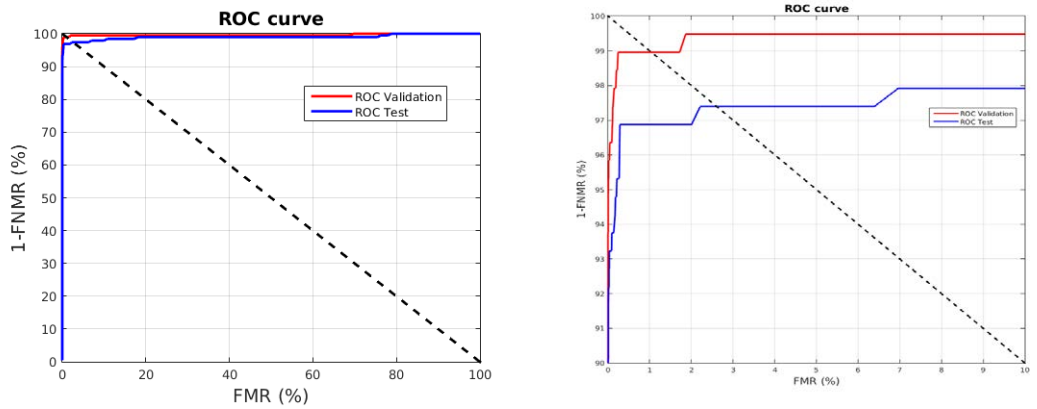

(a) ROC (b) ROC (zoomed)

Figure 43.: Validation and Test results obtained when features are extracted using LDP and compared by SVMs under realistic conditions. Region size is set to 16x16 and the involved directions are 0^o, 45^o, 90^o and 135^o.

10.2.5 *Curvelet*

In this case, the whole set of experiments have been repeated due to monomodal results under controlled conditions do not provide a clearly better combination of bands. Table 34 and Table 35 present the results of the evaluation under realistic conditions for Curvelet feature extraction when Euclidean distance and SVMs are employed to compare features respectively.

Algorithm Parameters		Results		
		Validation	Test	
Bands	PCA	EER (%)	FMR (%)	FNMR (%)
1	No	7.50	8.16	8.33
2	No	16.67	17.19	19.27
3	No	22.64	24.48	20.83
4	No	14.06	14.99	17.19
1, 2	No	8.33	9.06	8.33
1, 3	No	7.81	8.46	8.33
1, 4	No	7.77	8.44	8.33
2, 3	No	18.23	18.98	19.79
2, 4	No	16.67	17.33	17.71
3, 4	No	18.87	20.52	20.31
1, 2, 3	No	8.33	9.07	8.33
1, 2, 4	No	8.33	9.05	8.33
1, 3, 4	No	7.81	8.45	8.33
2, 3, 4	No	17.71	18.66	19.27
1, 2, 3, 4	No	8.33	9.04	8.33
1	Yes	7.51	8.17	8.33
2	Yes	15.63	16.15	16.67

Algorithm Parameters		Results		
		Validation	Test	
Bands	PCA	EER (%)	FMR (%)	FNMR (%)
3	Yes	14.01	14.47	14.58
4	Yes	8.18	8.45	11.98
1, 2	Yes	7.77	8.39	8.33
1, 3	Yes	7.30	8.01	8.33
1, 4	Yes	7.45	8.07	8.33
2, 3	Yes	14.39	14.73	15.63
2, 4	Yes	14.12	14.41	17.19
3, 4	Yes	11.24	11.52	15.10
1, 2, 3	Yes	7.55	8.23	8.33
1, 2, 4	Yes	7.64	8.32	8.33
1, 3, 4	Yes	7.29	8.02	8.33
2, 3, 4	Yes	13.54	13.90	15.10
1, 2, 3, 4	Yes	7.48	8.15	5.33

Table 34.: Palmprint Results using Curvelets to extract features and Euclidean distance to compare under realistic conditions.

Algorithm Parameters		Results		
		Validation	Test	
Bands	PCA	EER (%)	FMR (%)	FNMR (%)
1	No	1.37	1.34	3.65
2	No	8.04	7.36	12.50
3	No	10.94	9.62	14.58
4	No	6.87	5.64	7.29
1, 2	No	2.26	2.32	3.65
1, 3	No	1.53	1.59	3.65
1, 4	No	1.04	0.98	3.13
2, 3	No	7.81	7.00	11.98
2, 4	No	7.54	6.78	9.90
3, 4	No	9.74	8.33	10.94
1, 2, 3	No	1.79	1.80	4.17
1, 2, 4	No	1.09	1.17	3.13
1, 3, 4	No	1.07	1.06	3.65
2, 3, 4	No	6.77	5.86	11.46
1, 2, 3, 4	No	1.04	1.05	2.60
1	Yes	1.04	1.01	3.65
2	Yes	8.24	7.50	10.94
3	Yes	8.95	7.87	11.98
4	Yes	5.85	4.85	7.81
1, 2	Yes	1.46	1.35	2.08
1, 3	Yes	1.08	1.02	4.17
1, 4	Yes	1.06	1.01	4.17

Algorithm Parameters		Results		
		Validation	Test	
Bands	PCA	EER (%)	FMR (%)	FNMR (%)
2, 3	Yes	8.20	7.49	11.46
2, 4	Yes	8.33	7.58	10.94
3, 4	Yes	7.84	6.81	12.50
1, 2, 3	Yes	1.07	1.06	4.17
1, 2, 4	Yes	1.04	1.13	3.13
1, 3, 4	Yes	1.47	1.38	3.13
2, 3, 4	Yes	7.36	6.70	10.94
1, 2, 3, 4	Yes	1.04	0.97	3.13

Table 35.: Palmprint Results using Curvelets to extract features and SVMs to compare under realistic conditions.

Figure 44 depicts a comparison between the best validation results obtained when Curvelet is applied as feature extraction method under realistic conditions. Figures 44a and 44b compare the results obtained using Euclidean distance while Figures 44c and 44d compare the results obtained employing SVMs. Each graphic compares the results obtained by different configurations of parameter *bands*. PCA is applied for dimensionality reduction. Validation and Test results of the best case, which corresponds to bands 1, 2, 3 and 4, are compared in Figure 45.

10.3 HAND GEOMETRY

Table 36 presents the results of the evaluation under realistic conditions for Hand Geometry feature extraction.

Figure 46 depicts a comparison between validation results obtained when hand geometry features are extracted under controlled conditions. 30 features per finger are extracted and thumb is not included in the pattern. The graphic compares the results obtained when Euclidean distance and SVMs are used as matching approaches. Validation and Test results of the best case, which corresponds to 30 features per finger and SVMs, are compared in Figure 47.

Algorithm Parameters			Results		
			Validation	Test	
♯Features	Thumb	Comparison Method	EER (%)	FMR (%)	FNMR (%)
30	No	Euclidean Distance	12.28	13.02	13.54
30	No	SVMs	6.88	6.36	7.29

Table 36.: Hand Geometry Results under realistic conditions.

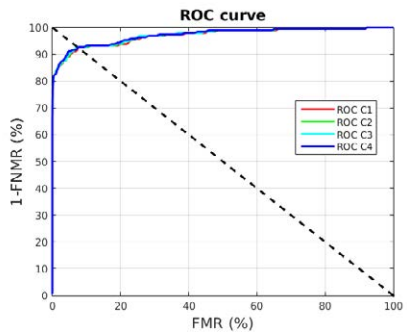

(a) Euclidean distance. C1: band 1. C2: bands 1 and 4. C3: bands 1, 3 and 4. C4: bands 1, 2, 3 and 4.

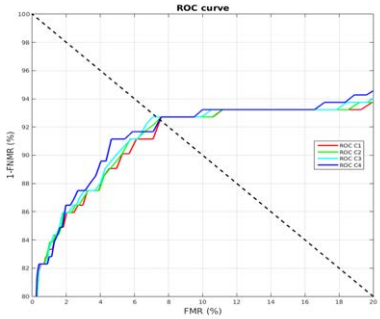

(b) Euclidean distance (zoomed). C1: band 1. C2: bands 1 and 4. C3: bands 1, 3 and 4. C4: bands 1, 2, 3 and 4.

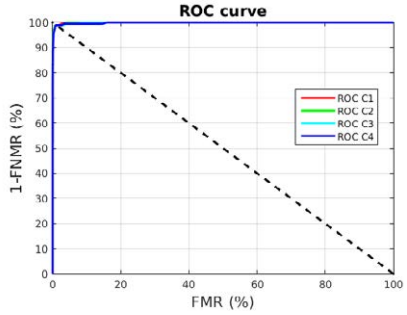

(c) SVMs. C1: band 1. C2: bands 1 and 4. C3: bands 1, 2 and 4. C4: bands 1, 2, 3 and 4.

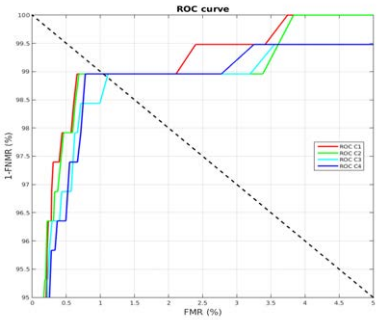

(d) SVMs (zoomed). C1: band 1. C2: bands 1 and 4. C3: bands 1, 2 and 4. C4: bands 1, 2, 3 and 4.

Figure 44.: Best palmprint results using Curvelet as feature extraction method and PCA under realistic conditions. Each graphic compares different configurations of parameter *bands*.

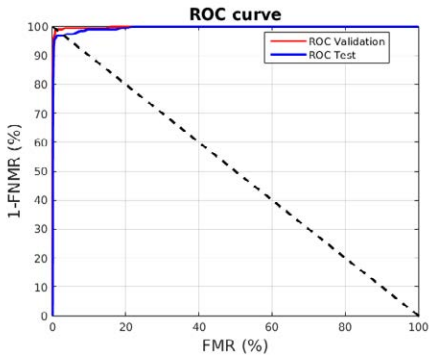

(a) ROC

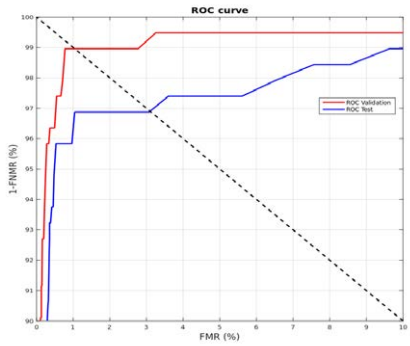

(b) ROC (zoomed)

Figure 45.: Validation and Test results obtained when features are extracted using Curvelet and compared by SVMs under realistic conditions. PCA is applied and 1, 2, 3 and 4 bands are involved in the feature extraction process.

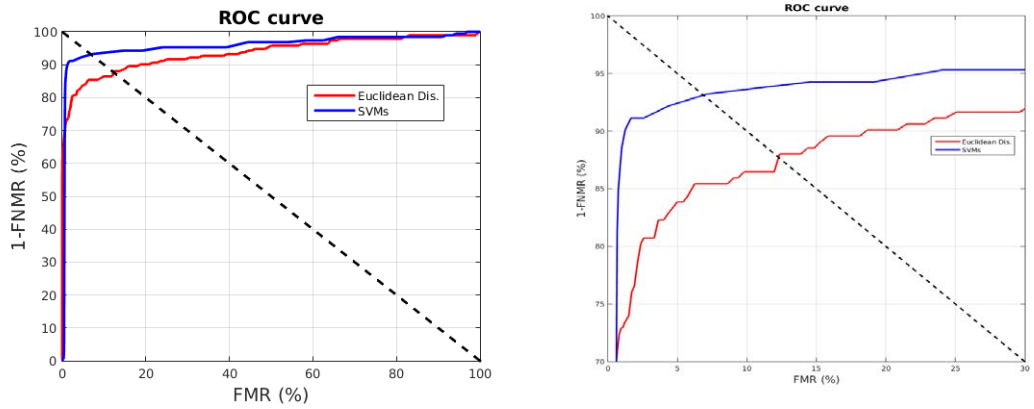

(a) Euclidean distance and SVMs comparison. (b) Euclidean distance and SVMs comparison (zoomed).

Figure 46.: Best hand geometry results under realistic conditions.

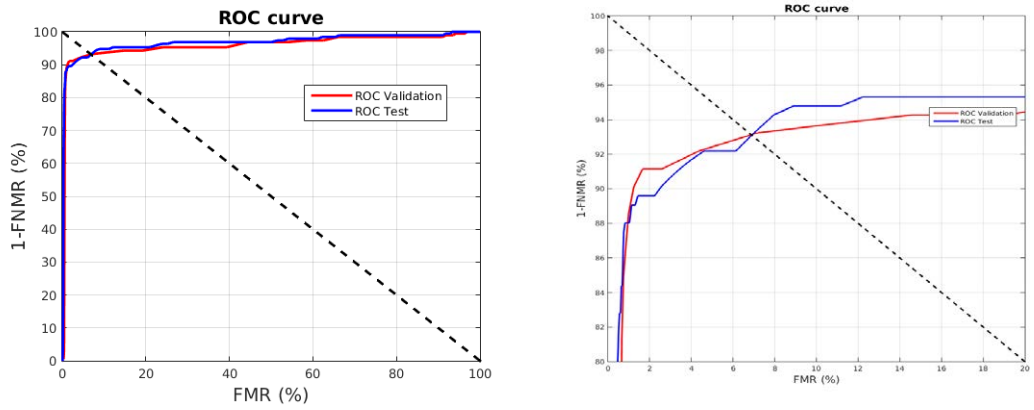

(a) ROC (b) ROC (zoomed)

Figure 47.: Validation and Test results obtained when hand geometry features are extracted using 30 features per finger, thumb is excluded, and compared by SVMs under realistic conditions.

10.4 ANALYSIS OF THE RESULTS

In view of the obtained results, a clear decrease on the performance with respect to the results under controlled conditions can be appreciated for every feature extraction independently on the comparison method. This highlights that lighting conditions not only influences the segmentation but also the feature extraction process.

A decrease on segmentation accuracy directly influences the extraction and alignment of the ROI, which is a crucial step for texture-based palmprint recognition. Most of texture recognition methods are sensitive to small translation and rotation variations of the analysed region. Even when it is possible to align and crop the ROI, there are variations in the texture captured by the camera due to illumination changes which also influences the recognition results.

As can be expected, hand geometry is more affected than palmprint. In addition to the problems that affect the segmentation process, which can lead into non-precise contour detection, it needs to deal with those drawbacks derived from the absence of pose restrictions during the capture. Small variations on the pose can derive into considerable variations of the silhouette of the projected hand, producing intra-user variations that clearly reduce the hand geometry recognition accuracy.

11

MULTIMODAL EVALUATION UNDER REALISTIC CONDITIONS

11.1 INTRODUCTION

This chapter presents an evaluation of different fusions of palmprint and hand geometry feature extraction methods presented in Chapter 5. The aim of this evaluation is to check to what extent the combination of multiple biometric modalities allows to increase the overall accuracy taking advantage of the strengths of each single modality, compensating the limitations derived from their nature and the capturing conditions.

Two fusion levels have been implemented in this thesis, as described in Chapter 7: score-level fusion and feature-level fusion. Scores as well as features need to be normalized previously to the fusion. To this end, min-max and z-score normalizations have been applied and compared. In addition, four rules have been tested for score-level fusion: min, max, sum and product. Moreover, for each fusion level two kinds of multibiometrics have been considered depending on the trait(s) involved in the fusion. On the one hand, some of the palmprint methods have been combined two-by-two to obtain different palmprint multibiometric approaches that allows for the evaluation of the intra-modal fusion. On the other hand, one or more palmprint methods have been fused with the hand geometry approach to evaluate different hand multibiometric solutions.

It has been decided to evaluate the multibiometric solutions under realistic conditions due to it is more challenging than the evaluation under controlled conditions, which already presents very good accuracy rates. To this end, gb2s_ID database have been employed keeping the same division of samples than monomodal evaluation under realistic conditions in order to make equitable comparisons. Each method involved in the fusion has been configured with the parameters that provides better results during the monomodal evaluation. In those cases that more than one parameter configuration provide the best accuracy, faster parameter combinations have been chosen. Particularly, images have been resized to 32×32 px. and threshold has been established into 0.1 for Sobel filter. In the case of Gabor filter, the values for filter size, frequency and σ parameters are 17×17, 0.0916 and 5.6179 respectively. Unary patterns, 8-neighbourhood and radio equal to 1 are employed for LBP feature extraction, while region size parameter takes value 8×8 when LBP is combined with distance-based matching and value 16×16 when SVMs are used for comparison. In the case of LDP, region size parameter is set to 16×16 and directions 0, 45 and 90 are involved in the feature extraction process. When Curvelets are combined with Euclidean distance just band 1 information is included in the feature vector, while band 3 information is

also added in the case that SVMs are used for feature matching. Finally, 30 widths per finger excluding the thumb are extracted for hand geometry recognition.

Multimodal evaluation results under realistic conditions are presented below.

11.2 SCORE LEVEL FUSION

11.2.1 *Palmprint multibiometrics*

11.2.1.1 *Sobel and Gabor Score-Level fusion*

Table 37 and Table 38 show the results of fusing Sobel and Gabor filter at score level when Euclidean distance and SVMs are used to obtain the matching scores respectively. In general, a small improvement can be seen in relation to monomodal results when Euclidean distance is employed, while SVMs almost maintain the accuracy of the best monomodal method. More in detail, results show that the rule which provides better results for Sobel and Gabor fusion is the min rule. In addition, it can be seen that both normalization techniques provide very similar results, which are almost identical in the case of Euclidean distance comparison.

Normalization Rule	Fusion Rule	w1	w2	Validation	Test	
				EER (%)	FMR (%)	FNMR (%)
min-max	sum	0.4111	0.6323	1.23	0	32.29
min-max	product	0.6955	0.7852	1.56	1.58	4.69
min-max	min	0.1652	0.5676	1.15	1.16	5.73
min-max	max	0.4174	0.3809	1.56	0.96	5.73
z-score	sum	0.3911	0.0630	1.23	0	28.13
z-score	product	0.6955	0.7852	1.56	2.40	4.17
z-score	min	0.2902	0.8894	1.15	3.53	3.13
z-score	max	0.7730	0.7513	1.56	2.64	4.69

Table 37.: Palmprint multibiometrics fusing Sobel and Gabor feature extraction methods at score level when Euclidean distance is used to compare. w1 and w2 stands for the weights given to Sobel and Gabor methods respectively.

Normalization Rule	Fusion Rule	w1	w2	Validation	Test	
				EER (%)	FMR (%)	FNMR (%)
min-max	sum	0.8825	0.8265	1.04	95.33	0
min-max	product	0.4285	0.5767	1.04	1.12	5.21
min-max	min	0.5816	0.9843	1.04	1.04	4.17
min-max	max	0.8181	0.8178	1.04	13.24	4.17
z-score	sum	0.4190	0.2917	1.04	15.73	1.56
z-score	product	1.8646	0.5927	1.92	2.01	6.25
z-score	min	0.0615	0.0329	1.02	0.21	5.21
z-score	max	0.5208	0.6600	1.04	2.91	1.56

Table 38.: Palmprint multibiometrics fusing Sobel and Gabor feature extraction methods at score level when SVMs are used to compare. w1 and w2 stands for the weights given to Sobel and Gabor methods respectively.

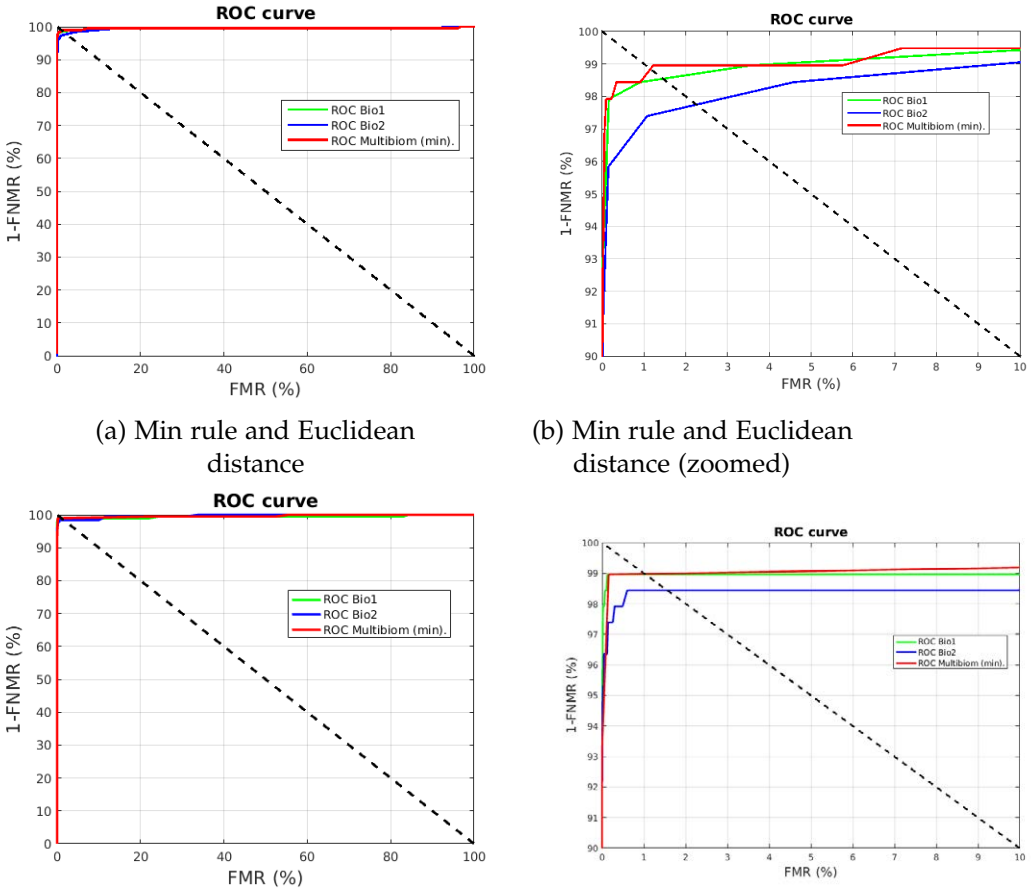

(a) Min rule and Euclidean distance

(b) Min rule and Euclidean distance (zoomed)

(c) Min rule and SVMs

(d) Min rule and SVMs (zoomed)

Figure 48.: Best score level fusion results involving Sobel (Bio1) and Gabor (Bio2) feature extraction methods when min-max normalization is applied.

Figure 48 depicts the best validation results of Sobel and Gabor fusion at score level when Euclidean distance and SVMs are used to obtain the matching scores and min-max normalization is applied. In addition, the corresponding monomodal results can also be seen in the figure.

11.2.1.2 *LBP and LDP Score-level fusion*

Table 39 and Table 40 show the results of LBP and LDP fusion at score level when Euclidean distance and SVMs are used to obtain the matching scores respectively. In general, a small improvement can be seen in relation to monomodal results when Euclidean distance is employed for some rules, while accuracy is maintained or decreased for SVMs. More in detail, sum and min are the rules that allows for certain improvement. In addition, it can be seen that both normalization techniques provide very similar results, which are almost identical in the case of Euclidean distance comparison.

Figure 49 shows the best validation results of LBP and LDP fusion at score level when Euclidean distance and SVMs are used to obtain the matching scores and min-

max normalization is applied. In addition, the corresponding monomodal results can also be seen in the figure.

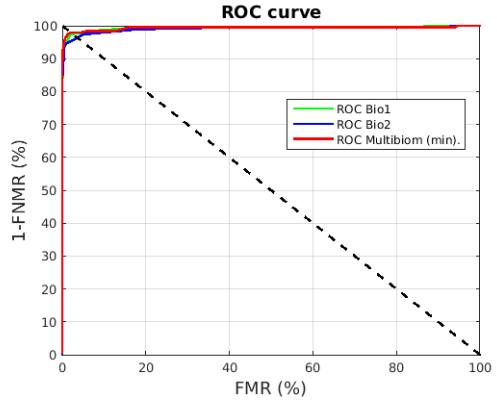

(a) Min rule and Euclidean distance

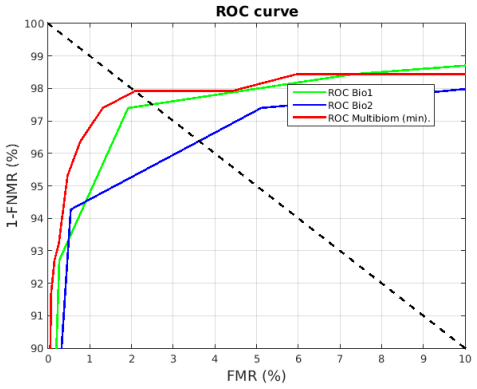

(b) Min rule and Euclidean distance (zoomed)

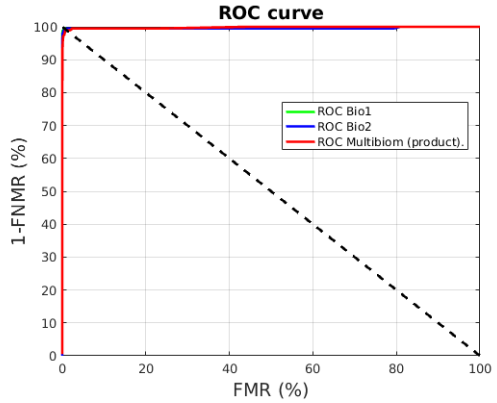

(c) Product rule and SVMs

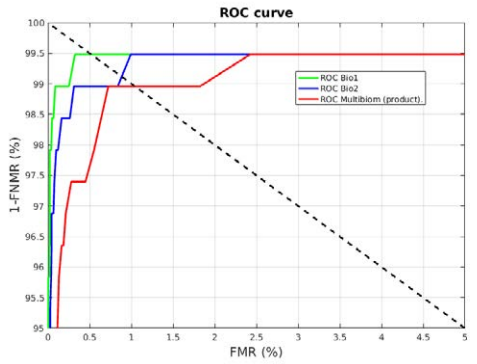

(d) Product rule and SVMs (zoomed)

Figure 49.: Best score level fusion results involving LBP (Bio1) and LDP (Bio2) feature extraction methods when min-max normalization is applied.

Normalization Rule	Fusion Rule	w1	w2	Validation	Test	
				EER (%)	FMR (%)	FNMR (%)
min-max	sum	0.9625	0.4159	2.08	0.005	27.60
min-max	product	0.7353	0.4709	2.36	2.62	6.77
min-max	min	0.3145	0.3091	2.08	2.49	5.73
min-max	max	0.7499	0.6162	2.15	0.09	9.90
z-score	sum	0.9625	0.4159	2.08	0.005	28.13
z-score	product	0.9871	0.8807	2.36	2.07	6.77
z-score	min	0.1959	0.2123	2.08	1.73	6.25
z-score	max	0.7143	0.6451	2.14	0.05	10.42

Table 39.: Palmprint multibiometrics fusing LBP and LDP feature extraction methods at score level when Euclidean distance is used to compare. w1 and w2 stands for the weights given to LBP and LDP methods respectively.

Normalization Rule	Fusion Rule	w1	w2	Validation	Test	
				EER (%)	FMR (%)	FNMR (%)
min-max	sum	0.6569	0.0422	0.52	95.50	0
min-max	product	0.0054	0.4813	0.52	0.38	3.13
min-max	min	0.0192	0.1746	0.52	0.43	3.13
min-max	max	0.5244	0.4237	0.52	39.91	2.60
z-score	sum	0.3329	0.4994	0.52	11.00	1.56
z-score	product	0.3916	0.3418	1.04	1.00	3.65
z-score	min	0.3129	0.4272	0.52	0.37	3.13
z-score	max	0.2971	0.0641	0.52	9.89	2.60

Table 40.: Palmprint multibiometrics fusing LBP and LDP feature extraction methods at score level when SVMs are used to compare. w1 and w2 stands for the weights given to LBP and LDP methods respectively.

11.2.1.3 *Sobel and Curvelets Score-Level fusion*

Table 41 and Table 42 show the results of fusing Sobel filter and Curvelets at score level when Euclidean distance and SVMs are used to obtain the matching scores respectively. In general, a small improvement can be seen in relation to monomodal results for some rules when Euclidean distance is employed, while SVMs almost maintain the accuracy of the best monomodal method. Regarding normalization approaches, it can be seen that both normalization techniques provide very similar results, which are almost identical in the case of Euclidean distance comparison. More in detail, for Euclidean distance comparison sum as well as min rules improve the monomodal results. When scores are obtained by means of SVMs certain improvement is obtained with min rule and z-score normalization.

Normalization Rule	Fusion Rule	w1	w2	Validation	Test	
				EER (%)	FMR (%)	FNMR (%)
min-max	sum	0.9775	0.0030	1.16	0	32.81
min-max	product	0.0460	0.9075	1.99	2.05	5.21
min-max	min	0.0720	0.9975	1.15	1.16	5.73
min-max	max	0.3923	0.9091	1.56	0	11.46
z-score	sum	0.6825	0.0047	1.16	0	26.56
z-score	product	0.2803	0.0296	1.99	7.66	3.65
z-score	min	0.0241	0.6855	1.15	3.56	3.13
z-score	max	0.0933	0.5220	1.56	0	8.85

Table 41.: Palmprint multibiometrics fusing Sobel and Curvelets feature extraction methods at score level when Euclidean distance is used to compare. w1 and w2 stands for the weights given to Sobel and Curvelets methods respectively.

Figure 50 illustrates the best validation results of Sobel and Curvelets fusion at score level when Euclidean distance and SVMs are used to obtain the matching scores and min-max normalization is applied. In addition, the corresponding monomodal results can also be seen in the figure.

Normalization Rule	Fusion Rule	w1	w2	Validation	Test	
				EER (%)	FMR (%)	FNMR (%)
min-max	sum	0.3873	0.5523	1.04	99.23	0
min-max	product	0.8259	0.6410	1.04	1.11	4.17
min-max	min	0.7364	0.3841	1.04	1.00	3.65
min-max	max	0.6291	0.6860	1.04	82.07	0
z-score	sum	0.0804	0.0994	1.04	16.77	1.04
z-score	product	0.4861	0.2186	1.20	1.10	6.25
z-score	min	0.6677	0.1364	0.90	0.71	3.65
z-score	max	0.5282	0.3085	1.04	0.42	1.04

Table 42.: Palmprint multibiometrics fusing Sobel and Curvelets feature extraction methods at score level when SVMs are used to compare. w1 and w2 stands for the weights given to Sobel and Curvelets methods respectively.

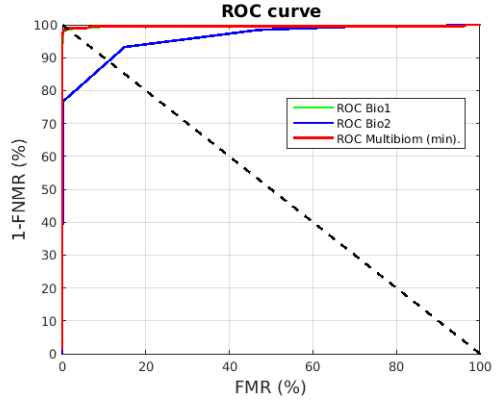

(a) Min rule and Euclidean distance

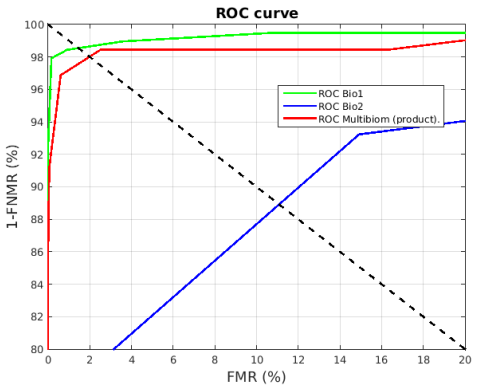

(b) Min rule and Euclidean distance (zoomed)

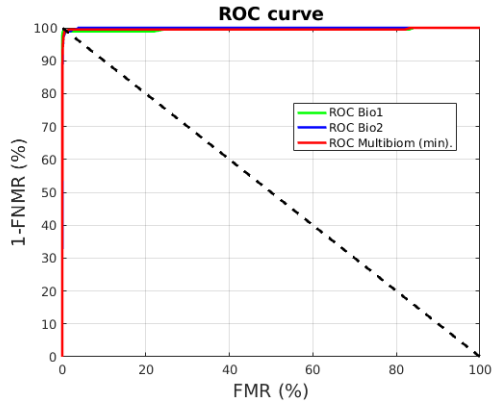

(c) Min rule and SVMs

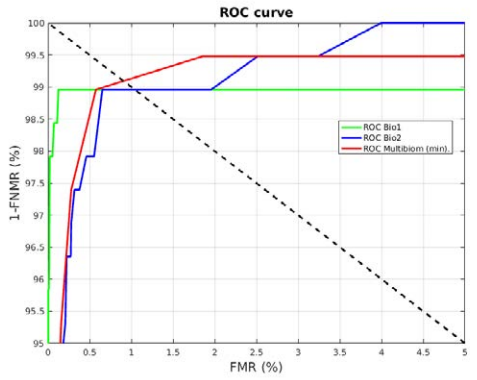

(d) Min rule and SVMs (zoomed)

Figure 50.: Best score level fusion results involving Sobel (Bio1) and Curvelets (Bio2) feature extraction methods when min-max normalization is applied.

11.2.1.4 *LBP and Curvelets Score-level fusion*

Table 43 and Table 44 show the results of fusing LBP and Curvelets at score level when Euclidean distance and SVMs are used to obtain the matching scores respec-

tively. In general, a small improvement can be seen in relation to monomodal results when Euclidean distance is employed for some rules, while accuracy is maintained or decreased for SVMs. More in detail, results show that sum and min are the rules that allows for certain improvement. In addition, it can be seen that both normalization techniques provide very similar results.

Normalization Rule	Fusion Rule	w1	w2	Validation	Test	
				EER (%)	FMR (%)	FNMR (%)
min-max	sum	0.7919	0.1155	2.08	0.005	28.65
min-max	product	0.9381	0.4128	3.61	3.76	5.21
min-max	min	0.0100	0.3518	2.32	2.81	5.21
min-max	max	0.4554	0.5422	2.83	0	11.46
z-score	sum	0.4616	0.1000	2.08	0.005	28.65
z-score	product	0.9381	0.4128	3.61	7.83	3.65
z-score	min	0.0100	0.3518	2.32	2.63	5.73
z-score	max	0.4477	0.9888	3.20	0.25	10.42

Table 43.: Palmprint multibiometrics fusing LBP and Curvelets feature extraction methods at score level when Euclidean distance is used to compare. w1 and w2 stands for the weights given to LBP and Curvelets methods respectively.

Normalization Rule	Fusion Rule	w1	w2	Validation	Test	
				EER (%)	FMR (%)	FNMR (%)
min-max	sum	0.9016	0.0582	0.52	96.09	0
min-max	product	0.8886	0.6128	0.52	0.47	2.60
min-max	min	0.2813	0.6164	0.52	0.43	3.13
min-max	max	0.6472	0.1242	0.52	97.11	0.52
z-score	sum	0.4506	0.6345	0.52	12.46	1.04
z-score	product	0.4672	0.5607	1.20	1.16	4.17
z-score	min	0.0308	0.9327	0.52	0.25	3.13
z-score	max	0.8220	0.2909	0.52	0.24	2.60

Table 44.: Palmprint multibiometrics fusing LBP and Curvelets feature extraction methods at score level when SVMs are used to compare. w1 and w2 stands for the weights given to LBP and Curvelets methods respectively.

Figure 51 depicts the best validation results of LBP and Curvelets fusion at score level when Euclidean distance and SVMs are used to obtain the matching scores and min-max normalization is applied. In addition, the corresponding monomodal results can also be seen in the figure.

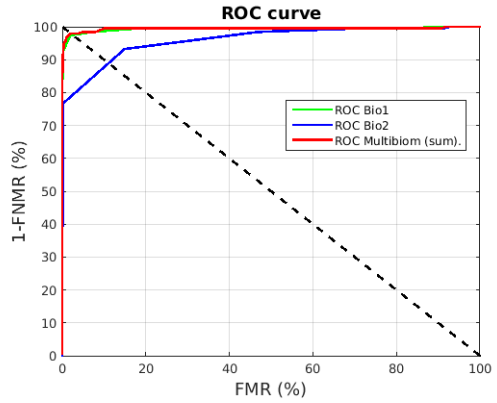

(a) Sum rule and Euclidean distance

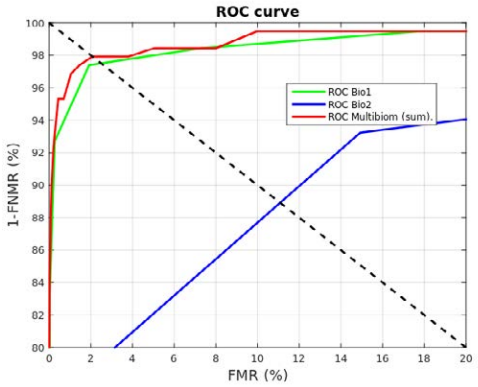

(b) Sum rule and Euclidean distance (zoomed)

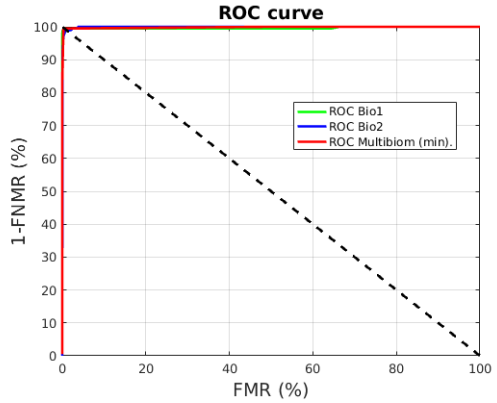

(c) Min rule and SVMs

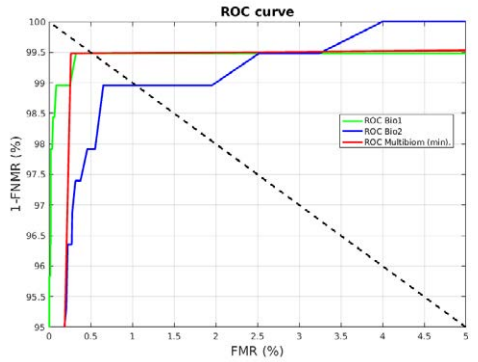

(d) Min rule and SVMs (zoomed)

Figure 51.: Best score level fusion results involving LBP (Bio1) and Curvelets (Bio2) feature extraction methods when min-max normalization is applied.

11.2.1.5 *Sobel and LBP Score-Level fusion*

Table 45 and Table 46 show the results of Sobel filter and LBP fusion at score level when Euclidean distance and SVMs are used to obtain the matching scores respectively. In general, a small improvement can be seen in relation to monomodal results when Euclidean distance is employed in combination with some rules, while accuracy is maintained or decreased for SVMs. In addition, it can be seen that both normalization techniques provide very similar results, which are almost identical in the case of Euclidean distance comparison. More in detail, table 45 results show that sum as well as min and max rules allows to improve monomodal results when Euclidean distance is used for scores calculation.

Figure 52 shows the best validation results of Sobel and LBP fusion at score level when Euclidean distance and SVMs are used to obtain the matching scores and min-max normalization is applied. In addition, the corresponding monomodal results can also be seen in the figure.

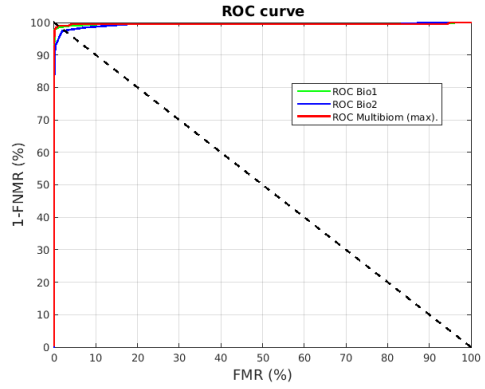

(a) Max rule and Euclidean distance

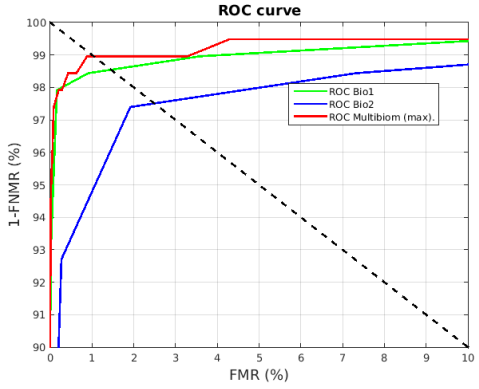

(b) Max rule and Euclidean distance (zoomed)

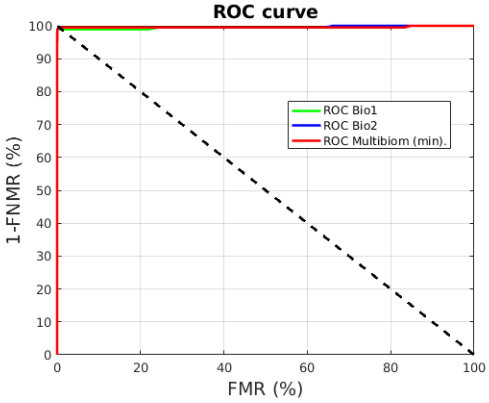

(c) Min rule and SVMs

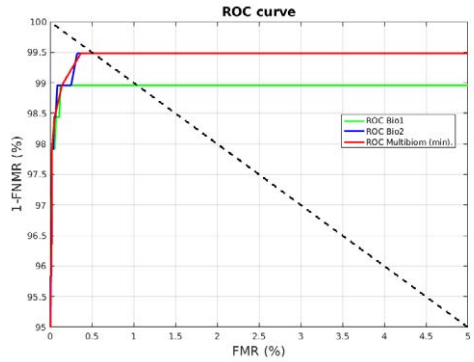

(d) Min rule and SVMs (zoomed)

Figure 52.: Best score level fusion results involving Sobel (Bio1) and LBP (Bio2) feature extraction methods when min-max normalization is applied.

Normalization Rule	Fusion Rule	w1	w2	Validation	Test	
				EER (%)	FMR (%)	FNMR (%)
min-max	sum	0.9679	0.7942	1.04	0	31.25
min-max	product	0.3774	0.2892	1.25	1.50	5.73
min-max	min	0.1556	0.2602	1.04	1.29	6.25
min-max	max	0.5368	0.7413	1.04	0	7.29
z-score	sum	0.0732	0.1652	1.04	0	26.56
z-score	product	0.3774	0.2892	1.25	2.27	4.17
z-score	min	0.2777	0.8658	1.04	1.98	4.69
z-score	max	0.3731	0.8794	1.04	6.08	6.77

Table 45.: Palmprint multibiometrics fusing Sobel and LBP feature extraction methods at score level when Euclidean distance is used to compare. w1 and w2 stands for the weights given to Sobel and LBP methods respectively.

Normalization Rule	Fusion Rule	w1	w2	Validation	Test	
				EER (%)	FMR (%)	FNMR (%)
min-max	sum	0.0194	0.2527	0.52	95.35	0
min-max	product	0.8298	0.1680	1.04	0.94	3.13
min-max	min	0.4965	0.1402	0.52	0.43	3.13
min-max	max	0.6223	0.9190	0.87	33.43	1.56
z-score	sum	0.0752	0.9943	0.52	10.78	2.60
z-score	product	0.1835	0.9888	1.04	0.96	4.17
z-score	min	0.3125	0.0824	0.52	0.40	3.13
z-score	max	0.1019	0.3389	0.62	7.07	2.60

Table 46.: Palmprint multibiometrics fusing Sobel and LBP feature extraction methods at score level when SVMs are used to compare. w1 and w2 stands for the weights given to Sobel and LBP methods respectively.

11.2.2 *Hand multibiometrics*

11.2.2.1 *Sobel and Hand Geometry Score-level fusion*

Table 47 and Table 48 show the results of fusing palmprint information extracted by means of Sobel filter and Hand Geometry at score level when Euclidean distance and SVMs are used to obtain the matching information respectively. In general, a small improvement can be seen in relation to monomodal results for some rules when Euclidean distance is employed, while SVMs almost maintain the accuracy of the best monomodal method. More in detail, for Euclidean distance comparison sum as well as min rules improve the monomodal results. In addition, it can be seen that both normalization techniques provide very similar results in most of the cases and that these results are almost identical in the case of Euclidean distance comparison.

Figure 53 shows the best validation results of Sobel and Hand Geometry fusion at score level when Euclidean distance and SVMs are used to obtain the matching scores and min-max normalization is applied. In addition, the corresponding monomodal results can also be seen in the figure.

Normalization Rule	Fusion Rule	w1	w2	Validation	Test	
				EER (%)	FMR (%)	FNMR (%)
min-max	sum	0.7655	0.1078	1.10	0	32.29
min-max	product	0.8663	0.3459	5.62	6.01	3.65
min-max	min	0.0355	0.7720	0.96	0.95	3.13
min-max	max	0.8526	0.0110	1.36	0	32.29
z-score	sum	0.9593	0.3439	1.10	0	28.65
z-score	product	0.8663	0.3459	5.62	0.14	13.54
z-score	min	0.0166	0.9038	0.96	2.91	3.13
z-score	max	0.7478	0.0110	1.38	0	26.04

Table 47.: Hand multibiometrics fusing Sobel and Hand Geometry feature extraction methods at score level when Euclidean distance is used to compare. w1 and w2 stands for the weights given to Sobel and Hand Geometry methods respectively.

Normalization Rule	Fusion Rule	w1	w2	Validation	Test	
				EER (%)	FMR (%)	FNMR (%)
min-max	sum	0.6059	0.2155	1.04	99.73	0
min-max	product	0.8753	0.0621	1.04	1.07	3.65
min-max	min	0.2656	0.2965	1.04	1.05	4.17
min-max	max	0.7016	0.4906	1.04	58.26	0
z-score	sum	0.6605	0.3109	1.04	14.47	1.04
z-score	product	0.7273	0.9029	4.89	4.02	4.69
z-score	min	0.0585	0.9837	4.01	0.13	7.29
z-score	max	0.4596	0.5196	1.56	18.31	0

Table 48.: Hand multibiometrics fusing Sobel and Hand Geometry feature extraction methods at score level when SVMs are used to compare. w1 and w2 stands for the weights given to Sobel and Hand Geometry methods respectively.

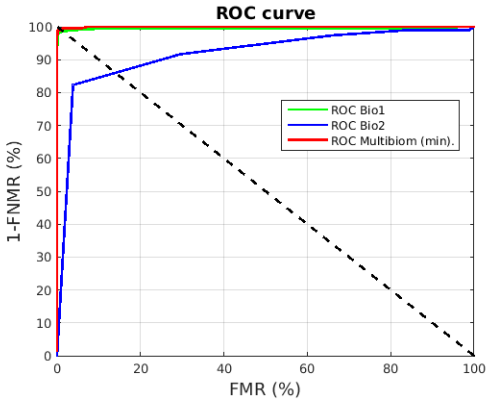

(a) Min rule and Euclidean distance

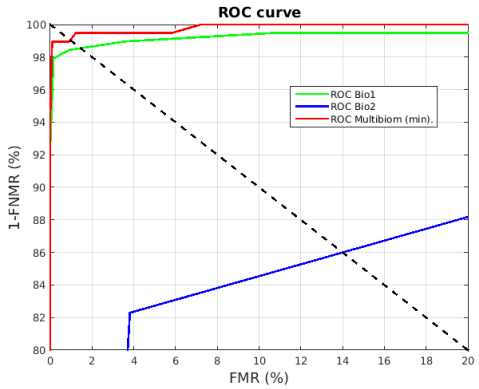

(b) Min rule and Euclidean distance (zoomed)

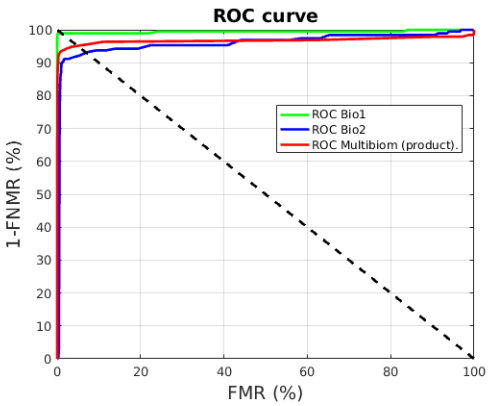

(c) Product rule and SVMs

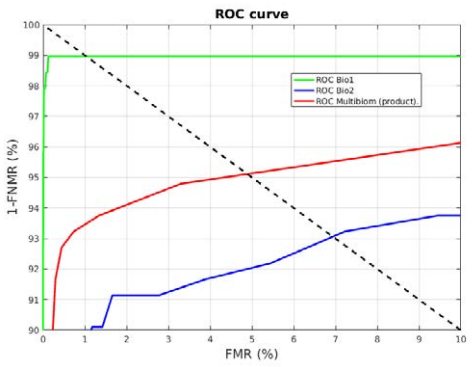

(d) Product rule and SVMs (zoomed)

Figure 53.: Best score level fusion results involving Sobel (Bio1) and Hand Geom. (Bio2) feature extraction methods when min-max normalization is used.

11.2.2.2 *Gabor and Hand Geometry Score-level fusion*

Table 49 and Table 50 show the results of fusing palmprint information extracted by means of Gabor filter and hand geometry information at score level when Euclidean distance and SVMs are used to obtain the matching scores respectively. In general, a small improvement can be seen in relation to monomodal results for some rules. Comparing both normalization techniques it can be seen that both approaches provide very similar results in most of the cases and that these results are almost identical in the case of Euclidean distance comparison. More in detail, for Euclidean distance comparison min rule improve the monomodal results while for SVMs the rule which improves the results for both normalizations is the sum rule. In addition, it can be seen that results are also improved when z-score normalization and max rule are applied in the case of SVMs comparison.

Figure 54 shows the best validation results of Gabor and Hand Geometry fusion at score level when Euclidean distance and SVMs are used to obtain the matching scores and min-max normalization is applied. In addition, the corresponding monomodal results can also be seen in the figure.

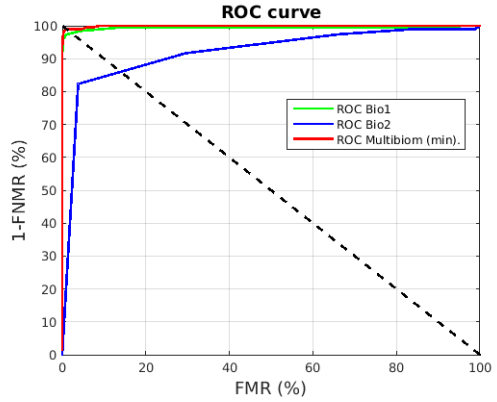

(a) Min rule and Euclidean distance

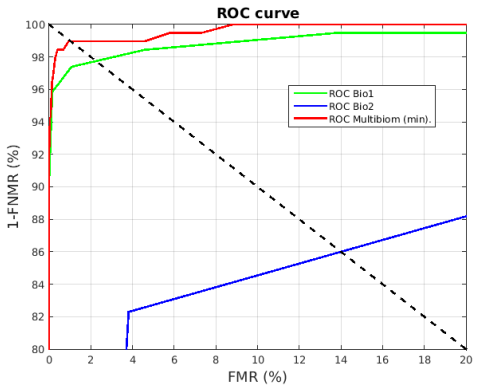

(b) Min rule and Euclidean distance (zoomed)

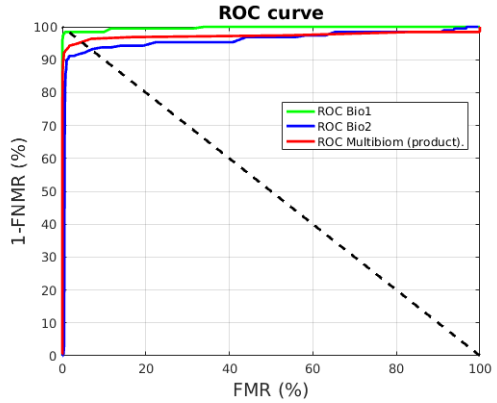

(c) Product rule and SVMs

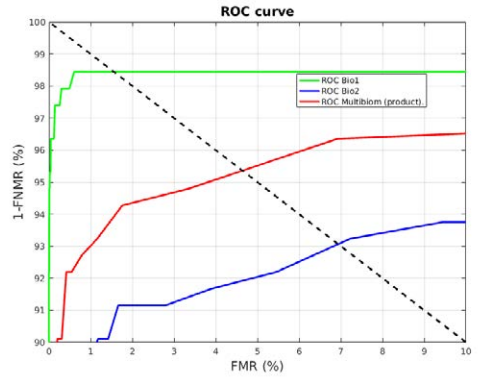

(d) Product rule and SVMs (zoomed)

Figure 54.: Best score level fusion results involving Gabor (Bio1) and Hand Geom. (Bio2) feature extraction methods when min-max normalization is used.

Normalization Rule	Fusion Rule	w1	w2	Validation	Test	
				EER (%)	FMR (%)	FNMR (%)
min-max	sum	0.8032	0.1463	1.56	0	34.90
min-max	product	0.7458	0.0945	5.86	6.09	4.17
min-max	min	0.0374	0.6839	1.04	1.01	3.65
min-max	max	0.5197	0.1747	2.08	0	31.77
z-score	sum	0.8032	0.1453	1.56	0	36.46
z-score	product	0.8950	0.2604	5.86	0.04	16.67
z-score	min	0.0196	0.8580	1.04	0.66	7.29
z-score	max	0.7669	0.6333	2.80	0	31.77

Table 49.: Hand multibiometrics fusing Gabor and Hand Geometry feature extraction methods at score level when Euclidean distance is used to compare. w1 and w2 stands for the weights given to Gabor and Hand Geometry methods respectively.

Normalization Rule	Fusion Rule	w1	w2	Validation	Test	
				EER (%)	FMR (%)	FNMR (%)
min-max	sum	0.2917	0.9915	1.19	1	0
min-max	product	0.2946	0.1521	1.56	1.70	3.65
min-max	min	0.4033	0.8553	1.56	1.63	4.17
min-max	max	0.7364	0.4766	1.56	57.87	0
z-score	sum	0.8715	0.8622	1.19	14.76	0
z-score	product	0.4736	0.1332	4.64	4.16	4.69
z-score	min	0.0476	0.4644	4.01	0.67	6.77
z-score	max	0.1520	0.1853	1.40	43.84	0.52

Table 50.: Hand multibiometrics fusing Gabor and Hand Geometry feature extraction methods at score level when SVMs are used to compare. w1 and w2 stands for the weights given to Gabor and Hand Geometry methods respectively.

11.2.2.3 *LBP and Hand Geometry Score-level fusion*

Table 51 and Table 52 show the results of fusing palmprint information extracted by means of LBP and hand geometry information at score level when Euclidean distance and SVMs are used to obtain the matching scores respectively. In general, a small improvement can be seen in relation to monomodal results when Euclidean distance is employed in combination with some rules, while accuracy is maintained or decreased for SVMs. More in detail, sum and min are the rules that improve the results when Euclidean distance is used. In addition, it can be seen that both normalization techniques provides very similar results in most of the cases and that these results are almost identical in the case of Euclidean distance comparison.

Figure 55 illustrates the best validation results of LBP and Hand Geometry fusion at score level when Euclidean distance and SVMs are used to obtain the matching scores and min-max normalization is applied. In addition, the corresponding monomodal results can also be seen in the figure.

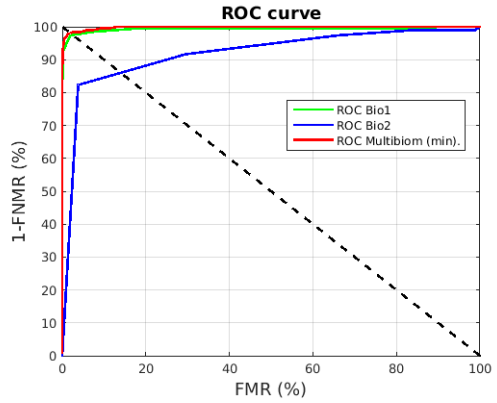

(a) Min rule and Euclidean distance

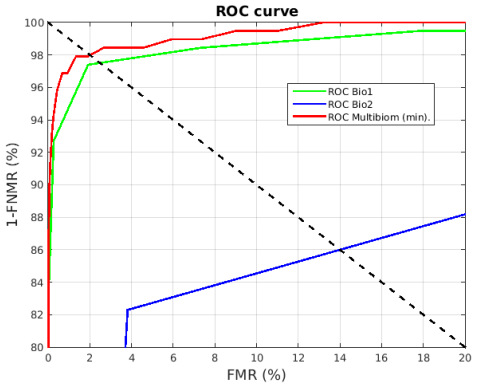

(b) Min rule and Euclidean distance (zoomed)

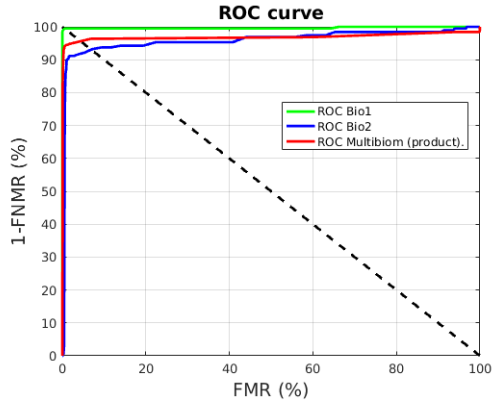

(c) Product rule and SVMs

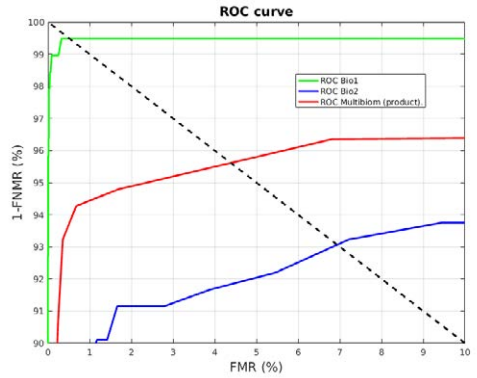

(d) Product rule and SVMs (zoomed)

Figure 55.: Best score level fusion results involving LBP (Bio1) and Hand Geom. (Bio2) feature extraction methods when min-max normalization is used.

Normalization Rule	Fusion Rule	w1	w2	Validation	Test	
				EER (%)	FMR (%)	FNMR (%)
min-max	sum	0.3312	0.0399	2.08	0.0055	28.65
min-max	product	0.2917	0.3756	5.70	6.30	3.13
min-max	min	0.0775	0.7524	2.01	2.51	3.65
min-max	max	0.6387	0.0885	2.08	3.09	26.04
z-score	sum	0.4630	0.0862	2.08	0	31.77
z-score	product	0.4753	0.0594	5.70	0.16	11.98
z-score	min	0.0147	0.2216	2.01	2.28	5.73
z-score	max	0.9088	0.1995	2.08	3.23	26.04

Table 51.: Hand multibiometrics fusing LBP and Hand Geometry feature extraction methods at score level when Euclidean distance is used to compare. w1 and w2 stands for the weights given to LBP and Hand Geometry methods respectively.

Normalization Rule	Fusion Rule	w1	w2	Validation	Test	
				EER (%)	FMR (%)	FNMR (%)
min-max	sum	0.7749	0.3219	0.52	99.85	0
min-max	product	0.7052	0.7012	0.52	0.42	3.13
min-max	min	0.0129	0.2168	0.52	0.43	3.13
min-max	max	0.9870	0.2186	0.52	20.27	0.52
z-score	sum	0.8004	0.4435	0.52	9.12	2.08
z-score	product	0.2985	0.7625	4.39	2.98	5.21
z-score	min	0.0444	0.7310	3.54	0.44	5.21
z-score	max	0.5024	0.1750	0.52	20.53	2.60

Table 52.: Hand multibiometrics fusing LBP and Hand Geometry feature extraction methods at score level when SVMs are used to compare. w1 and w2 stands for the weights given to LBP and Hand Geometry methods respectively.

11.2.2.4 *LDP and Hand Geometry Score-level fusion*

Table 53 and Table 54 show the results of fusing palmprint information extracted by means of LDP and hand geometry information at score level when Euclidean distance and SVMs are used to obtain the matching scores respectively. In general, a small improvement can be seen in relation to monomodal results for some rules and both comparison methods. In addition, it can be seen that both normalization techniques provide very similar results in most of the cases and that these results are almost identical in the case of Euclidean distance comparison. More in detail, sum and min are the rules that improve the results when Euclidean distance is used to compute the scores while improvement in the case of SVMs depends on the normalization approach. In the case of SVMs and min-max normalization all the rules produce certain increase of the results, while for z-score normalization improvements are only obtained when sum and max rules are applied.

Figure 56 depicts the best validation results of LDP and Hand Geometry fusion at score level when Euclidean distance and SVMs are used to obtain the matching scores

Normalization Rule	Fusion Rule	w1	w2	Validation	Test	
				EER (%)	FMR (%)	FNMR (%)
min-max	sum	0.8711	0.1611	2.94	0	29.69
min-max	product	0.7054	0.8319	6.11	6.09	4.69
min-max	min	0.1361	0.6212	2.60	2.72	3.65
min-max	max	0.9891	0.1991	3.14	0.027	25.00
z-score	sum	0.8015	0.2095	2.94	0	36.46
z-score	product	0.2661	0.5064	6.11	0.14	14.58
z-score	min	0.1529	0.9864	2.60	0.33	9.38
z-score	max	0.9490	0.2703	3.14	0.03	27.08

Table 53.: Hand multibiometrics fusing LDP and Hand Geometry feature extraction methods at score level when Euclidean distance is used to compare. w1 and w2 stands for the weights given to LDP and Hand Geometry methods respectively.

and min-max normalization is applied. In addition, the corresponding monomodal results can also be seen in the figure.

Normalization Rule	Fusion Rule	w1	w2	Validation	Test	
				EER (%)	FMR (%)	FNMR (%)
min-max	sum	0.3507	0.4719	0.52	1	0
min-max	product	0.8922	0.0369	0.52	0.38	3.13
min-max	min	0.7487	0.7075	0.52	0.53	3.65
min-max	max	0.7324	0.0374	0.52	0.027	0
z-score	sum	0.5160	0.1846	0.52	10.65	1.04
z-score	product	0.6556	0.4643	4.62	3.97	4.17
z-score	min	0.0589	0.9393	3.55	0.98	4.69
z-score	max	0.7879	0.1115	0.54	2.22	1.04

Table 54.: Hand multibiometrics fusing LDP and Hand Geometry feature extraction methods at score level when SVMs are used to compare. w1 and w2 stands for the weights given to LDP and Hand Geometry methods respectively.

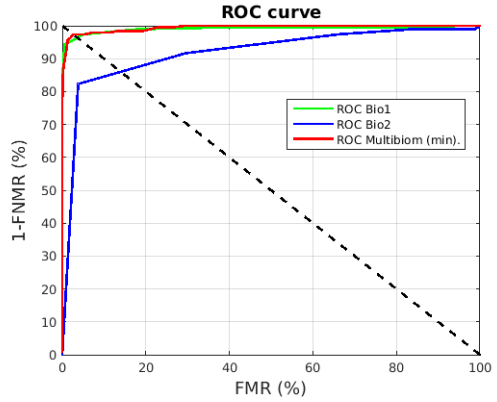

(a) Min rule and Euclidean distance

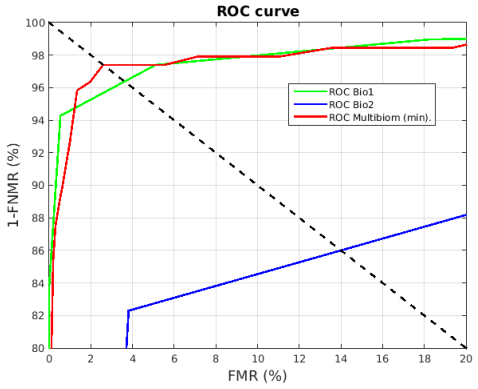

(b) Min rule and Euclidean distance (zoomed)

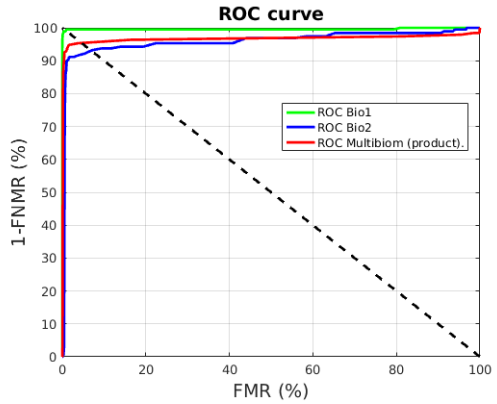

(c) Product rule and SVMs

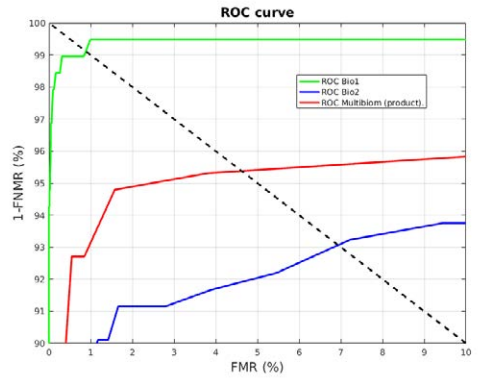

(d) Product rule and SVMs (zoomed)

Figure 56.: Best score level fusion results involving LDP (Bio1) and Hand Geom. (Bio2) feature extraction methods when min-max normalization is used.

11.2.2.5 *Curvelets and Hand Geometry Score-level fusion*

Table 55 and Table 56 show the results of fusing palmprint information extracted by means of Curvelets and hand geometry information at score level when Euclidean distance and SVMs are used to obtain the matching scores respectively. In general, a small improvement can be seen in relation to monomodal results for some rules and both comparison methods. In addition, it can be seen that both normalization techniques provide very similar results in most of the cases and that these results are almost identical in the case of Euclidean distance comparison. More in detail, sum and min are the rules that improve the results when Euclidean distance is used to compute the scores while improvement in the case of SVMs depends on the normalization approach. In the case of SVMs and min-max normalization all the rules produce an increase of the results, while for z-score normalization improvements are only obtained when sum and max rules are employed.

Normalization Rule	Fusion Rule	w1	w2	Validation	Test	
				EER (%)	FMR (%)	FNMR (%)
min-max	sum	0.4756	0.2688	6.94	0	23.44
min-max	product	0.6908	0.1869	8.24	7.81	3.65
min-max	min	0.5359	0.8924	5.98	6.45	4.17
min-max	max	0.6937	0.0642	8.80	3.17	22.92
z-score	sum	0.4267	0.2551	6.94	0	38.02
z-score	product	0.5626	0.7165	8.24	0.79	11.98
z-score	min	0.4693	0.8340	5.98	12.19	5.73
z-score	max	0.4237	0.0412	8.81	0.82	13.02

Table 55.: Hand multibiometrics fusing Curvelets and Hand Geometry feature extraction methods at score level when Euclidean distance is used to compare. w1 and w2 stands for the weights given to Curvelets and Hand Geometry methods respectively.

Normalization Rule	Fusion Rule	w1	w2	Validation	Test	
				EER (%)	FMR (%)	FNMR (%)
min-max	sum	0.5020	0.8106	0.71	1	0
min-max	product	0.4138	0.8475	0.81	0.77	2.08
min-max	min	0.2075	0.2459	1.04	1.04	2.06
min-max	max	0.4623	0.0825	1.02	98.27	0
z-score	sum	0.9454	0.4452	0.71	13.85	0.52
z-score	product	0.9303	0.9751	4.62	3.84	3.13
z-score	min	0.0667	0.5978	3.09	2.38	3.65
z-score	max	0.4172	0.1798	0.74	35.22	1.56

Table 56.: Hand multibiometrics fusing Curvelets and Hand Geometry feature extraction methods at score level when SVMs are used to compare. w1 and w2 stands for the weights given to Curvelets and Hand Geometry methods respectively.

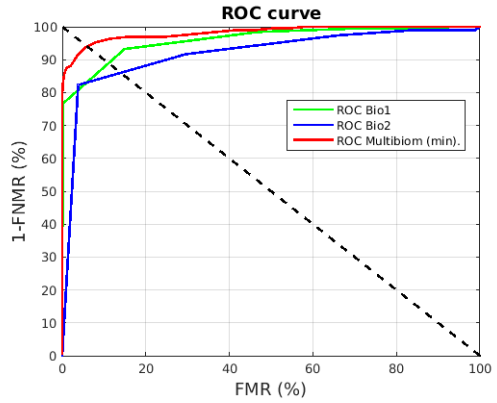

(a) Min rule and Euclidean distance

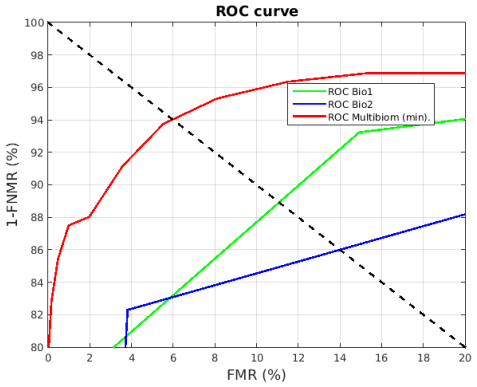

(b) Min rule and Euclidean distance (zoomed)

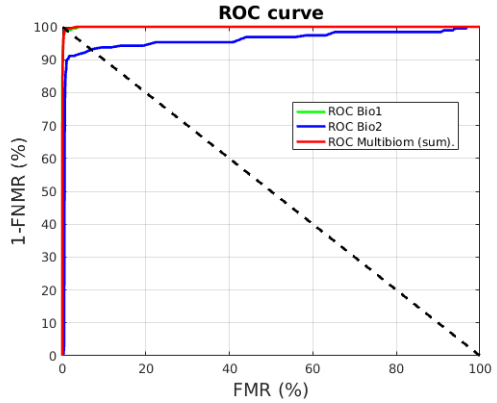

(c) Sum rule and SVMs

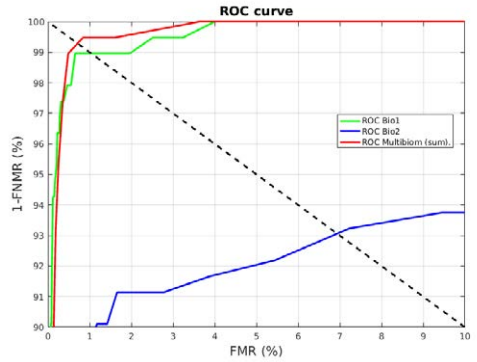

(d) Sum rule and SVMs (zoomed)

Figure 57.: Best score level fusion results involving Curvelets (Bio1) and Hand Geom. (Bio2) feature extraction methods when min-max normalization is used.

Figure 57 shows the best validation results of Curvelets and Hand Geometry fusion at score level when Euclidean distance and SVMs are used to obtain the matching scores and min-max normalization is applied. In addition, the corresponding monomodal results can also be seen in the figure.

11.2.2.6 *Sobel, Gabor and Hand Geometry Score-Level fusion*

Table 57 and Table 58 show the results of fusing palmprint information extracted by means of Sobel filter and Gabor filter together with hand geometry information at score level when Euclidean distance and SVMs are used to obtain the matching scores respectively. In general, a small improvement can be seen in relation to monomodal results for some rules when Euclidean distance is employed, while SVMs maintain or decrease the accuracy of the best monomodal method. In addition, it can be seen that results provided by Sobel-Gabor or Sobel-Geom fusions are in general equalled or decreased, while Gabor-Geom fusion results are slightly improved. It can also be seen that both normalization techniques provide practically identical results. More in detail, for Euclidean distance comparison sum as well as min rules improve the

Normalization Rule	Fusion Rule	w1	w2	w3	Validation	Test	
					EER (%)	FMR (%)	FNMR (%)
min-max	sum	0.1455	0.9841	0.0133	1.11	0	72.92
min-max	product	0.3881	0.0634	0.4907	3.41	3.37	2.08
min-max	min	0.2478	0.0120	0.0949	0.96	7.70	1.56
min-max	max	0.0003	0.7975	0.7260	1.56	0	19.79
z-score	sum	0.3804	0.9937	0.0170	1.12	0	75
z-score	product	0.5945	0.3510	0.4332	3.41	0.13	6.77
z-score	min	0.2135	0.0036	0.0137	0.96	48.02	0.52
z-score	max	0.0187	0.9626	0.9358	1.56	0	17.71

Table 57.: Hand multibiometrics fusing Sobel, Gabor and Hand Geometry feature extraction methods at score level when Euclidean distance is used to compare. w1, w2 and w3 stands for the weights given to Sobel, Gabor and Hand Geometry methods respectively.

Normalization Rule	Fusion Rule	w1	w2	w3	Validation	Test	
					EER (%)	FMR (%)	FNMR (%)
min-max	sum	0.2360	0.6793	0.2450	1.04	99.98	0
min-max	product	0.7181	0.1905	0.7659	1.27	1.28	3.13
min-max	min	0.5973	0.4868	0.7226	1.04	0.31	6.77
min-max	max	0.3802	0.5352	0.4711	1.08	99.99	0
z-score	sum	0.5147	0.7578	0.2088	1.04	39.28	1.04
z-score	product	0.0892	0.3751	0.5263	1.27	21.45	3.13
z-score	min	0.6231	0.6053	0.8808	1.04	7.54	4.17
z-score	max	0.4104	0.5914	0.5473	1.08	49.84	0

Table 58.: Hand multibiometrics fusing Sobel, Gabor and Hand Geometry feature extraction methods at score level when SVMs are used to compare. w1, w2 and w3 stands for the weights given to Sobel, Gabor and Hand Geometry methods respectively.

monomodal results and Sobel-Gabor fusion while product rule improves Sobel-Geom fusion result. Gabor-Geom results are improved for all the possible comparison method and fusion rule combinations.

Figure 58 depicts the best validation results of Sobel, Gabor and Hand Geometry fusion at score level when Euclidean distance and SVMs are used to obtain the matching scores and min-max normalization is applied. In addition, the corresponding monomodal results can also be seen in the figure.

11.2.2.7 *LBP, LDP and Hand Geometry Score-level fusion*

Table 59 and Table 60 show the results of fusing palmprint information extracted by means of LBP and LBP together with hand geometry information at score level when Euclidean distance and SVMs are used to obtain the matching scores respectively. In general, a small improvement can be seen in relation to monomodal results for some rules when Euclidean distance is employed, while SVMs maintain the accuracy of the best monomodal method. In addition, a small improvement can also be seen for some rules in relation to the results provided by two-by-two fusions. Regarding normalization techniques, it can be seen that both approaches provide practically

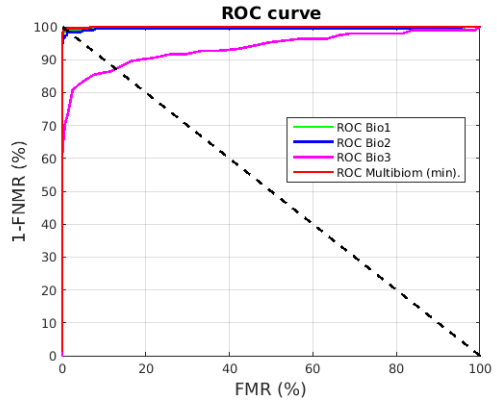

(a) Min rule and Euclidean distance

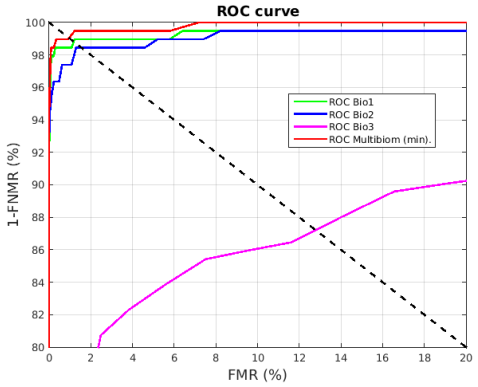

(b) Min rule and Euclidean distance (zoom)

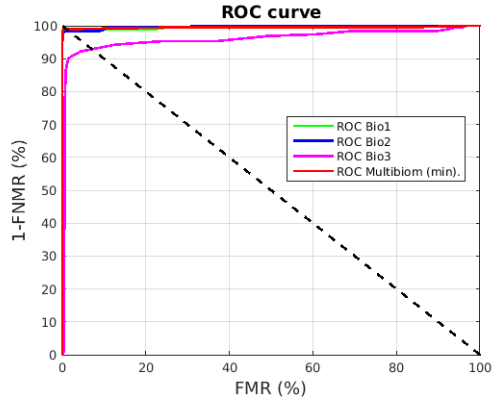

(c) Min rule and SVMs

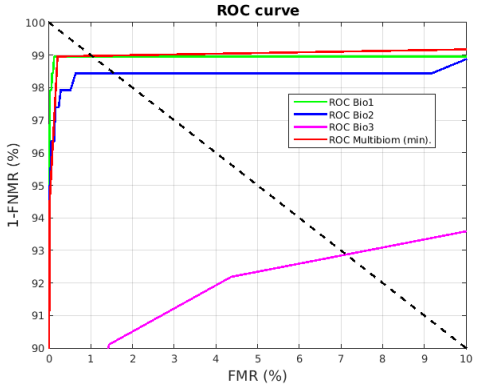

(d) Min rule and SVMs (zoom)

Figure 58.: Best score level fusion results involving Sobel (Bio1), Gabor (Bio2), and Hand Geometry (Bio3) feature extraction methods when min-max normalization is applied.

identical results. More in detail, for Euclidean distance comparison sum and min rules improve the monomodal and LBP-LDP fusion results. The four rules obtain better results when compared to LBP-Geom and LDP-Geom fusions. In the case of SVMs and z-score normalization product rule obtains better results than LBP-LDP, LBP-Geom, LDP-Geom fusions; min rule improves the results achieved by LBP-Geom and LDP-Geom, and max-rule overcome LDP-Geom fusion results.

Figure 59 depicts the best validation results of LBP, LDP and Hand Geometry fusion at score level when Euclidean distance and SVMs are used to obtain the matching scores and min-max normalization is applied. In addition, the corresponding monomodal results can also be seen in the figure.

Normalization Rule	Fusion Rule	w1	w2	w3	Validation	Test	
					EER (%)	FMR (%)	FNMR (%)
min-max	sum	0.0898	0.7723	0.6547	1.94	0	33.85
min-max	product	0.0957	0.2528	0.8683	4.43	4.69	3.13
min-max	min	0.8218	0.0902	0.0909	1.56	87.82	0
min-max	max	0.1948	0.9346	0.7394	2.40	0.049	15.63
z-score	sum	0.1771	0.9493	0.8823	1.93	0	42.19
z-score	product	0.4723	0.3174	0.8200	4.43	0.27	8.33
z-score	min	0.9602	0.0747	0.0925	1.56	45.08	1.04
z-score	max	0.3208	0.9549	0.8333	2.38	0.049	18.23

Table 59.: Hand multibiometrics fusing LBP, LDP and Hand Geometry feature extraction methods at score level when Euclidean distance is used to compare. w1, w2 and w3 stands for the weights given to LBP, LDP and Hand Geometry methods respectively.

Normalization Rule	Fusion Rule	w1	w2	w3	Validation	Test	
					EER (%)	FMR (%)	FNMR (%)
min-max	sum	0.7587	0.5469	0.1000	0.52	99.91	0
min-max	product	0.3997	0.2900	0.2811	0.52	0.44	3.13
min-max	min	0.7163	0.6484	0.8077	0.52	3.40	2.60
min-max	max	0.2628	0.8419	0.4974	0.52	99.97	0
z-score	sum	0.1924	0.5382	0.6439	0.52	35.30	0
z-score	product	0.8722	0.4411	0.4709	0.52	16.60	3.13
z-score	min	0.7425	0.2398	0.8492	0.52	9.67	4.69
z-score	max	0.6640	0.9920	0.0054	0.52	33.53	1.04

Table 60.: Hand multibiometrics fusing LBP, LDP and Hand Geometry feature extraction methods at score level when SVMs are used to compare. w1, w2 and w3 stands for the weights given to LBP, LDP and Hand Geometry methods respectively.

11.2.2.8 *Sobel, Curvelets and Hand Geometry Score-Level fusion*

Table 61 and Table 62 show the results of fusing palmprint information extracted by means of Sobel filter and Curvelets together with hand geometry information at score level when Euclidean distance and SVMs are used to obtain the matching scores respectively. In general, a small improvement can be seen in relation to monomodal results or two-by-two fusions is obtained for some rules when Euclidean distance and SVMs are employed. Regarding normalization techniques, it can be seen that both approaches provide quite similar results. More in detail, when compared to monomodal biometrics and Sobel-Curvelets fusion it can be seen that sum rule provides better results for SVMs as well as Euclidean distance comparison, and that also min rule improves the results in the latter case. When compared to Sobel-Geom results it can be seen better results when product rule and Euclidean distance are applied. In the case of SVMs comparison Sobel-Geom results are improved by sum rule in the case of min-max normalization and the four rules if scores are normalized by z-score approach. Finally, it can be seen that results obtained using Euclidean distance comparison improve Curvelets-Geom fusion results. In the case of SVMs

comparison Curvelets-Geom results are also improved by prod and min rules when z-score is employed and by sum rule independently of the normalization approach.

Normalization Rule	Fusion Rule	w1	w2	w3	Validation	Test	
					EER (%)	FMR (%)	FNMR (%)
min-max	sum	0.1200	0.8576	0.0079	1.10	4.63	4.17
min-max	product	0.5677	0.4406	0.6445	4.51	4.78	2.60
min-max	min	0.5005	0.0229	0.7913	0.96	94.01	1.04
min-max	max	0.0280	0.4811	0.9641	1.56	28.46	7.29
z-score	sum	0.3228	0.7360	0.0637	1.10	0	10.94
z-score	product	0.8915	0.4269	0.8585	4.51	0.69	4.17
z-score	min	0.2695	0.0047	0.5393	0.96	1	0
z-score	max	0.0581	0.1716	0.5968	1.56	0	0.1563

Table 61.: Hand multibiometrics fusing Sobel, Curvelets and Hand Geometry feature extraction methods at score level when Euclidean distance is used to compare. w1, w2 and w3 stands for the weights given to Sobel, Curvelets and Hand Geometry methods respectively.

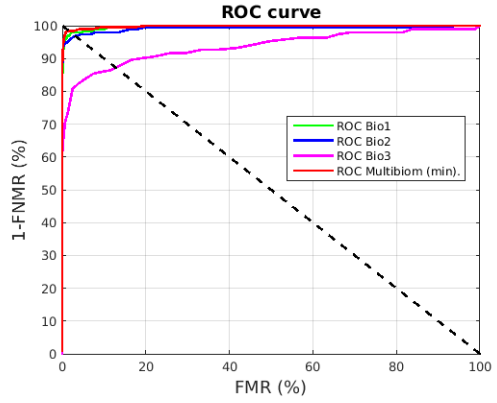

(a) Min rule and Euclidean distance

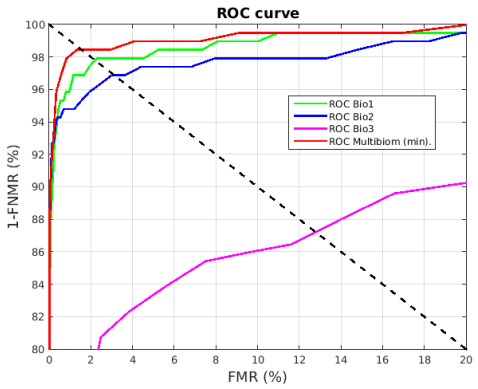

(b) Min rule and Euclidean distance (zoomed)

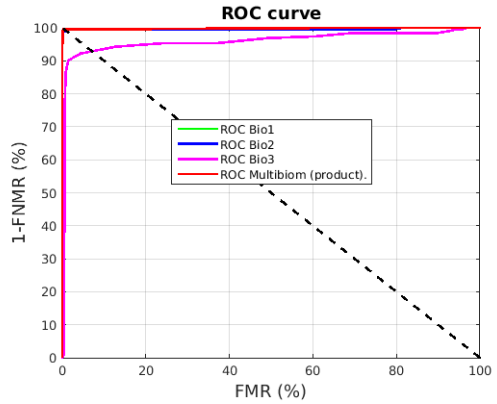

(c) Product rule and SVMs

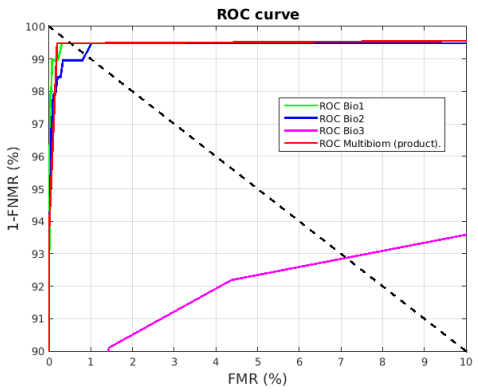

(d) Product rule and SVMs (zoomed)

Figure 59.: Best score level fusion results involving LBP (Bio1), LDP (Bio2), and Hand Geometry (Bio3) feature extraction methods when min-max normalization is applied.

Figure 60 depicts the best validation results of Sobel, Curvelets and Hand Geometry fusion at score level when Euclidean distance and SVMs are used to obtain the matching scores and min-max normalization is applied. In addition, the corresponding monomodal results can also be seen in the figure.

Normalization Rule	Fusion Rule	w1	w2	w3	Validation	Test	
					EER (%)	FMR (%)	FNMR (%)
min-max	sum	0.8612	0.0696	0.5347	0.68	1	0
min-max	product	0.5132	0.2635	0.6493	1.04	1.06	3.13
min-max	min	0.9460	0.6887	0.7179	1.04	58.15	1.04
min-max	max	0.6908	0.9739	0.0901	1.04	99.19	0
z-score	sum	0.6243	0.0487	0.3951	0.70	32.94	1.04
z-score	product	0.1172	0.2967	0.9752	1.04	13.40	3.65
z-score	min	0.6946	0.7383	0.3852	1.03	2.66	6.25
z-score	max	0.4917	0.6926	0.1165	1.04	47.06	0

Table 62.: Hand multibiometrics fusing Sobel, Curvelets and Hand Geometry feature extraction methods at score level when SVMs are used to compare. w1, w2 and w3 stands for the weights given to Sobel, Curvelets and Hand Geometry methods respectively.

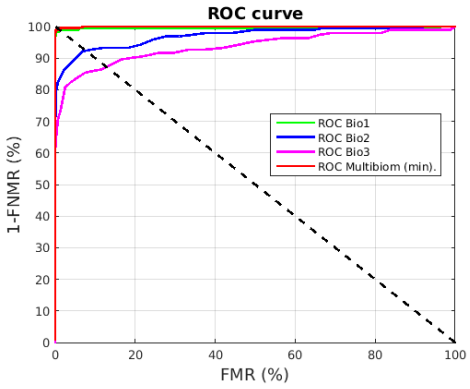

(a) Min rule and Euclidean distance

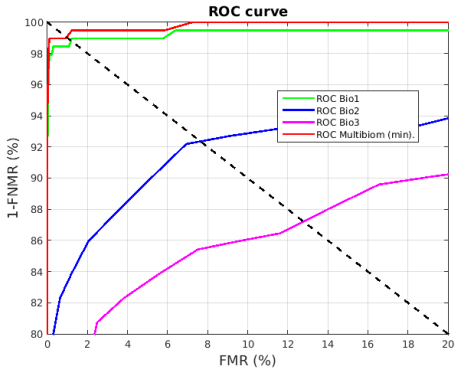

(b) Min rule and Euclidean distance (zoomed)

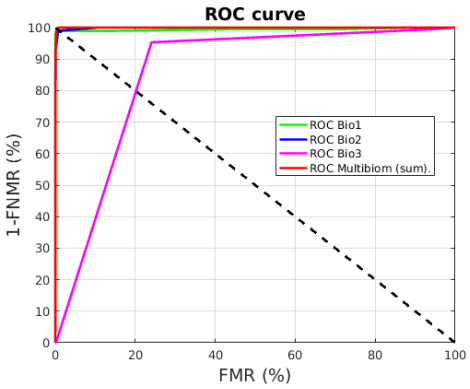

(c) Sum rule and SVMs

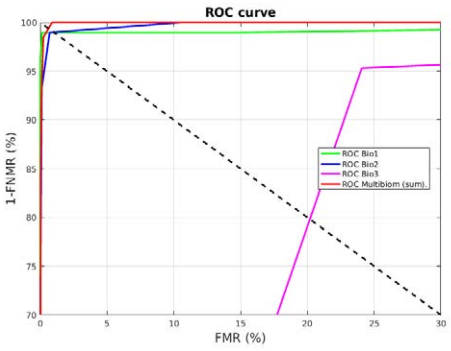

(d) Sum rule and SVMs (zoomed)

Figure 60.: Best score level fusion results involving Sobel (Bio1), Curvelets (Bio2), and Hand Geometry (Bio3) feature extraction methods when min-max normalization is applied.

11.2.2.9 *LBP, Curvelets and Hand Geometry Score-level fusion*

Table 63 and Table 64 show the results of fusing palmprint information extracted by means of LBP and Curvelets together with hand geometry information at score level when Euclidean distance and SVMs are used to obtain the matching scores respectively. In general, a small improvement can be seen in relation to monomodal results is obtained for some rules when Euclidean distance is applied while SVMs maintain the same performance. In adition, it can be seen than two-by-two fusions are also improved by some rules. Regarding normalization techniques, it can be seen that both approaches provide quite similar results. In particular, sum and min rules overcome monomodal results when Euclidean distance is used to compare features. In addition, results provided by LBP-Curvelets fusion are improved by min rule when scores are obtained by Euclidean distance and by product rule when scores are calculated by SVMs and z-scrore normalization is applied. When compared to LBP-Geom fusion results, certain improvement can be seen when product and min rules are used to fuse scores provided by SVMs in combination with z-score normalization. Finally, Curvelets-Geom results are improved by all the rule, comparison method and normalization approach possible combinations.

Normalization Rule	Fusion Rule	w1	w2	w3	Validation	Test	
					EER (%)	FMR (%)	FNMR (%)
min-max	sum	0.1143	0.6728	0.2078	2.08	0.022	16.67
min-max	product	0.2840	0.1241	0.4174	6.81	7.17	3.13
min-max	min	0.5962	0.0613	0.5023	2.01	82.51	0.52
min-max	max	0.1880	0.6441	0.9219	3.10	14.55	7.81
z-score	sum	0.1403	0.5638	0.2424	2.08	0.011	21.88
z-score	product	0.3227	0.4458	0.2577	6.81	1.20	4.69
z-score	min	0.9329	0.0615	0.9006	2.01	93.53	1.04
z-score	max	0.0596	0.2407	0.4348	2.72	0.071	20.83

Table 63.: Hand multibiometrics fusing LBP, Curvelets and Hand Geometry feature extraction methods at score level when Euclidean distance is used to compare. w1, w2 and w3 stands for the weights given to LBP, Curvelets and Hand Geometry methods respectively.

Normalization Rule	Fusion Rule	w1	w2	w3	Validation	Test	
					EER (%)	FMR (%)	FNMR (%)
min-max	sum	0.5905	0.7743	0.6236	0.52	1	0
min-max	product	0.3257	0.7191	0.2553	0.52	0.49	2.60
min-max	min	0.9800	0.0667	0.7027	0.52	92.71	0
min-max	max	0.3260	0.5847	0.3736	0.52	97.24	0
z-score	sum	0.6522	0.3448	0.1912	0.52	35.11	0.52
z-score	product	0.9528	0.6122	0.0738	0.52	12.96	4.17
z-score	min	0.7415	0.0344	0.1377	0.52	11.03	4.17
z-score	max	0.2697	0.9537	0.3450	0.52	49.16	0

Table 64.: Hand multibiometrics fusing LBP, Curvelets and Hand Geometry feature extraction methods at score level when SVMs are used to compare. w1, w2 and w3 stands for the weights given to LBP, Curvelets and Hand Geometry methods respectively.

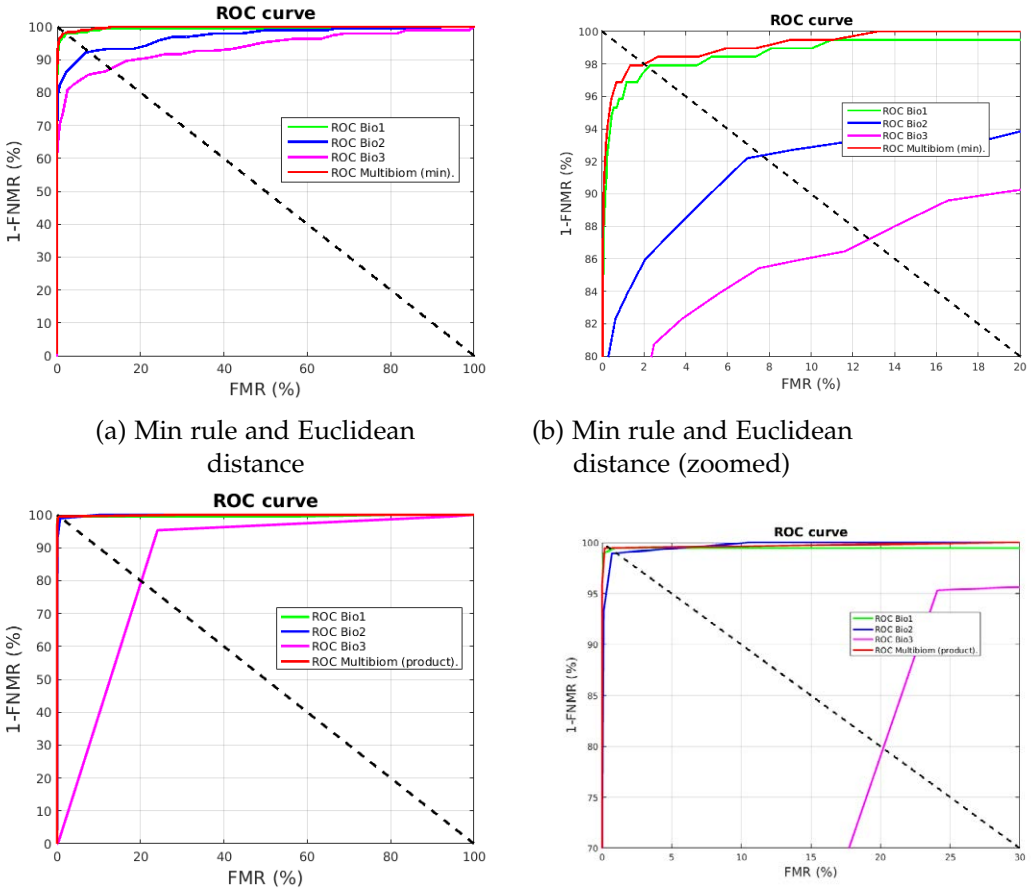

(a) Min rule and Euclidean distance

(b) Min rule and Euclidean distance (zoomed)

(c) Product rule and SVMs

(d) Product rule and SVMs (zoomed)

Figure 61.: Best score level fusion results involving LBP (Bio1), Curvelets (Bio2), and Hand Geometry (Bio3) feature extraction methods when min-max normalization is applied.

Figure 61 depicts the best validation results of LBP, Curvelets and Hand Geometry fusion at score level when Euclidean distance and SVMs are used to obtain the matching scores and min-max normalization is applied. In addition, the corresponding monomodal results can also be seen in the figure.

11.2.2.10 *Sobel, LBP and Hand Geometry Score-Level fusion*

Table 65 and Table 66 show the results of fusing palmprint information extracted by means of Sobel filter and LBP together with hand geometry information at score level when Euclidean distance and SVMs are used to obtain the matching scores respectively. In general, a small improvement can be seen in relation to monomodal and two-by-two fusions results when Euclidean distance is applied, while SVMs accuracy is maintained or decreased. Regarding normalization techniques, it can be seen that both approaches provide quite similar results. More in detail, when results are compared to monomodal results improvements are obtained by sum, min and max rules when Euclidean distance is applied to calculate the scores. In the case of comparison

with Sobel-LBP fusion, min distance is able to improve the results when Euclidean distance is used to compute the scores. If results are compared to Sobel-Geom fusion results, certain improvement can be seen for all the rules, comparison methods and normalization approaches with the exception of product rule when SVMs are employed to obtain the scores that are normalized by min-max method. Finally, when compared to LBP-Geom fusion improvements can be seen for all the rules when scores are computed by means of Euclidean distance as well as for product rule and min rule when scores are provided by SVMs and normalized by z-score.

Figure 62 depicts the best validation results of Sobel, LBP and Hand Geometry fusion at score level when Euclidean distance and SVMs are used to obtain the matching scores and min-max normalization applied. In addition, the corresponding monomodal results can also be seen in the figure.

Normalization Rule	Fusion Rule	w1	w2	w3	Validation	Test	
					EER (%)	FMR (%)	FNMR (%)
min-max	sum	0.0106	0.9261	0.3516	1.04	0.011	15.63
min-max	product	0.1640	0.0462	0.4371	3.41	3.03	2.08
min-max	min	0.9295	0.0570	0.1120	0.52	90.10	0
min-max	max	0.0964	0.6693	0.8977	1.07	4.23	4.69
z-score	sum	0.2083	0.3795	0.5346	1.04	0	29.69
z-score	product	0.6421	0.2277	0.5537	3.41	0.19	6.77
z-score	min	0.6464	0.0139	0.0429	0.52	96.88	0
z-score	max	0.1808	0.3897	0.9160	1.13	8.62	6.25

Table 65.: Hand multibiometrics fusing Sobel, LBP and Hand Geometry feature extraction methods at score level when Euclidean distance is used to compare. w1, w2 and w3 stands for the weights given to Sobel, LBP and Hand Geometry methods respectively.

Normalization Rule	Fusion Rule	w1	w2	w3	Validation	Test	
					EER (%)	FMR (%)	FNMR (%)
min-max	sum	0.4061	0.2037	0.3916	0.52	1	0
min-max	product	0.4697	0.9411	0.8113	1.04	0.94	2.60
min-max	min	0.9306	0.7652	0.4589	0.52	78.91	0
min-max	max	0.4355	0.5784	0.7379	0.91	1	0
z-score	sum	0.3375	0.0842	0.4026	0.52	35.21	0
z-score	product	0.8721	0.1202	0.0704	1.04	18.92	3.13
z-score	min	0.5115	0.2107	0.0986	0.52	6.64	5.21
z-score	max	0.0568	0.0137	0.6362	0.52	62.44	0.52

Table 66.: Hand multibiometrics fusing Sobel, LBP and Hand Geometry feature extraction methods at score level when SVMs are used to compare. w1, w2 and w3 stands for the weights given to Sobel, LBP and Hand Geometry methods respectively.

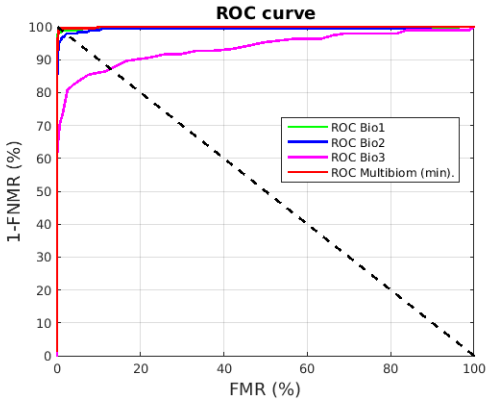

(a) Min rule and Euclidean distance

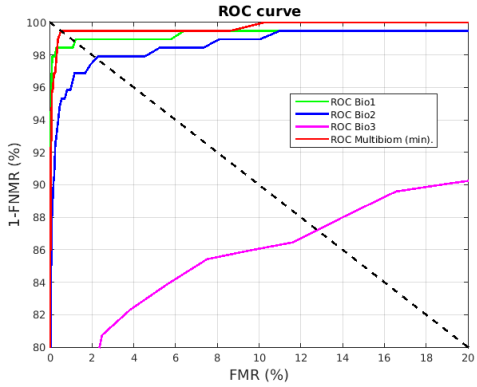

(b) Min rule and Euclidean distance (zoomed)

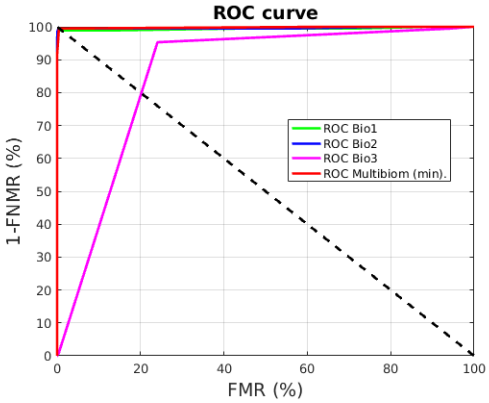

(c) Min rule and SVMs

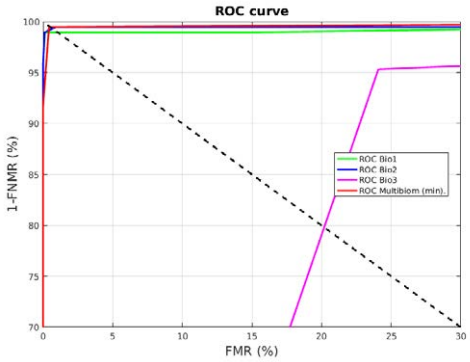

(d) Min rule and SVMs (zoomed)

Figure 62.: Best score level fusion results involving Sobel (Bio1), LBP (Bio2), and Hand Geometry (Bio3) feature extraction methods when min-max normalization is applied.

11.3 FEATURE LEVEL FUSION

11.3.1 *Palmprint multibiometrics*

11.3.1.1 *Sobel and Gabor Feature-Level fusion*

Table 67 shows the results of fusing the features extracted by Sobel and Gabor filters after z-score normalization. Opposite to expected, it cannot be seen any improvement of the recognition accuracy and the result is equal to the worst monomodal biometrics. This behaviour can be explained because there is a substantial difference in the length of the feature vectors extracted by Sobel and Gabor filters and results could be biased towards Gabor filter because its feature vector is longer. Accordingly, it can be stated that Sobel and Gabor filters are not compatible for feature level fusion.

Comparison Method	Validation	Test	
	EER (%)	FMR (%)	FNMR (%)
Euclidean Distance	1.56	1.56	5.73
Support Vector Machines	1.56	1.67	3.65

Table 67.: Palmprint multibiometrics fusing features extracted by Sobel and Gabor filters. z-score normalization is applied to the features previously to the fusion.

Figure 63 depicts the best validation results of Sobel and Gabor fusion at feature level when Euclidean distance and SVMs are used to obtain the matching scores and z-score normalization is applied. In addition, the corresponding monomodal results can also be seen in the figure.

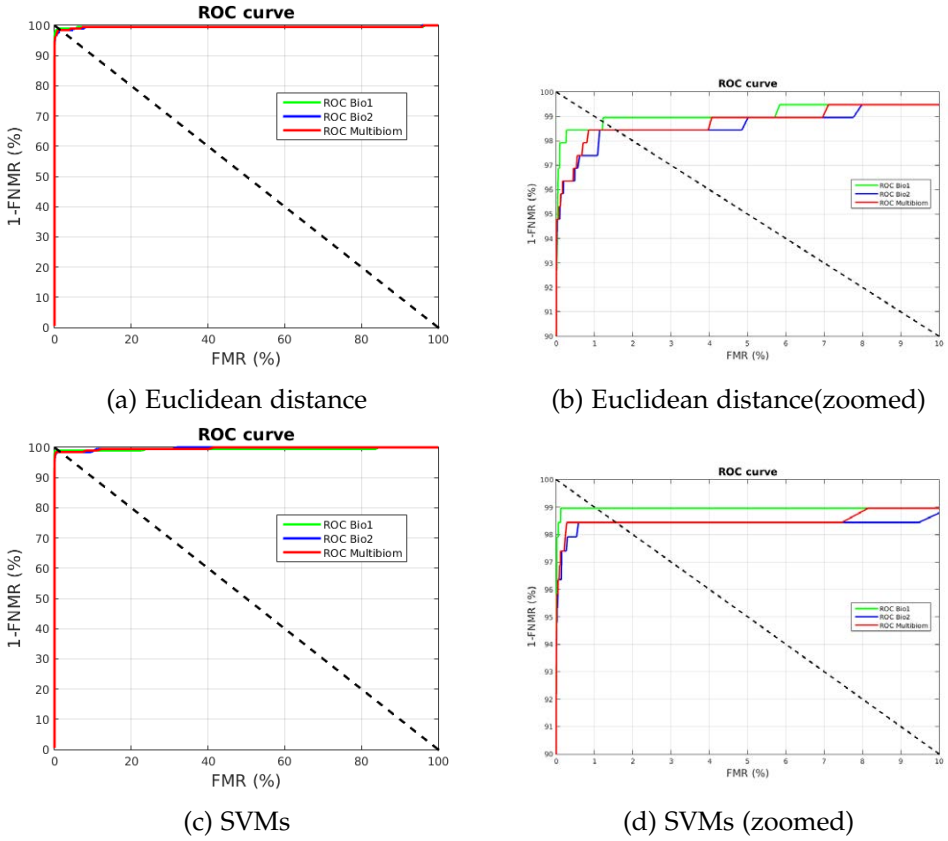

(a) Euclidean distance

(b) Euclidean distance(zoomed)

(c) SVMs

(d) SVMs (zoomed)

Figure 63.: Best feature level fusion results involving Sobel (Bio1) and Gabor (Bio2) methods. z-score normalization is applied to the features previously to the fusion.

11.3.1.2 *LBP and LDP Feature-level fusion*

Table 68 shows the results of fusing the features extracted by LBP and LDP after z-score normalization. It can be seen that a little improvement is obtained with this fusion in relation to the results of the monomodal biometrics when Euclidean dis-

tance is used for comparison. On the contrary, no improvements are achieved in the case of SVMs comparison, although the obtained result is really close to the best of the monomodal biometrics. It could be explained because LBP and LDP are texture descriptors that share a common basis and the models learned by SVMs in this case cannot extract additional information from the combination of features. Figure 64 shows the best validation results of LBP and LDP fusion at feature level when Euclidean distance and SVMs are used to obtain the matching scores and z-score normalization is applied. In addition, the corresponding monomodal results can also be seen in the figure.

Comparison Method	Validation	Test	
	EER (%)	FMR (%)	FNMR (%)
Euclidean Distance	2.08	2.65	5.21
Support Vector Machines	0.54	0.44	3.13

Table 68.: Palmprint multibiometrics fusing features extracted by LBP and LDP. z-score normalization is applied to the features previously to the fusion.

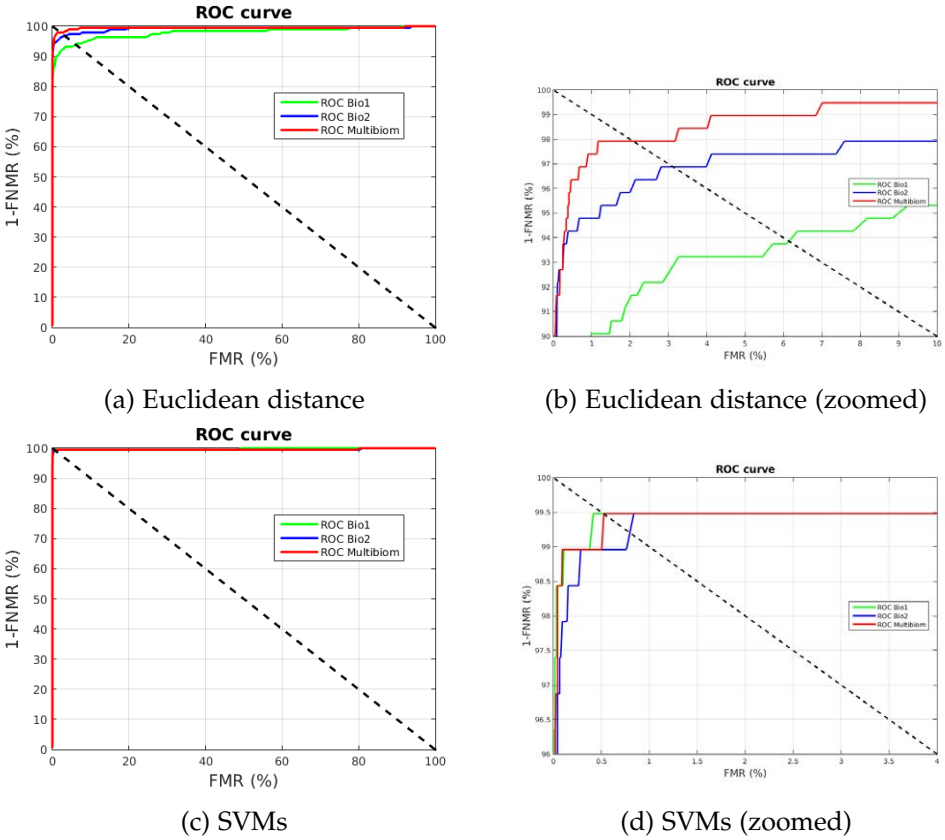

(a) Euclidean distance

(b) Euclidean distance (zoomed)

(c) SVMs

(d) SVMs (zoomed)

Figure 64.: Best feature level fusion results involving LBP (Bio1) and LDP (Bio2) methods. z-score normalization is applied to the features previously to the fusion.

11.3.1.3 *Sobel and Curvelets Feature-Level fusion*

Table 69 shows the results of fusing the features extracted by Sobel filter and Curvelets after z-score normalization. In this case, it cannot be seen any improvement on the results. In addition, it can be seen that for Euclidean distance comparison the obtained accuracy is slightly worse than the best monomodal result while for SVMs matching the best monomodal result is equalled. It could be derived that features extracted by Curvelets are introducing some noise that SVMs are able to manage but not Euclidean distance. Accordingly, it can be stated that Sobel and Curvelets are not compatible for feature level fusion.

Figure 65 depicts the best validation results of Sobel and Curvelets fusion at feature level when Euclidean distance and SVMs are used to obtain the matching scores and z-score normalization is applied. In addition, the corresponding monomodal results can also be seen in the figure.

Comparison Method	Validation	Test	
	EER (%)	FMR (%)	FNMR (%)
Euclidean Distance	1.56	1.56	4.69
Support Vector Machines	1.04	1.24	4.17

Table 69.: Palmprint multibiometrics fusing features extracted by Sobel and Curvelets. z-score normalization is applied to the features previously to the fusion.

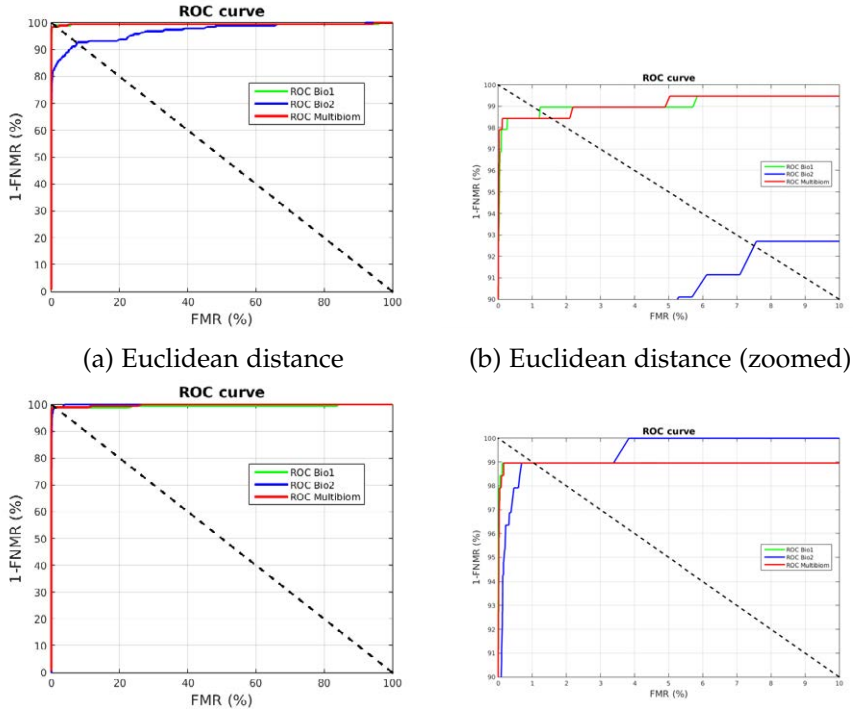

(a) Euclidean distance

(b) Euclidean distance (zoomed)

(c) SVMs

(d) SVMs (zoomed)

Figure 65.: Best feature level fusion results involving Sobel (Bio1) and Curvelets (Bio2) methods. z-score normalization is applied to the features previously to the fusion.

11.3.1.4 *LBP and Curvelets Feature-level fusion*

Table 70 shows the results of fusing the features extracted by LBP and Curvelets after z-score normalization. It can be seen that a little improvement is obtained fusing LBP and Curvelets in relation to the results of the monomodal biometrics when Euclidean distance is used for comparison. On the contrary, no improvements are achieved in the case of SVMs comparison that equals the result of the best monomodal biometric. It could be explained because LBP extract more representative features and the models learned by SVMs in this case cannot extract additional information from the combination of features.

Figure 66 depicts the best validation results of LBP and Curvelets fusion at feature level when Euclidean distance and SVMs are used to obtain the matching scores and z-score normalization is applied. In addition, the corresponding monomodal results can also be seen in the figure.

Comparison Method	Validation	Test	
	EER (%)	FMR (%)	FNMR (%)
Euclidean Distance	2.08	2.58	4.69
Support Vector Machines	0.52	0.56	2.60

Table 70.: Palmprint multibiometrics fusing features extracted by LBP and Curvelets. z-score normalization is applied to the features previously to the fusion.

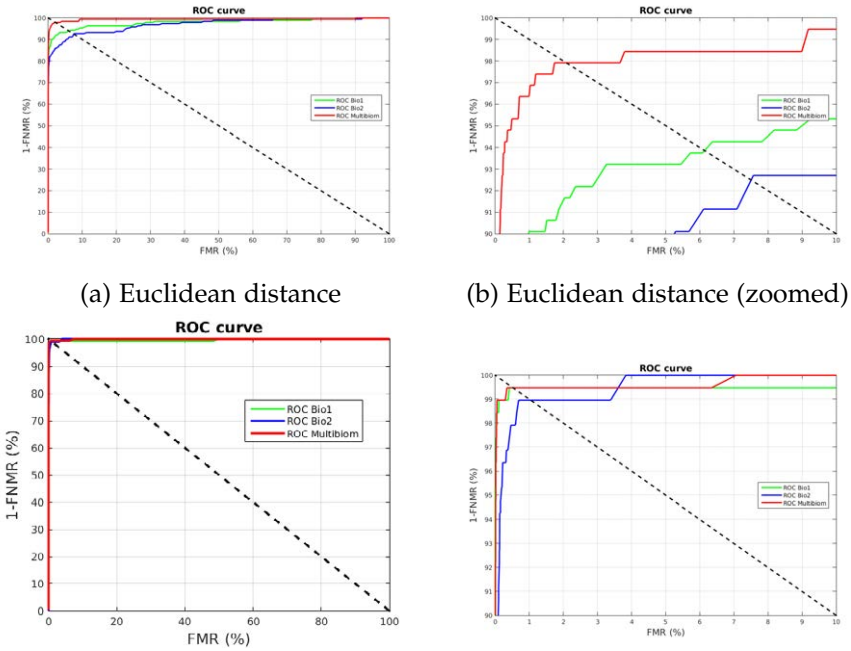

(a) Euclidean distance (b) Euclidean distance (zoomed)

(c) SVMs (d) SVMs (zoomed)

Figure 66.: Best feature level fusion results involving LBP (Bio1) and Curvelets (Bio2) methods. z-score normalization is applied to the features previously to the fusion.

11.3.1.5 *Sobel and LBP Feature-level fusion*

Table 71 shows the results of fusing the features extracted by Sobel filter and LBP after z-score normalization. In this case, it cannot be seen any improvement on the results. In addition, it can be seen that for Euclidean distance comparison the obtained accuracy is slightly worst than the best monomodal result while for SVMs matching the best monomodal result is equalled. It could be derived that features extracted by LBPs are more representative and are biasing the results. Accordingly, it can be stated that Sobel and LBP are not compatible for feature level fusion.

Figure 67 depicts the best validation results of Sobel and LBP fusion at feature level when Euclidean distance and SVMs are used to obtain the matching scores and z-score normalization is applied. In addition, the corresponding monomodal results can also be seen in the figure.

Comparison Method	Validation	Test	
	EER (%)	FMR (%)	FNMR (%)
Euclidean Distance	1.56	2.01	4.69
Support Vector Machines	1.04	1.06	2.60

Table 71.: Palmprint multibiometrics fusing features extracted by Sobel and LBP. z-score normalization is applied to the features previously to the fusion.

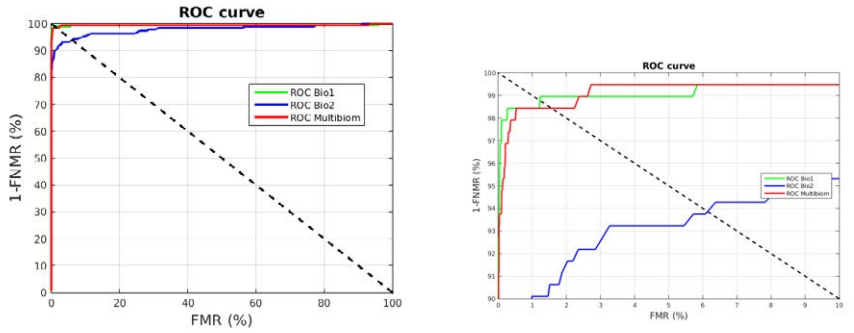

(a) Euclidean distance

(b) Euclidean distance (zoomed)

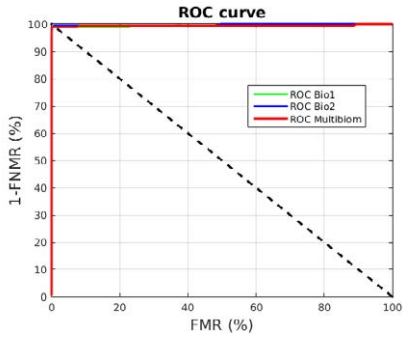

(c) SVMs

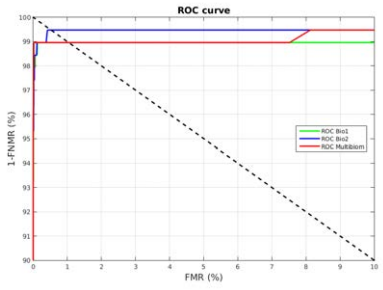

(d) SVMs (zoomed)

Figure 67.: Best feature level fusion results involving Sobel (Bio1) and LBP (Bio2) methods. z-score normalization is applied to the features previously to the fusion.

11.3.2 *Hand multibiometrics*

11.3.2.1 *Sobel and Hand Geometry Feature-level fusion*

Table 72 shows the results of fusing the palmprint features extracted by Sobel filter and hand geometry features after z-score normalization. It can be seen that a little improvement is obtained fusing Sobel and hand geometry features in relation to the results of the monomodal biometrics when Euclidean distance is used for comparison. On the contrary, no improvements are achieved in the case of SVMs comparison that equals the result of the best of the monomodal biometrics. It could be derived that Sobel filter extract more representative features and the models learned by SVMs in this case cannot extract additional information from the combination of features.

Figure 68 illustrates the best validation results of Sobel and Hand Geometry fusion at feature level when Euclidean distance and SVMs are used to obtain the matching scores and z-score normalization is applied. In addition, the corresponding monomodal results can also be seen in the figure.

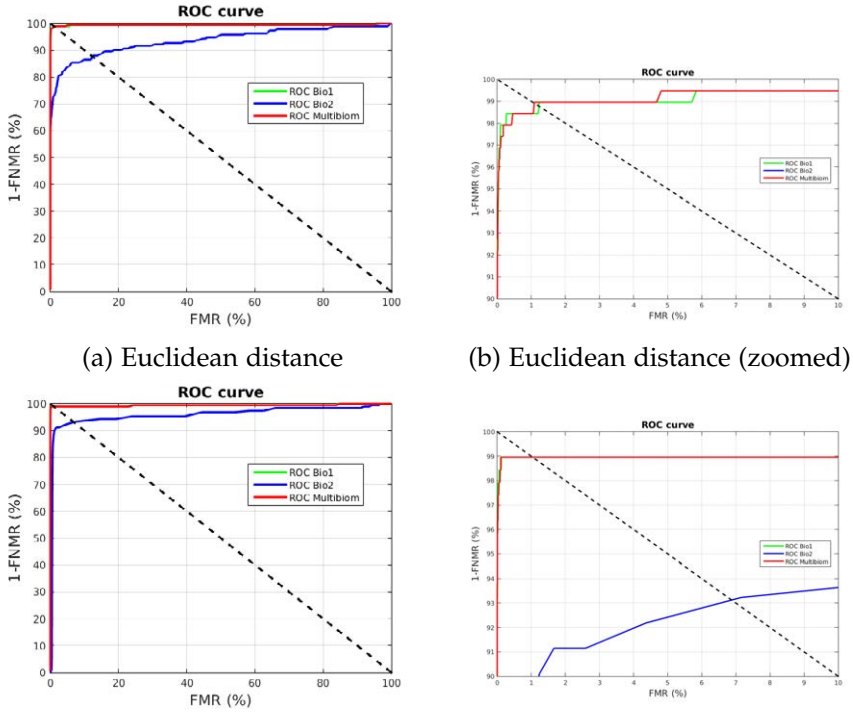

(a) Euclidean distance (b) Euclidean distance (zoomed)

(c) SVMs (d) SVMs (zoomed)

Figure 68.: Best feature level fusion results involving Sobel (Bio1) and Hand Geometry (Bio2) methods. z-score normalization is applied to the features previously to the fusion.

Comparison Method	Validation	Test	
	EER (%)	FMR (%)	FNMR (%)
Euclidean Distance	1.09	1.16	5.73
Support Vector Machines	1.04	1.05	3.65

Table 72.: Hand multibiometrics fusing palmprint features extracted by Sobel filter together with hand geometry features. z-score normalization is applied to the features previously to the fusion.

11.3.2.2 *Gabor and Hand Geometry Feature-level fusion*

Table 73 shows the results of fusing the palmprint features extracted by Gabor filter and hand geometry features after z-score normalization. It can be seen that the results of the best monomodal method is maintained for both Euclidean distance and SVMs comparison. It could be derived that features extracted by Gabor filter are more representative than the features provided by hand geometry method. Accordingly, it can be stated that Gabor and hand geometry are not compatible for feature level fusion.

Figure 69 shows the best validation results of Gabor and Hand Geometry fusion at feature level when Euclidean distance and SVMs are used to obtain the matching scores and z-score normalization is applied. In addition, the corresponding monomodal results can also be seen in the figure.

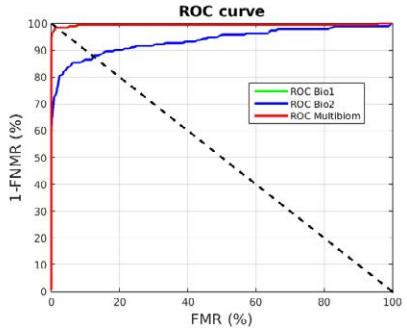

(a) Euclidean distance

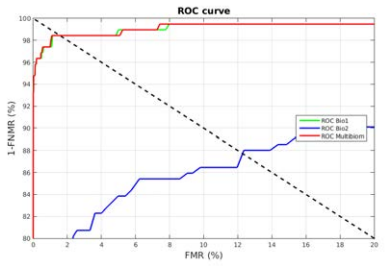

(b) Euclidean distance (zoomed)

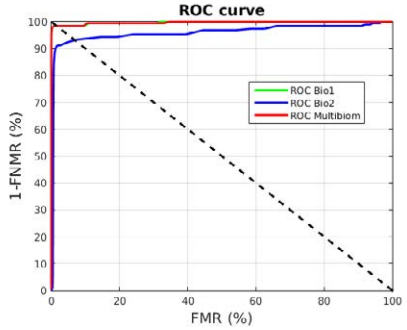

(c) SVMs

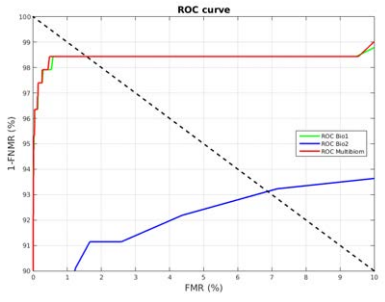

(d) SVMs (zoomed)

Figure 69.: Best feature level fusion results involving Gabor (Bio1) and Hand Geometry (Bio2) methods. z-score normalization is applied to the features previously to the fusion.

Comparison Method	Validation	Test	
	EER (%)	FMR (%)	FNMR (%)
Euclidean Distance	1.56	1.52	6.25
Support Vector Machines	1.56	1.69	4.17

Table 73.: Hand multibiometrics fusing palmprint features extracted by Gabor filter together with hand geometry features. z-score normalization is applied to the features previously to the fusion.

11.3.2.3 *LBP and Hand Geometry Feature-level fusion*

Table 74 shows the results of fusing the palmprint features extracted by LBP and hand geometry features after z-score normalization. It can be seen that a little improvement is obtained with the fusion of LBP and hand geometry features in relation to the results of the monomodal biometrics when Euclidean distance is used for comparison. On the contrary, no improvements are achieved in the case of SVMs matching that equals the result of the best of the monomodal biometrics. It could be explained because LBP extract more representative features and the models learned by SVMs in this case cannot extract additional information from the combination of features.

Figure 70 illustrates the best validation results of LBP and Hand Geometry fusion at feature level when Euclidean distance and SVMs are used to obtain the matching scores and z-score normalization is applied. In addition, the corresponding monomodal results can also be seen in the figure.

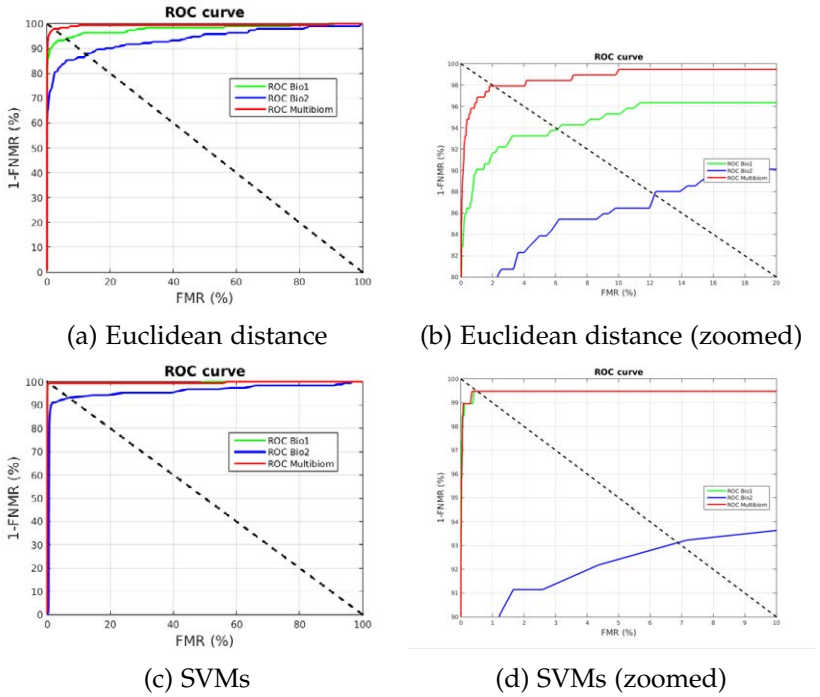

(a) Euclidean distance (b) Euclidean distance (zoomed)

(c) SVMs (d) SVMs (zoomed)

Figure 70.: Best feature level fusion results involving LBP (Bio1) and Hand Geometry (Bio2) methods. z-score normalization is applied to the features previously to the fusion.

Comparison Method	Validation	Test	
	EER (%)	FMR (%)	FNMR (%)
Euclidean Distance	2.08	2.56	5.21
Support Vector Machines	0.52	0.36	3.13

Table 74.: Hand multibiometrics fusing palmprint features extracted by LBP together with hand geometry features. z-score normalization is applied to the features previously to the fusion.

11.3.2.4 *LDP and Hand Geometry Feature-level fusion*

Table 75 shows the results of fusing the palmprint features extracted by LDP and hand geometry features after z-score normalization. Results show a small decrease of the accuracy in relation to monomodal biometrics when Euclidean distance is used to compare features. On the contrary, little improvement can be seen when SVMs are used for the comparison. Accordingly, it could be stated that LDP and hand geometry extract complementary features that requires from machine learning techniques to be found.

Figure 71 shows the best validation results of LDP and Hand Geometry fusion at feature level when Euclidean distance and SVMs are used to obtain the matching scores and z-score normalization is applied. In addition, the corresponding monomodal results can also be seen in the figure.

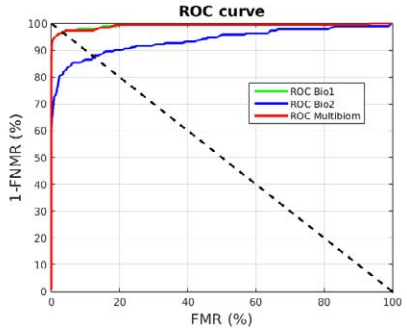

(a) Euclidean distance

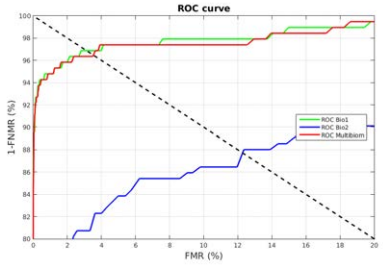

(b) Euclidean distance (zoomed)

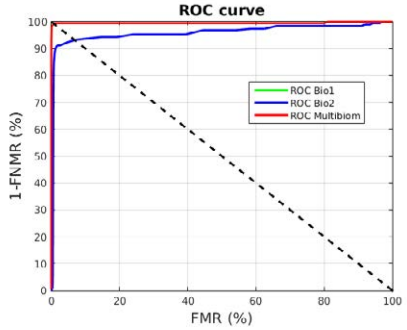

(c) SVMs

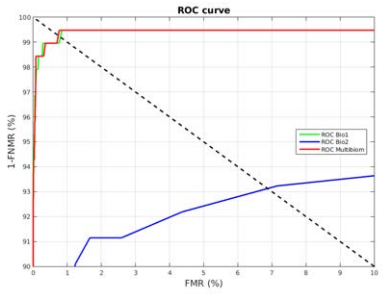

(d) SVMs (zoomed)

Figure 71.: Best feature level fusion results involving LDP (Bio1) and Hand Geometry (Bio2) methods. z-score normalization is applied to the features previously to the fusion.

Comparison Method	Validation	Test	
	EER (%)	FMR (%)	FNMR (%)
Euclidean Distance	3.53	3.71	5.21
Support Vector Machines	0.74	0.60	3.13

Table 75.: Hand multibiometrics fusing palmprint features extracted by LDP together with hand geometry features. z-score normalization is applied to the features previously to the fusion.

11.3.2.5 *Curvelets and Hand Geometry Feature-level fusion*

Table 76 shows the results of fusing the palmprint features extracted by Curvelets and hand geometry features after z-score normalization. Results show that there is a small decrease of the accuracy when compared with the monomodal results. Nevertheless, they keep close to the best monomodal biometric. Accordingly, it can be stated that Curvelets and hand geometry are not compatible for feature level fusion.

Figure 72 depicts the best validation results of Curvelets and Hand Geometry fusion at feature level when Euclidean distance and SVMs are used to obtain the matching scores and z-score normalization is applied. In addition, the corresponding monomodal results can also be seen in the figure.

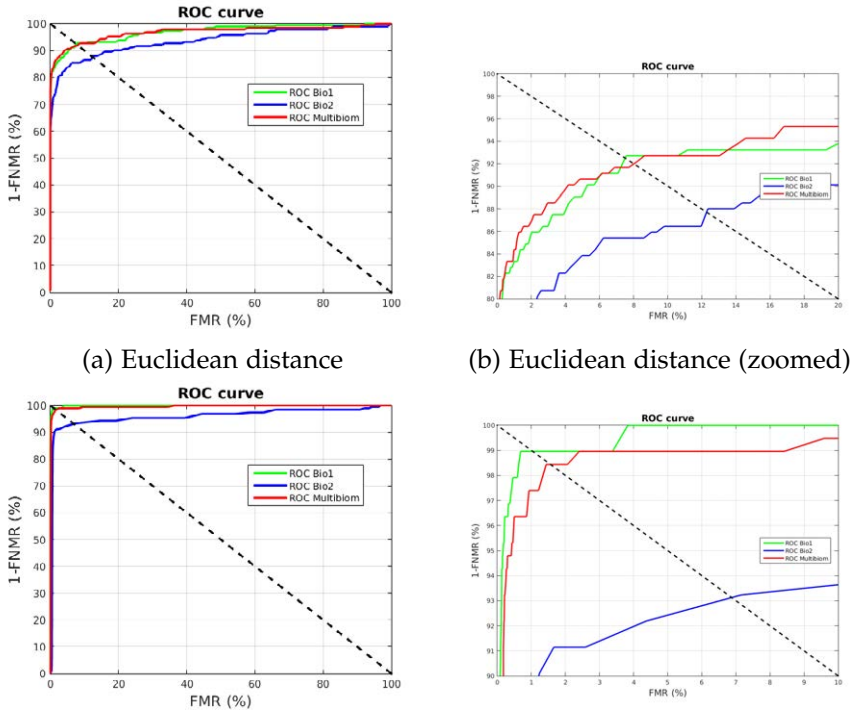

(a) Euclidean distance (b) Euclidean distance (zoomed)

(c) SVMs (d) SVMs (zoomed)

Figure 72.: Best feature level fusion results involving Curvelets (Bio1) and Hand Geometry (Bio2) methods. z-score normalization is applied to the features previously to the fusion.

Comparison Method	Validation	Test	
	EER (%)	FMR (%)	FNMR (%)
Euclidean Distance	8.02	8.57	6.25
Support Vector Machines	1.56	1.24	2.60

Table 76.: Hand multibiometrics fusing palmprint features extracted by Curvelets together with hand geometry features. z-score normalization is applied to the features previously to the fusion.

11.3.2.6 *Sobel, Gabor and Hand Geometry Feature-Level fusion*

Table 77 shows the results of fusing the palmprint features extracted by Sobel and Gabor filters together with hand geometry features after z-score normalization. It can be seen that no improvements are made when fusion results are compared to the best monomodal biometric neither when the comparison is made with the two-by-two fusions. In addition, it seems that results are biased by the features extracted by Gabor filter. It could be a consequence of a higher representativeness of Gabor features or the difference of the feature vectors length. In any case, it could be stated that Sobel, Gabor and hand geometry methods seems not to be compatible for feature level fusion.

Figure 73 depicts the best validation results of Sobel, Gabor and Hand Geometry fusion at feature level when Euclidean distance and SVMs are used to obtain the matching scores and z-score normalization is applied. In addition, the corresponding monomodal results can also be seen in the figure together with the results of the two-by-two fusions.

Comparison Method	Validation	Test	
	EER (%)	FMR (%)	FNMR (%)
Euclidean Distance	1.56	1.56	5.73
Support Vector Machines	1.56	1.69	3.65

Table 77.: Hand multibiometrics fusing palmprint features extracted by Sobel and Gabor filters together with hand geometry features. z-score normalization is applied to the features previously to the fusion.

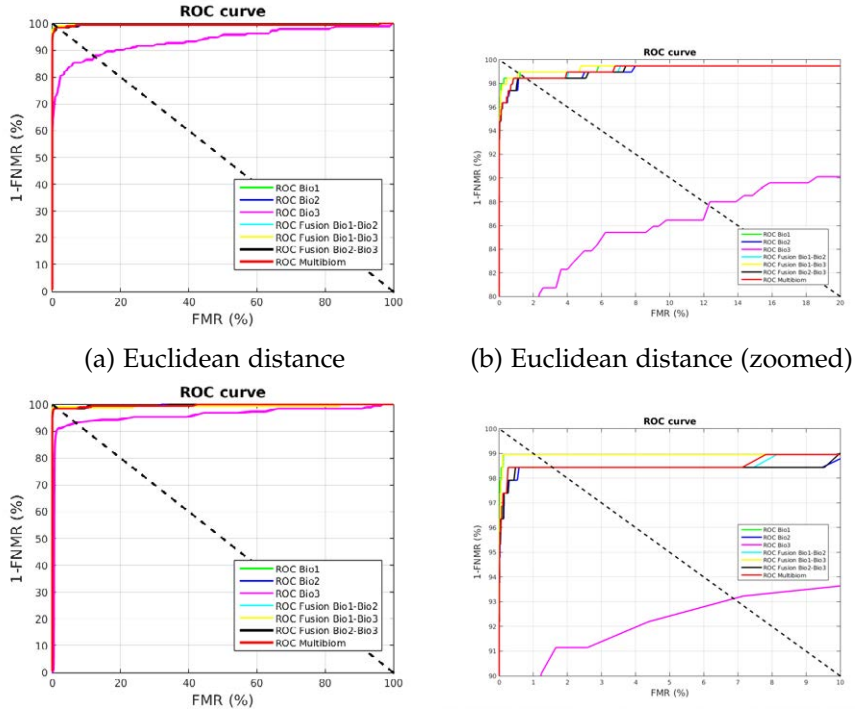

(a) Euclidean distance

(b) Euclidean distance (zoomed)

(c) SVMs

(d) SVMs (zoomed)

Figure 73.: Best feature level fusion results involving Sobel (Bio1), Gabor (Bio2) and Hand Geometry (Bio3) methods. z-score normalization is applied to the features previously to the fusion.

11.3.2.7 *LBP, LDP and Hand Geometry Feature-level fusion*

Table 78 shows the results of fusing the palmprint features extracted by LBP and LDP together with hand geometry features after z-score normalization. It can be seen a little improvement of the best monomodal result when features are compared by means of Euclidean distance, while a light decrease is obtained for SVMs comparison. In addition, it can be seen that the results of better two-by-two fusions (LBP-LDP and LBP-Geom) are almost maintained. Accordingly, it can be stated that the fusion of LBP, LDP and Hand Geometry features is not an alternative to increase the overall performance.

Figure 74 shows the best validation results of LBP, LDP and Hand Geometry fusion at feature level when Euclidean distance and SVMs are used to obtain the matching scores and z-score normalization is applied. In addition, the corresponding monomodal results can also be seen in the figure together with the results of the two-by-two fusions.

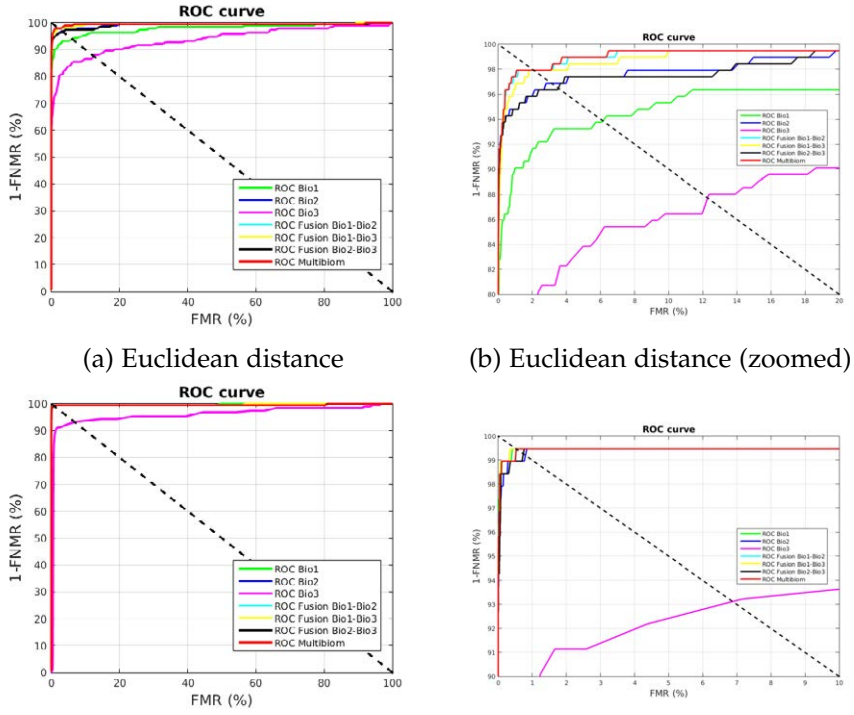

(a) Euclidean distance (b) Euclidean distance (zoomed)

(c) SVMs (d) SVMs (zoomed)

Figure 74.: Best feature level fusion results involving LBP (Bio1), LDP (Bio2) and Hand Geometry (Bio3) methods. z-score normalization is applied to the features previously to the fusion.

Comparison Method	Validation	Test	
	EER (%)	FMR (%)	FNMR (%)
Euclidean Distance	2.08	2.59	4.69
Support Vector Machines	0.53	0.46	3.13

Table 78.: Hand multibiometrics fusing palmprint features extracted by LBP and LDP together with hand geometry features. z-score normalization is applied to the features previously to the fusion.

11.3.2.8 *Sobel, Curvelets and Hand Geometry Feature-Level fusion*

Table 79 shows the results of fusing the palmprint features extracted by Sobel filter and Curvelets together with hand geometry features after z-score normalization. When the obtained results are compared to monomodal results as well as the best two-by-two fusion (Sobel-Hand Geometry) it can be observed that the accuracy is decreased if Euclidean distance is used for feature matching while it is maintained in the case of SVMs comparison. Accordingly, it can be stated that the fusion of Sobel, Curvelets and Hand Geometry features is not an alternative to increase the overall performance.

Figure 75 shows the best validation results of Sobel, Curvelets and Hand Geometry fusion at feature level when Euclidean distance and SVMs are used to obtain the matching scores and z-score normalization is applied. In addition, the corresponding

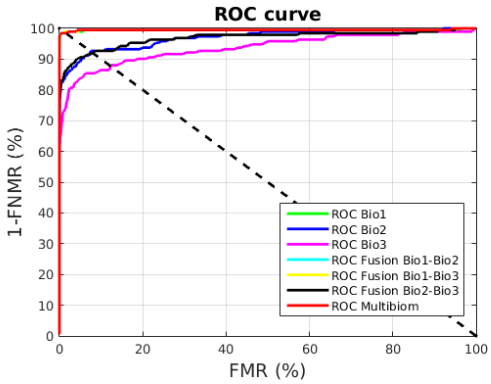

(a) Euclidean distance

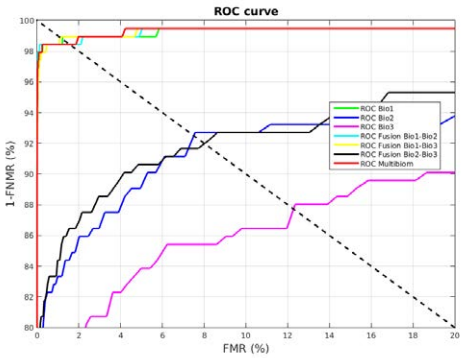

(b) Euclidean distance (zoomed)

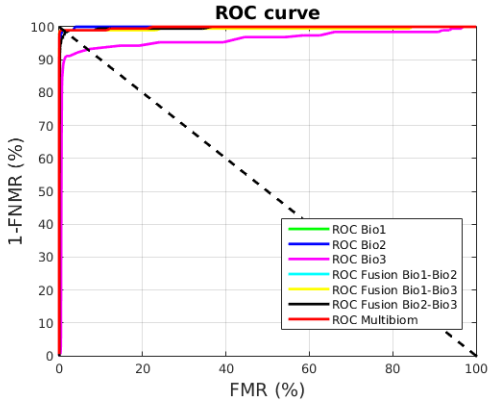

(c) SVMs

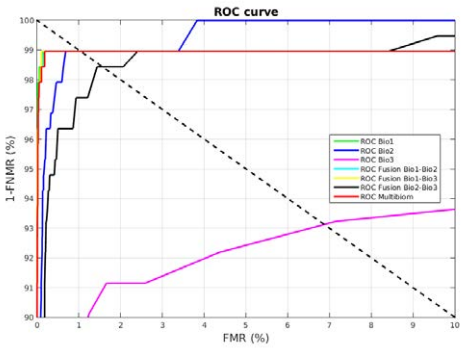

(d) SVMs (zoomed)

Figure 75.: Best feature level fusion results involving Sobel (Bio1), Curvelets (Bio2) and Hand Geometry (Bio3) methods. z-score normalization is applied to the features previously to the fusion.

Comparison Method	Validation	Test	
	EER (%)	FMR (%)	FNMR (%)
Euclidean Distance	1.56	1.60	3.65
Support Vector Machines	1.04	1.25	3.65

Table 79.: Hand multibiometrics fusing palmprint features extracted by Sobel filter and Curvelets together with hand geometry features. z-score normalization is applied to the features previously to the fusion.

monomodal results can also be seen in the figure together with the results of the two-by-two fusions.

11.3.2.9 *LBP, Curvelets and Hand Geometry Feature-level fusion*

Table 80 shows the results of fusing the palmprint features extracted by LBP and Curvelets together with hand geometry features after z-score normalization. It can be seen a little improvement of the best monomodal result when features are compared by means of Euclidean distance, while performance is maintained for SVMs

comparison. In addition it can be seen that the results of the best two-by-two fusions are also maintained. Accordingly, it can be stated that the fusion of LBP, Curvelets and Hand Geometry features is not an alternative to increase the overall performance.

Figure 76 shows the best validation results of LBP, Curvelets and Hand Geometry fusion at feature level when Euclidean distance and SVMs are used to obtain the matching scores and z-score normalization is applied. In addition, the corresponding monomodal results can also be seen in the figure together with the results of the two-by-two fusions.

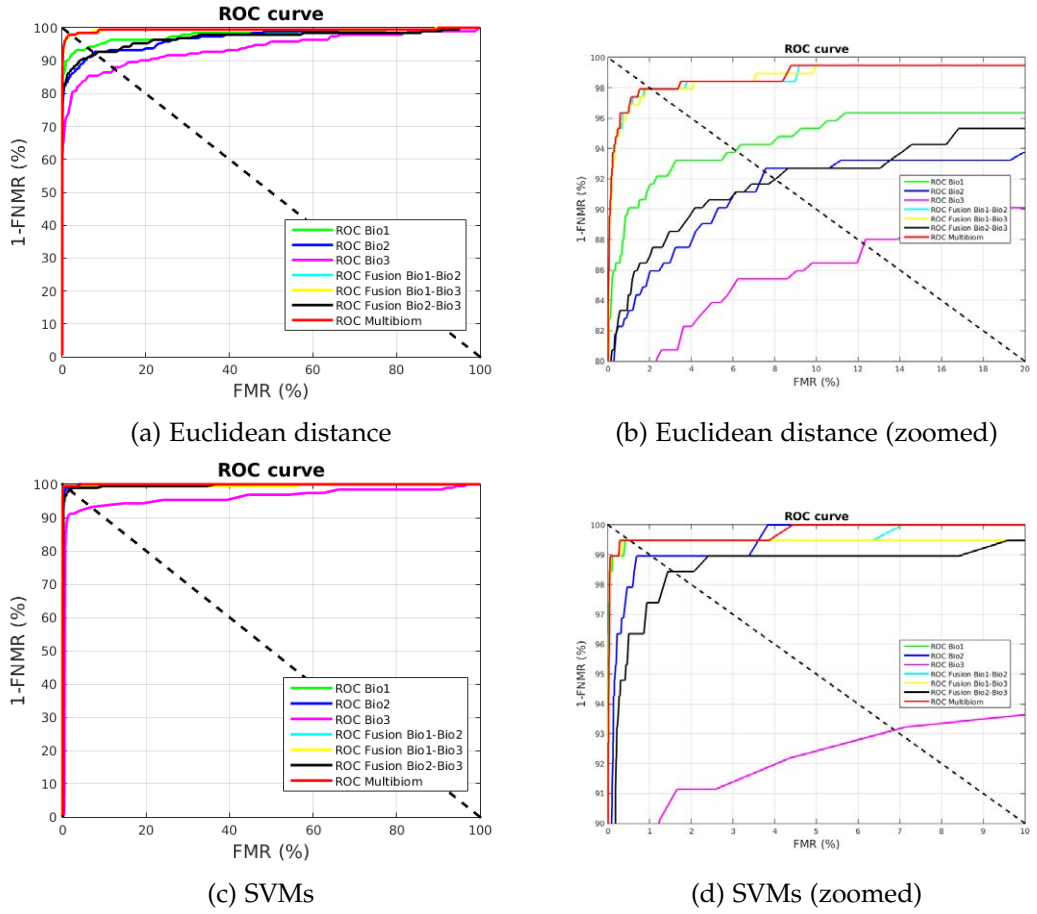

(a) Euclidean distance

(b) Euclidean distance (zoomed)

(c) SVMs

(d) SVMs (zoomed)

Figure 76.: Best feature level fusion results involving LBP (Bio1), Curvelets (Bio2) and Hand Geometry (Bio3) methods. z-score normalization is applied to the features previously to the fusion.

Comparison Method	Validation	Test	
	EER (%)	FMR (%)	FNMR (%)
Euclidean Distance	2.08	2.55	4.69
Support Vector Machines	0.52	0.60	2.60

Table 80.: Hand multibiometrics fusing palmprint features extracted by LBP and Curvelets together with hand geometry features. z-score normalization is applied to the features previously to the fusion.

11.3.2.10 *Sobel, LBP and Hand Geometry Feature-Level fusion*

Table 81 shows the results of fusing the palmprint features extracted by Sobel filter and LBP together with hand geometry features after z-score normalization. A decrease of the accuracy can be observed when the results provided by this fusion are compared to the best monomodal results as well as two-by-two fusions. Accordingly, it can be stated that the fusion of Sobel, LBP and Hand Geometry features is not an alternative to increase the overall performance.

Figure 77 shows the best validation results of Sobel, LBP and Hand Geometry fusion at feature level when Euclidean distance and SVMs are used to obtain the matching scores and z-score normalization is applied. In addition, the corresponding monomodal results can also be seen in the figure together with the results of the two-by-two fusions.

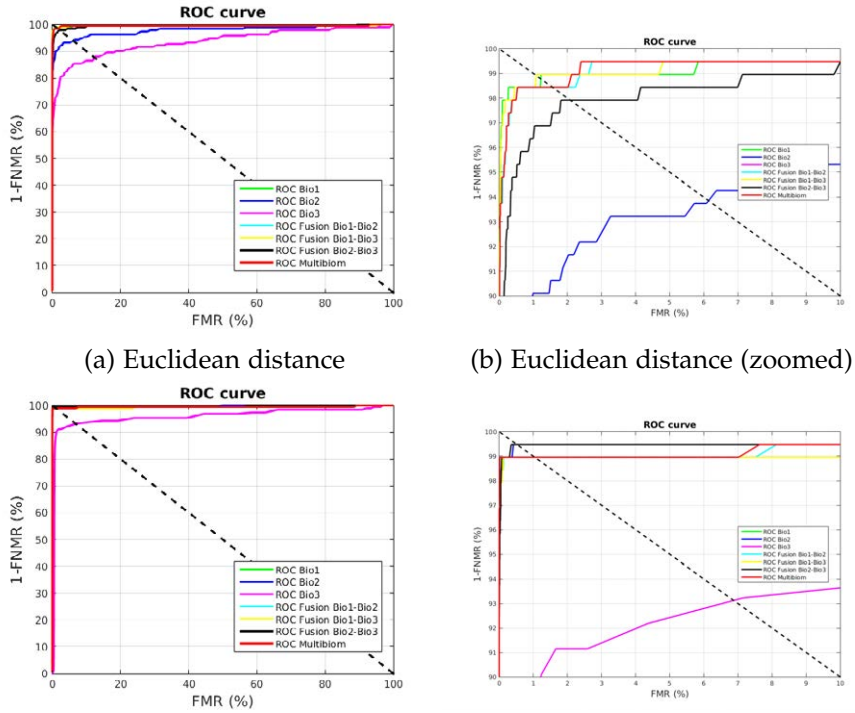

(a) Euclidean distance

(b) Euclidean distance (zoomed)

(c) SVMs

(d) SVMs (zoomed)

Figure 77.: Best feature level fusion results involving Sobel (Bio1), LBP (Bio2) and Hand Geometry (Bio3) methods. z-score normalization is applied to the features previously to the fusion.

Comparison Method	Validation	Test	
	EER (%)	FMR (%)	FNMR (%)
Euclidean Distance	1.56	2.02	4.17
Support Vector Machines	1.04	1.02	2.08

Table 81.: Hand multibiometrics fusing palmprint features extracted by Sobel filter and LBP together with hand geometry features. z-score normalization is applied to the features previously to the fusion.

Part V

CONCLUSIONS AND FUTURE RESEARCH LINES

12

CONCLUSIONS AND FUTURE RESEARCH LINES

12.1 CONCLUSIONS

In this thesis different techniques of image processing, machine learning and information fusion have been analysed in relation to their applicability to contact-less biometrics. To this end, a modular and configurable system that explodes the multimodal nature of the hand to increase its robustness and accuracy have been designed, implemented and evaluated. The evaluation is aimed to provide a fair comparative of methods under different environmental conditions that helps to adapt the system to the specific requirements of a concrete final application. Special attention have been paid to segmentation, feature extraction, comparison and information fusion modules, which gather the main contributions of this thesis.

First contribution of this thesis is a comparative study of different segmentation methods that include well-known methods such as global thresholding and graph cuts as well as a novelty flooding-based method which combines different image-based segmentation approaches and is presented as the second contribution of this thesis. These methods have been compared in terms of accuracy and computation time using diverse datasets of images which cover a wide spectrum of capturing conditions. To this end, a subset of each dataset have been manually segmented in order to have a real ground-truth against which to compare the results of the segmentation algorithms. It is worth noting that one of the employed datasets, the gb2sμMOD database, have been recorded during this thesis aimed to cover the lack of datasets captured in real and adverse environments.

Results show that when the images are captured under uniform lighting conditions and present dark well-contrasted background, global thresholding method, which is the simplest and fasted method included in the system, achieves the best results. Nevertheless, as soon as little difficulties are introduced the precision of this method drastically falls and more complex methods are required. On the other hand, it can be appreciated a similar performance between the remaining methods in almost every situation, being the flooding method proposed in this thesis considerably faster than the other one (Graph Cuts).

Regarding the capturing conditions, it can be seen that illumination and background are the leading causes of the loss of accuracy in the segmented contour. Cluttered background, blurriness or difficult lighting conditions makes the segmentation process specially challenging. Lighting conditions also vary the quality of the captured image. Accordingly, if the image is highly or poorly illuminated texture details are indistinguishable because the hand seems saturated or almost uniformly

black, which directly impact on palmprint recognition results. On the other hand, difficulties can be also produced because the user does not follow the provided recommendations for the capturing process. Most common errors produced by user's behaviour are non centred hand as well as non stretched and non separated fingers. Given the assumptions made by some of the segmentation approaches, the position of the hand directly influences the result, diminishing their accuracy when the hand is not located in the centre of the image. Wrong fingers positioning often lead into segmented hands that only contain four fingers. The four-fingers error is also produced by the use of rings, specially when rings contrast with the skin colour. In these cases the finger wearing the ring does not appear in the segmented image.

Third contribution presented in this thesis is a comprehensive evaluation of different palmprint feature extraction methods comprising Gabor and Sobel filters, Local Binary Patterns, Local Derivative Patterns and Curvelets. Different parameter configurations have also been tested with the aim of finding out which arrangement provides better results for each method. Obtained results under controlled capturing conditions are very promising, even when the methods are simple, easy to implement and low-resource consuming, with the exception of Curvelets from which a higher performance was expected because its higher complexity. On the contrary, a clear decrease of the performance can be appreciated when realistic environmental conditions are introduced. Most of texture recognition methods are sensitive to small translation and rotation variations of the analysed region such as those produced by misalignment of ROIs derived from non-accurate segmentations. Variations in the texture captured by the camera due to illumination changes also influences the recognition results. Nevertheless, these results are acceptable for a wide number of mobile phone applications.

In addition to palmprint, also hand geometry features have been extracted. Results show low discriminative ability of this biometric trait when compared to palmprint methods performance. It can be seen that hand geometry is more affected than palmprint by environmental conditions. In addition to the problems that affect the segmentation process which can lead into non-precise contour detection, it needs to deal with those drawbacks derived from the absence of pose restrictions during the capture. Nevertheless, its simplicity and rapidness make it a good candidate to complement other techniques.

Fourthly, distance-based and Support Vector Machine methods have been compared for feature matching as another contribution of this thesis. As might be expected, SVMs outperform distance based approach, specially when combined with PCA to select the most representative features, getting results near to 0 for some feature extraction methods. Nevertheless, computational cost is higher than distance-based approach because of the training, although this time increase can be partially compensated if dimensionality reduction is applied. In addition, SVMs requires inter-class data to construct the model, which involves data from various individuals and make them more suitable for closed-environments.

Fifth contribution of this thesis is the evaluation of the feasibility of combining different feature extraction methods at different levels to yield into a more precise and robust solution under semi-controlled environmental conditions. When biometric information is fused at score level, a improvement of the results is obtained when

compared against monomodal result. This increase on the accuracy is larger for euclidean distance than SVMs comparison and for those biometrics which present worse monomodal results. Nevertheless, there is not very significant increase in any case, probably due to the fact that monomodal results were quite good. In addition, it can be also appreciated that in general mean-std normalization provides better results and that the best rules to fuse the information are min and sum. On the other hand, results obtained from the fusion of biometric information at feature level show very little improvement regarding to monomodal results and are quite similar to the best monomodal result. It can also be seen that fusing more than two feature extraction approaches in general do not provide any increase on the accuracy of the final result. Finally, when two fusions levels are compared it can be stated that score level generally outperforms the results, what is explained because of the difficulty to find compatible features.

Last but not least, an evaluation methodology that allows for a fair comparison between different methods has been proposed as a contribution of this thesis. In particular, an evaluation protocol is offered with the aim of not only obtaining an extensive evaluation of the complete system under different environmental conditions, and testing multiple combinations of methods for each module, but also providing a basis against which to compare future methods.

12.2 DIFFUSION OF THE RESULTS

Partial results of this thesis have been published in some national and international conferences as well as a journal.

Contributions to conferences are presented here below:

- Belén Ríos-Sánchez, Miguel Viana-Matesanz and Carmen Sánchez-Ávila. Multibiometría de huella palmar y geometría de mano para un sistema sin contacto orientado a dispositivos móviles. XXI Simposium Nacional de la Unión Científica Internacional de Radio. Madrid, Spain. 5-7 Sept. 2016.

  In this conference paper a contactless hand multibiometric system oriented to mobile devices was presented. The system fuses information coming from palmprint and hand geometry at score level.

- Javier Guerra-Casanova, Belén Ríos-Sánchez, Miguel Viana-Matesanz, Gonzalo Bailador, Carmen Sánchez-Ávila and María José Melcón de Giles. Comfort and Security Perception of Biometrics in Mobile Phones with Widespread Sensors. Workshop on Mobility and Cloud Security & Privacy. In conjunction with 35th IEEE Symposium on Reliable Distributed Systems (SRDS). Budapest, Hungary. Sept, 2016.

  This conference paper presents an evaluation of different biometric modalities including hand in terms of user perception about comfort and security.

- Belén Ríos-Sánchez, Miguel Viana-Matesanz, Carmen Sánchez-Ávila and María José Melcón de Giles. A Configurable multibiometric system for authentication at different security levels using mobile devices. Workshop on Mobility

and Cloud Security & Privacy. In conjunction with 35th IEEE Symposium on Reliable Distributed Systems (SRDS). Budapest, Hungary. Sept, 2016.

In this conference paper a configurable multibiometric system for user authentication at different security levels using mobile devices was presented. The system include hand, face and in-air signature biometrics and became more robust as more modalities are involved in the authentication by means of biometric fusion at score level. In addition, hand scores was obtained from a previous fusion of palmprint and hand geometry biometrics.

The contribution of this thesis presented in an international journal (JCR) is detailed hereafter:

- Belén Ríos-Sánchez, Miguel F. Arriaga-Gomez, Javier Guerra-Casanova, Daniel de Santos-Sierra, Ignacio de Mendizabal-Vázquez, Gonzalo Bailador, Carmen Sánchez-Ávila. gb2sμMOD: A MUltiMODal biometric video database using visible and IR light. Information Fusion Journal, vol 32, PartB, pp. 64-79. Nov. 2016.

  This article presents a multimodal biometric database including face, hand and iris images aimed to overcome the absence of hand videos and the lack of infrared images in multimodal databases, as well as to provide touch-less realistic images captured under different environmental conditions.

12.3 FUTURE RESEARCH LINES

This thesis leaves open several research lines on the image segmentation, feature extraction and matching and information fusion fields that could be of great interest for the improvement of contact-less biometric recognition techniques under different usability conditions.

It has been demonstrated that a precise segmentation is crucial for a reliable extraction of the biometric information because it directly influences the detection of characteristic points such as inter-finger valleys and fingertips, as well as the extraction of the region of interest which contains most of the relevant information about the palmprint. Given the results obtained in this thesis, it can be stated that segmentation it is the bottleneck of the system. With the aim to improve segmentation results more complex methods such as deep learning or statistical shape models combined with graph cuts could be an alternative in those cases where computational resources and large population are available. In other cases, to warrant that the hand is centred in the image and the fingers are stretched, it will be possible to add some guidance such as a generic hand in the centre of screen to help the user to place the hand during the capturing process

Regarding segmentation failures, it should be interesting to improve the quality control module in such a way that it will be able to detect more inaccuracies and to repair them when feasible. For instance, it could be possible to repair those images that split one finger because of the use of rings. In addition, an automatic module to discard incorrect ROIs could be included. It is possible to implement some mecha-

nism that discard ROIs which greatly differ from a set of properly extracted ROIs by comparing against the mean and standard deviation of this training set.

In relation to meaningful points detection and ROI extraction, given the fact that it is a sensitive stage, it also will be interesting to carry out a deep study and evaluation of different methods as performed for segmentation, feature extraction, matching and fusion stages. To this end, a reference dataset where the points of interest are known should be labelled.

On the other hand, given the modular design of the system, new methods at each stage are easy to introduce. Accordingly, more elaborated hand geometry features or more complex classifiers such as neural networks, as well as new normalization techniques, could improve the system performance.

In relation to multibiometrics, results have showed that higher improvement is achieved when the fused biometric techniques presented lower monomodal performance. This hypothesis could be tested by extending the experiments to adverse environmental situations as those presented by gb2sμMOD database.

Liveness detection is an important research topic that should be taken into account. Infrared cameras are able to capture hand veins information and thus, could became a reference tool to fight against spoofing attacks. Infrared images provided by gb2sμMOD database can be used to this end as well as to fuse information of the same individuals captured with different devices.

Concerning the biometric application, identification is also an important modality with a wide application field. An extension of the proposed evaluation protocol as well as the evaluation of the combination of different methods for this purpose seems to be interesting.

Finally, with the objective of putting into practice all the knowledge generated throughout the development of this thesis, the different modules of the proposed system could be assembled into a prototype including desktop and mobile phone interfaces. Accordingly, scenario, or even operational, evaluation could be performed.

Appendices

A

GRAPH CUTS RESULTS USING DIFFERENT PARAMETER CONFIGURATIONS

A.1 GRAPH CUTS SEGMENTATION

A complete evaluation of different parameter configurations for Graph Cuts segmentation has been conducted with the aim to find the best arrangement. Obtained results are shown hereafter for each dataset.

A.1.1 *Dataset1*

Image Size (px.)	Balancing Terms	Lambda	F-Score	Average time
640x480	0	0.15	0.9469	11.2690
640x480	0	0.5	0.9425	11.0902
640x480	0	0.75	0.9392	11.3982
640x480	0	1	0.9374	11.4650
640x480	0	1.5	0.9347	11.4887
640x480	0	3	0.9308	11.4741
640x480	0	10	0.9230	11.4997
640x480	0	15	0.9197	11.5866
640x480	0	30	0.9132	11.5834
640x480	0.15	0.15	0.9436	11.6023
640x480	0.15	0.5	0.9421	11.8347
640x480	0.15	0.75	0.9408	11.5939
640x480	0.15	1	0.9398	11.5216
640x480	0.15	1.5	0.9369	11.5400
640x480	0.15	3	0.9317	11.9287
640x480	0.15	10	0.9222	11.0797
640x480	0.15	15	0.9200	11.0526
640x480	0.15	30	0.9144	11.2587
640x480	0.25	0.15	0.9389	11.9172
640x480	0.25	0.5	0.9382	11.9033
640x480	0.25	0.75	0.9370	11.7950
640x480	0.25	1	0.9363	11.0622
640x480	0.25	1.5	0.9341	11.7568
640x480	0.25	3	0.9293	11.8013

Image Size (px.)	Balancing Terms	Lambda	F-Score	Average time
640x480	0.25	10	0.9178	11.6135
640x480	0.25	15	0.9149	11.6330
640x480	0.25	30	0.9103	11.6146
640x480	0.35	0.15	0.9336	11.8315
640x480	0.35	0.5	0.9327	12.1231
640x480	0.35	0.75	0.9323	11.9960
640x480	0.35	1	0.9316	11.7867
640x480	0.35	1.5	0.9305	12.0411
640x480	0.35	3	0.9255	11.9126
640x480	0.35	10	0.9120	11.6159
640x480	0.35	15	0.9089	11.6154
640x480	0.35	30	0.9035	11.6266
640x480	0.45	0.15	0.9272	11.9726
640x480	0.45	0.5	0.9265	11.8843
640x480	0.45	0.75	0.9250	11.9253
640x480	0.45	1	0.9238	11.9806
640x480	0.45	1.5	0.9229	11.8102
640x480	0.45	3	0.9193	12.4471
640x480	0.45	10	0.9037	11.6333
640x480	0.45	15	0.8996	11.7434
640x480	0.45	30	0.8936	11.6604
640x480	0.5	0.15	0.9225	11.7873
640x480	0.5	0.5	0.9217	12.4093
640x480	0.5	0.75	0.9210	12.0484
640x480	0.5	1	0.9204	11.8543
640x480	0.5	1.5	0.9190	12.3863
640x480	0.5	3	0.9149	11.6998
640x480	0.5	10	0.8987	11.6298
640x480	0.5	15	0.8945	11.7001
640x480	0.5	30	0.8883	11.6051
640x480	0.55	0.15	0.9195	12.0149
640x480	0.55	0.5	0.9189	12.1307
640x480	0.55	0.75	0.9179	11.9725
640x480	0.55	1	0.9167	11.8874
640x480	0.55	1.5	0.9152	12.3101
640x480	0.55	3	0.9110	12.2222
640x480	0.55	10	0.8928	11.8693
640x480	0.55	15	0.8871	11.8200
640x480	0.55	30	0.8806	11.8145
640x480	0.65	0.15	0.9090	11.7489
640x480	0.65	0.5	0.9091	12.4287
640x480	0.65	0.75	0.9082	12.2613
640x480	0.65	1	0.9078	11.7698
640x480	0.65	1.5	0.9059	12.1212

Image Size (px.)	Balancing Terms	Lambda	F-Score	Average time
640x480	0.65	3	0.9002	11.9916
640x480	0.65	10	0.8778	11.7497
640x480	0.65	15	0.8722	11.8246
640x480	0.65	30	0.8654	11.5928
640x480	0.75	0.15	0.8952	11.8450
640x480	0.75	0.5	0.8935	11.9395
640x480	0.75	0.75	0.8923	11.8119
640x480	0.75	1	0.8918	11.8197
640x480	0.75	1.5	0.8900	12.8844
640x480	0.75	3	0.8858	11.7446
640x480	0.75	10	0.8624	11.6734
640x480	0.75	15	0.8537	11.6383
640x480	0.75	30	0.8438	11.6299
640x480	0.85	0.15	0.8505	11.8060
640x480	0.85	0.5	0.8493	11.8215
640x480	0.85	0.75	0.8488	11.8179
640x480	0.85	1	0.8480	11.7822
640x480	0.85	1.5	0.8466	11.8779
640x480	0.85	3	0.8389	11.7683
640x480	0.85	10	0.8163	11.6602
640x480	0.85	15	0.8063	11.6501
640x480	0.85	30	0.7945	11.6291
640x480	1	0.15	0.2854	11.7535
640x480	1	0.5	0.2852	11.8427
640x480	1	0.75	0.2852	11.8995
640x480	1	1	0.2855	11.7964
640x480	1	1.5	0.2846	11.7867
640x480	1	3	0.2789	11.8192
640x480	1	10	0.2672	11.6642
640x480	1	15	0.2634	11.6715
640x480	1	30	0.2631	11.6309
480x360	0	0.15	0.9371	6.4866
480x360	0	0.5	0.9319	6.4763
480x360	0	0.75	0.9296	6.4613
480x360	0	1	0.9276	6.4708
480x360	0	1.5	0.9238	6.4596
480x360	0	3	0.9193	6.4590
480x360	0	10	0.9106	6.4783
480x360	0	15	0.9076	6.4803
480x360	0	30	0.9014	6.5236
480x360	0.15	0.15	0.9317	6.5371
480x360	0.15	0.5	0.9302	6.5131
480x360	0.15	0.75	0.9295	6.4765
480x360	0.15	1	0.9285	6.4793

Image Size (px.)	Balancing Terms	Lambda	F-Score	Average time
480x360	0.15	1.5	0.9263	6.4717
480x360	0.15	3	0.9215	6.4537
480x360	0.15	10	0.9115	6.4494
480x360	0.15	15	0.9080	6.4732
480x360	0.15	30	0.9023	6.4554
480x360	0.25	0.15	0.9279	6.4997
480x360	0.25	0.5	0.9265	6.5259
480x360	0.25	0.75	0.9256	6.4916
480x360	0.25	1	0.9251	6.4879
480x360	0.25	1.5	0.9236	6.4780
480x360	0.25	3	0.9190	6.5010
480x360	0.25	10	0.9071	6.4716
480x360	0.25	15	0.9036	6.4677
480x360	0.25	30	0.8988	6.4712
480x360	0.35	0.15	0.9226	6.4869
480x360	0.35	0.5	0.9221	6.4735
480x360	0.35	0.75	0.9210	6.5613
480x360	0.35	1	0.9204	6.4939
480x360	0.35	1.5	0.9193	6.4870
480x360	0.35	3	0.9152	6.4755
480x360	0.35	10	0.9020	6.4714
480x360	0.35	15	0.8990	6.4622
480x360	0.35	30	0.8915	6.4698
480x360	0.45	0.15	0.9151	6.4957
480x360	0.45	0.5	0.9146	6.4837
480x360	0.45	0.75	0.9139	6.4695
480x360	0.45	1	0.9136	6.4844
480x360	0.45	1.5	0.9126	6.4802
480x360	0.45	3	0.9086	6.4590
480x360	0.45	10	0.8939	6.4628
480x360	0.45	15	0.8886	6.4678
480x360	0.45	30	0.8816	6.4608
480x360	0.5	0.15	0.9100	6.5945
480x360	0.5	0.5	0.9094	6.6032
480x360	0.5	0.75	0.9094	6.5529
480x360	0.5	1	0.9089	6.5095
480x360	0.5	1.5	0.9078	6.4822
480x360	0.5	3	0.9037	6.4890
480x360	0.5	10	0.8887	6.4842
480x360	0.5	15	0.8836	6.4801
480x360	0.5	30	0.8764	6.4813
480x360	0.55	0.15	0.9061	6.4801
480x360	0.55	0.5	0.9053	6.5078
480x360	0.55	0.75	0.9047	6.4889

Image Size (px.)	Balancing Terms	Lambda	F-Score	Average time
480x360	0.55	1	0.9036	6.4795
480x360	0.55	1.5	0.9026	6.4902
480x360	0.55	3	0.8981	6.4641
480x360	0.55	10	0.8832	6.4473
480x360	0.55	15	0.8774	6.4506
480x360	0.55	30	0.8711	6.4456
480x360	0.65	0.15	0.8925	6.4617
480x360	0.65	0.5	0.8920	6.4701
480x360	0.65	0.75	0.8916	6.5445
480x360	0.65	1	0.8915	6.4965
480x360	0.65	1.5	0.8901	6.5792
480x360	0.65	3	0.8872	6.5157
480x360	0.65	10	0.8726	6.4934
480x360	0.65	15	0.8667	6.5014
480x360	0.65	30	0.8570	6.4571
480x360	0.75	0.15	0.8763	6.4665
480x360	0.75	0.5	0.8758	6.5786
480x360	0.75	0.75	0.8760	6.4822
480x360	0.75	1	0.8757	6.4829
480x360	0.75	1.5	0.8752	6.4892
480x360	0.75	3	0.8718	6.4668
480x360	0.75	10	0.8552	6.4694
480x360	0.75	15	0.8482	6.4692
480x360	0.75	30	0.8377	6.4603
480x360	0.85	0.15	0.8405	6.4862
480x360	0.85	0.5	0.8409	6.4849
480x360	0.85	0.75	0.8406	6.4814
480x360	0.85	1	0.8400	6.4870
480x360	0.85	1.5	0.8393	6.4810
480x360	0.85	3	0.8351	6.4718
480x360	0.85	10	0.8173	6.4746
480x360	0.85	15	0.8079	6.4820
480x360	0.85	30	0.7952	6.4653
480x360	1	0.15	0.3188	6.4806
480x360	1	0.5	0.3186	6.4941
480x360	1	0.75	0.3182	6.4797
480x360	1	1	0.3176	6.5005
480x360	1	1.5	0.3167	6.4740
480x360	1	3	0.3132	6.4792
480x360	1	10	0.2988	6.4771
480x360	1	15	0.2930	6.4675
480x360	1	30	0.2865	6.4624

Table 82.: Graph Cuts segmentation results using Dataset1 and multiple parameter configurations.

A.1.2 *Dataset2*

Image Size (px.)	Balancing Terms	Lambda	F-Score	Average time
640x480	0	0.15	0.8801	9.0712
640x480	0	0.5	0.8797	9.0851
640x480	0	0.75	0.8793	9.2987
640x480	0	1	0.8788	9.4978
640x480	0	1.5	0.8778	9.4962
640x480	0	3	0.8739	9.5142
640x480	0	10	0.8644	9.5141
640x480	0	15	0.8594	9.5164
640x480	0	30	0.8552	9.5381
640x480	0.15	0.15	0.8877	9.5141
640x480	0.15	0.5	0.8869	9.5140
640x480	0.15	0.75	0.8869	9.5176
640x480	0.15	1	0.8868	9.5239
640x480	0.15	1.5	0.8868	9.5183
640x480	0.15	3	0.8841	9.5432
640x480	0.15	10	0.8759	9.5144
640x480	0.15	15	0.8743	9.5229
640x480	0.15	30	0.8751	9.5140
640x480	0.25	0.15	0.8867	9.4878
640x480	0.25	0.5	0.8867	9.4881
640x480	0.25	0.75	0.8867	9.4958
640x480	0.25	1	0.8867	9.5314
640x480	0.25	1.5	0.8867	9.4987
640x480	0.25	3	0.8863	9.5184
640x480	0.25	10	0.8840	9.5105
640x480	0.25	15	0.8795	9.5278
640x480	0.25	30	0.8806	9.5282
640x480	0.35	0.15	0.8913	9.5227
640x480	0.35	0.5	0.8913	9.5126
640x480	0.35	0.75	0.8913	9.5286
640x480	0.35	1	0.8913	9.5175
640x480	0.35	1.5	0.8912	9.5230
640x480	0.35	3	0.8911	9.5122
640x480	0.35	10	0.8864	9.5090
640x480	0.35	15	0.8850	9.5048
640x480	0.35	30	0.8817	9.5526
640x480	0.45	0.15	0.8923	9.5189
640x480	0.45	0.5	0.8924	9.5172
640x480	0.45	0.75	0.8925	9.5148
640x480	0.45	1	0.8925	9.5260
640x480	0.45	1.5	0.8925	9.5422
640x480	0.45	3	0.8922	9.5141

Image Size (px.)	Balancing Terms	Lambda	F-Score	Average time
640x480	0.45	10	0.8880	9.5242
640x480	0.45	15	0.8867	9.5178
640x480	0.45	30	0.8833	9.5147
640x480	0.5	0.15	0.8920	9.5305
640x480	0.5	0.5	0.8936	9.5294
640x480	0.5	0.75	0.8936	9.5278
640x480	0.5	1	0.8935	9.5225
640x480	0.5	1.5	0.8934	9.5115
640x480	0.5	3	0.8932	9.5103
640x480	0.5	10	0.8894	9.5109
640x480	0.5	15	0.8880	9.5170
640x480	0.5	30	0.8819	9.5162
640x480	0.55	0.15	0.8866	9.5137
640x480	0.55	0.5	0.8865	9.5731
640x480	0.55	0.75	0.8865	9.5400
640x480	0.55	1	0.8877	9.5345
640x480	0.55	1.5	0.8877	9.5388
640x480	0.55	3	0.8875	9.5415
640x480	0.55	10	0.8836	9.5292
640x480	0.55	15	0.8827	9.5360
640x480	0.55	30	0.8784	9.5290
640x480	0.65	0.15	0.8780	9.5325
640x480	0.65	0.5	0.8780	9.5361
640x480	0.65	0.75	0.8778	9.5201
640x480	0.65	1	0.8778	9.5071
640x480	0.65	1.5	0.8777	9.5345
640x480	0.65	3	0.8774	9.5197
640x480	0.65	10	0.8756	9.4979
640x480	0.65	15	0.8742	9.5029
640x480	0.65	30	0.8708	9.5171
640x480	0.75	0.15	0.8769	9.5100
640x480	0.75	0.5	0.8764	9.5352
640x480	0.75	0.75	0.8763	9.5582
640x480	0.75	1	0.8758	9.5387
640x480	0.75	1.5	0.8752	9.5411
640x480	0.75	3	0.8751	9.5936
640x480	0.75	10	0.8734	9.5343
640x480	0.75	15	0.8719	9.5182
640x480	0.75	30	0.8670	9.5250
640x480	0.85	0.15	0.8115	9.5302
640x480	0.85	0.5	0.8110	9.5266
640x480	0.85	0.75	0.8109	9.5241
640x480	0.85	1	0.8108	9.5124
640x480	0.85	1.5	0.8107	9.5228

Image Size (px.)	Balancing Terms	Lambda	F-Score	Average time
640x480	0.85	3	0.8103	9.5295
640x480	0.85	10	0.8075	9.5207
640x480	0.85	15	0.8062	9.5618
640x480	0.85	30	0.8028	9.5422
640x480	1	0.15	0.6349	9.5482
640x480	1	0.5	0.6349	9.5360
640x480	1	0.75	0.6349	9.5157
640x480	1	1	0.6348	9.5220
640x480	1	1.5	0.6347	9.5414
640x480	1	3	0.6344	9.5291
640x480	1	10	0.6319	9.5196
640x480	1	15	0.6306	9.5129
640x480	1	30	0.6247	9.5042
480x360	0	0.15	0.8862	5.2988
480x360	0	0.5	0.8854	5.2961
480x360	0	0.75	0.8845	5.3003
480x360	0	1	0.8822	5.3019
480x360	0	1.5	0.8798	5.2977
480x360	0	3	0.8757	5.3015
480x360	0	10	0.8657	5.3043
480x360	0	15	0.8628	5.3066
480x360	0	30	0.8564	5.3017
480x360	0.15	0.15	0.8922	5.2986
480x360	0.15	0.5	0.8921	5.2972
480x360	0.15	0.75	0.8920	5.3030
480x360	0.15	1	0.8918	5.3000
480x360	0.15	1.5	0.8890	5.3061
480x360	0.15	3	0.8873	5.3085
480x360	0.15	10	0.8807	5.3055
480x360	0.15	15	0.8783	5.3156
480x360	0.15	30	0.8747	5.3085
480x360	0.25	0.15	0.8935	5.3061
480x360	0.25	0.5	0.8934	5.3077
480x360	0.25	0.75	0.8934	5.3118
480x360	0.25	1	0.8933	5.3098
480x360	0.25	1.5	0.8932	5.3094
480x360	0.25	3	0.8929	5.3011
480x360	0.25	10	0.8859	5.3024
480x360	0.25	15	0.8836	5.2972
480x360	0.25	30	0.8806	5.2973
480x360	0.35	0.15	0.8993	5.2959
480x360	0.35	0.5	0.8993	5.2996
480x360	0.35	0.75	0.8995	5.2983
480x360	0.35	1	0.8994	5.2824

Image Size (px.)	Balancing Terms	Lambda	F-Score	Average time
480x360	0.35	1.5	0.8993	5.2972
480x360	0.35	3	0.8996	5.2926
480x360	0.35	10	0.8918	5.2987
480x360	0.35	15	0.8886	5.2959
480x360	0.35	30	0.8813	5.2978
480x360	0.45	0.15	0.9006	5.2991
480x360	0.45	0.5	0.9005	5.2989
480x360	0.45	0.75	0.9004	5.2978
480x360	0.45	1	0.9004	5.3171
480x360	0.45	1.5	039002	5.3109
480x360	0.45	3	0.8998	5.3043
480x360	0.45	10	0.8937	5.3039
480x360	0.45	15	0.8918	5.3113
480x360	0.45	30	0.8848	5.3061
480x360	0.5	0.15	0.9013	5.3062
480x360	0.5	0.5	0.9011	5.3263
480x360	0.5	0.75	0.9011	5.3080
480x360	0.5	1	0.9010	5.3032
480x360	0.5	1.5	0.9009	5.3238
480x360	0.5	3	0.9007	5.3077
480x360	0.5	10	0.8965	5.3065
480x360	0.5	15	0.8938	5.3073
480x360	0.5	30	0.8870	5.3071
480x360	0.55	0.15	0.9009	5.3067
480x360	0.55	0.5	0.9010	5.3167
480x360	0.55	0.75	0.9010	5.3163
480x360	0.55	1	0.9010	5.3011
480x360	0.55	1.5	0.9009	5.3216
480x360	0.55	3	0.8981	5.3027
480x360	0.55	10	0.8972	5.3283
480x360	0.55	15	0.8951	5.3091
480x360	0.55	30	0.8881	5.2929
480x360	0.65	0.15	0.8972	5.2954
480x360	0.65	0.5	0.8981	5.3214
480x360	0.65	0.75	0.8981	5.3141
480x360	0.65	1	0.8979	5.3072
480x360	0.65	1.5	0.8977	5.3151
480x360	0.65	3	0.8968	5.3075
480x360	0.65	10	0.8899	5.3105
480x360	0.65	15	0.8881	5.3165
480x360	0.65	30	0.8837	5.3079
480x360	0.75	0.15	0.8933	5.3198
480x360	0.75	0.5	0.8930	5.3194
480x360	0.75	0.75	0.8927	5.3143

Image Size (px.)	Balancing Terms	Lambda	F-Score	Average time
480x360	0.75	1	0.8929	5.3074
480x360	0.75	1.5	0.8927	5.3072
480x360	0.75	3	0.8920	5.3081
480x360	0.75	10	0.8893	5.3168
480x360	0.75	15	0.8910	5.3152
480x360	0.75	30	0.8851	5.3118
480x360	0.85	0.15	0.8634	5.3147
480x360	0.85	0.5	0.8633	5.3199
480x360	0.85	0.75	0.8631	5.3152
480x360	0.85	1	0.8629	5.3079
480x360	0.85	1.5	0.8631	5.3096
480x360	0.85	3	0.8615	5.3048
480x360	0.85	10	0.8571	5.2980
480x360	0.85	15	0.8547	5.3032
480x360	0.85	30	0.8533	5.2953
480x360	1	0.15	0.7488	5.2926
480x360	1	0.5	0.7488	5.2973
480x360	1	0.75	0.7487	5.3050
480x360	1	1	0.7487	5.3040
480x360	1	1.5	0.7485	5.3007
480x360	1	3	0.7473	5.2958
480x360	1	10	0.7430	5.3040
480x360	1	15	0.7409	5.3067
480x360	1	30	0.7314	5.3157

Table 83.: Graph Cuts segmentation results using Dataset2 and multiple parameter configurations.

A.1.3 *Dataset3*

Image Size (px.)	Balancing Terms	Lambda	F-Score	Average time
640x480	0	0.15	0.6807	9.5554
640x480	0	0.5	0.6800	9.5347
640x480	0	0.75	0.6803	9.5309
640x480	0	1	0.6786	9.5355
640x480	0	1.5	0.6813	9.5420
640x480	0	3	0.6826	9.5457
640x480	0	10	0.6866	9.5858
640x480	0	15	0.6874	9.5609
640x480	0	30	0.6880	9.6248
640x480	0.15	0.15	0.7080	9.5469
640x480	0.15	0.5	0.7073	9.5360
640x480	0.15	0.75	0.7071	9.5328
640x480	0.15	1	0.7072	9.5091
640x480	0.15	1.5	0.7069	9.5382
640x480	0.15	3	0.7069	9.5346
640x480	0.15	10	0.7084	9.5432
640x480	0.15	15	0.7096	9.5577
640x480	0.15	30	0.7113	9.5527
640x480	0.25	0.15	0.7269	9.5551
640x480	0.25	0.5	0.7262	9.5350
640x480	0.25	0.75	0.7260	9.5503
640x480	0.25	1	0.7260	9.5529
640x480	0.25	1.5	0.7258	9.5293
640x480	0.25	3	0.7251	9.5322
640x480	0.25	10	0.7253	9.5622
640x480	0.25	15	0.7258	9.5711
640x480	0.25	30	0.7270	9.5494
640x480	0.35	0.15	0.7415	9.5400
640x480	0.35	0.5	0.7407	9.5431
640x480	0.35	0.75	0.7405	9.5341
640x480	0.35	1	0.7405	9.5350
640x480	0.35	1.5	0.7403	9.5669
640x480	0.35	3	0.7400	9.5540
640x480	0.35	10	0.7403	9.5481
640x480	0.35	15	0.7404	9.5470
640x480	0.35	30	0.7408	9.5496
640x480	0.45	0.15	0.7526	9.5308
640x480	0.45	0.5	0.7520	9.5621
640x480	0.45	0.75	0.7519	9.5564
640x480	0.45	1	0.7517	9.5486
640x480	0.45	1.5	0.7517	9.5384
640x480	0.45	3	0.7517	9.5396

Image Size (px.)	Balancing Terms	Lambda	F-Score	Average time
640x480	0.45	10	0.7521	9.5417
640x480	0.45	15	0.7521	9.5383
640x480	0.45	30	0.7513	9.5318
640x480	0.5	0.15	0.7569	9.5334
640x480	0.5	0.5	0.7562	9.5423
640x480	0.5	0.75	0.7560	9.5304
640x480	0.5	1	0.7559	9.5574
640x480	0.5	1.5	0.7558	9.5349
640x480	0.5	3	0.7559	9.5669
640x480	0.5	10	0.7555	9.5398
640x480	0.5	15	0.7554	9.5463
640x480	0.5	30	0.7545	9.5420
640x480	0.55	0.15	0.7587	9.5423
640x480	0.55	0.5	0.7581	9.5416
640x480	0.55	0.75	0.7579	9.5447
640x480	0.55	1	0.7578	9.5434
640x480	0.55	1.5	0.7577	9.5394
640x480	0.55	3	0.7574	9.5246
640x480	0.55	10	0.7567	9.5425
640x480	0.55	15	0.7566	9.5242
640x480	0.55	30	0.7555	9.5235
640x480	0.65	0.15	0.7556	9.5667
640x480	0.65	0.5	0.7552	9.5463
640x480	0.65	0.75	0.7550	9.5445
640x480	0.65	1	0.7548	9.5544
640x480	0.65	1.5	0.7545	9.5565
640x480	0.65	3	0.7541	9.5660
640x480	0.65	10	0.7535	9.5494
640x480	0.65	15	0.7531	9.5530
640x480	0.65	30	0.7519	9.5389
640x480	0.75	0.15	0.7409	9.5341
640x480	0.75	0.5	0.7406	9.5284
640x480	0.75	0.75	0.7405	9.5212
640x480	0.75	1	0.7404	9.5557
640x480	0.75	1.5	0.7403	9.5475
640x480	0.75	3	0.7397	9.5201
640x480	0.75	10	0.7383	9.5450
640x480	0.75	15	0.7379	9.5434
640x480	0.75	30	0.7347	9.5435
640x480	0.85	0.15	0.7027	9.5456
640x480	0.85	0.5	0.7024	9.5958
640x480	0.85	0.75	0.7023	9.5374
640x480	0.85	1	0.7021	9.5518
640x480	0.85	1.5	0.7017	9.5349

Image Size (px.)	Balancing Terms	Lambda	F-Score	Average time
640x480	0.85	3	0.7009	9.5474
640x480	0.85	10	0.6998	9.5502
640x480	0.85	15	0.6987	9.5339
640x480	0.85	30	0.6950	9.5419
640x480	1	0.15	0.5903	9.5312
640x480	1	0.5	0.5901	9.5118
640x480	1	0.75	0.5899	9.5289
640x480	1	1	0.5896	9.5404
640x480	1	1.5	0.5890	9.5236
640x480	1	3	0.5873	9.5470
640x480	1	10	0.5836	9.5422
640x480	1	15	0.5823	9.5662
640x480	1	30	0.5768	9.5493
480x360	0	0.15	0.6850	5.3306
480x360	0	0.5	0.6871	5.3182
480x360	0	0.75	0.6875	5.3157
480x360	0	1	0.6879	5.3179
480x360	0	1.5	0.6886	5.3239
480x360	0	3	0.6910	5.3193
480x360	0	10	0.6930	5.3359
480x360	0	15	0.6933	5.3907
480x360	0	30	0.6919	5.3567
480x360	0.15	0.15	0.5624	5.3219
480x360	0.15	0.5	0.5588	5.3241
480x360	0.15	0.75	0.5583	5.3228
480x360	0.15	1	0.5579	5.3187
480x360	0.15	1.5	0.5574	5.3164
480x360	0.15	3	0.7105	5.3600
480x360	0.15	10	0.7132	5.3151
480x360	0.15	15	0.7139	5.3237
480x360	0.15	30	0.7149	5.3229
480x360	0.25	0.15	0.5860	5.3033
480x360	0.25	0.5	0.5837	5.3244
480x360	0.25	0.75	0.5818	5.3192
480x360	0.25	1	0.5811	5.3575
480x360	0.25	1.5	0.5809	5.3192
480x360	0.25	3	0.7211	5.3221
480x360	0.25	10	0.7284	5.3286
480x360	0.25	15	0.7291	5.3314
480x360	0.25	30	0.7298	5.3375
480x360	0.35	0.15	0.6062	5.5515
480x360	0.35	0.5	0.6044	5.3690
480x360	0.35	0.75	0.6035	5.3338
480x360	0.35	1	0.6026	5.3335

Image Size (px.)	Balancing Terms	Lambda	F-Score	Average time
480x360	0.35	1.5	0.6021	5.3315
480x360	0.35	3	0.7410	5.3244
480x360	0.35	10	0.7422	5.3232
480x360	0.35	15	0.7424	5.3578
480x360	0.35	30	0.7426	5.3364
480x360	0.45	0.15	0.6210	5.3213
480x360	0.45	0.5	0.6190	5.3227
480x360	0.45	0.75	0.6187	5.3293
480x360	0.45	1	0.6184	5.3305
480x360	0.45	1.5	0.6177	5.3359
480x360	0.45	3	0.7539	5.3189
480x360	0.45	10	0.7540	5.3251
480x360	0.45	15	0.7538	5.3150
480x360	0.45	30	0.7530	5.3678
480x360	0.5	0.15	0.6236	5.3198
480x360	0.5	0.5	0.6232	5.3273
480x360	0.5	0.75	0.6224	5.3214
480x360	0.5	1	0.6222	5.3177
480x360	0.5	1.5	0.6226	5.3183
480x360	0.5	3	0.7587	5.3197
480x360	0.5	10	0.7584	5.3221
480x360	0.5	15	0.7581	5.3284
480x360	0.5	30	0.7567	5.3260
480x360	0.55	0.15	0.6205	5.3258
480x360	0.55	0.5	0.6199	5.3295
480x360	0.55	0.75	0.6193	5.3256
480x360	0.55	1	0.6193	5.3205
480x360	0.55	1.5	0.6189	5.3312
480x360	0.55	3	0.7614	5.3353
480x360	0.55	10	0.7612	5.3275
480x360	0.55	15	0.7606	5.3182
480x360	0.55	30	0.7591	5.3276
480x360	0.65	0.15	0.6232	5.3322
480x360	0.65	0.5	0.6221	5.3400
480x360	0.65	0.75	0.6216	5.3252
480x360	0.65	1	0.6220	5.3251
480x360	0.65	1.5	0.6214	5.3368
480x360	0.65	3	0.7621	5.3219
480x360	0.65	10	0.7616	5.3136
480x360	0.65	15	0.7608	5.3158
480x360	0.65	30	0.7592	5.3148
480x360	0.75	0.15	0.6215	5.3132
480x360	0.75	0.5	0.6197	5.3157
480x360	0.75	0.75	0.6195	5.3224

Image Size (px.)	Balancing Terms	Lambda	F-Score	Average time
480x360	0.75	1	0.6196	5.3000
480x360	0.75	1.5	0.6208	5.3243
480x360	0.75	3	0.7532	5.3372
480x360	0.75	10	0.7520	5.3262
480x360	0.75	15	0.7507	5.3229
480x360	0.75	30	0.7477	5.3063
480x360	0.85	0.15	0.5853	5.3275
480x360	0.85	0.5	0.5843	5.3182
480x360	0.85	0.75	0.5838	5.3088
480x360	0.85	1	0.5844	5.3234
480x360	0.85	1.5	0.5842	5.3229
480x360	0.85	3	0.7296	5.3168
480x360	0.85	10	0.7277	5.3357
480x360	0.85	15	0.7258	5.3270
480x360	0.85	30	0.7213	5.3233
480x360	1	0.15	0.5376	5.3303
480x360	1	0.5	0.5373	5.3278
480x360	1	0.75	0.5364	5.3298
480x360	1	1	0.5360	5.3313
480x360	1	1.5	0.5354	5.3181
480x360	1	3	0.6519	5.3337
480x360	1	10	0.6484	5.3228
480x360	1	15	0.6465	5.3189
480x360	1	30	0.6400	5.3181

Table 84.: Graph Cuts segmentation results using Dataset3 and multiple parameter configurations.

A.1.4 *Dataset4*

Image Size (px.)	Balancing Terms	Lambda	F-Score	Average time
640x480	0	0.15	0.5833	11.6030
640x480	0	0.5	0.5812	11.5914
640x480	0	0.75	0.5803	11.5872
640x480	0	1	0.5792	11.5919
640x480	0	1.5	0.5774	11.5778
640x480	0	3	0.5735	11.5760
640x480	0	10	0.5673	11.5876
640x480	0	15	0.5684	11.5858
640x480	0	30	0.5652	11.6107
640x480	0.15	0.15	0.6033	11.5759
640x480	0.15	0.5	0.6032	11.5956
640x480	0.15	0.75	0.6028	11.6104
640x480	0.15	1	0.6003	11.5834
640x480	0.15	1.5	0.5997	11.5794
640x480	0.15	3	0.5985	11.5711
640x480	0.15	10	0.5966	11.5762
640x480	0.15	15	0.5933	11.5786
640x480	0.15	30	0.5909	11.6517
640x480	0.25	0.15	0.6195	11.6027
640x480	0.25	0.5	0.6194	11.5872
640x480	0.25	0.75	0.6195	11.5996
640x480	0.25	1	0.6190	11.5751
640x480	0.25	1.5	0.6189	11.6186
640x480	0.25	3	0.6172	11.5887
640x480	0.25	10	0.6131	11.5883
640x480	0.25	15	0.6108	11.6008
640x480	0.25	30	0.6081	11.6316
640x480	0.35	0.15	0.6303	11.6133
640x480	0.35	0.5	0.6295	11.6120
640x480	0.35	0.75	0.6299	11.6075
640x480	0.35	1	0.6298	11.6483
640x480	0.35	1.5	0.6291	11.6051
640x480	0.35	3	0.6282	11.5833
640x480	0.35	10	0.6267	11.5707
640x480	0.35	15	0.6233	11.5843
640x480	0.35	30	0.6215	11.5942
640x480	0.45	0.15	0.6432	11.6043
640x480	0.45	0.5	0.6426	11.6135
640x480	0.45	0.75	0.6428	11.5964
640x480	0.45	1	0.6432	11.6134
640x480	0.45	1.5	0.6432	11.6187
640x480	0.45	3	0.6428	11.6013

Image Size (px.)	Balancing Terms	Lambda	F-Score	Average time
640x480	0.45	10	0.6394	11.6461
640x480	0.45	15	0.6366	11.6285
640x480	0.45	30	0.6342	11.5549
640x480	0.5	0.15	0.6480	11.5442
640x480	0.5	0.5	0.6476	11.5757
640x480	0.5	0.75	0.6463	11.5329
640x480	0.5	1	0.6464	11.5408
640x480	0.5	1.5	0.6463	11.5730
640x480	0.5	3	0.6484	11.5684
640x480	0.5	10	0.6430	11.5528
640x480	0.5	15	0.6420	11.5945
640x480	0.5	30	0.6373	11.5692
640x480	0.55	0.15	0.6505	11.6206
640x480	0.55	0.5	0.6497	11.5752
640x480	0.55	0.75	0.6497	11.5501
640x480	0.55	1	0.6498	11.5481
640x480	0.55	1.5	0.6496	11.5575
640x480	0.55	3	0.6507	11.5249
640x480	0.55	10	0.6478	11.5227
640x480	0.55	15	0.6475	11.5376
640x480	0.55	30	0.6452	11.5457
640x480	0.65	0.15	0.6566	11.5392
640x480	0.65	0.5	0.6551	11.5701
640x480	0.65	0.7	0.6549	11.5489
640x480	0.65	1	0.6549	11.5577
640x480	0.65	1.5	0.6544	11.5402
640x480	0.65	3	0.6540	11.5686
640x480	0.65	10	0.6552	11.5544
640x480	0.65	15	0.6529	11.5709
640x480	0.65	30	0.6521	11.5587
640x480	0.75	0.15	0.6539	11.5420
640x480	0.75	0.5	0.6539	11.5555
640x480	0.75	0.75	0.6534	11.5939
640x480	0.75	1	0.6537	11.5692
640x480	0.75	1.5	0.6534	11.5938
640x480	0.75	3	0.6533	11.5713
640x480	0.75	10	0.6524	11.5696
640x480	0.75	15	0.6511	11.6380
640x480	0.75	30	0.6450	11.5847
640x480	0.85	0.15	0.6330	11.5667
640x480	0.85	0.5	0.6329	11.5690
640x480	0.85	0.75	0.6328	11.5931
640x480	0.85	1	0.6324	11.5692
640x480	0.85	1.5	0.6322	11.5424

Image Size (px.)	Balancing Terms	Lambda	F-Score	Average time
640x480	0.85	3	0.6326	11.5503
640x480	0.85	10	0.6396	11.5353
640x480	0.85	15	0.6292	11.5543
640x480	0.85	30	0.6226	11.5536
640x480	1	0.15	0.5708	11.5525
640x480	1	0.5	0.5706	11.5643
640x480	1	0.75	0.5706	11.5518
640x480	1	1	0.5706	11.5426
640x480	1	1.5	0.5709	11.5559
640x480	1	3	0.5702	11.5717
640x480	1	10	0.5680	11.5638
640x480	1	15	0.5651	11.5642
640x480	1	30	0.5598	11.6328
480x360	0	0.15	0.5886	6.4387
480x360	0	0.5	0.5862	6.4439
480x360	0	0.75	0.5836	6.4374
480x360	0	1	0.5826	6.4478
480x360	0	1.5	0.5820	6.4448
480x360	0	3	0.5780	6.4633
480x360	0	10	0.5735	6.4562
480x360	0	15	0.5726	6.4494
480x360	0	30	0.5709	6.4628
480x360	0.15	0.15	0.6057	6.4452
480x360	0.15	0.5	0.6040	6.4811
480x360	0.15	0.75	0.6040	6.4455
480x360	0.15	1	0.6042	6.4404
480x360	0.15	1.5	0.6048	6.4371
480x360	0.15	3	0.6030	6.4433
480x360	0.15	10	0.5984	6.4500
480x360	0.15	15	0.5966	6.4547
480x360	0.15	30	0.5925	6.4514
480x360	0.25	0.15	0.6198	6.4478
480x360	0.25	0.5	0.6180	6.4411
480x360	0.25	0.75	0.6182	6.4437
480x360	0.25	1	0.6181	6.4494
480x360	0.25	1.5	0.6170	6.4368
480x360	0.25	3	0.6169	6.4409
480x360	0.25	10	0.6148	6.4390
480x360	0.25	15	0.6116	6.4285
480x360	0.25	30	0.6089	6.4369
480x360	0.35	0.15	0.6326	6.4397
480x360	0.35	0.5	0.6332	6.4520
480x360	0.35	0.75	0.6323	6.4398
480x360	0.35	1	0.6318	6.4415

Image Size (px.)	Balancing Terms	Lambda	F-Score	Average time
480x360	0.35	1.5	0.6326	6.4426
480x360	0.35	3	0.6332	6.4336
480x360	0.35	10	0.6304	6.4364
480x360	0.35	15	0.6278	6.4385
480x360	0.35	30	0.6241	6.4417
480x360	0.45	0.15	0.6445	6.4341
480x360	0.45	0.5	0.6438	6.4353
480x360	0.45	0.75	0.6437	6.4400
480x360	0.45	1	0.6440	6.4342
480x360	0.45	1.5	0.6451	6.4398
480x360	0.45	3	0.6470	6.4511
480x360	0.45	10	0.6435	6.4328
480x360	0.45	15	0.6416	6.4295
480x360	0.45	30	0.6353	6.4360
480x360	0.5	0.15	0.6464	6.4465
480x360	0.5	0.5	0.6478	6.4446
480x360	0.5	0.75	0.6477	6.4356
480x360	0.5	1	0.6478	6.4369
480x360	0.5	1.5	0.6481	6.4433
480x360	0.5	3	0.6508	6.4481
480x360	0.5	10	0.6484	6.4300
480x360	0.5	15	0.6460	6.4538
480x360	0.5	30	0.6410	6.4707
480x360	0.55	0.15	0.6548	6.4504
480x360	0.55	0.5	0.6538	6.4498
480x360	0.55	0.75	0.6539	6.4482
480x360	0.55	1	0.6545	6.4516
480x360	0.55	1.5	0.6546	6.4590
480x360	0.55	3	0.6571	6.4401
480x360	0.55	10	0.6546	6.4406
480x360	0.55	15	0.6534	6.4624
480x360	0.55	30	0.6480	6.4456
480x360	0.65	0.15	0.6679	6.4436
480x360	0.65	0.5	0.6677	6.4402
480x360	0.65	0.75	0.6678	6.4417
480x360	0.65	1	0.6674	6.4427
480x360	0.65	1.5	0.6669	6.4441
480x360	0.65	3	0.6680	6.4388
480x360	0.65	10	0.6661	6.4430
480x360	0.65	15	0.6633	6.4414
480x360	0.65	30	0.6595	6.4383
480x360	0.75	0.15	0.6699	6.4302
480x360	0.75	0.5	0.6694	6.4377
480x360	0.75	0.75	0.6692	6.4399

Image Size (px.)	Balancing Terms	Lambda	F-Score	Average time
480x360	0.75	1	0.6691	6.4476
480x360	0.75	1.5	0.6705	6.4404
480x360	0.75	3	0.6705	6.4426
480x360	0.75	10	0.6701	6.4413
480x360	0.75	15	0.6679	6.4449
480x360	0.75	30	0.6615	6.4390
480x360	0.85	0.15	0.6543	6.4488
480x360	0.85	0.5	0.6546	6.4498
480x360	0.85	0.75	0.6539	6.4441
480x360	0.85	1	0.6536	6.4478
480x360	0.85	1.5	0.6538	6.4442
480x360	0.85	3	0.6523	6.4512
480x360	0.85	10	0.6507	6.4441
480x360	0.85	15	0.6480	6.4661
480x360	0.85	30	0.6399	6.4533
480x360	1	0.15	0.5949	6.4351
480x360	1	0.5	0.5948	6.4377
480x360	1	0.75	0.5949	6.4308
480x360	1	1	0.5949	6.4524
480x360	1	1.5	0.5950	6.4377
480x360	1	3	0.5942	6.4441
480x360	1	10	0.5929	6.4473
480x360	1	15	0.5900	6.4481
480x360	1	30	0.5856	6.4509

Table 85.: Graph Cuts segmentation results using Dataset4 and multiple parameter configurations.

Image Size (px.)	Balancing Terms	Lambda	F-Score
640x480	0	0.15	0.6762
640x480	0	0.5	0.6725
640x480	0	0.75	0.6709
640x480	0	1	0.6704
640x480	0	1.5	0.6725
640x480	0	3	0.6728
640x480	0	10	0.6699
640x480	0	15	0.6786
640x480	0	30	0.6716
640x480	0.15	0.15	0.6975
640x480	0.15	0.5	0.6957
640x480	0.15	0.75	0.6952
640x480	0.15	1	0.6933
640x480	0.15	1.5	0.6914
640x480	0.15	3	0.6905
640x480	0.15	10	0.6891
640x480	0.15	15	0.6894
640x480	0.15	30	0.6909
640x480	0.25	0.15	0.7062
640x480	0.25	0.5	0.7064
640x480	0.25	0.75	0.7058
640x480	0.25	1	0.7054
640x480	0.25	1.5	0.7026
640x480	0.25	3	0.7019
640x480	0.25	10	0.7019
640x480	0.25	15	0.7017
640x480	0.25	30	0.7062
640x480	0.35	0.15	0.7169
640x480	0.35	0.5	0.7174
640x480	0.35	0.75	0.7179
640x480	0.35	1	0.7175
640x480	0.35	1.5	0.7157
640x480	0.35	3	0.7121
640x480	0.35	10	0.7114
640x480	0.35	15	0.7080
640x480	0.35	30	0.7123
640x480	0.45	0.15	0.7258
640x480	0.45	0.5	0.7251
640x480	0.45	0.75	0.7254
640x480	0.45	1	0.7254
640x480	0.45	1.5	0.7252
640x480	0.45	3	0.7280
640x480	0.45	10	0.7221
640x480	0.45	15	0.7220

Image Size (px.)	Balancing Terms	Lambda	F-Score
640x480	0.45	30	0.7276
640x480	0.5	0.15	0.7217
640x480	0.5	0.5	0.7214
640x480	0.5	0.75	0.7213
640x480	0.5	1	0.7211
640x480	0.5	1.5	0.7202
640x480	0.5	3	0.7336
640x480	0.5	10	0.7197
640x480	0.5	15	0.7171
640x480	0.5	30	0.7235
640x480	0.55	0.15	0.7238
640x480	0.55	0.5	0.7226
640x480	0.55	0.75	0.7228
640x480	0.55	1	0.7228
640x480	0.55	1.5	0.7230
640x480	0.55	3	0.7290
640x480	0.55	10	0.7185
640x480	0.55	15	0.7170
640x480	0.55	30	0.7227
640x480	0.65	0.15	0.7342
640x480	0.65	0.5	0.7324
640x480	0.65	0.75	0.7322
640x480	0.65	1	0.7320
640x480	0.65	1.5	0.7319
640x480	0.65	3	0.7292
640x480	0.65	10	0.7330
640x480	0.65	15	0.7335
640x480	0.65	30	0.7324
640x480	0.75	0.15	0.7173
640x480	0.75	0.5	0.7175
640x480	0.75	0.75	0.7173
640x480	0.75	1	0.7176
640x480	0.75	1.5	0.7167
640x480	0.75	3	0.7166
640x480	0.75	10	0.7160
640x480	0.75	15	0.7154
640x480	0.75	30	0.7113
640x480	0.85	0.15	0.6765
640x480	0.85	0.5	0.6766
640x480	0.85	0.75	0.6766
640x480	0.85	1	0.6763
640x480	0.85	1.5	0.6760
640x480	0.85	3	0.6762
640x480	0.85	10	0.6730

Image Size (px.)	Balancing Terms	Lambda	F-Score
640x480	0.85	15	0.6720
640x480	0.85	30	0.6681
640x480	1	0.15	0.5927
640x480	1	0.5	0.5926
640x480	1	0.75	0.5927
640x480	1	1	0.5927
640x480	1	1.5	0.5925
640x480	1	3	0.5923
640x480	1	10	0.5887
640x480	1	15	0.5871
640x480	1	30	0.5821
480x360	0	0.15	0.6693
480x360	0	0.5	0.6670
480x360	0	0.75	0.6657
480x360	0	1	0.6647
480x360	0	1.5	0.6652
480x360	0	3	0.6615
480x360	0	10	0.6634
480x360	0	15	0.6641
480x360	0	30	0.6602
480x360	0.15	0.15	0.6884
480x360	0.15	0.5	0.6848
480x360	0.15	0.75	0.6877
480x360	0.15	1	0.6878
480x360	0.15	1.5	0.6871
480x360	0.15	3	0.6840
480x360	0.15	10	0.6828
480x360	0.15	15	0.6837
480x360	0.15	30	0.6840
480x360	0.25	0.15	0.6945
480x360	0.25	0.5	0.6940
480x360	0.25	0.75	0.6929
480x360	0.25	1	0.6920
480x360	0.25	1.5	0.6946
480x360	0.25	3	0.6947
480x360	0.25	10	0.6982
480x360	0.25	15	0.6912
480x360	0.25	30	0.6940
480x360	0.35	0.15	0.7093
480x360	0.35	0.5	0.7089
480x360	0.35	0.75	0.7096
480x360	0.35	1	0.7080
480x360	0.35	1.5	0.7098
480x360	0.35	3	0.7001

Image Size (px.)	Balancing Terms	Lambda	F-Score
480x360	0.35	10	0.7141
480x360	0.35	15	0.7116
480x360	0.35	30	0.7058
480x360	0.45	0.15	0.7240
480x360	0.45	0.5	0.7245
480x360	0.45	0.75	0.7243
480x360	0.45	1	0.7242
480x360	0.45	1.5	0.7305
480x360	0.45	3	0.7316
480x360	0.45	10	0.7280
480x360	0.45	15	0.7284
480x360	0.45	30	0.7247
480x360	0.5	0.15	0.7255
480x360	0.5	0.5	0.7269
480x360	0.5	0.75	0.7269
480x360	0.5	1	0.7271
480x360	0.5	1.5	0.7272
480x360	0.5	3	0.7309
480x360	0.5	10	0.7299
480x360	0.5	15	0.7318
480x360	0.5	30	0.7268
480x360	0.55	0.15	0.7270
480x360	0.55	0.5	0.7265
480x360	0.55	0.75	0.7284
480x360	0.55	1	0.7286
480x360	0.55	1.5	0.7289
480x360	0.55	3	0.7317
480x360	0.55	10	0.7291
480x360	0.55	15	0.7300
480x360	0.55	30	0.7268
480x360	0.65	0.15	0.7548
480x360	0.65	0.5	0.7532
480x360	0.65	0.75	0.7532
480x360	0.65	1	0.7532
480x360	0.65	1.5	0.7535
480x360	0.65	3	0.7561
480x360	0.65	10	0.7563
480x360	0.65	15	0.7538
480x360	0.65	30	0.7454
480x360	0.75	0.15	0.7335
480x360	0.75	0.5	0.7333
480x360	0.75	0.75	0.7322
480x360	0.75	1	0.7322
480x360	0.75	1.5	0.7383

Image Size (px.)	Balancing Terms	Lambda	F-Score
480x360	0.75	3	0.7385
480x360	0.75	10	0.7404
480x360	0.75	15	0.7179
480x360	0.75	30	0.7267
480x360	0.85	0.15	0.6944
480x360	0.85	0.5	0.6950
480x360	0.85	0.75	0.6942
480x360	0.85	1	0.6942
480x360	0.85	1.5	0.6942
480x360	0.85	3	0.6884
480x360	0.85	10	0.6890
480x360	0.85	15	0.6882
480x360	0.85	30	0.6849
480x360	1	0.15	0.6113
480x360	1	0.5	0.6104
480x360	1	0.75	0.6103
480x360	1	1	0.6104
480x360	1	1.5	0.6103
480x360	1	3	0.6098
480x360	1	10	0.6083
480x360	1	15	0.6057
480x360	1	30	0.6021

Table 86.: Graph Cuts segmentation results using multiple parameter configurations and the subset of images from Dataset4 which were captured with natural lighting conditions.

Image Size (px.)	Balancing Terms	Lambda	F-Score
640x480	0	0.15	0.5953
640x480	0	0.5	0.5969
640x480	0	0.75	0.5965
640x480	0	1	0.5951
640x480	0	1.5	0.5916
640x480	0	3	0.5826
640x480	0	10	0.5753
640x480	0	15	0.5723
640x480	0	30	0.5699
640x480	0.15	0.15	0.6149
640x480	0.15	0.5	0.6798
640x480	0.15	0.75	0.6195
640x480	0.15	1	0.6181
640x480	0.15	1.5	0.6206
640x480	0.15	3	0.6183
640x480	0.15	10	0.6132
640x480	0.15	15	0.6094
640x480	0.15	30	0.6034
640x480	0.25	0.15	0.6327
640x480	0.25	0.5	0.6332
640x480	0.25	0.75	0.6334
640x480	0.25	1	0.6334
640x480	0.25	1.5	0.6374
640x480	0.25	3	0.6398
640x480	0.25	10	0.6315
640x480	0.25	15	0.6301
640x480	0.25	30	0.6280
640x480	0.35	0.15	0.6472
640x480	0.35	0.5	0.6447
640x480	0.35	0.75	0.6459
640x480	0.35	1	0.6459
640x480	0.35	1.5	0.6460
640x480	0.35	3	0.6507
640x480	0.35	10	0.6481
640x480	0.35	15	0.6441
640x480	0.35	30	0.6398
640x480	0.45	0.15	0.6546
640x480	0.45	0.5	0.6531
640x480	0.45	0.75	0.6540
640x480	0.45	1	0.6560
640x480	0.45	1.5	0.6568
640x480	0.45	3	0.6549
640x480	0.45	10	0.6552
640x480	0.45	15	0.6467

Image Size (px.)	Balancing Terms	Lambda	F-Score
640x480	0.45	30	0.6442
640x480	0.5	0.15	0.6627
640x480	0.5	0.5	0.6623
640x480	0.5	0.75	0.6557
640x480	0.5	1	0.6567
640x480	0.5	1.5	0.6573
640x480	0.5	3	0.6563
640x480	0.5	10	0.6601
640x480	0.5	15	0.6602
640x480	0.5	30	0.6421
640x480	0.55	0.15	0.6567
640x480	0.55	0.5	0.6564
640x480	0.55	0.75	0.6560
640x480	0.55	1	0.6561
640x480	0.55	1.5	0.6557
640x480	0.55	3	0.6562
640x480	0.55	10	0.6599
640x480	0.55	15	0.6651
640x480	0.55	30	0.6515
640x480	0.65	0.15	0.6727
640x480	0.65	0.5	0.6721
640x480	0.65	0.75	0.6723
640x480	0.65	1	0.6725
640x480	0.65	1.5	0.6721
640x480	0.65	3	0.6729
640x480	0.65	10	0.6729
640x480	0.65	15	0.6711
640x480	0.65	30	0.6673
640x480	0.75	0.15	0.6697
640x480	0.75	0.5	0.6696
640x480	0.75	0.75	0.6688
640x480	0.75	1	0.6727
640x480	0.75	1.5	0.6733
640x480	0.75	3	0.6731
640x480	0.75	10	0.6721
640x480	0.75	15	0.6706
640x480	0.75	30	0.6634
640x480	0.85	0.15	0.6640
640x480	0.85	0.5	0.6642
640x480	0.85	0.75	0.6639
640x480	0.85	1	0.6641
640x480	0.85	1.5	0.6643
640x480	0.85	3	0.6653
640x480	0.85	10	0.6633

Image Size (px.)	Balancing Terms	Lambda	F-Score
640x480	0.85	15	0.6641
640x480	0.85	30	0.6520
640x480	1	0.15	0.6061
640x480	1	0.5	0.6061
640x480	1	0.75	0.6059
640x480	1	1	0.6058
640x480	1	1.5	0.6082
640x480	1	3	0.6079
640x480	1	10	0.6027
640x480	1	15	0.5985
640x480	1	30	0.5913
480x360	0	0.15	0.6050
480x360	0	0.5	0.6004
480x360	0	0.75	0.5958
480x360	0	1	0.5925
480x360	0	1.5	0.5904
480x360	0	3	0.5904
480x360	0	10	0.5774
480x360	0	15	0.5745
480x360	0	30	0.5761
480x360	0.15	0.15	0.6169
480x360	0.15	0.5	0.6193
480x360	0.15	0.75	0.6200
480x360	0.15	1	0.6223
480x360	0.15	1.5	0.6233
480x360	0.15	3	0.6193
480x360	0.15	10	0.6142
480x360	0.15	15	0.6126
480x360	0.15	30	0.6043
480x360	0.25	0.15	0.6366
480x360	0.25	0.5	0.6363
480x360	0.25	0.75	0.6404
480x360	0.25	1	0.6412
480x360	0.25	1.5	0.6408
480x360	0.25	3	0.6421
480x360	0.25	10	0.6324
480x360	0.25	15	0.6295
480x360	0.25	30	0.6249
480x360	0.35	0.15	0.6487
480x360	0.35	0.5	0.6474
480x360	0.35	0.75	0.6471
480x360	0.35	1	0.6471
480x360	0.35	1.5	0.6509
480x360	0.35	3	0.6558

Image Size (px.)	Balancing Terms	Lambda	F-Score
480x360	0.35	10	0.6444
480x360	0.35	15	0.6401
480x360	0.35	30	0.6376
480x360	0.45	0.15	0.6587
480x360	0.45	0.5	0.6577
480x360	0.45	0.75	0.6578
480x360	0.45	1	0.6590
480x360	0.45	1.5	0.6589
480x360	0.45	3	0.6684
480x360	0.45	10	0.6632
480x360	0.45	15	0.6550
480x360	0.45	30	0.6410
480x360	0.5	0.15	0.6546
480x360	0.5	0.5	0.6622
480x360	0.5	0.75	0.6621
480x360	0.5	1	0.6621
480x360	0.5	1.5	0.6625
480x360	0.5	3	0.6680
480x360	0.5	10	0.6712
480x360	0.5	15	0.6599
480x360	0.5	30	0.6515
480x360	0.55	0.15	0.6680
480x360	0.55	0.5	0.6657
480x360	0.55	0.75	0.6664
480x360	0.55	1	0.6684
480x360	0.55	1.5	0.6684
480x360	0.55	3	0.6738
480x360	0.55	10	0.6760
480x360	0.55	15	0.6756
480x360	0.55	30	0.6634
480x360	0.65	0.15	0.6804
480x360	0.65	0.5	0.6810
480x360	0.65	0.75	0.6812
480x360	0.65	1	0.6809
480x360	0.65	1.5	0.6805
480x360	0.65	3	0.6800
480x360	0.65	10	0.6804
480x360	0.65	15	0.6790
480x360	0.65	30	0.6711
480x360	0.75	0.15	0.6996
480x360	0.75	0.5	0.6992
480x360	0.75	0.75	0.6985
480x360	0.75	1	0.6985
480x360	0.75	1.5	0.6996

Image Size (px.)	Balancing Terms	Lambda	F-Score
480x360	0.75	3	0.6994
480x360	0.75	10	0.7013
480x360	0.75	15	0.6991
480x360	0.75	30	0.6918
480x360	0.85	0.15	0.6948
480x360	0.85	0.5	0.6944
480x360	0.85	0.75	0.6942
480x360	0.85	1	0.6940
480x360	0.85	1.5	0.6939
480x360	0.85	3	0.6925
480x360	0.85	10	0.6954
480x360	0.85	15	0.6926
480x360	0.85	30	0.6853
480x360	1	0.15	0.6332
480x360	1	0.5	0.6329
480x360	1	0.75	0.6334
480x360	1	1	0.6333
480x360	1	1.5	0.6324
480x360	1	3	0.6321
480x360	1	10	0.6350
480x360	1	15	0.6291
480x360	1	30	0.6249

Table 87.: Graph Cuts segmentation results using multiple parameter configurations and the subset of images from Dataset4 which were captured with severe shadows on the hand.

Image Size (px.)	Balancing Terms	Lambda	F-Score
640x480	0	0.15	0.5270
640x480	0	0.5	0.5229
640x480	0	0.75	0.5200
640x480	0	1	0.5185
640x480	0	1.5	0.5173
640x480	0	3	0.5103
640x480	0	10	0.4994
640x480	0	15	0.4984
640x480	0	30	0.4980
640x480	0.15	0.15	0.5495
640x480	0.15	0.5	0.5488
640x480	0.15	0.75	0.5478
640x480	0.15	1	0.5473
640x480	0.15	1.5	0.5446
640x480	0.15	3	0.5424
640x480	0.15	10	0.5365
640x480	0.15	15	0.5293
640x480	0.15	30	0.5261
640x480	0.25	0.15	0.5593
640x480	0.25	0.5	0.5585
640x480	0.25	0.75	0.5580
640x480	0.25	1	0.5585
640x480	0.25	1.5	0.5569
640x480	0.25	3	0.5517
640x480	0.25	10	0.5487
640x480	0.25	15	0.5446
640x480	0.25	30	0.5374
640x480	0.35	0.15	0.5097
640x480	0.35	0.5	0.5688
640x480	0.35	0.75	0.5687
640x480	0.35	1	0.5686
640x480	0.35	1.5	0.5677
640x480	0.35	3	0.5626
640x480	0.35	10	0.5601
640x480	0.35	15	0.5569
640x480	0.35	30	0.5540
640x480	0.45	0.15	0.5875
640x480	0.45	0.5	0.5864
640x480	0.45	0.75	0.5861
640x480	0.45	1	0.5861
640x480	0.45	1.5	0.5856
640x480	0.45	3	0.5819
640x480	0.45	10	0.5781
640x480	0.45	15	0.5754

Image Size (px.)	Balancing Terms	Lambda	F-Score
640x480	0.45	30	0.5691
640x480	0.5	0.15	0.5881
640x480	0.5	0.5	0.5877
640x480	0.5	0.75	0.5878
640x480	0.5	1	0.5882
640x480	0.5	1.5	0.5885
640x480	0.5	3	0.5875
640x480	0.5	10	0.5790
640x480	0.5	15	0.5776
640x480	0.5	30	0.5745
640x480	0.55	0.15	0.5911
640x480	0.55	0.5	0.5889
640x480	0.55	0.75	0.5891
640x480	0.55	1	0.5893
640x480	0.55	1.5	0.5885
640x480	0.55	3	0.5892
640x480	0.55	10	0.5832
640x480	0.55	15	0.5799
640x480	0.55	30	0.5753
640x480	0.65	0.15	0.5875
640x480	0.65	0.5	0.5872
640x480	0.65	0.75	0.5866
640x480	0.65	1	0.5866
640x480	0.65	1.5	0.5856
640x480	0.65	3	0.5847
640x480	0.65	10	0.5791
640x480	0.65	15	0.5775
640x480	0.65	30	0.5714
640x480	0.75	0.15	0.5888
640x480	0.75	0.5	0.5884
640x480	0.75	0.75	0.5874
640x480	0.75	1	0.5870
640x480	0.75	1.5	0.5866
640x480	0.75	3	0.5851
640x480	0.75	10	0.5851
640x480	0.75	15	0.5831
640x480	0.75	30	0.5716
640x480	0.85	0.15	0.5885
640x480	0.85	0.5	0.5883
640x480	0.85	0.75	0.5882
640x480	0.85	1	0.5877
640x480	0.85	1.5	0.5876
640x480	0.85	3	0.5861
640x480	0.85	10	0.5826

Image Size (px.)	Balancing Terms	Lambda	F-Score
640x480	0.85	15	0.5804
640x480	0.85	30	0.5726
640x480	1	0.15	0.5922
640x480	1	0.5	0.5919
640x480	1	0.75	0.5918
640x480	1	1	0.5922
640x480	1	1.5	0.5914
640x480	1	3	0.5858
640x480	1	10	0.5853
640x480	1	15	0.5774
640x480	1	30	0.5679
480x360	0	0.15	0.5195
480x360	0	0.5	0.5150
480x360	0	0.75	0.5121
480x360	0	1	0.5116
480x360	0	1.5	0.5102
480x360	0	3	0.5039
480x360	0	10	0.4996
480x360	0	15	0.5017
480x360	0	30	0.4998
480x360	0.15	0.15	0.5424
480x360	0.15	0.5	0.5401
480x360	0.15	0.75	0.5389
480x360	0.15	1	0.5376
480x360	0.15	1.5	0.5394
480x360	0.15	3	0.5368
480x360	0.15	10	0.5238
480x360	0.15	15	0.5195
480x360	0.15	30	0.5167
480x360	0.25	0.15	0.5511
480x360	0.25	0.5	0.5502
480x360	0.25	0.75	0.5495
480x360	0.25	1	0.5486
480x360	0.25	1.5	0.5496
480x360	0.25	3	0.5501
480x360	0.25	10	0.5430
480x360	0.25	15	0.5397
480x360	0.25	30	0.5335
480x360	0.35	0.15	0.5639
480x360	0.35	0.5	0.5626
480x360	0.35	0.75	0.5626
480x360	0.35	1	0.5618
480x360	0.35	1.5	0.5600
480x360	0.35	3	0.5593

Image Size (px.)	Balancing Terms	Lambda	F-Score
480x360	0.35	10	0.5571
480x360	0.35	15	0.5541
480x360	0.35	30	0.5483
480x360	0.45	0.15	0.5771
480x360	0.45	0.5	0.5758
480x360	0.45	0.75	0.5746
480x360	0.45	1	0.5747
480x360	0.45	1.5	0.5744
480x360	0.45	3	0.5741
480x360	0.45	10	0.5659
480x360	0.45	15	0.5655
480x360	0.45	30	0.5588
480x360	0.5	0.15	0.5776
480x360	0.5	0.5	0.5770
480x360	0.5	0.75	0.5758
480x360	0.5	1	0.5768
480x360	0.5	1.5	0.5777
480x360	0.5	3	0.5772
480x360	0.5	10	0.5709
480x360	0.5	15	0.5684
480x360	0.5	30	0.5631
480x360	0.55	0.15	0.5826
480x360	0.55	0.5	0.5825
480x360	0.55	0.75	0.5809
480x360	0.55	1	0.5817
480x360	0.55	1.5	0.5822
480x360	0.55	3	0.5807
480x360	0.55	10	0.5742
480x360	0.55	15	0.5706
480x360	0.55	30	0.5662
480x360	0.65	0.15	0.5841
480x360	0.65	0.5	0.5845
480x360	0.65	0.75	0.5843
480x360	0.65	1	0.5838
480x360	0.65	1.5	0.5830
480x360	0.65	3	0.5818
480x360	0.65	10	0.5840
480x360	0.65	15	0.5687
480x360	0.65	30	0.5646
480x360	0.75	0.15	0.5881
480x360	0.75	0.5	0.5866
480x360	0.75	0.75	0.5867
480x360	0.75	1	0.5860
480x360	0.75	1.5	0.5864

Image Size (px.)	Balancing Terms	Lambda	F-Score
480x360	0.75	3	0.5851
480x360	0.75	10	0.5824
480x360	0.75	15	0.5792
480x360	0.75	30	0.5708
480x360	0.85	0.15	0.5920
480x360	0.85	0.5	0.5930
480x360	0.85	0.75	0.5924
480x360	0.85	1	0.5914
480x360	0.85	1.5	0.5920
480x360	0.85	3	0.5904
480x360	0.85	10	0.5842
480x360	0.85	15	0.5778
480x360	0.85	30	0.5607
480x360	1	0.15	0.5895
480x360	1	0.5	0.5892
480x360	1	0.75	0.5892
480x360	1	1	0.5895
480x360	1	1.5	0.5879
480x360	1	3	0.5863
480x360	1	10	0.5806
480x360	1	15	0.5791
480x360	1	30	0.5700

Table 88.: Graph Cuts segmentation results using multiple parameter configurations and the subset of images from Dataset4 which were captured under highly brilliant lighting conditions.

Image Size (px.)	Balancing Terms	Lambda	F-Score
640x480	0	0.15	0.6108
640x480	0	0.5	0.6090
640x480	0	0.75	0.6093
640x480	0	1	0.6090
640x480	0	1.5	0.6047
640x480	0	3	0.6058
640x480	0	10	0.5999
640x480	0	15	0.6016
640x480	0	30	0.5993
640x480	0.15	0.15	0.6289
640x480	0.15	0.5	0.6271
640x480	0.15	0.75	0.6273
640x480	0.15	1	0.6248
640x480	0.15	1.5	0.6248
640x480	0.15	3	0.6250
640x480	0.15	10	0.6283
640x480	0.15	15	0.6255
640x480	0.15	30	0.6249
640x480	0.25	0.15	0.6538
640x480	0.25	0.5	0.6538
640x480	0.25	0.75	0.6543
640x480	0.25	1	0.6528
640x480	0.25	1.5	0.6526
640x480	0.25	3	0.6483
640x480	0.25	10	0.6508
640x480	0.25	15	0.6498
640x480	0.25	30	0.6476
640x480	0.35	0.15	0.6596
640x480	0.35	0.5	0.6603
640x480	0.35	0.75	0.6604
640x480	0.35	1	0.6604
640x480	0.35	1.5	0.6604
640x480	0.35	3	0.6607
640x480	0.35	10	0.6623
640x480	0.35	15	0.6618
640x480	0.35	30	0.6605
640x480	0.45	0.15	0.6874
640x480	0.45	0.5	0.6865
640x480	0.45	0.75	0.6865
640x480	0.45	1	0.6866
640x480	0.45	1.5	0.6864
640x480	0.45	3	0.6873
640x480	0.45	10	0.6873
640x480	0.45	15	0.6855

Image Size (px.)	Balancing Terms	Lambda	F-Score
640x480	0.45	30	0.6818
640x480	0.5	0.15	0.7038
640x480	0.5	0.5	0.7029
640x480	0.5	0.75	0.7029
640x480	0.5	1	0.7021
640x480	0.5	1.5	0.7018
640x480	0.5	3	0.7020
640x480	0.5	10	0.6954
640x480	0.5	15	0.6953
640x480	0.5	30	0.6932
640x480	0.55	0.15	0.7101
640x480	0.55	0.5	0.7085
640x480	0.55	0.75	0.7086
640x480	0.55	1	0.7089
640x480	0.55	1.5	0.7091
640x480	0.55	3	0.7094
640x480	0.55	10	0.7103
640x480	0.55	15	0.7094
640x480	0.55	30	0.7086
640x480	0.65	0.15	0.7152
640x480	0.65	0.5	0.7092
640x480	0.65	0.75	0.7092
640x480	0.65	1	0.7093
640x480	0.65	1.5	0.7085
640x480	0.65	3	0.7107
640x480	0.65	10	0.7198
640x480	0.65	15	0.7122
640x480	0.65	30	0.7196
640x480	0.75	0.15	0.7222
640x480	0.75	0.5	0.7227
640x480	0.75	0.75	0.7226
640x480	0.75	1	0.7206
640x480	0.75	1.5	0.7206
640x480	0.75	3	0.7221
640x480	0.75	10	0.7205
640x480	0.75	15	0.7183
640x480	0.75	30	0.7130
640x480	0.85	0.15	0.6591
640x480	0.85	0.5	0.6592
640x480	0.85	0.75	0.6592
640x480	0.85	1	0.6592
640x480	0.85	1.5	0.6592
640x480	0.85	3	0.6621
640x480	0.85	10	0.6614

Image Size (px.)	Balancing Terms	Lambda	F-Score
640x480	0.85	15	0.6618
640x480	0.85	30	0.6608
640x480	1	0.15	0.5240
640x480	1	0.5	0.5239
640x480	1	0.75	0.5239
640x480	1	1	0.5239
640x480	1	1.5	0.5239
640x480	1	3	0.5262
640x480	1	10	0.5258
640x480	1	15	0.5258
640x480	1	30	0.5228
480x360	0	0.15	0.6372
480x360	0	0.5	0.6382
480x360	0	0.75	0.6362
480x360	0	1	0.6374
480x360	0	1.5	0.6355
480x360	0	3	0.6324
480x360	0	10	0.6287
480x360	0	15	0.6263
480x360	0	30	0.6246
480x360	0.15	0.15	0.6565
480x360	0.15	0.5	0.6571
480x360	0.15	0.75	0.6547
480x360	0.15	1	0.6546
480x360	0.15	1.5	0.6560
480x360	0.15	3	0.6570
480x360	0.15	10	0.6565
480x360	0.15	15	0.6537
480x360	0.15	30	0.6499
480x360	0.25	0.15	0.6723
480x360	0.25	0.5	0.6706
480x360	0.25	0.75	0.6692
480x360	0.25	1	0.6700
480x360	0.25	1.5	0.6681
480x360	0.25	3	0.6674
480x360	0.25	10	0.6700
480x360	0.25	15	0.6686
480x360	0.25	30	0.6680
480x360	0.35	0.15	0.6838
480x360	0.35	0.5	0.6861
480x360	0.35	0.75	0.6861
480x360	0.35	1	0.6861
480x360	0.35	1.5	0.6859
480x360	0.35	3	0.6857

Image Size (px.)	Balancing Terms	Lambda	F-Score
480x360	0.35	10	0.6855
480x360	0.35	15	0.6844
480x360	0.35	30	0.6829
480x360	0.45	0.15	0.6891
480x360	0.45	0.5	0.6890
480x360	0.45	0.75	0.6890
480x360	0.45	1	0.6890
480x360	0.45	1.5	0.6889
480x360	0.45	3	0.6893
480x360	0.45	10	0.6923
480x360	0.45	15	0.6929
480x360	0.45	30	0.6898
480x360	0.5	0.15	0.7009
480x360	0.5	0.5	0.6996
480x360	0.5	0.75	0.7000
480x360	0.5	1	0.7001
480x360	0.5	1.5	0.7004
480x360	0.5	3	0.7063
480x360	0.5	10	0.7032
480x360	0.5	15	0.7049
480x360	0.5	30	0.7037
480x360	0.55	0.15	0.7129
480x360	0.55	0.5	0.7109
480x360	0.55	0.75	0.7099
480x360	0.55	1	0.7100
480x360	0.55	1.5	0.7098
480x360	0.55	3	0.7185
480x360	0.55	10	0.7149
480x360	0.55	15	0.7164
480x360	0.55	30	0.7153
480x360	0.65	0.15	0.7400
480x360	0.65	0.5	0.7396
480x360	0.65	0.75	0.7392
480x360	0.65	1	0.7381
480x360	0.65	1.5	0.7379
480x360	0.65	3	0.7426
480x360	0.65	10	0.7435
480x360	0.65	15	0.7387
480x360	0.65	30	0.7410
480x360	0.75	0.15	0.7491
480x360	0.75	0.5	0.7490
480x360	0.75	0.75	0.7490
480x360	0.75	1	0.7493
480x360	0.75	1.5	0.7492

Image Size (px.)	Balancing Terms	Lambda	F-Score
480x360	0.75	3	0.7517
480x360	0.75	10	0.7500
480x360	0.75	15	0.7479
480x360	0.75	30	0.7410
480x360	0.85	0.15	0.7058
480x360	0.85	0.5	0.7056
480x360	0.85	0.75	0.7055
480x360	0.85	1	0.7057
480x360	0.85	1.5	0.7057
480x360	0.85	3	0.7081
480x360	0.85	10	0.7075
480x360	0.85	15	0.7047
480x360	0.85	30	0.7022
480x360	1	0.15	0.5955
480x360	1	0.5	0.5956
480x360	1	0.75	0.5956
480x360	1	1	0.5956
480x360	1	1.5	0.5986
480x360	1	3	0.5972
480x360	1	10	0.5943
480x360	1	15	0.5935
480x360	1	30	0.5910

Table 89.: Graph Cuts segmentation results using multiple parameter configurations and the subset of images from Dataset4 which were captured under low intensity lighting conditions.

A.2 GRAPH CUTS FOR FLOODING-BASED SEGMENTATION

A complete evaluation of different parameter configurations for Graph Cuts segmentation has been conducted with the aim to find the best arrangement when used as initial segmentation for flooding-based segmentation. Obtained results are shown hereafter for each dataset.

A.2.1 *Dataset1*

Image Size (px.)	Balancing Terms	Lambda	F-Score	Average time
640x480	0	0.15	0.9000	9.4472
640x480	0	0.5	0.8980	9.1262
640x480	0	0.75	0.8952	9.1248
640x480	0	1	0.8941	9.1244
640x480	0	1.5	0.8932	9.1271
640x480	0	3	0.8916	9.1308
640x480	0	10	0.8864	9.1521
640x480	0	15	0.8824	9.1640
640x480	0	30	0.8799	9.1793
640x480	0.15	0.15	0.8952	9.2143
640x480	0.15	0.5	0.8925	9.1629
640x480	0.15	0.75	0.8916	9.1518
640x480	0.15	1	0.8918	9.1400
640x480	0.15	1.5	0.8900	9.1775
640x480	0.15	3	0.8868	9.1947
640x480	0.15	10	0.8814	9.2031
640x480	0.15	15	0.8798	9.9337
640x480	0.15	30	0.8774	9.8597
640x480	0.25	0.15	0.8895	9.6151
640x480	0.25	0.5	0.8887	9.9812
640x480	0.25	0.75	0.8874	9.8161
640x480	0.25	1	0.8769	9.5414
640x480	0.25	1.5	0.8862	9.2339
640x480	0.25	3	0.8825	9.2924
640x480	0.25	10	0.8744	9.3085
640x480	0.25	15	0.8730	9.3138
640x480	0.25	30	0.8696	9.3200
640x480	0.35	0.15	0.8811	9.3820
640x480	0.35	0.5	0.8828	9.3545
640x480	0.35	0.75	0.8817	9.3469
640x480	0.35	1	0.8813	9.3365
640x480	0.35	1.5	0.8810	9.3249
640x480	0.35	3	0.8772	9.3147
640x480	0.35	10	0.8684	9.3336
640x480	0.35	15	0.8662	9.3392

Image Size (px.)	Balancing Terms	Lambda	F-Score	Average time
640x480	0.35	30	0.8599	9.3354
640x480	0.45	0.15	0.8726	9.3894
640x480	0.45	0.5	0.8726	9.2890
640x480	0.45	0.75	0.8709	9.2687
640x480	0.45	1	0.8713	9.2676
640x480	0.45	1.5	0.8708	9.2522
640x480	0.45	3	0.8669	9.2051
640x480	0.45	10	0.8576	9.2344
640x480	0.45	15	0.8547	9.2447
640x480	0.45	30	0.8500	9.2510
640x480	0.5	0.15	0.8664	9.2990
640x480	0.5	0.5	0.8657	9.2858
640x480	0.5	0.75	0.8637	9.2844
640x480	0.5	1	0.8655	9.2748
640x480	0.5	1.5	0.8650	9.2878
640x480	0.5	3	0.8619	9.2458
640x480	0.5	10	0.8513	9.2628
640x480	0.5	15	0.8488	9.2646
640x480	0.5	30	0.8460	9.2719
640x480	0.55	0.15	0.8620	9.2825
640x480	0.55	0.5	0.8617	9.2695
640x480	0.55	0.75	0.8612	9.2615
640x480	0.55	1	0.8617	9.2752
640x480	0.55	1.5	0.8596	9.2671
640x480	0.55	3	0.8561	9.2544
640x480	0.55	10	0.8439	9.2587
640x480	0.55	15	0.8413	9.2629
640x480	0.55	30	0.8377	9.2694
640x480	0.65	0.15	0.8481	9.3199
640x480	0.65	0.5	0.8480	9.2932
640x480	0.65	0.75	0.8467	9.3035
640x480	0.65	1	0.8461	9.2967
640x480	0.65	1.5	0.8461	9.2886
640x480	0.65	3	0.8424	9.2696
640x480	0.65	10	0.8266	9.2751
640x480	0.65	15	0.8255	9.2789
640x480	0.65	30	0.8230	9.2860
640x480	0.75	0.15	0.8317	9.3339
640x480	0.75	0.5	0.8312	9.3249
640x480	0.75	0.75	0.8301	9.3254
640x480	0.75	1	0.8298	9.3156
640x480	0.75	1.5	0.8287	9.3089
640x480	0.75	3	0.8244	9.2895
640x480	0.75	10	0.8100	9.2980

Image Size (px.)	Balancing Terms	Lambda	F-Score	Average time
640x480	0.75	15	0.8055	9.3028
640x480	0.75	30	0.8003	9.3098
640x480	0.85	0.15	0.7966	9.3737
640x480	0.85	0.5	0.7964	9.3654
640x480	0.85	0.75	0.7957	9.3615
640x480	0.85	1	0.7938	9.3555
640x480	0.85	1.5	0.7902	9.3484
640x480	0.85	3	0.7817	9.3353
640x480	0.85	10	0.7656	9.3275
640x480	0.85	15	0.7611	9.3319
640x480	0.85	30	0.7579	9.3317
640x480	1	0.15	0.2935	9.4441
640x480	1	0.5	0.2919	9.4559
640x480	1	0.75	0.2902	9.4475
640x480	1	1	0.2884	9.4438
640x480	1	1.5	0.2882	9.4382
640x480	1	3	0.2922	9.4196
640x480	1	10	0.2847	9.4034
640x480	1	15	0.2837	9.4081
640x480	1	30	0.2832	9.4121
480x360	0	0.15	0.8969	5.4141
480x360	0	0.5	0.8973	5.4109
480x360	0	0.75	0.8961	5.4110
480x360	0	1	0.8945	5.4146
480x360	0	1.5	0.8936	5.4233
480x360	0	3	0.8900	5.4190
480x360	0	10	0.8852	5.4226
480x360	0	15	0.8844	5.4245
480x360	0	30	0.8765	5.4345
480x360	0.15	0.15	0.8913	5.4458
480x360	0.15	0.5	0.8898	5.4440
480x360	0.15	0.75	0.8911	5.4428
480x360	0.15	1	0.8913	5.4386
480x360	0.15	1.5	0.8899	5.4307
480x360	0.15	3	0.8877	5.4363
480x360	0.15	10	0.8817	5.4390
480x360	0.15	15	0.8794	5.4459
480x360	0.15	30	0.8751	5.4490
480x360	0.25	0.15	0.8859	5.4522
480x360	0.25	0.5	0.8853	5.4551
480x360	0.25	0.75	0.8852	5.4553
480x360	0.25	1	0.8857	5.4526
480x360	0.25	1.5	0.8848	5.4560
480x360	0.25	3	0.8803	5.4551

Image Size (px.)	Balancing Terms	Lambda	F-Score	Average time
480x360	0.25	10	0.8758	5.4553
480x360	0.25	15	0.8746	5.4603
480x360	0.25	30	0.8686	5.4684
480x360	0.35	0.15	0.8796	5.4679
480x360	0.35	0.5	0.8803	5.4634
480x360	0.35	0.75	0.8824	5.4564
480x360	0.35	1	0.8822	5.4608
480x360	0.35	1.5	0.8803	5.4602
480x360	0.35	3	0.8742	5.6584
480x360	0.35	10	0.8682	5.8028
480x360	0.35	15	0.8671	5.8401
480x360	0.35	30	0.8607	5.64505
480x360	0.45	0.15	0.8726	5.9464
480x360	0.45	0.5	0.8713	5.8235
480x360	0.45	0.75	0.8707	5.8727
480x360	0.45	1	0.8707	5.8092
480x360	0.45	1.5	0.8723	5.5171
480x360	0.45	3	0.8663	5.8168
480x360	0.45	10	0.8589	5.8564
480x360	0.45	15	0.8544	5.5614
480x360	0.45	30	0.8472	5.5589
480x360	0.5	0.15	0.8672	5.5600
480x360	0.5	0.5	0.8662	5.5675
480x360	0.5	0.75	0.8660	5.5576
480x360	0.5	1	0.8658	5.5688
480x360	0.5	1.5	0.8645	5.5578
480x360	0.5	3	0.8609	5.5651
480x360	0.5	10	0.8520	5.5844
480x360	0.5	15	0.8481	5.5782
480x360	0.5	30	0.8409	5.5862
480x360	0.55	0.15	0.8622	5.5709
480x360	0.55	0.5	0.8589	5.5741
480x360	0.55	0.75	0.8591	5.5736
480x360	0.55	1	0.8578	5.5728
480x360	0.55	1.5	0.8567	5.5680
480x360	0.55	3	0.8552	5.5735
480x360	0.55	10	0.8454	5.5170
480x360	0.55	15	0.8401	5.5170
480x360	0.55	30	0.8377	5.5199
480x360	0.65	0.15	0.8454	5.5181
480x360	0.65	0.5	0.8420	5.5173
480x360	0.65	0.75	0.8422	5.5208
480x360	0.65	1	0.8418	5.8703
480x360	0.65	1.5	0.8425	5.5512

Image Size (px.)	Balancing Terms	Lambda	F-Score	Average time
480x360	0.65	3	0.8401	5.6479
480x360	0.65	10	0.8319	5.6353
480x360	0.65	15	0.8273	5.6728
480x360	0.65	30	0.8209	5.66085
480x360	0.75	0.15	0.8242	5.5914
480x360	0.75	0.5	0.8210	5.6328
480x360	0.75	0.75	0.8209	5.7065
480x360	0.75	1	0.8208	5.6327
480x360	0.75	1.5	0.8213	5.6475
480x360	0.75	3	0.8190	6.8284
480x360	0.75	10	0.8113	7.1818
480x360	0.75	15	0.8072	6.0312
480x360	0.75	30	0.7986	6.1076
480x360	0.85	0.15	0.7855	6.1264
480x360	0.85	0.5	0.7840	6.0489
480x360	0.85	0.75	0.7836	5.7990
480x360	0.85	1	0.7831	5.8174
480x360	0.85	1.5	0.7819	5.7986
480x360	0.85	3	0.7819	5.6364
480x360	0.85	10	0.7684	5.6529
480x360	0.85	15	0.7592	5.6764
480x360	0.85	30	0.7516	5.6501
480x360	1	0.15	0.3215	5.7392
480x360	1	0.5	0.3246	5.7405
480x360	1	0.75	0.3241	5.7358
480x360	1	1	0.3218	5.7379
480x360	1	1.5	0.3215	5.7406
480x360	1	3	0.3144	5.7074
480x360	1	10	0.3060	5.6902
480x360	1	15	0.2997	5.7286
480x360	1	30	0.3059	5.7403

Table 90.: Flooding based segmentation results using Graph Cuts as initial segmentation and multiple parameter configurations over Dataset1.

A.2.2 *Dataset2*

Image Size (px.)	Balancing Terms	Lambda	F-Score	Average time
640x480	0	0.15	0.8934	9.5611
640x480	0	0.5	0.8934	9.6802
640x480	0	0.75	0.8932	9.7355
640x480	0	1	0.8929	9.7273
640x480	0	1.5	0.8880	9.7401
640x480	0	3	0.8872	9.7523
640x480	0	10	0.8837	9.7502
640x480	0	15	0.8839	9.7375
640x480	0	30	0.8810	9.7460
640x480	0.15	0.15	0.9026	9.7663
640x480	0.15	0.5	0.9017	9.7895
640x480	0.15	0.75	0.9017	9.7874
640x480	0.15	1	0.9019	10.5735
640x480	0.15	1.5	0.9018	9.7487
640x480	0.15	3	0.9021	10.3902
640x480	0.15	10	0.8997	9.7472
640x480	0.15	15	0.8989	9.7454
640x480	0.15	30	0.8965	9.7434
640x480	0.25	0.15	0.9041	9.7648
640x480	0.25	0.5	0.9041	9.8057
640x480	0.25	0.75	0.9041	9.8410
640x480	0.25	1	0.9040	9.8357
640x480	0.25	1.5	0.9040	9.8089
640x480	0.25	3	0.9041	11.1102
640x480	0.25	10	0.9024	10.8051
640x480	0.25	15	0.9011	11.3709
640x480	0.25	30	0.8988	11.2345
640x480	0.35	0.15	0.9072	10.5827
640x480	0.35	0.5	0.9072	10.6757
640x480	0.35	0.75	0.9072	10.5332
640x480	0.35	1	0.9071	10.8905
640x480	0.35	1.5	0.9071	10.7931
640x480	0.35	3	0.9068	11.2117
640x480	0.35	10	0.9055	9.8653
640x480	0.35	15	0.9045	10.3245
640x480	0.35	30	0.9025	11.3028
640x480	0.45	0.15	0.9088	9.7528
640x480	0.45	0.5	0.9088	9.7779
640x480	0.45	0.75	0.9090	9.7628
640x480	0.45	1	0.9090	9.7795
640x480	0.45	1.5	0.9090	9.7707
640x480	0.45	3	0.9087	9.7749

Image Size (px.)	Balancing Terms	Lambda	F-Score	Average time
640x480	0.45	10	0.9076	9.7791
640x480	0.45	15	0.9076	9.7868
640x480	0.45	30	0.9043	9.7887
640x480	0.5	0.15	0.9095	9.7828
640x480	0.5	0.5	0.9114	9.7794
640x480	0.5	0.75	0.9115	9.7734
640x480	0.5	1	0.9115	9.7847
640x480	0.5	1.5	0.9114	9.7937
640x480	0.5	3	0.9122	9.8199
640x480	0.5	10	0.9099	9.8023
640x480	0.5	15	0.9083	9.7886
640x480	0.5	30	0.9052	9.7969
640x480	0.55	0.15	0.9036	9.7985
640x480	0.55	0.5	0.9049	9.7883
640x480	0.55	0.75	0.9048	10.2877
640x480	0.55	1	0.9048	10.8265
640x480	0.55	1.5	0.9047	11.3334
640x480	0.55	3	0.9044	11.3159
640x480	0.55	10	0.9033	11.5653
640x480	0.55	15	0.9022	10.7665
640x480	0.55	30	0.8997	10.3259
640x480	0.65	0.15	0.9030	10.0063
640x480	0.65	0.5	0.9029	9.8503
640x480	0.65	0.75	0.9029	10.1301
640x480	0.65	1	0.9028	9.8327
640x480	0.65	1.5	0.9027	10.7660
640x480	0.65	3	0.9023	11.6473
640x480	0.65	10	0.9001	11.6250
640x480	0.65	15	0.8989	11.7554
640x480	0.65	30	0.8947	10.1274
640x480	0.75	0.15	0.8851	9.9342
640x480	0.75	0.5	0.8847	9.9113
640x480	0.75	0.75	0.8847	9.9199
640x480	0.75	1	0.8846	9.8954
640x480	0.75	1.5	0.8849	9.8916
640x480	0.75	3	0.8848	9.9016
640x480	0.75	10	0.8822	9.8982
640x480	0.75	15	0.8808	9.8918
640x480	0.75	30	0.8777	9.8861
640x480	0.85	0.15	0.8341	11.2415
640x480	0.85	0.5	0.8334	11.3565
640x480	0.85	0.75	0.8337	10.1059
640x480	0.85	1	0.8337	10.6384
640x480	0.85	1.5	0.8336	10.7300

Image Size (px.)	Balancing Terms	Lambda	F-Score	Average time
640x480	0.85	3	0.8334	10.0954
640x480	0.85	10	0.8334	10.0943
640x480	0.85	15	0.8331	10.1007
640x480	0.85	30	0.8267	11.3902
640x480	1	0.15	0.7491	11.3475
640x480	1	0.5	0.7491	10.3036
640x480	1	0.75	0.7491	10.2797
640x480	1	1	0.7490	35.9366
640x480	1	1.5	0.7489	11.7524
640x480	1	3	0.7487	10.9261
640x480	1	10	0.7469	10.3100
640x480	1	15	0.7465	10.2669
640x480	1	30	0.7416	10.2869
480x360	0	0.15	0.8962	6.1629
480x360	0	0.5	0.8958	5.7087
480x360	0	0.75	0.8953	5.6953
480x360	0	1	0.8949	5.6149
480x360	0	1.5	0.8946	5.6184
480x360	0	3	0.8927	5.6188
480x360	0	10	0.8842	5.6192
480x360	0	15	0.8822	5.6085
480x360	0	30	0.8808	5.6104
480x360	0.15	0.15	0.9036	5.6348
480x360	0.15	0.5	0.9034	5.6289
480x360	0.15	0.75	0.9033	5.6271
480x360	0.15	1	0.9032	5.6292
480x360	0.15	1.5	0.9031	5.6270
480x360	0.15	3	0.9029	5.6261
480x360	0.15	10	0.8998	5.6312
480x360	0.15	15	0.8982	5.6312
480x360	0.15	30	0.8950	5.6312
480x360	0.25	0.15	0.9056	5.6354
480x360	0.25	0.5	0.9053	5.6407
480x360	0.25	0.75	0.9053	5.6351
480x360	0.25	1	0.9061	5.6389
480x360	0.25	1.5	0.9054	5.6403
480x360	0.25	3	0.9052	5.6424
480x360	0.25	10	0.9031	5.6456
480x360	0.25	15	0.9016	5.6550
480x360	0.25	30	0.8985	5.6414
480x360	0.35	0.15	0.9082	5.6453
480x360	0.35	0.5	0.9082	5.6450
480x360	0.35	0.75	0.9083	5.6468
480x360	0.35	1	0.9082	5.6482

Image Size (px.)	Balancing Terms	Lambda	F-Score	Average time
480x360	0.35	1.5	0.9081	5.6456
480x360	0.35	3	0.9077	5.6457
480x360	0.35	10	0.9054	5.6475
480x360	0.35	15	0.9050	5.6380
480x360	0.35	30	0.9019	5.6444
480x360	0.45	0.15	0.9094	5.6525
480x360	0.45	0.5	0.9094	5.6485
480x360	0.45	0.75	0.9093	5.6632
480x360	0.45	1	0.9093	5.6649
480x360	0.45	1.5	0.9092	5.6643
480x360	0.45	3	0.9088	5.6654
480x360	0.45	10	0.9065	5.6610
480x360	0.45	15	0.9051	5.6562
480x360	0.45	30	0.9017	5.6512
480x360	0.5	0.15	0.9105	5.6625
480x360	0.5	0.5	0.9104	5.6673
480x360	0.5	0.75	0.9103	5.7548
480x360	0.5	1	0.9102	5.7725
480x360	0.5	1.5	0.9101	5.6719
480x360	0.5	3	0.9098	5.6659
480x360	0.5	10	0.9093	5.6685
480x360	0.5	15	0.9065	5.6669
480x360	0.5	30	0.9038	5.6646
480x360	0.55	0.15	0.9087	5.6780
480x360	0.55	0.5	0.9106	5.6737
480x360	0.55	0.75	0.9106	5.6824
480x360	0.55	1	0.9105	5.6781
480x360	0.55	1.5	0.9105	5.6760
480x360	0.55	3	0.9111	5.6750
480x360	0.55	10	0.9094	5.6789
480x360	0.55	15	0.9077	5.6788
480x360	0.55	30	0.9044	5.6748
480x360	0.65	0.15	0.9064	5.7036
480x360	0.65	0.5	0.9063	5.7114
480x360	0.65	0.75	0.9063	5.7088
480x360	0.65	1	0.9062	5.7106
480x360	0.65	1.5	0.9061	5.7091
480x360	0.65	3	0.9052	5.7080
480x360	0.65	10	0.9031	5.7265
480x360	0.65	15	0.8994	5.7071
480x360	0.65	30	0.8960	5.6881
480x360	0.75	0.15	0.8983	5.7950
480x360	0.75	0.5	0.8982	5.7343
480x360	0.75	0.75	0.8984	5.7275

Image Size (px.)	Balancing Terms	Lambda	F-Score	Average time
480x360	0.75	1	0.8982	5.7278
480x360	0.75	1.5	0.8981	5.7312
480x360	0.75	3	0.8975	5.7275
480x360	0.75	10	0.8950	5.7319
480x360	0.75	15	0.8924	5.7360
480x360	0.75	30	0.8881	5.7312
480x360	0.85	0.15	0.8558	5.8282
480x360	0.85	0.5	0.8558	5.8302
480x360	0.85	0.75	0.8557	5.8405
480x360	0.85	1	0.8556	5.8352
480x360	0.85	1.5	0.8560	5.8320
480x360	0.85	3	0.8569	5.8362
480x360	0.85	10	0.8550	5.8398
480x360	0.85	15	0.8535	5.8385
480x360	0.85	30	0.8508	5.8370
480x360	1	0.15	0.8026	5.9631
480x360	1	0.5	0.8026	5.9652
480x360	1	0.75	0.8021	5.9666
480x360	1	1	0.8020	5.9706
480x360	1	1.5	0.8019	5.9619
480x360	1	3	0.8014	5.9565
480x360	1	10	0.7996	5.9634
480x360	1	15	0.7993	5.9621
480x360	1	30	0.7948	5.9701

Table 91.: Flooding based segmentation results using Graph Cuts as initial segmentation and multiple parameter configurations over Dataset2.

A.2.3 *Dataset3*

Image Size (px.)	Balancing Terms	Lambda	F-Score	Average time
640x480	0	0.15	0.7631	9.5945
640x480	0	0.5	0.7323	10.1590
640x480	0	0.75	0.7624	9.2242
640x480	0	1	0.7621	12.6461
640x480	0	1.5	0.7630	10.6195
640x480	0	3	0.7642	15.0753
640x480	0	10	0.7668	15.1436
640x480	0	15	0.7677	15.2305
640x480	0	30	0.7669	15.2305
640x480	0.15	0.15	0.7846	14.7104
640x480	0.15	0.5	0.7842	14.6424
640x480	0.15	0.75	0.7839	14.6532
640x480	0.15	1	0.7839	14.6585
640x480	0.15	1.5	0.7838	14.6672
640x480	0.15	3	0.7838	14.6733
640x480	0.15	10	0.7835	14.6865
640x480	0.15	15	0.7841	14.7033
640x480	0.15	30	0.7845	14.7831
640x480	0.25	0.15	0.7979	14.8354
640x480	0.25	0.5	0.7975	15.0942
640x480	0.25	0.75	0.7973	14.8632
640x480	0.25	1	0.7973	14.8647
640x480	0.25	1.5	0.7970	14.9285
640x480	0.25	3	0.7970	14.9872
640x480	0.25	10	0.7955	14.7683
640x480	0.25	15	0.7958	14.7856
640x480	0.25	30	0.7964	14.8362
640x480	0.35	0.15	0.8075	14.8185
640x480	0.35	0.5	0.8074	14.7956
640x480	0.35	0.75	0.8074	14.9589
640x480	0.35	1	0.8074	14.8864
640x480	0.35	1.5	0.8074	14.9543
640x480	0.35	3	0.8071	14.9117
640x480	0.35	10	0.8054	14.9151
640x480	0.35	15	0.8054	14.8531
640x480	0.35	30	0.8050	14.8938
640x480	0.45	0.15	0.8147	14.8757
640x480	0.45	0.5	0.8146	14.9307
640x480	0.45	0.75	0.8146	14.9410
640x480	0.45	1	0.8146	14.9718
640x480	0.45	1.5	0.8146	14.9742
640x480	0.45	3	0.8143	14.9967

Image Size (px.)	Balancing Terms	Lambda	F-Score	Average time
640x480	0.45	10	0.8124	14.9950
640x480	0.45	15	0.8108	15.1228
640x480	0.45	30	0.8089	15.1189
640x480	0.5	0.15	0.8145	15.2039
640x480	0.5	0.5	0.8146	15.1192
640x480	0.5	0.75	0.8147	15.1448
640x480	0.5	1	0.8148	15.0852
640x480	0.5	1.5	0.8151	15.0869
640x480	0.5	3	0.8148	15.0464
640x480	0.5	10	0.8121	15.0933
640x480	0.5	15	0.8112	15.1123
640x480	0.5	30	0.8093	15.1108
640x480	0.55	0.15	0.8129	13.4528
640x480	0.55	0.5	0.8128	13.4472
640x480	0.55	0.75	0.8128	13.4462
640x480	0.55	1	0.8127	13.4583
640x480	0.55	1.5	0.8127	13.6249
640x480	0.55	3	0.8122	13.4716
640x480	0.55	10	0.8103	13.4690
640x480	0.55	15	0.8094	13.4603
640x480	0.55	30	0.8079	13.4639
640x480	0.65	0.15	0.8033	13.4528
640x480	0.65	0.5	0.8033	13.4472
640x480	0.65	0.75	0.8033	13.4462
640x480	0.65	1	0.8032	13.4583
640x480	0.65	1.5	0.8031	13.6249
640x480	0.65	3	0.8026	13.7416
640x480	0.65	10	0.8009	13.4690
640x480	0.65	15	0.8002	13.4603
640x480	0.65	30	0.7986	13.4639
640x480	0.75	0.15	0.7834	13.7013
640x480	0.75	0.5	0.7833	13.5736
640x480	0.75	0.75	0.7833	13.5715
640x480	0.75	1	0.7831	13.5724
640x480	0.75	1.5	0.7832	13.5823
640x480	0.75	3	0.7829	13.5807
640x480	0.75	10	0.7816	13.7416
640x480	0.75	15	0.7800	13.5966
640x480	0.75	30	0.7776	13.6417
640x480	0.85	0.15	0.7444	13.7597
640x480	0.85	0.5	0.7443	13.7933
640x480	0.85	0.75	0.7442	13.7633
640x480	0.85	1	0.7441	13.8040
640x480	0.85	1.5	0.7440	13.7668

Image Size (px.)	Balancing Terms	Lambda	F-Score	Average time
640x480	0.85	3	0.7432	13.7795
640x480	0.85	10	0.7421	13.8067
640x480	0.85	15	0.7401	13.7525
640x480	0.85	30	0.7363	13.7505
640x480	1	0.15	0.6408	13.9801
640x480	1	0.5	0.6407	14.0079
640x480	1	0.75	0.6406	13.9960
640x480	1	1	0.6405	14.1738
640x480	1	1.5	0.6401	14.0259
640x480	1	3	0.6393	14.0570
640x480	1	10	0.6364	14.0074
640x480	1	15	0.6352	14.0392
640x480	1	30	0.6315	14.0254
480x360	0	0.15	0.7604	6.2487
480x360	0	0.5	0.7608	6.4849
480x360	0	0.75	0.7613	6.0273
480x360	0	1	0.7612	5.6648
480x360	0	1.5	0.7611	6.2391
480x360	0	3	0.7629	5.5624
480x360	0	10	0.7632	5.4941
480x360	0	15	0.7627	5.4298
480x360	0	30	0.7606	5.3267
480x360	0.15	0.15	0.6566	5.2729
480x360	0.15	0.5	0.6539	5.4385
480x360	0.15	0.75	0.6544	5.3259
480x360	0.15	1	0.6536	5.4628
480x360	0.15	1.5	0.6524	5.5300
480x360	0.15	3	0.7788	5.7401
480x360	0.15	10	0.7797	5.7067
480x360	0.15	15	0.7802	5.5674
480x360	0.15	30	0.7805	5.5667
480x360	0.25	0.15	0.6737	5.5621
480x360	0.25	0.5	0.6705	5.6507
480x360	0.25	0.75	0.6701	5.6418
480x360	0.25	1	0.6695	6.5981
480x360	0.25	1.5	0.6695	6.4710
480x360	0.25	3	0.7923	5.3020
480x360	0.25	10	0.7911	5.2937
480x360	0.25	15	0.7921	6.2078
480x360	0.25	30	0.7921	6.6490
480x360	0.35	0.15	0.6880	5.2024
480x360	0.35	0.5	0.6876	5.1660
480x360	0.35	0.75	0.6872	5.2019
480x360	0.35	1	0.6875	5.2080

Image Size (px.)	Balancing Terms	Lambda	F-Score	Average time
480x360	0.35	1.5	0.6857	5.2048
480x360	0.35	3	0.8028	5.1480
480x360	0.35	10	0.8013	5.2307
480x360	0.35	15	0.8012	5.1826
480x360	0.35	30	0.8002	5.1452
480x360	0.45	0.15	0.7028	5.1550
480x360	0.45	0.5	0.7024	5.1837
480x360	0.45	0.75	0.7013	5.1591
480x360	0.45	1	0.6995	5.1537
480x360	0.45	1.5	0.6993	5.1542
480x360	0.45	3	0.8106	5.1683
480x360	0.45	10	0.8082	5.1747
480x360	0.45	15	0.8078	5.2289
480x360	0.45	30	0.8053	5.2386
480x360	0.5	0.15	0.7043	5.2002
480x360	0.5	0.5	0.7016	5.1902
480x360	0.5	0.75	0.7013	5.2056
480x360	0.5	1	0.7007	5.1960
480x360	0.5	1.5	0.6996	5.1799
480x360	0.5	3	0.8120	5.1747
480x360	0.5	10	0.8094	5.2002
480x360	0.5	15	0.8085	5.1970
480x360	0.5	30	0.8065	5.2289
480x360	0.55	0.15	0.6958	5.2276
480x360	0.55	0.5	0.6964	5.2502
480x360	0.55	0.75	0.6949	5.2401
480x360	0.55	1	0.6944	5.2365
480x360	0.55	1.5	0.6945	5.2294
480x360	0.55	3	0.8114	5.2214
480x360	0.55	10	0.8094	5.2367
480x360	0.55	15	0.8080	5.2139
480x360	0.55	30	0.8060	5.2405
480x360	0.65	0.15	0.6905	5.3006
480x360	0.65	0.5	0.6892	5.3103
480x360	0.65	0.75	0.6897	5.2875
480x360	0.65	1	0.6893	5.2732
480x360	0.65	1.5	0.6873	5.2885
480x360	0.65	3	0.8059	5.2677
480x360	0.65	10	0.8042	5.2750
480x360	0.65	15	0.8030	5.2718
480x360	0.65	30	0.8010	5.3086
480x360	0.75	0.15	0.6781	5.3420
480x360	0.75	0.5	0.6764	5.3308
480x360	0.75	0.75	0.6764	5.3069

Image Size (px.)	Balancing Terms	Lambda	F-Score	Average time
480x360	0.75	1	0.6773	5.3192
480x360	0.75	1.5	0.6734	5.3101
480x360	0.75	3	0.7920	5.3186
480x360	0.75	10	0.7897	5.3319
480x360	0.75	15	0.7878	5.3351
480x360	0.75	30	0.7847	5.3182
480x360	0.85	0.15	0.6296	5.4071
480x360	0.85	0.5	0.6288	5.4246
480x360	0.85	0.75	0.6266	5.4059
480x360	0.85	1	0.6252	5.4276
480x360	0.85	1.5	0.6241	5.4060
480x360	0.85	3	0.7669	5.3988
480x360	0.85	10	0.7635	5.4178
480x360	0.85	15	0.7613	5.4262
480x360	0.85	30	0.7571	5.4135
480x360	1	0.15	0.5671	5.5514
480x360	1	0.5	0.5670	5.5122
480x360	1	0.75	0.5664	5.5250
480x360	1	1	0.5661	5.5247
480x360	1	1.5	0.5658	5.5003
480x360	1	3	0.6988	5.4872
480x360	1	10	0.6957	5.5149
480x360	1	15	0.6937	5.5331
480x360	1	30	0.6899	5.5133

Table 92.: Flooding based segmentation results using Graph Cuts as initial segmentation and multiple parameter configurations over Dataset3.

A.2.4 *Dataset4*

Image Size (px.)	Balancing Terms	Lambda	F-Score	Average time
640x480	0	0.15	0.5502	12.7085
640x480	0	0.5	0.5505	12.5533
640x480	0	0.75	0.5506	12.5937
640x480	0	1	0.5505	12.5619
640x480	0	1.5	0.5504	12.5494
640x480	0	3	0.5501	12.5541
640x480	0	10	0.5490	12.5559
640x480	0	15	0.5490	12.5597
640x480	0	30	0.5484	12.7931
640x480	0.15	0.15	0.5618	12.7728
640x480	0.15	0.5	0.5620	12.2424
640x480	0.15	0.75	0.5622	12.1539
640x480	0.15	1	0.5624	12.4423
640x480	0.15	1.5	0.5626	12.5529
640x480	0.15	3	0.5631	12.5456
640x480	0.15	10	0.5633	12.5518
640x480	0.15	15	0.5631	12.5493
640x480	0.15	30	0.5627	12.5404
640x480	0.25	0.15	0.5706	12.5398
640x480	0.25	0.5	0.5708	12.5811
640x480	0.25	0.75	0.5709	12.5390
640x480	0.25	1	0.5711	12.5222
640x480	0.25	1.5	0.5713	12.5291
640x480	0.25	3	0.5718	12.5264
640x480	0.25	10	0.5725	12.5125
640x480	0.25	15	0.5725	12.5223
640x480	0.25	30	0.5722	12.5250
640x480	0.35	0.15	0.5760	12.5187
640x480	0.35	0.5	0.5762	12.5440
640x480	0.35	0.75	0.5764	12.5131
640x480	0.35	1	0.5765	12.5171
640x480	0.35	1.5	0.5768	14.8339
640x480	0.35	3	0.5774	12.6477
640x480	0.35	10	0.5785	14.2229
640x480	0.35	15	0.5787	15.5507
640x480	0.35	30	005788	14.7068
640x480	0.45	0.15	0.5859	14.9660
640x480	0.45	0.5	0.5861	14.3942
640x480	0.45	0.75	0.5863	14.7251
640x480	0.45	1	0.5864	15.4286
640x480	0.45	1.5	0.5867	14.5070
640x480	0.45	3	0.5872	12.9714

Image Size (px.)	Balancing Terms	Lambda	F-Score	Average time
640x480	0.45	10	0.5884	13.8318
640x480	0.45	15	0.5885	12.7667
640x480	0.45	30	0.5885	12.5442
640x480	0.5	0.15	0.5891	12.5474
640x480	0.5	0.5	0.5893	14.4069
640x480	0.5	0.75	0.5895	15.7388
640x480	0.5	1	0.5896	12.7004
640x480	0.5	1.5	0.5899	12.6175
640x480	0.5	3	0.5905	12.9887
640x480	0.5	10	0.5916	13.8670
640x480	0.5	15	0.5918	14.4771
640x480	0.5	30	0.5918	14.3951
640x480	0.55	0.15	0.5911	14.3848
640x480	0.55	0.5	0.5913	15.2052
640x480	0.55	0.75	0.5915	14.1069
640x480	0.55	1	0.5916	13.8463
640x480	0.55	1.5	0.5919	14.4827
640x480	0.55	3	0.5925	13.0389
640x480	0.55	10	0.5936	12.9825
640x480	0.55	15	0.5939	14.7365
640x480	0.55	30	0.5941	14.6152
640x480	0.65	0.15	0.5980	13.8788
640x480	0.65	0.5	0.5981	14.8040
640x480	0.65	0.75	0.5982	12.5426
640x480	0.65	1	0.5983	12.5633
640x480	0.65	1.5	0.5985	12.5460
640x480	0.65	3	0.5990	12.5349
640x480	0.65	10	0.5999	12.5268
640x480	0.65	15	0.6001	12.5397
640x480	0.65	30	0.6003	12.5342
640x480	0.75	0.15	0.6030	12.5407
640x480	0.75	0.5	0.6032	12.5449
640x480	0.75	0.75	0.6033	12.5504
640x480	0.75	1	0.6034	12.5307
640x480	0.75	1.5	0.6036	12.5571
640x480	0.75	3	0.6039	12.5362
640x480	0.75	10	0.6046	12.5370
640x480	0.75	15	0.6047	12.5385
640x480	0.75	30	0.6046	12.5406
640x480	0.85	0.15	0.5947	12.5661
640x480	0.85	0.5	0.5948	12.5224
640x480	0.85	0.75	0.5949	12.5137
640x480	0.85	1	0.5949	12.7208
640x480	0.85	1.5	0.5951	12.5076

Image Size (px.)	Balancing Terms	Lambda	F-Score	Average time
640x480	0.85	3	0.5954	12.5116
640x480	0.85	10	0.5961	12.5210
640x480	0.85	15	0.5963	12.5285
640x480	0.85	30	0.5962	12.5188
640x480	1	0.15	0.5598	12.4826
640x480	1	0.5	0.5598	12.4851
640x480	1	0.75	0.5598	12.4782
640x480	1	1	0.5598	12.4723
640x480	1	1.5	0.5598	12.4868
640x480	1	3	0.5598	12.4885
640x480	1	10	0.5595	12.4704
640x480	1	15	0.5592	12.4704
640x480	1	30	0.5582	12.4785
480x360	0	0.15	0.5579	7.4426
480x360	0	0.5	0.5583	7.4906
480x360	0	0.75	0.5584	7.4539
480x360	0	1	0.5584	7.4499
480x360	0	1.5	0.5584	7.4439
480x360	0	3	0.5581	7.4617
480x360	0	10	0.5571	7.4576
480x360	0	15	0.5567	7.4660
480x360	0	30	0.5560	7.4649
480x360	0.15	0.15	0.5697	7.4597
480x360	0.15	0.5	0.5700	7.4429
480x360	0.15	0.75	0.5702	7.4416
480x360	0.15	1	0.5704	7.4503
480x360	0.15	1.5	0.5707	7.4515
480x360	0.15	3	0.5712	7.4577
480x360	0.15	10	0.5715	7.4558
480x360	0.15	15	0.5714	7.4606
480x360	0.15	30	0.5709	7.4693
480x360	0.25	0.15	0.5770	7.4541
480x360	0.25	0.5	0.5772	7.4468
480x360	0.25	0.75	0.5774	7.4451
480x360	0.25	1	0.5775	7.4493
480x360	0.25	1.5	0.5778	7.4518
480x360	0.25	3	0.5784	7.4556
480x360	0.25	10	0.5794	7.4543
480x360	0.25	15	0.5795	7.4547
480x360	0.25	30	0.5795	7.4722
480x360	0.35	0.15	0.5847	7.4483
480x360	0.35	0.5	0.5750	7.4499
480x360	0.35	0.75	0.5752	7.4562
480x360	0.35	1	0.5853	7.4592

Image Size (px.)	Balancing Terms	Lambda	F-Score	Average time
480x360	0.35	1.5	0.5855	7.4567
480x360	0.35	3	0.5855	7.4629
480x360	0.35	10	0.5861	7.4616
480x360	0.35	15	0.5875	7.4599
480x360	0.35	30	0.5877	7.4578
480x360	0.45	0.15	0.5939	7.4533
480x360	0.45	0.5	0.5941	7.4592
480x360	0.45	0.75	0.5942	7.4528
480x360	0.45	1	0.5943	7.4534
480x360	0.45	1.5	0.5945	7.4493
480x360	0.45	3	0.5950	7.4437
480x360	0.45	10	0.5963	7.4451
480x360	0.45	15	0.5966	7.4577
480x360	0.45	30	0.5967	7.4540
480x360	0.5	0.15	0.5977	7.4632
480x360	0.5	0.5	0.5980	7.4649
480x360	0.5	0.75	0.5981	7.4645
480x360	0.5	1	0.5982	7.4513
480x360	0.5	1.5	0.5985	7.4488
480x360	0.5	3	0.5990	7.4500
480x360	0.5	10	0.6002	7.4441
480x360	0.5	15	0.6005	7.4445
480x360	0.5	30	0.6007	7.4583
480x360	0.55	0.15	0.6013	7.4512
480x360	0.55	0.5	0.6015	7.4516
480x360	0.55	0.75	0.6017	7.4567
480x360	0.55	1	0.6018	7.4558
480x360	0.55	1.5	0.6020	7.4582
480x360	0.55	3	0.6025	7.4531
480x360	0.55	10	0.6037	7.4558
480x360	0.55	15	0.6039	7.4640
480x360	0.55	30	0.6041	7.4606
480x360	0.65	0.15	0.6103	7.4672
480x360	0.65	0.5	0.6104	7.4648
480x360	0.65	0.75	0.6105	7.4707
480x360	0.65	1	0.6106	7.4636
480x360	0.65	1.5	0.6108	7.4844
480x360	0.65	3	0.6111	7.4786
480x360	0.65	10	0.6119	7.6496
480x360	0.65	15	0.6121	7.4644
480x360	0.65	30	0.6121	7.4672
480x360	0.75	0.15	0.6140	7.4616
480x360	0.75	0.5	0.6142	7.4568
480x360	0.75	0.75	0.6143	7.4672

Image Size (px.)	Balancing Terms	Lambda	F-Score	Average time
480x360	0.75	1	0.6143	7.4584
480x360	0.75	1.5	0.6145	7.4834
480x360	0.75	3	0.6147	7.4578
480x360	0.75	10	0.6151	7.4581
480x360	0.75	15	0.6151	7.4561
480x360	0.75	30	0.6151	7.4622
480x360	0.85	0.15	0.6069	7.4487
480x360	0.85	0.5	0.6070	7.4443
480x360	0.85	0.75	0.6070	7.4435
480x360	0.85	1	0.6070	7.4471
480x360	0.85	1.5	0.6071	7.4330
480x360	0.85	3	0.6072	7.4284
480x360	0.85	10	0.6077	7.4259
480x360	0.85	15	0.6078	7.4310
480x360	0.85	30	0.6077	7.4309
480x360	1	0.15	0.5765	7.4023
480x360	1	0.5	0.5765	7.4036
480x360	1	0.75	0.5765	7.4039
480x360	1	1	0.5765	7.3931
480x360	1	1.5	0.5765	7.3986
480x360	1	3	0.5764	7.3983
480x360	1	10	0.5759	7.4000
480x360	1	15	0.5755	7.3953
480x360	1	30	0.5746	7.3952

Table 93.: Flooding based segmentation results using Graph Cuts as initial segmentation and multiple parameter configurations over Dataset4.

Image Size (px.)	Balancing Terms	Lambda	F-Score
640x480	0	0.15	0.6133
640x480	0	0.5	0.6136
640x480	0	0.75	0.6136
640x480	0	1	0.6137
640x480	0	1.5	0.6139
640x480	0	3	0.6136
640x480	0	10	0.6123
640x480	0	15	0.6119
640x480	0	30	0.6111
640x480	0.15	0.15	0.6254
640x480	0.15	0.5	0.6255
640x480	0.15	0.75	0.6256
640x480	0.15	1	0.6257
640x480	0.15	1.5	0.6259
640x480	0.15	3	0.6263
640x480	0.15	10	0.6267
640x480	0.15	15	0.6264
640x480	0.15	30	0.6258
640x480	0.25	0.15	0.6314
640x480	0.25	0.5	0.6317
640x480	0.25	0.75	0.6319
640x480	0.25	1	0.6320
640x480	0.25	1.5	0.6323
640x480	0.25	3	0.6329
640x480	0.25	10	0.6339
640x480	0.25	15	0.6341
640x480	0.25	30	0.6338
640x480	0.35	0.15	0.6358
640x480	0.35	0.5	0.6361
640x480	0.35	0.75	0.6364
640x480	0.35	1	0.6366
640x480	0.35	1.5	0.6369
640x480	0.35	3	0.6377
640x480	0.35	10	0.6388
640x480	0.35	15	0.6391
640x480	0.35	30	0.6390
640x480	0.45	0.15	0.6454
640x480	0.45	0.5	0.6455
640x480	0.45	0.75	0.6457
640x480	0.45	1	0.6458
640x480	0.45	1.5	0.6460
640x480	0.45	3	0.6465
640x480	0.45	10	0.6476
640x480	0.45	15	0.6478

Image Size (px.)	Balancing Terms	Lambda	F-Score
640x480	0.45	30	0.6476
640x480	0.5	0.15	0.6470
640x480	0.5	0.5	0.6471
640x480	0.5	0.75	0.6472
640x480	0.5	1	0.6473
640x480	0.5	1.5	0.6475
640x480	0.5	3	0.6479
640x480	0.5	10	0.6488
640x480	0.5	15	0.6490
640x480	0.5	30	0.6488
640x480	0.55	0.15	0.6463
640x480	0.55	0.5	0.6465
640x480	0.55	0.75	0.6467
640x480	0.55	1	0.6468
640x480	0.55	1.5	0.6471
640x480	0.55	3	0.6477
640x480	0.55	10	0.6488
640x480	0.55	15	0.6490
640x480	0.55	30	0.6490
640x480	0.65	0.15	0.6489
640x480	0.65	0.5	0.6490
640x480	0.65	0.75	0.6490
640x480	0.65	1	0.6491
640x480	0.65	1.5	0.6491
640x480	0.65	3	0.6495
640x480	0.65	10	0.6503
640x480	0.65	15	0.6505
640x480	0.65	30	0.6504
640x480	0.75	0.15	0.6453
640x480	0.75	0.5	0.6454
640x480	0.75	0.75	0.6456
640x480	0.75	1	0.6457
640x480	0.75	1.5	0.6459
640x480	0.75	3	0.6464
640x480	0.75	10	0.6476
640x480	0.75	15	0.6480
640x480	0.75	30	0.6481
640x480	0.85	0.15	0.6307
640x480	0.85	0.5	0.6307
640x480	0.85	0.75	0.6308
640x480	0.85	1	0.6308
640x480	0.85	1.5	0.6309
640x480	0.85	3	0.6312
640x480	0.85	10	0.6316

Image Size (px.)	Balancing Terms	Lambda	F-Score
640x480	0.85	15	0.6317
640x480	0.85	30	0.6315
640x480	1	0.15	0.5799
640x480	1	0.5	0.5799
640x480	1	0.75	0.5799
640x480	1	1	0.5799
640x480	1	1.5	0.5798
640x480	1	3	0.5797
640x480	1	10	0.5790
640x480	1	15	0.5784
640x480	1	30	0.5769
480x360	0	0.15	0.6116
480x360	0	0.5	0.6117
480x360	0	0.75	0.6119
480x360	0	1	0.6120
480x360	0	1.5	0.6120
480x360	0	3	0.6115
480x360	0	10	0.6101
480x360	0	15	0.6094
480x360	0	30	0.6088
480x360	0.15	0.15	0.6245
480x360	0.15	0.5	0.6247
480x360	0.15	0.75	0.6247
480x360	0.15	1	0.6248
480x360	0.15	1.5	0.6249
480x360	0.15	3	0.6253
480x360	0.15	10	0.6254
480x360	0.15	15	0.6251
480x360	0.15	30	0.6242
480x360	0.25	0.15	0.6309
480x360	0.25	0.5	0.6312
480x360	0.25	0.75	0.6313
480x360	0.25	1	0.6315
480x360	0.25	1.5	0.6317
480x360	0.25	3	0.6323
480x360	0.25	10	0.6334
480x360	0.25	15	0.6335
480x360	0.25	30	0.6330
480x360	0.35	0.15	0.6384
480x360	0.35	0.5	0.6388
480x360	0.35	0.75	0.6390
480x360	0.35	1	0.6392
480x360	0.35	1.5	0.6394
480x360	0.35	3	0.6400

Image Size (px.)	Balancing Terms	Lambda	F-Score
480x360	0.35	10	0.6409
480x360	0.35	15	0.6412
480x360	0.35	30	0.6409
480x360	0.45	0.15	0.6504
480x360	0.45	0.5	0.6504
480x360	0.45	0.75	0.6505
480x360	0.45	1	0.6506
480x360	0.45	1.5	0.6507
480x360	0.45	3	0.6511
480x360	0.45	10	0.6520
480x360	0.45	15	0.6521
480x360	0.45	30	0.6515
480x360	0.5	0.15	0.6527
480x360	0.5	0.5	0.6531
480x360	0.5	0.75	0.6532
480x360	0.5	1	0.6534
480x360	0.5	1.5	0.6537
480x360	0.5	3	0.6542
480x360	0.5	10	0.6551
480x360	0.5	15	0.6551
480x360	0.5	30	0.6547
480x360	0.55	0.15	0.6558
480x360	0.55	0.5	0.6561
480x360	0.55	0.75	0.6563
480x360	0.55	1	0.6565
480x360	0.55	1.5	0.6567
480x360	0.55	3	0.6572
480x360	0.55	10	0.6579
480x360	0.55	15	0.6580
480x360	0.55	30	0.6576
480x360	0.65	0.15	0.6652
480x360	0.65	0.5	0.6653
480x360	0.65	0.75	0.6653
480x360	0.65	1	0.6654
480x360	0.65	1.5	0.6654
480x360	0.65	3	0.6656
480x360	0.65	10	0.6658
480x360	0.65	15	0.6656
480x360	0.65	30	0.6649
480x360	0.75	0.15	0.6614
480x360	0.75	0.5	0.6615
480x360	0.75	0.75	0.6616
480x360	0.75	1	0.6617
480x360	0.75	1.5	0.6618

Image Size (px.)	Balancing Terms	Lambda	F-Score
480x360	0.75	3	0.6619
480x360	0.75	10	0.6621
480x360	0.75	15	0.6618
480x360	0.75	30	0.6610
480x360	0.85	0.15	0.6437
480x360	0.85	0.5	0.6438
480x360	0.85	0.75	0.6438
480x360	0.85	1	0.6438
480x360	0.85	1.5	0.6439
480x360	0.85	3	0.6439
480x360	0.85	10	0.6441
480x360	0.85	15	0.6439
480x360	0.85	30	0.6432
480x360	1	0.15	0.5980
480x360	1	0.5	0.5979
480x360	1	0.75	0.5979
480x360	1	1	0.5979
480x360	1	1.5	0.5977
480x360	1	3	0.5975
480x360	1	10	0.5963
480x360	1	15	0.5954
480x360	1	30	0.5935

Table 94.: Flooding based segmentation results using Graph Cuts as initial segmentation and multiple parameter configurations over the subset of images from Dataset4 which were captured with natural lighting conditions.

Image Size (px.)	Balancing Terms	Lambda	F-Score
640x480	0	0.15	0.5281
640x480	0	0.5	0.5286
640x480	0	0.75	0.5288
640x480	0	1	0.5287
640x480	0	1.5	0.5287
640x480	0	3	0.5286
640x480	0	10	0.5279
640x480	0	15	0.5276
640x480	0	30	0.5278
640x480	0.15	0.15	0.5432
640x480	0.15	0.5	0.5436
640x480	0.15	0.75	0.5438
640x480	0.15	1	0.5441
640x480	0.15	1.5	0.5444
640x480	0.15	3	0.5449
640x480	0.15	10	0.5453
640x480	0.15	15	0.5452
640x480	0.15	30	0.5450
640x480	0.25	0.15	0.5553
640x480	0.25	0.5	0.5557
640x480	0.25	0.75	0.5559
640x480	0.25	1	0.5562
640x480	0.25	1.5	0.5567
640x480	0.25	3	0.5575
640x480	0.25	10	0.5582
640x480	0.25	15	0.5582
640x480	0.25	30	0.5577
640x480	0.35	0.15	0.5644
640x480	0.35	0.5	0.5647
640x480	0.35	0.75	0.5650
640x480	0.35	1	0.5652
640x480	0.35	1.5	0.5657
640x480	0.35	3	0.5666
640x480	0.35	10	0.5679
640x480	0.35	15	0.5682
640x480	0.35	30	0.5682
640x480	0.45	0.15	0.5744
640x480	0.45	0.5	0.5747
640x480	0.45	0.75	0.5749
640x480	0.45	1	0.5751
640x480	0.45	1.5	0.5755
640x480	0.45	3	0.5764
640x480	0.45	10	0.5776
640x480	0.45	15	0.5777

Image Size (px.)	Balancing Terms	Lambda	F-Score
640x480	0.45	30	0.5778
640x480	0.5	0.15	0.5768
640x480	0.5	0.5	0.5774
640x480	0.5	0.75	0.5777
640x480	0.5	1	0.5779
640x480	0.5	1.5	0.5784
640x480	0.5	3	0.5794
640x480	0.5	10	0.5811
640x480	0.5	15	0.5814
640x480	0.5	30	0.5715
640x480	0.55	0.15	0.5808
640x480	0.55	0.5	0.5811
640x480	0.55	0.75	0.5814
640x480	0.55	1	0.5816
640x480	0.55	1.5	0.5821
640x480	0.55	3	0.5831
640x480	0.55	10	0.5848
640x480	0.55	15	0.5853
640x480	0.55	30	0.5855
640x480	0.65	0.15	0.5947
640x480	0.65	0.5	0.5951
640x480	0.65	0.75	0.5953
640x480	0.65	1	0.5956
640x480	0.65	1.5	0.5959
640x480	0.65	3	0.5968
640x480	0.65	10	0.5981
640x480	0.65	15	0.5982
640x480	0.65	30	0.5981
640x480	0.75	0.15	0.6050
640x480	0.75	0.5	0.6054
640x480	0.75	0.75	0.6056
640x480	0.75	1	0.6058
640x480	0.75	1.5	0.6061
640x480	0.75	3	0.6068
640x480	0.75	10	0.6077
640x480	0.75	15	0.6077
640x480	0.75	30	0.6075
640x480	0.85	0.15	0.6136
640x480	0.85	0.5	0.6138
640x480	0.85	0.75	0.6140
640x480	0.85	1	0.6141
640x480	0.85	1.5	0.6143
640x480	0.85	3	0.6148
640x480	0.85	10	0.6156

Image Size (px.)	Balancing Terms	Lambda	F-Score
640x480	0.85	15	0.6157
640x480	0.85	30	0.6154
640x480	1	0.15	0.5809
640x480	1	0.5	0.5810
640x480	1	0.75	0.5810
640x480	1	1	0.5810
640x480	1	1.5	0.5811
640x480	1	3	0.5812
640x480	1	10	0.5808
640x480	1	15	0.5803
640x480	1	30	0.5791
480x360	0	0.15	0.5408
480x360	0	0.5	0.5412
480x360	0	0.75	0.5414
480x360	0	1	0.5414
480x360	0	1.5	0.5415
480x360	0	3	0.5414
480x360	0	10	0.5409
480x360	0	15	0.5408
480x360	0	30	0.5410
480x360	0.15	0.15	0.5545
480x360	0.15	0.5	0.5550
480x360	0.15	0.75	0.5553
480x360	0.15	1	0.5556
480x360	0.15	1.5	0.5559
480x360	0.15	3	0.5564
480x360	0.15	10	0.5569
480x360	0.15	15	0.5568
480x360	0.15	30	0.5563
480x360	0.25	0.15	0.5637
480x360	0.25	0.5	0.5640
480x360	0.25	0.75	0.5643
480x360	0.25	1	0.5645
480x360	0.25	1.5	0.5648
480x360	0.25	3	0.5654
480x360	0.25	10	0.5664
480x360	0.25	15	0.5665
480x360	0.25	30	0.5665
480x360	0.35	0.15	0.5739
480x360	0.35	0.5	0.5742
480x360	0.35	0.75	0.5744
480x360	0.35	1	0.5746
480x360	0.35	1.5	0.5749
480x360	0.35	3	0.5755

Image Size (px.)	Balancing Terms	Lambda	F-Score
480x360	0.35	10	0.5769
480x360	0.35	15	0.5769
480x360	0.35	30	0.5768
480x360	0.45	0.15	0.5854
480x360	0.45	0.5	0.5858
480x360	0.45	0.75	0.5860
480x360	0.45	1	0.5861
480x360	0.45	1.5	0.5865
480x360	0.45	3	0.5872
480x360	0.45	10	0.5886
480x360	0.45	15	0.5887
480x360	0.45	30	0.5884
480x360	0.5	0.15	0.5905
480x360	0.5	0.5	0.5909
480x360	0.5	0.75	0.5911
480x360	0.5	1	0.5913
480x360	0.5	1.5	0.5917
480x360	0.5	3	0.5925
480x360	0.5	10	0.5940
480x360	0.5	15	0.5941
480x360	0.5	30	0.5941
480x360	0.55	0.15	0.5962
480x360	0.55	0.5	0.5965
480x360	0.55	0.75	0.5967
480x360	0.55	1	0.5969
480x360	0.55	1.5	0.5974
480x360	0.55	3	0.5983
480x360	0.55	10	0.6000
480x360	0.55	15	0.6002
480x360	0.55	30	0.6003
480x360	0.65	0.15	0.6116
480x360	0.65	0.5	0.6119
480x360	0.65	0.75	0.6120
480x360	0.65	1	0.6122
480x360	0.65	1.5	0.6124
480x360	0.65	3	0.6130
480x360	0.65	10	0.6139
480x360	0.65	15	0.6141
480x360	0.65	30	0.6136
480x360	0.75	0.15	0.6222
480x360	0.75	0.5	0.6225
480x360	0.75	0.75	0.6226
480x360	0.75	1	0.6227
480x360	0.75	1.5	0.6229

Image Size (px.)	Balancing Terms	Lambda	F-Score
480x360	0.75	3	0.6234
480x360	0.75	10	0.6240
480x360	0.75	15	0.6239
480x360	0.75	30	0.6233
480x360	0.85	0.15	0.6295
480x360	0.85	0.5	0.6296
480x360	0.85	0.75	0.6296
480x360	0.85	1	0.6297
480x360	0.85	1.5	0.6298
480x360	0.85	3	0.6300
480x360	0.85	10	0.6302
480x360	0.85	15	0.6301
480x360	0.85	30	0.6297
480x360	1	0.15	0.6029
480x360	1	0.5	0.6029
480x360	1	0.75	0.6029
480x360	1	1	0.6030
480x360	1	1.5	0.6030
480x360	1	3	0.6029
480x360	1	10	0.6022
480x360	1	15	0.6016
480x360	1	30	0.6002

Table 95.: Flooding based segmentation results using Graph Cuts as initial segmentation and multiple parameter configurations over the subset of images from Dataset4 which were captured with severe shadows on the hand.

Image Size (px.)	Balancing Terms	Lambda	F-Score
640x480	0	0.15	0.4700
640x480	0	0.5	0.4705
640x480	0	0.75	0.4708
640x480	0	1	0.4709
640x480	0	1.5	0.4711
640x480	0	3	0.4715
640x480	0	10	0.4728
640x480	0	15	0.4733
640x480	0	30	0.4748
640x480	0.15	0.15	0.4768
640x480	0.15	0.5	0.4772
640x480	0.15	0.75	0.4774
640x480	0.15	1	0.4775
640x480	0.15	1.5	0.4778
640x480	0.15	3	0.4783
640x480	0.15	10	0.4792
640x480	0.15	15	0.4795
640x480	0.15	30	0.4801
640x480	0.25	0.15	0.4804
640x480	0.25	0.5	0.4806
640x480	0.25	0.75	0.4808
640x480	0.25	1	0.4809
640x480	0.25	1.5	0.4812
640x480	0.25	3	0.4819
640x480	0.25	10	0.4832
640x480	0.25	15	0.4837
640x480	0.25	30	0.4844
640x480	0.35	0.15	0.4850
640x480	0.35	0.5	0.4851
640x480	0.35	0.75	0.4852
640x480	0.35	1	0.4854
640x480	0.35	1.5	0.4856
640x480	0.35	3	0.4863
640x480	0.35	10	0.4878
640x480	0.35	15	0.4884
640x480	0.35	30	0.4893
640x480	0.45	0.15	0.4918
640x480	0.45	0.5	0.4920
640x480	0.45	0.75	0.4922
640x480	0.45	1	0.4923
640x480	0.45	1.5	0.4926
640x480	0.45	3	0.4932
640x480	0.45	10	0.4948
640x480	0.45	15	0.4954

Image Size (px.)	Balancing Terms	Lambda	F-Score
640x480	0.45	30	0.4964
640x480	0.5	0.15	0.4938
640x480	0.5	0.5	0.4943
640x480	0.5	0.75	0.4945
640x480	0.5	1	0.4947
640x480	0.5	1.5	0.4951
640x480	0.5	3	0.4960
640x480	0.5	10	0.4978
640x480	0.5	15	0.4984
640x480	0.5	30	0.4992
640x480	0.55	0.15	0.4959
640x480	0.55	0.5	0.4962
640x480	0.55	0.75	0.4963
640x480	0.55	1	0.4965
640x480	0.55	1.5	0.4968
640x480	0.55	3	0.4974
640x480	0.55	10	0.4991
640x480	0.55	15	0.4998
640x480	0.55	30	0.5009
640x480	0.65	0.15	0.5006
640x480	0.65	0.5	0.5008
640x480	0.65	0.75	0.5011
640x480	0.65	1	0.5013
640x480	0.65	1.5	0.5016
640x480	0.65	3	0.5022
640x480	0.65	10	0.5037
640x480	0.65	15	0.5041
640x480	0.65	30	0.5049
640x480	0.75	0.15	0.5081
640x480	0.75	0.5	0.5084
640x480	0.75	0.75	0.5085
640x480	0.75	1	0.5086
640x480	0.75	1.5	0.5089
640x480	0.75	3	0.5093
640x480	0.75	10	0.5105
640x480	0.75	15	0.5109
640x480	0.75	30	0.5118
640x480	0.85	0.15	0.5165
640x480	0.85	0.5	0.5167
640x480	0.85	0.75	0.5167
640x480	0.85	1	0.5168
640x480	0.85	1.5	0.5170
640x480	0.85	3	0.5173
640x480	0.85	10	0.5183

Image Size (px.)	Balancing Terms	Lambda	F-Score
640x480	0.85	15	0.5187
640x480	0.85	30	0.5193
640x480	1	0.15	0.5157
640x480	1	0.5	0.5157
640x480	1	0.75	0.5157
640x480	1	1	0.5158
640x480	1	1.5	0.5158
640x480	1	3	0.5158
640x480	1	10	0.5159
640x480	1	15	0.5160
640x480	1	30	0.5160
480x360	0	0.15	0.4663
480x360	0	0.5	0.4671
480x360	0	0.75	0.4675
480x360	0	1	0.4677
480x360	0	1.5	0.4682
480x360	0	3	0.4690
480x360	0	10	0.4710
480x360	0	15	0.4721
480x360	0	30	0.4734
480x360	0.15	0.15	0.4738
480x360	0.15	0.5	0.4741
480x360	0.15	0.75	0.4744
480x360	0.15	1	0.4746
480x360	0.15	1.5	0.4749
480x360	0.15	3	0.4756
480x360	0.15	10	0.4768
480x360	0.15	15	0.4773
480x360	0.15	30	0.4784
480x360	0.25	0.15	0.4781
480x360	0.25	0.5	0.4783
480x360	0.25	0.75	0.4785
480x360	0.25	1	0.4787
480x360	0.25	1.5	0.4790
480x360	0.25	3	0.4800
480x360	0.25	10	0.4817
480x360	0.25	15	0.4827
480x360	0.25	30	0.4840
480x360	0.35	0.15	0.4848
480x360	0.35	0.5	0.4851
480x360	0.35	0.75	0.4853
480x360	0.35	1	0.4855
480x360	0.35	1.5	0.4858
480x360	0.35	3	0.4866

Image Size (px.)	Balancing Terms	Lambda	F-Score
480x360	0.35	10	0.4887
480x360	0.35	15	0.4893
480x360	0.35	30	0.4905
480x360	0.45	0.15	0.4894
480x360	0.45	0.5	0.4896
480x360	0.45	0.75	0.4897
480x360	0.45	1	0.4898
480x360	0.45	1.5	0.4902
480x360	0.45	3	0.4909
480x360	0.45	10	0.4930
480x360	0.45	15	0.4939
480x360	0.45	30	0.4951
480x360	0.5	0.15	0.4920
480x360	0.5	0.5	0.4923
480x360	0.5	0.75	0.4924
480x360	0.5	1	0.4925
480x360	0.5	1.5	0.4928
480x360	0.5	3	0.4934
480x360	0.5	10	0.4953
480x360	0.5	15	0.4961
480x360	0.5	30	0.4974
480x360	0.55	0.15	0.4970
480x360	0.55	0.5	0.4972
480x360	0.55	0.75	0.4973
480x360	0.55	1	0.4974
480x360	0.55	1.5	0.4977
480x360	0.55	3	0.4982
480x360	0.55	10	0.5002
480x360	0.55	15	0.5010
480x360	0.55	30	0.5020
480x360	0.65	0.15	0.5018
480x360	0.65	0.5	0.5023
480x360	0.65	0.75	0.5025
480x360	0.65	1	0.5027
480x360	0.65	1.5	0.5030
480x360	0.65	3	0.5034
480x360	0.65	10	0.5053
480x360	0.65	15	0.5059
480x360	0.65	30	0.5071
480x360	0.75	0.15	0.5083
480x360	0.75	0.5	0.5084
480x360	0.75	0.75	0.5085
480x360	0.75	1	0.5086
480x360	0.75	1.5	0.5088

Image Size (px.)	Balancing Terms	Lambda	F-Score
480x360	0.75	3	0.5092
480x360	0.75	10	0.5106
480x360	0.75	15	0.5110
480x360	0.75	30	0.5121
480x360	0.85	0.15	0.5187
480x360	0.85	0.5	0.5189
480x360	0.85	0.75	0.5189
480x360	0.85	1	0.5189
480x360	0.85	1.5	0.5191
480x360	0.85	3	0.5194
480x360	0.85	10	0.5203
480x360	0.85	15	0.5206
480x360	0.85	30	0.5213
480x360	1	0.15	0.5218
480x360	1	0.5	0.5218
480x360	1	0.75	0.5218
480x360	1	1	0.5218
480x360	1	1.5	0.5218
480x360	1	3	0.5218
480x360	1	10	0.5220
480x360	1	15	0.5223
480x360	1	30	0.5227

Table 96.: Flooding based segmentation results using Graph Cuts as initial segmentation and multiple parameter configurations over the subset of images from Dataset4 which were captured under highly brilliant lighting conditions.

Image Size (px.)	Balancing Terms	Lambda	F-Score
640x480	0	0.15	0.5769
640x480	0	0.5	0.5771
640x480	0	0.75	0.5771
640x480	0	1	0.5771
640x480	0	1.5	0.5769
640x480	0	3	0.5764
640x480	0	10	0.5742
640x480	0	15	0.5731
640x480	0	30	0.5715
640x480	0.15	0.15	0.5889
640x480	0.15	0.5	0.5891
640x480	0.15	0.75	0.5893
640x480	0.15	1	0.5895
640x480	0.15	1.5	0.5897
640x480	0.15	3	0.5903
640x480	0.15	10	0.5911
640x480	0.15	15	0.5909
640x480	0.15	30	0.5902
640x480	0.25	0.15	0.6012
640x480	0.25	0.5	0.6014
640x480	0.25	0.75	0.6015
640x480	0.25	1	0.6017
640x480	0.25	1.5	0.6019
640x480	0.25	3	0.6023
640x480	0.25	10	0.6033
640x480	0.25	15	0.6034
640x480	0.25	30	0.6031
640x480	0.35	0.15	0.6049
640x480	0.35	0.5	0.6050
640x480	0.35	0.75	0.6051
640x480	0.35	1	0.6053
640x480	0.35	1.5	0.6056
640x480	0.35	3	0.6063
640x480	0.35	10	0.6083
640x480	0.35	15	0.6087
640x480	0.35	30	0.6091
640x480	0.45	0.15	0.6200
640x480	0.45	0.5	0.6202
640x480	0.45	0.75	0.6203
640x480	0.45	1	0.6205
640x480	0.45	1.5	0.6207
640x480	0.45	3	0.6212
640x480	0.45	10	0.6224
640x480	0.45	15	0.6227

Image Size (px.)	Balancing Terms	Lambda	F-Score
640x480	0.45	30	0.6225
640x480	0.5	0.15	0.6261
640x480	0.5	0.5	0.6262
640x480	0.5	0.75	0.6262
640x480	0.5	1	0.6263
640x480	0.5	1.5	0.6265
640x480	0.5	3	0.6269
640x480	0.5	10	0.6281
640x480	0.5	15	0.6285
640x480	0.5	30	0.6285
640x480	0.55	0.15	0.6279
640x480	0.55	0.5	0.6280
640x480	0.55	0.75	0.6281
640x480	0.55	1	0.6282
640x480	0.55	1.5	0.6283
640x480	0.55	3	0.6289
640x480	0.55	10	0.6301
640x480	0.55	15	0.6303
640x480	0.55	30	0.6306
640x480	0.65	0.15	0.6454
640x480	0.65	0.5	0.6455
640x480	0.65	0.75	0.6456
640x480	0.65	1	0.6456
640x480	0.65	1.5	0.6457
640x480	0.65	3	0.6460
640x480	0.65	10	0.6466
640x480	0.65	15	0.6467
640x480	0.65	30	0.6171
640x480	0.75	0.15	0.6616
640x480	0.75	0.5	0.6617
640x480	0.75	0.75	0.6617
640x480	0.75	1	0.6617
640x480	0.75	1.5	0.6617
640x480	0.75	3	0.6616
640x480	0.75	10	0.6611
640x480	0.75	15	0.6606
640x480	0.75	30	0.6596
640x480	0.85	0.15	0.6302
640x480	0.85	0.5	0.6301
640x480	0.85	0.75	0.6302
640x480	0.85	1	0.6302
640x480	0.85	1.5	0.6303
640x480	0.85	3	0.6306
640x480	0.85	10	0.6316

Image Size (px.)	Balancing Terms	Lambda	F-Score
640x480	0.85	15	0.6321
640x480	0.85	30	0.6326
640x480	1	0.15	0.5626
640x480	1	0.5	0.5626
640x480	1	0.75	0.5625
640x480	1	1	0.5625
640x480	1	1.5	0.5625
640x480	1	3	0.5624
640x480	1	10	0.5618
640x480	1	15	0.5612
640x480	1	30	0.5596
480x360	0	0.15	0.5940
480x360	0	0.5	0.5944
480x360	0	0.75	0.5945
480x360	0	1	0.5945
480x360	0	1.5	0.5945
480x360	0	3	0.5939
480x360	0	10	0.5915
480x360	0	15	0.5900
480x360	0	30	0.5879
480x360	0.15	0.15	0.6074
480x360	0.15	0.5	0.6078
480x360	0.15	0.75	0.6081
480x360	0.15	1	0.6084
480x360	0.15	1.5	0.6087
480x360	0.15	3	0.6093
480x360	0.15	10	0.6096
480x360	0.15	15	0.6092
480x360	0.15	30	0.6080
480x360	0.25	0.15	0.6164
480x360	0.25	0.5	0.6167
480x360	0.25	0.75	0.6169
480x360	0.25	1	0.6170
480x360	0.25	1.5	0.6173
480x360	0.25	3	0.6178
480x360	0.25	10	0.6190
480x360	0.25	15	0.6190
480x360	0.25	30	0.6184
480x360	0.35	0.15	0.6252
480x360	0.35	0.5	0.6254
480x360	0.35	0.75	0.6256
480x360	0.35	1	0.6257
480x360	0.35	1.5	0.6258
480x360	0.35	3	0.6264

Image Size (px.)	Balancing Terms	Lambda	F-Score
480x360	0.35	10	0.6277
480x360	0.35	15	0.6281
480x360	0.35	30	0.6282
480x360	0.45	0.15	0.6327
480x360	0.45	0.5	0.6328
480x360	0.45	0.75	0.6328
480x360	0.45	1	0.6329
480x360	0.45	1.5	0.6330
480x360	0.45	3	0.6335
480x360	0.45	10	0.6352
480x360	0.45	15	0.6357
480x360	0.45	30	0.6361
480x360	0.5	0.15	0.6390
480x360	0.5	0.5	0.6392
480x360	0.5	0.75	0.6393
480x360	0.5	1	0.6394
480x360	0.5	1.5	0.6396
480x360	0.5	3	0.6104
480x360	0.5	10	0.6417
480x360	0.5	15	0.6423
480x360	0.5	30	0.6425
480x360	0.55	0.15	0.6431
480x360	0.55	0.5	0.6433
480x360	0.55	0.75	0.6435
480x360	0.55	1	0.6436
480x360	0.55	1.5	0.6438
480x360	0.55	3	0.6445
480x360	0.55	10	0.6461
480x360	0.55	15	0.6464
480x360	0.55	30	0.6466
480x360	0.65	0.15	0.6674
480x360	0.65	0.5	0.6675
480x360	0.65	0.75	0.6675
480x360	0.65	1	0.6676
480x360	0.65	1.5	0.6677
480x360	0.65	3	0.6678
480x360	0.65	10	0.6683
480x360	0.65	15	0.6682
480x360	0.65	30	0.6675
480x360	0.75	0.15	0.6813
480x360	0.75	0.5	0.6816
480x360	0.75	0.75	0.6817
480x360	0.75	1	0.6817
480x360	0.75	1.5	0.6818

Image Size (px.)	Balancing Terms	Lambda	F-Score
480x360	0.75	3	0.6817
480x360	0.75	10	0.6810
480x360	0.75	15	0.6806
480x360	0.75	30	0.6801
480x360	0.85	0.15	0.6596
480x360	0.85	0.5	0.6596
480x360	0.85	0.75	0.6595
480x360	0.85	1	0.6595
480x360	0.85	1.5	0.6594
480x360	0.85	3	0.6594
480x360	0.85	10	0.6597
480x360	0.85	15	0.6600
480x360	0.85	30	0.6601
480x360	1	0.15	0.6045
480x360	1	0.5	0.6045
480x360	1	0.75	0.6044
480x360	1	1	0.6044
480x360	1	1.5	0.6044
480x360	1	3	0.6042
480x360	1	10	0.6033
480x360	1	15	0.6027
480x360	1	30	0.6007

Table 97.: Flooding based segmentation results using Graph Cuts as initial segmentation and multiple parameter configurations over the subset of images from Dataset4 which were captured under low intensity lighting conditions.

B

PALMPRINT RESULTS USING DIFFERENT PARAMETER CONFIGURATIONS UNDER CONTROLLED CONDITIONS

A complete evaluation of different parameter configurations for feature extraction using different monomodal feature extraction methods has been conducted with the aim to find the best arrangement for each of them. Different comparison methods and a dimensionality reduction technique (PCA) have also been included in this evaluation.

Since the objective is to provide a wide evaluation of different feature extraction methods, 2DHK database has been used to this end. As detailed in Sec. 2.3.1, it provides images captured under controlled conditions together with the most representative part of the palmprint properly aligned and cropped that makes it suitable for a fair analysis of different feature extraction methods.

B.1 SOBEL FILTER

B.1.1 *Sobel filter and Euclidean Distance*

Algorithm Parameters			Results		
			Validation	Test	
Imsize	Threshold	Angles	EER (%)	FMR (%)	FNMR (%)
32x32	0.1	0	1.98	1.91	2.26
32x32	0.1	45	1.38	1.39	2.54
32x32	0.1	90	0.56	0.57	2.54
32x32	0.1	135	0.85	0.82	1.41
32x32	0.1	0, 45, 90, 135	0.56	0.55	1.41
32x32	0.25	0	1.69	1.57	2.54
32x32	0.25	45	1.85	1.77	2.82
32x32	0.25	90	1.98	2.02	2.26
32x32	0.25	135	1.13	1.11	1.69
32x32	0.25	0, 45, 90, 135	0.94	0.90	1.41
32x32	0.35	0	1.69	1.59	1.69
32x32	0.35	45	1.98	1.78	3.95
32x32	0.35	90	2.72	2.69	3.95
32x32	0.35	135	1.13	1.15	1.98
32x32	0.35	0, 45, 90, 135	1.17	1.09	1.41
32x32	0.50	0	1.61	1.65	2.26
32x32	0.50	45	3.11	2.97	5.37
32x32	0.50	90	6.40	6.47	6.78

Algorithm Parameters			Results		
			Validation	Test	
Imsize	Threshold	Angles	EER (%)	FMR (%)	FNMR (%)
32x32	0.50	135	2.56	2.64	3.39
32x32	0.50	0, 45, 90, 135	1.41	1.40	2.82
64x64	0.1	0	3.16	3.14	4.24
64x64	0.1	45	1.98	1.99	3.67
64x64	0.1	90	1.69	1.65	3.11
64x64	0.1	135	1.69	1.63	2.26
64x64	0.1	0, 45, 90, 135	1.41	1.32	3.11
64x64	0.25	0	2.64	2.53	3.67
64x64	0.25	45	4.39	4.35	6.78
64x64	0.25	90	5.45	5.30	7.91
64x64	0.25	135	2.82	2.85	3.11
64x64	0.25	0, 45, 90, 135	2.66	2.53	4.8
64x64	0.35	0	3.62	3.45	3.95
64x64	0.35	45	9.52	9.59	9.89
64x64	0.35	90	10.37	10.05	11.86
64x64	0.35	135	4.52	4.54	7.34
64x64	0.35	0, 45, 90, 135	4.52	4.31	6.78
64x64	0.50	0	6.44	6.19	6.78
64x64	0.50	45	18.13	18.01	20.34
64x64	0.50	90	18.33	18.37	20.62
64x64	0.50	135	9.75	10.00	10.73
64x64	0.50	0, 45, 90, 135	10.45	10.47	14.41
128x128	0.1	0	5.39	5.28	9.04
128x128	0.1	45	6.21	6.17	7.06
128x128	0.1	90	4.49	4.46	7.06
128x128	0.1	135	2.34	2.48	3.95
128x128	0.1	0, 45, 90, 135	3.39	3.33	5.37
128x128	0.25	0	10.81	10.48	13.56
128x128	0.25	45	17.81	17.17	20.34
128x128	0.25	90	17.59	17.54	20.62
128x128	0.25	135	9.16	9.52	11.58
128x128	0.25	0, 45, 90, 135	12.43	12.27	16.10
128x128	0.35	0	17.57	17.21	21.47
128x128	0.35	45	26.89	26.02	30.51
128x128	0.35	90	26.24	26.00	28.53
128x128	0.35	135	17.89	18.51	22.60
128x128	0.35	0, 45, 90, 135	20.92	20.86	20.53
128x128	0.50	0	27.97	27.59	29.38
128x128	0.50	45	35.03	34.12	35.03
128x128	0.50	90	34.75	34.96	35.59
128x128	0.50	135	30.57	30.79	32.49
128x128	0.50	0, 45, 90, 135	30.79	30.82	32.77

Table 98.: Palmprint Results using Sobel filter to extract features and Euclidean distance to compare.

B.1.2 *Sobel filter, PCA and Euclidean Distance*

Algorithm Parameters			Results		
			Validation	Test	
Imsize	Threshold	Angles	EER (%)	FMR (%)	FNMR (%)
32x32	0.1	0, 45, 90, 135	0.56	0.39	0.85
32x32	0.25	0, 45, 90, 135	0.28	0.19	0.85
32x32	0.35	0, 45, 90, 135	0.49	0.37	0.85
32x32	0.50	0, 45, 90, 135	0.92	0.73	0.56
64x64	0.1	0, 45, 90, 135	0.56	0.34	0.85
64x64	0.25	0, 45, 90, 135	0.85	0.56	1.13
64x64	0.35	0, 45, 90, 135	1.03	0.72	1.69
64x64	0.50	0, 45, 90, 135	2.27	1.73	3.11
128x128	0.1	0, 45, 90, 135	1.41	0.99	1.69
128x128	0.25	0, 45, 90, 135	1.60	1.11	2.82
128x128	0.35	0, 45, 90, 135	3.13	2.21	6.21
128x128	0.50	0, 45, 90, 135	8.48	6.64	10.73

Table 99.: Palmprint Results using Sobel filter and PCA to extract features and Euclidean distance to compare.

B.1.3 *Sobel filter and Support Vector Machines*

Algorithm Parameters			Results		
			Validation	Test	
Imsize	Threshold	Angles	EER (%)	FMR (%)	FNMR (%)
32x32	0.1	0	0.28	0.56	0.34
32x32	0.1	45	0.0063	0.28	0.011
32x32	0.1	90	0.067	0.29	0.10
32x32	0.1	135	0.28	0.28	0.35
32x32	0.1	0, 45, 90, 135	0.0048	0.046	0.0096
32x32	0.25	0	0.28	0.28	0.37
32x32	0.25	45	0.13	0.28	0.17
32x32	0.25	90	0.11	0.50	0.14
32x32	0.25	135	0.28	0.28	0.35
32x32	0.25	0, 45, 90, 135	0.0016	0.24	0.0016
32x32	0.35	0	0.28	0.32	0.36
32x32	0.35	45	0.56	0.28	0.68
32x32	0.35	90	0.56	0.56	0.59
32x32	0.35	135	0.28	0.31	0.30
32x32	0.35	0, 45, 90, 135	0.0095	0.28	0.0080
32x32	0.50	0	0.28	0.17	0.33
32x32	0.50	45	0.82	0.56	0.96
32x32	0.50	90	0.96	0.78	1.01
32x32	0.50	135	0.56	0.56	0.65
32x32	0.50	0, 45, 90, 135	0.089	0.20	0.11
64x64	0.1	0	0.35	0.85	0.39
64x64	0.1	45	0.033	0.64	0.043
64x64	0.1	90	0.28	0.28	0.35

Algorithm Parameters			Results		
			Validation	Test	
Imsize	Threshold	Angles	EER (%)	FMR (%)	FNMR (%)
64x64	0.1	135	0.40	0.28	0.49
64x64	0.1	0, 45, 90, 135	0.019	0.083	0.022
64x64	0.25	0	0.25	0.56	0.31
64x64	0.25	45	0.28	0.56	0.33
64x64	0.25	90	0.28	0.56	0.30
64x64	0.25	135	0.28	0.28	0.36
64x64	0.25	0, 45, 90, 135	0.11	0.28	0.14
64x64	0.35	0	0.67	0.84	0.76
64x64	0.35	45	0.28	0.85	0.36
64x64	0.35	90	0.66	0.56	0.70
64x64	0.35	135	0.33	0.56	0.40
64x64	0.35	0, 45, 90, 135	0.23	0.56	0.40
64x64	0.50	0	1.41	0.85	1.55
64x64	0.50	45	1.01	1.13	1.15
64x64	0.50	90	1.98	1.41	2.11
64x64	0.50	135	0.56	1.13	0.69
64x64	0.50	0, 45, 90, 135	0.56	0.28	0.69
128x128	0.1	0	0.28	0.57	0.33
128x128	0.1	45	0.50	0.85	0.64
128x128	0.1	90	0.56	0.62	0.61
128x128	0.1	135	0.77	0.28	0.97
128x128	0.1	0, 45, 90, 135	0.24	0.28	0.31
128x128	0.25	0	1.13	0.88	1.20
128x128	0.25	45	0.29	0.13	0.37
128x128	0.25	90	0.88	1.13	0.95
128x128	0.25	135	1.13	0.80	1.29
128x128	0.25	0, 45, 90, 135	0.28	0.28	0.32
128x128	0.35	0	2.53	2.54	2.71
128x128	0.35	45	1.07	1.70	1.22
128x128	0.35	90	1.69	1.78	1.13
128x128	0.35	135	1.13	1.30	1.41
128x128	0.35	0, 45, 90, 135	0.85	0.30	0.95
128x128	0.50	0	3.81	4.11	5.65
128x128	0.50	45	2.25	2.48	3.67
128x128	0.50	90	3.37	3.52	3.67
128x128	0.50	135	2.26	2.47	2.54
128x128	0.50	0, 45, 90, 135	0.86	1.02	1.13

Table 100.: Palmprint Results using Sobel filter to extract features and SVMs to compare.

B.1.4 *Sobel filter, PCA and Support Vector Machines*

Algorithm Parameters			Results		
			Validation	Test	
Imsize	Threshold	Angles	EER (%)	FMR (%)	FNMR (%)
32x32	0.1	0, 45, 90, 135	0	0.28	0
32x32	0.25	0, 45, 90, 135	0	0.28	0.0016
32x32	0.35	0, 45, 90, 135	0.0048	0.28	0.0032
32x32	0.50	0, 45, 90, 135	0.0032	0.28	0.0064
64x64	0.1	0, 45, 90, 135	0.018	0.28	0.022
64x64	0.25	0, 45, 90, 135	0.025	0.28	0.045
64x64	0.35	0, 45, 90, 135	0.092	0.41	0.13
64x64	0.50	0, 45, 90, 135	0.28	0.56	0.37
128x128	0.1	0, 45, 90, 135	0.052	0.10	0.088
128x128	0.25	0, 45, 90, 135	0.093	0.37	0.15
128x128	0.35	0, 45, 90, 135	0.42	0.56	0.59
128x128	0.50	0, 45, 90, 135	1.16	1.52	0.85

Table 101.: Palmprint Results using Sobel filter and PCA to extract features and SVMs to compare.

B.2 ZERO DC CIRCULAR GABOR FILTER

B.2.1 *Gabor filter and Euclidean Distance*

Algorithm Parameters			Results		
			Validation	Test	
Filter Size	Frequency	σ	EER (%)	FMR (%)	FNMR (%)
9x9	0.0916	1.4045	0.56	0.56	1.41
9x9	0.0916	2.8090	1.13	1.16	1.98
9x9	0.0916	5.6179	0.74	0.77	1.13
9x9	0.1833	1.4045	0.56	0.58	1.69
9x9	0.1833	2.8090	1.07	1.11	1.41
9x9	0.1833	5.6179	3.95	3.94	5.08
9x9	0.3666	1.4045	0.64	0.68	2.82
9x9	0.3666	2.8090	1.13	1.13	1.69
9x9	0.3666	5.6179	4.53	4.70	5.08
17x17	0.0916	1.4045	0.73	0.77	2.26
17x17	0.0916	2.8090	0.97	0.99	1.98
17x17	0.0916	5.6179	0.56	0.55	1.41
17x17	0.1833	1.4045	0.75	0.77	2.26
17x17	0.1833	2.8090	0.85	0.90	1.98
17x17	0.1833	5.6179	3.81	3.90	5.37
17x17	0.3666	1.4045	1.13	1.20	3.67
17x17	0.3666	2.8090	1.98	2.04	3.95
17x17	0.3666	5.6179	8.46	8.52	8.47
35x35	0.0916	1.4045	1.92	1.88	2.82
35x35	0.0916	2.8090	2.10	2.02	3.11
35x35	0.0916	5.6179	0.85	0.87	1.98
35x35	0.1833	1.4045	2.12	2.06	2.82
35x35	0.1833	2.8090	1.98	1.97	2.82
35x35	0.1833	5.6179	5.08	5.04	6.21
35x35	0.3666	1.4045	4.71	4.71	4.52
35x35	0.3666	2.8090	5.91	6.00	7.34
35x35	0.3666	5.6179	13.77	13.90	14.69

Table 102.: Palmprint Results using Gabor filter to extract features and Euclidean distance to compare.

B.2.2 *Gabor filter, PCA and Euclidean Distance*

Algorithm Parameters			Results		
			Validation	Test	
Filter Size	Frequency	σ	EER (%)	FMR (%)	FNMR (%)
9x9	0.0916	1.4045	0.56	0.36	0.28
9x9	0.0916	2.8090	1.41	1.02	1.69
9x9	0.0916	5.6179	0.56	0.37	0.56
9x9	0.1833	1.4045	0.85	0.60	0.28
9x9	0.1833	2.8090	1.42	0.97	1.98
9x9	0.1833	5.6179	5.08	3.43	7.63
9x9	0.3666	1.4045	1.13	0.77	1.69
9x9	0.3666	2.8090	0.93	0.59	1.13
9x9	0.3666	5.6179	4.63	3.44	6.78
17x17	0.0916	1.4045	0.37	0.35	1.41
17x17	0.0916	2.8090	0.56	0.45	1.13
17x17	0.0916	5.6179	0.56	0.39	0.56
17x17	0.1833	1.4045	0.42	0.37	1.13
17x17	0.1833	2.8090	0.85	0.58	1.69
17x17	0.1833	5.6179	2.90	2.11	3.95
17x17	0.3666	1.4045	0.56	0.43	1.13
17x17	0.3666	2.8090	0.56	0.47	0.85
17x17	0.3666	5.6179	3.92	3.37	5.37
35x35	0.0916	1.4045	1.13	0.94	1.98
35x35	0.0916	2.8090	1.13	0.93	1.98
35x35	0.0916	5.6179	0.56	0.44	0.56
35x35	0.1833	1.4045	1.13	0.99	1.98
35x35	0.1833	2.8090	1.41	0.98	1.98
35x35	0.1833	5.6179	2.54	1.82	3.95
35x35	0.3666	1.4045	1.13	0.97	1.98
35x35	0.3666	2.8090	0.85	0.75	1.69
35x35	0.3666	5.6179	1.98	1.70	2.26

Table 103.: Palmprint Results using Gabor filter and PCA to extract features and Euclidean distance to compare.

B.2.3 *Gabor filter and Support Vector Machines*

Algorithm Parameters			Results		
			Validation	Test	
Filter Size	Frequency	σ	EER (%)	FMR (%)	FNMR (%)
9x9	0.0916	1.4045	0.28	0.32	0.56
9x9	0.0916	2.8090	0.85	1.01	0.85
9x9	0.0916	5.6179	0.28	0.34	0.28
9x9	0.1833	1.4045	0.28	0.32	0.56
9x9	0.1833	2.8090	0.85	0.98	0.85
9x9	0.1833	5.6179	2.74	3.08	4.24
9x9	0.3666	1.4045	0.28	0.31	0.85
9x9	0.3666	2.8090	0.46	0.49	0.85
9x9	0.3666	5.6179	1.69	1.68	1.98
17x17	0.0916	1.4045	0.28	0.35	0.56
17x17	0.0916	2.8090	0.28	0.35	0.28
17x17	0.0916	5.6179	0.27	0.31	0.28
17x17	0.1833	1.4045	0.28	0.35	0.56
17x17	0.1833	2.8090	0.28	0.36	0.85
17x17	0.1833	5.6179	1.80	2.10	2.26
17x17	0.3666	1.4045	0.28	0.34	0.85
17x17	0.3666	2.8090	0.28	0.32	0.85
17x17	0.3666	5.6179	1.01	1.01	0.85
35x35	0.0916	1.4045	0.28	0.33	0.56
35x35	0.0916	2.8090	0.28	0.32	0.56
35x35	0.0916	5.6179	0.28	0.33	0.56
35x35	0.1833	1.4045	0.28	0.32	0.56
35x35	0.1833	2.8090	0.28	0.39	0.56
35x35	0.1833	5.6179	1.41	1.70	1.41
35x35	0.3666	1.4045	0.28	0.34	0.85
35x35	0.3666	2.8090	0.28	0.28	0.56
35x35	0.3666	5.6179	0.56	0.60	0.85

Table 104.: Palmprint Results using Gabor filter to extract features and SVMs to compare.

B.2.4 *Gabor filter, PCA and Support Vector Machines*

Algorithm Parameters			Results		
			Validation	Test	
Filter Size	Frequency	σ	EER (%)	FMR (%)	FNMR (%)
9x9	0.0916	1.4045	0.28	0.35	0.56
9x9	0.0916	2.8090	0.85	1.04	0.85
9x9	0.0916	5.6179	0.24	0.34	0.28
9x9	0.1833	1.4045	0.25	0.30	0.56
9x9	0.1833	2.8090	0.78	0.92	0.28
9x9	0.1833	5.6179	4.45	5.23	4.80
9x9	0.3666	1.4045	0.28	0.37	0.56
9x9	0.3666	2.8090	0.49	0.57	0.85
9x9	0.3666	5.6179	2.00	2.04	2.26
17x17	0.0916	1.4045	0.045	0.047	1.13
17x17	0.0916	2.8090	0.039	0.059	1.13
17x17	0.0916	5.6179	0.054	0.059	0.56
17x17	0.1833	1.4045	0.027	0.026	1.13
17x17	0.1833	2.8090	0.22	0.28	0.28
17x17	0.1833	5.6179	1.38	1.74	1.98
17x17	0.3666	1.4045	0.022	0.022	1.13
17x17	0.3666	2.8090	0.033	0.027	1.13
17x17	0.3666	5.6179	0.65	0.64	0.85
35x35	0.0916	1.4045	0.28	0.36	0.56
35x35	0.0916	2.8090	0.28	0.34	0.56
35x35	0.0916	5.6179	0.024	0.019	0.85
35x35	0.1833	1.4045	0.28	0.35	0.56
35x35	0.1833	2.8090	0.071	0.11	0.56
35x35	0.1833	5.6179	1.13	1.39	1.98
35x35	0.3666	1.4045	0.22	0.25	0.56
35x35	0.3666	2.8090	0.28	0.32	0.56
35x35	0.3666	5.6179	0.31	0.29	1.13

Table 105.: Palmprint Results using Gabor filter and PCA to extract features and SVMs to compare.

B.3 LOCAL BINARY PATTERN

B.3.1 *Local Binary Pattern and Euclidean Distance*

Algorithm Parameters				Results		
				Validation	Test	
Region Size	Radio	♯Neighboors	Uniform	EER (%)	FMR (%)	FNMR (%)
8x8	1	8	Yes	2.54	2.50	1.98
8x8	1	8	No	2.54	2.56	2.54
8x8	2	8	Yes	2.82	2.69	3.11
8x8	2	8	No	2.93	2.76	3.11
8x8	2	16	Yes	4.06	3.75	4.80
8x8	3	8	Yes	2.91	2.90	2.54
8x8	3	8	No	3.12	3.10	2.54
8x8	3	16	Yes	6.21	6.67	7.06
16x16	1	8	Yes	2.64	2.56	1.98
16x16	1	8	No	2.62	2.55	1.98
16x16	2	8	Yes	2.66	2.58	1.98
16x16	2	8	No	3.03	2.96	2.26
16x16	2	16	Yes	3.11	3.00	2.82
16x16	3	8	Yes	2.92	2.78	2.26
16x16	3	8	No	3.39	3.18	2.26
16x16	3	16	Yes	3.23	3.03	3.39
32x32	1	8	Yes	3.39	3.41	2.54
32x32	1	8	No	3.39	3.41	2.82
32x32	2	8	Yes	3.06	2.90	3.11
32x32	2	8	No	3.11	3.01	3.39
32x32	2	16	Yes	3.28	3.14	3.39
32x32	3	8	Yes	3.39	3.12	2.26
32x32	3	8	No	3.20	3.09	2.82
32x32	3	16	Yes	3.14	3.02	3.11
64x64	1	8	Yes	4.68	4.80	3.95
64x64	1	8	No	4.52	4.66	3.67
64x64	2	8	Yes	4.02	3.97	3.67
64x64	2	8	No	4.24	4.33	4.24
64x64	2	16	Yes	5.37	5.38	5.08
64x64	3	8	Yes	4.52	4.36	2.82
64x64	3	8	No	4.24	4.13	3.95
64x64	3	16	Yes	5.51	5.60	4.52
128x128	1	8	Yes	7.01	7.26	4.80
128x128	1	8	No	7.01	7.30	4.80
128x128	2	8	Yes	6.78	7.25	4.52
128x128	2	8	No	5.93	6.46	4.52
128x128	2	16	Yes	8.05	8.30	8.47
128x128	3	8	Yes	6.50	6.73	4.52
128x128	3	8	No	6.86	6.86	5.08
128x128	3	16	Yes	9.98	10.38	9.60

Table 106.: Palmprint Results using Local Binary Pattern to extract features and Euclidean distance to compare.

B.3.2 *Local Binary Pattern, PCA and Euclidean Distance*

Algorithm Parameters				Results		
				Validation	Test	
Region Size	Radio	♯Neighboors	Uniform	EER (%)	FMR (%)	FNMR (%)
8x8	1	8	Yes	1.61	1.32	1.41
8x8	1	8	No	1.69	1.42	1.41
8x8	2	8	Yes	2.52	1.77	2.26
8x8	2	8	No	2.67	1.84	2.26
8x8	2	16	Yes	2.62	1.96	2.54
8x8	3	8	Yes	4.24	2.79	5.65
8x8	3	8	No	4.32	2.80	7.63
8x8	3	16	Yes	3.67	2.46	4.80
16x16	1	8	Yes	2.54	2.41	1.98
16x16	1	8	No	2.39	2.28	1.98
16x16	2	8	Yes	2.82	2.60	1.98
16x16	2	8	No	2.82	2.64	2.54
16x16	2	16	Yes	2.82	2.57	1.98
16x16	3	8	Yes	2.68	2.25	2.26
16x16	3	8	No	2.82	2.39	2.54
16x16	3	16	Yes	2.54	2.26	2.26
32x32	1	8	Yes	3.39	3.42	2.54
32x32	1	8	No	3.39	3.41	3.11
32x32	2	8	Yes	3.00	2.86	3.11
32x32	2	8	No	3.11	3.01	3.39
32x32	2	16	Yes	3.37	3.28	3.67
32x32	3	8	Yes	3.39	3.09	2.26
32x32	3	8	No	3.11	2.91	3.39
32x32	3	16	Yes	2.82	2.64	3.39
64x64	1	8	Yes	4.68	4.80	3.95
64x64	1	8	No	4.52	4.66	3.67
64x64	2	8	Yes	4.02	3.97	3.67
64x64	2	8	No	4.24	4.34	4.24
64x64	2	16	Yes	5.37	5.40	5.65
64x64	3	8	Yes	4.52	4.36	2.82
64x64	3	8	No	4.24	4.14	3.95
64x64	3	16	Yes	5.50	5.59	4.52
128x128	1	8	Yes	7.01	7.26	4.80
128x128	1	8	No	7.01	7.30	4.80
128x128	2	8	Yes	6.78	7.25	4.52
128x128	2	8	No	5.93	6.46	4.52
128x128	2	16	Yes	8.05	8.30	8.47
128x128	3	8	Yes	6.50	6.73	4.52
128x128	3	8	No	6.86	6.86	5.08
128x128	3	16	Yes	9.98	10.38	9.60

Table 107.: Palmprint Results using Local Binary Pattern and PCA to extract features and Euclidean distance to compare.

B.3.3 *Local Binary Pattern and Chi-Square Distance*

Algorithm Parameters				Results		
				Validation	Test	
Region Size	Radio	♯Neighboors	Uniform	EER (%)	FMR (%)	FNMR (%)
8x8	1	8	Yes	0.34	0.32	0.85
8x8	1	8	No	0.30	0.31	0.85
8x8	2	8	Yes	0.28	0.28	1.41
8x8	2	8	No	0.61	0.57	1.69
8x8	2	16	Yes	1.41	1.38	0.85
8x8	3	8	Yes	1.07	0.98	0.85
8x8	3	8	No	1.40	1.29	1.98
8x8	3	16	Yes	1.41	1.38	0.85
16x16	1	8	Yes	0.64	0.62	1.41
16x16	1	8	No	0.28	0.28	1.13
16x16	2	8	Yes	0.28	0.26	1.13
16x16	2	8	No	0.075	0.059	0.85
16x16	2	16	Yes	0.28	0.26	0.85
16x16	3	8	Yes	0.21	0.20	0.85
16x16	3	8	No	0.043	0.0334	1.13
16x16	3	16	Yes	0.28	0.26	0.85
32x32	1	8	Yes	2.18	2.08	1.69
32x32	1	8	No	1.69	1.60	1.41
32x32	2	8	Yes	1.69	1.66	1.41
32x32	2	8	No	1.13	1.12	1.41
32x32	2	16	Yes	1.13	1.15	1.41
32x32	3	8	Yes	1.41	1.36	1.41
32x32	3	8	No	0.69	0.70	1.13
32x32	3	16	Yes	1.03	0.97	1.41
64x64	1	8	Yes	3.67	3.73	3.11
64x64	1	8	No	3.39	3.42	2.26
64x64	2	8	Yes	2.82	2.87	1.98
64x64	2	8	No	2.26	2.36	1.98
64x64	2	16	Yes	2.57	2.57	1.98
64x64	3	8	Yes	2.54	2.50	1.69
64x64	3	8	No	1.71	1.78	1.41
64x64	3	16	Yes	2.29	2.33	1.41
128x128	1	8	Yes	5.08	5.36	4.24
128x128	1	8	No	4.61	4.88	3.95
128x128	2	8	Yes	4.40	4.70	3.39
128x128	2	8	No	3.90	4.22	3.11
128x128	2	16	Yes	4.29	4.50	2.82
128x128	3	8	Yes	4.25	4.31	3.67
128x128	3	8	No	3.44	3.36	2.54
128x128	3	16	Yes	4.01	4.02	3.11

Table 108.: Palmprint Results using Local Binary Pattern to extract features and Chi-Square distance to compare.

B.3.4 *Local Binary Pattern and Histogram Intersection*

Algorithm Parameters				Results		
				Validation	Test	
Region Size	Radio	♯Neighboors	Uniform	EER (%)	FMR (%)	FNMR (%)
8x8	1	8	Yes	0.51	0.47	0.85
8x8	1	8	No	0.28	0.28	1.13
8x8	2	8	Yes	0.53	0.50	0.85
8x8	2	8	No	0.56	0.55	1.98
8x8	2	16	Yes	1.38	1.32	0.56
8x8	3	8	Yes	1.11	1.03	0.85
8x8	3	8	No	1.27	1.14	1.98
8x8	3	16	Yes	3.67	4.11	4.52
16x16	1	8	Yes	0.64	0.61	1.41
16x16	1	8	No	0.30	0.29	1.41
16x16	2	8	Yes	0.53	0.49	1.13
16x16	2	8	No	0.14	0.12	0.85
16x16	2	16	Yes	0.28	0.28	1.13
16x16	3	8	Yes	0.28	0.23	0.85
16x16	3	8	No	0.079	0.074	1.13
16x16	3	16	Yes	0.85	0.76	1.13
32x32	1	8	Yes	1.73	1.64	1.41
32x32	1	8	No	1.41	1.33	1.41
32x32	2	8	Yes	1.50	1.46	1.41
32x32	2	8	No	1.13	1.14	1.41
32x32	2	16	Yes	1.41	1.39	1.41
32x32	3	8	Yes	1.69	1.61	1.41
32x32	3	8	No	0.85	0.89	1.13
32x32	3	16	Yes	1.69	1.62	1.41
64x64	1	8	Yes	3.67	3.70	3.39
64x64	1	8	No	3.11	3.12	2.82
64x64	2	8	Yes	2.80	2.80	1.69
64x64	2	8	No	1.98	2.08	1.69
64x64	2	16	Yes	2.60	2.59	1.98
64x64	3	8	Yes	2.54	2.56	1.69
64x64	3	8	No	1.98	2.00	1.41
64x64	3	16	Yes	2.82	2.85	1.69
128x128	1	8	Yes	5.37	5.63	5.08
128x128	1	8	No	5.06	5.34	3.95
128x128	2	8	Yes	4.68	4.90	3.67
128x128	2	8	No	4.19	4.45	2.82
128x128	2	16	Yes	4.91	5.16	4.52
128x128	3	8	Yes	4.80	4.84	4.24
128x128	3	8	No	3.75	3.72	2.82
128x128	3	16	Yes	5.08	5.14	4.24

Table 109.: Palmprint Results using Local Binary Pattern to extract features and Histogram Intersection to compare.

B.3.5 *Local Binary Pattern and Support Vector Machines*

Algorithm Parameters				Results		
				Validation	Test	
Region Size	Radio	♯Neighboors	Uniform	EER (%)	FMR (%)	FNMR (%)
8x8	1	8	Yes	0.0048	0.0048	0.28
8x8	1	8	No	0.0064	0.0064	0.28
8x8	2	8	Yes	0.083	0.083	0.28
8x8	2	8	No	0.10	0.10	0.28
8x8	2	16	Yes	0.28	0.30	0.28
8x8	3	8	Yes	0.40	0.45	0.56
8x8	3	8	No	0.28	0.35	0.56
8x8	3	16	Yes	0.85	0.97	0.28
16x16	1	8	Yes	0	0.0016	0.85
16x16	1	8	No	0	0.0016	0.85
16x16	2	8	Yes	0	0.0016	0.56
16x16	2	8	No	0	0	0.56
16x16	2	16	Yes	0.0031	0	1.13
16x16	3	8	Yes	0	0.0016	0.56
16x16	3	8	No	0	0.0016	0.56
16x16	3	16	Yes	0	0	1.13
32x32	1	8	Yes	0.28	0.31	0.28
32x32	1	8	No	0.21	0.22	0.28
32x32	2	8	Yes	0.14	0.12	0.85
32x32	2	8	No	0.23	0.24	0
32x32	2	16	Yes	0.17	0.19	0.85
32x32	3	8	Yes	0.21	0.20	0.85
32x32	3	8	No	0.055	0.055	0.28
32x32	3	16	Yes	0.24	0.23	0.85
64x64	1	8	Yes	1.13	1.05	1.41
64x64	1	8	No	0.85	0.83	1.41
64x64	2	8	Yes	0.85	0.84	1.13
64x64	2	8	No	0.85	0.92	0.85
64x64	2	16	Yes	1.13	1.15	1.13
64x64	3	8	Yes	0.85	0.79	1.13
64x64	3	8	No	0.85	0.84	0.85
64x64	3	16	Yes	0.90	0.85	1.13
128x128	1	8	Yes	4.78	4.51	5.93
128x128	1	8	No	4.24	3.86	5.93
128x128	2	8	Yes	2.26	2.17	4.24
128x128	2	8	No	1.41	1.36	4.80
128x128	2	16	Yes	2.26	2.24	1.98
128x128	3	8	Yes	1.69	1.75	1.69
128x128	3	8	No	1.41	1.50	1.69
128x128	3	16	Yes	1.69	1.61	1.41

Table 110.: Palmprint Results using Local Binary Pattern to extract features and SVMs to compare.

B.3.6 *Local Binary Pattern, PCA and Support Vector Machines*

Algorithm Parameters				Results		
				Validation	Test	
Region Size	Radio	♯Neighboors	Uniform	EER (%)	FMR (%)	FNMR (%)
8x8	1	8	Yes	0.0032	0.0048	0.56
8x8	1	8	No	0.0078	0.0048	0.56
8x8	2	8	Yes	0.056	0.095	0.56
8x8	2	8	No	0.078	0.13	0.56
8x8	2	16	Yes	0.28	0.35	0.56
8x8	3	8	Yes	0.56	0.73	0.85
8x8	3	8	No	0.66	0.85	0.85
8x8	3	16	Yes	1.13	1.28	1.13
16x16	1	8	Yes	0	0.0016	0.85
16x16	1	8	No	0	0.0032	1.41
16x16	2	8	Yes	0	0.0016	0.56
16x16	2	8	No	0	0.0016	0.56
16x16	2	16	Yes	0.0016	0	0.85
16x16	3	8	Yes	0	0.0032	0.56
16x16	3	8	No	0	0	0.56
16x16	3	16	Yes	0	0	1.13
32x32	1	8	Yes	0.28	0.31	0.28
32x32	1	8	No	0.27	0.29	0.28
32x32	2	8	Yes	0.17	0.15	0.85
32x32	2	8	No	0.28	0.27	0
32x32	2	16	Yes	0.25	0.29	0.85
32x32	3	8	Yes	0.23	0.22	0.85
32x32	3	8	No	0.070	0.061	0.28
32x32	3	16	Yes	0.20	0.20	0.85
64x64	1	8	Yes	1.13	1.05	1.41
64x64	1	8	No	0.85	0.83	1.41
64x64	2	8	Yes	0.85	0.84	1.13
64x64	2	8	No	0.85	0.91	1.13
64x64	2	16	Yes	1.13	1.16	1.13
64x64	3	8	Yes	0.85	0.80	1.13
64x64	3	8	No	0.85	0.84	0.85
64x64	3	16	Yes	1.04	0.96	1.13
128x128	1	8	Yes	4.78	4.51	5.93
128x128	1	8	No	4.24	3.86	5.93
128x128	2	8	Yes	2.26	2.17	4.24
128x128	2	8	No	1.41	1.36	4.80
128x128	2	16	Yes	2.26	2.24	1.98
128x128	3	8	Yes	1.69	1.75	1.69
128x128	3	8	No	1.41	1.50	1.69
128x128	3	16	Yes	1.69	1.60	1.41

Table 111.: Palmprint Results using Local Binary Pattern and PCA to extract features and SVMs to compare.

B.4 LOCAL DERIVATIVE PATTERN

B.4.1 *Local Derivative Pattern and Euclidean Distance*

Algorithm Parameters		Results		
		Validation	Test	
Region Size	Directions	EER (%)	FMR (%)	FNMR (%)
8x8	0	2.23	2.04	3.11
8x8	45	2.54	2.55	1.41
8x8	90	1.69	1.86	2.26
8x8	135	1.69	1.38	1.69
8x8	0, 45	1.59	1.51	1.41
8x8	0, 90	1.69	1.56	1.13
8x8	0, 135	1.72	1.61	1.98
8x8	45, 90	1.93	2.03	1.13
8x8	45, 135	1.13	1.15	1.13
8x8	90, 135	1.13	1.15	3.11
8x8	0, 45, 90	1.41	1.34	1.69
8x8	0, 45, 135	1.41	1.33	1.13
8x8	0, 90, 135	1.41	1.38	1.69
8x8	45, 90, 135	1.13	1.17	1.13
8x8	0, 45, 90, 135	1.13	1.14	0.85
16x16	0	1.98	1.82	2.54
16x16	45	2.82	2.69	1.69
16x16	90	2.89	2.87	2.26
16x16	135	1.75	1.75	3.11
16x16	0, 45	2.54	2.36	1.41
16x16	0, 90	1.98	1.88	1.41
16x16	0, 135	1.45	1.37	1.98
16x16	45, 90	2.54	2.44	1.69
16x16	45, 135	2.14	2.06	1.69
16x16	90, 135	1.92	1.95	1.98
16x16	0, 45, 90	2.26	2.13	1.41
16x16	0, 45, 135	1.97	1.87	1.14
16x16	0, 90, 135	1.41	1.33	1.41
16x16	45, 90, 135	2.23	2.21	1.69
16x16	0, 45, 90, 135	2.26	2.24	1.41
32x32	0	2.54	2.65	4.24
32x32	45	3.67	3.53	3.67
32x32	90	3.39	3.30	3.67
32x32	135	2.54	2.82	4.52
32x32	0, 45	2.93	2.91	2.54
32x32	0, 90	2.82	2.90	2.26
32x32	0, 135	1.98	2.25	3.11
32x32	45, 90	3.94	3.83	2.82

Algorithm Parameters		Results		
		Validation	Test	
Region Size	Directions	EER (%)	FMR (%)	FNMR (%)
32x32	45, 135	2.82	2.83	2.26
32x32	90, 135	3.11	3.27	3.11
32x32	0, 45, 90	3.11	3.07	2.54
32x32	0, 45, 135	2.54	2.63	1.98
32x32	0, 90, 135	2.72	2.86	2.54
32x32	45, 90, 135	3.11	3.13	2.82
32x32	0, 45, 90, 135	2.82	2.90	2.54
64x64	0	7.63	7.72	8.19
64x64	45	6.50	6.33	7.34
64x64	90	6.86	6.80	6.50
64x64	135	6.57	6.86	8.19
64x64	0, 45	5.69	5.69	5.08
64x64	0, 90	4.52	4.70	4.24
64x64	0, 135	3.95	4.19	5.08
64x64	45, 90	5.94	5.99	5.08
64x64	45, 135	5.08	5.17	4.24
64x64	90, 135	5.16	5.35	4.52
64x64	0, 45, 90	5.13	5.18	4.24
64x64	0, 45, 135	4.52	4.61	3.67
64x64	0, 90, 135	4.24	4.45	4.52
64x64	45, 90, 135	4.80	4.91	4.24
64x64	0, 45, 90, 135	4.52	4.69	3.95
128x128	0	14.68	14.89	17.80
128x128	45	15.80	16.26	15.25
128x128	90	14.91	15.34	13.84
128x128	135	13.87	14.05	14.69
128x128	0, 45	9.99	10.25	11.30
128x128	0, 90	9.73	10.11	9.04
128x128	0, 135	8.78	8.76	9.32
128x128	45, 90	12.79	13.12	9.04
128x128	45, 135	8.76	8.92	9.04
128x128	90, 135	9.86	9.97	9.04
128x128	0, 45, 90	8.93	9.29	8.47
128x128	0, 45, 135	7.10	7.18	7.63
128x128	0, 90, 135	7.77	7.95	7.63
128x128	45, 90, 135	8.55	8.85	7.91
128x128	0, 45, 90, 135	7.34	7.49	6.78

Table 112.: Palmprint Results using Local Derivative Pattern to extract features and Euclidean distance to compare.

B.4.2 *Local Derivative Pattern, PCA and Euclidean Distance*

Algorithm Parameters		Results		
		Validation	Test	
Region Size	Directions	EER (%)	FMR (%)	FNMR (%)
8x8	0	1.98	1.71	1.69
8x8	45	1.98	1.81	1.98
8x8	90	1.69	1.72	1.41
8x8	135	1.69	1.66	3.11
8x8	0, 45	1.69	1.38	1.69
8x8	0, 90	1.67	1.39	0.85
8x8	0, 135	1.41	1.07	1.13
8x8	45, 90	1.40	1.29	1.13
8x8	45, 135	1.13	0.90	0.28
8x8	90, 135	0.97	0.85	1.41
8x8	0, 45, 90	1.43	1.16	1.41
8x8	0, 45, 135	1.41	1.07	0.85
8x8	0, 90, 135	1.13	0.93	0.85
8x8	45, 90, 135	1.00	0.83	0.56
8x8	0, 45, 90, 135	1.38	1.12	0.56
16x16	0	1.98	1.82	2.54
16x16	45	2.82	2.67	1.69
16x16	90	2.82	2.77	2.26
16x16	135	1.88	1.94	2.82
16x16	0, 45	2.54	2.34	1.41
16x16	0, 90	1.98	1.87	1.41
16x16	0, 135	1.69	1.62	1.98
16x16	45, 90	2.54	2.39	1.69
16x16	45, 135	2.03	1.91	1.69
16x16	90, 135	2.03	2.07	1.98
16x16	0, 45, 90	2.55	2.37	1.69
16x16	0, 45, 135	1.70	1.59	1.41
16x16	0, 90, 135	1.41	1.32	1.41
16x16	45, 90, 135	2.26	2.18	1.69
16x16	0, 45, 90, 135	2.17	2.10	1.41
32x32	0	2.54	2.66	4.24
32x32	45	3.67	3.53	3.67
32x32	90	3.39	3.30	3.67
32x32	135	2.54	2.82	4.52
32x32	0, 45	3.00	2.96	2.54
32x32	0, 90	2.82	2.89	2.26
32x32	0, 135	1.98	2.25	3.11
32x32	45, 90	3.95	3.83	2.82
32x32	45, 135	2.82	2.82	2.26

Algorithm Parameters		Results		
		Validation	Test	
Region Size	Directions	EER (%)	FMR (%)	FNMR (%)
32x32	90, 135	3.11	3.28	3.11
32x32	0, 45, 90	3.11	3.06	2.54
32x32	0, 45, 135	2.56	2.63	1.98
32x32	0, 90, 135	2.71	2.85	2.54
32x32	45, 90, 135	3.11	3.13	2.82
32x32	0, 45, 90, 135	2.82	2.89	2.54
64x64	0	7.63	7.73	8.47
64x64	45	6.49	6.33	7.34
64x64	90	6.88	6.81	6.50
64x64	135	6.50	6.80	8.19
64x64	0, 45	5.82	5.85	5.08
64x64	0, 90	4.52	4.69	4.24
64x64	0, 135	3.95	4.19	5.65
64x64	45, 90	6.01	6.06	5.08
64x64	45, 135	5.08	5.18	4.24
64x64	90, 135	5.22	5.42	4.52
64x64	0, 45, 90	5.15	5.22	4.52
64x64	0, 45, 135	4.52	4.62	3.95
64x64	0, 90, 135	4.24	4.45	4.52
64x64	45, 90, 135	4.88	4.98	4.24
64x64	0, 45, 90, 135	4.52	4.69	3.95
128x128	0	14.68	14.89	17.80
128x128	45	15.80	16.26	15.25
128x128	90	14.91	15.34	13.84
128x128	135	13.87	14.05	14.69
128x128	0, 45	9.99	10.25	11.30
128x128	0, 90	9.73	10.11	9.04
128x128	0, 135	8.78	8.76	9.32
128x128	45, 90	12.79	13.12	9.04
128x128	45, 135	8.76	8.92	9.04
128x128	90, 135	9.86	9.97	9.04
128x128	0, 45, 90	8.94	9.31	8.47
128x128	0, 45, 135	7.06	7.15	7.91
128x128	0, 90, 135	7.79	7.97	7.63
128x128	45, 90, 135	8.48	8.77	7.91
128x128	0, 45, 90, 135	7.39	7.54	6.78

Table 113.: Palmprint Results using Local Derivative Pattern and PCA to extract features and Euclidean distance to compare.

B.4.3 *Local Derivative Pattern and Chi-Square Distance*

Algorithm Parameters		Results		
		Validation	Test	
Region Size	Directions	EER (%)	FMR (%)	FNMR (%)
8x8	0	5.08	4.87	6.50
8x8	45	3.39	3.39	5.65
8x8	90	8.10	8.09	11.58
8x8	135	10.00	10.07	11.02
8x8	0, 45	2.54	2.47	3.95
8x8	0, 90	3.34	3.20	4.80
8x8	0, 135	3.28	3.16	3.39
8x8	45, 90	5.00	4.98	5.93
8x8	45, 135	3.93	3.82	5.65
8x8	90, 135	8.15	8.21	9.32
8x8	0, 45, 90	3.17	3.09	4.24
8x8	0, 45, 135	2.54	2.40	3.67
8x8	0, 90, 135	3.53	3.45	4.52
8x8	45, 90, 135	4.80	4.70	6.78
8x8	0, 45, 90, 135	3.10	2.96	4.80
16x16	0	2.26	2.26	3.11
16x16	45	2.26	2.26	1.69
16x16	90	6.34	6.10	7.34
16x16	135	3.95	3.73	5.93
16x16	0, 45	1.30	1.29	0.85
16x16	0, 90	2.20	2.11	1.13
16x16	0, 135	1.02	0.95	0.85
16x16	45, 90	3.22	3.16	2.54
16x16	45, 135	1.95	1.83	1.69
16x16	90, 135	4.24	4.05	5.93
16x16	0, 45, 90	1.98	1.91	1.13
16x16	0, 45, 135	0.99	0.99	0.85
16x16	0, 90, 135	1.66	1.56	1.69
16x16	45, 90, 135	2.82	2.68	2.82
16x16	0, 45, 90, 135	1.69	1.62	1.13
32x32	0	3.11	3.30	1.98
32x32	45	1.88	2.09	1.41
32x32	90	3.92	4.01	3.95
32x32	135	3.11	3.07	3.39
32x32	0, 45	1.65	1.80	1.13
32x32	0, 90	1.69	1.84	1.13
32x32	0, 135	1.58	1.52	1.13
32x32	45, 90	1.98	2.16	1.98
32x32	45, 135	1.69	1.73	1.41

Algorithm Parameters		Results		
		Validation	Test	
Region Size	Directions	EER (%)	FMR (%)	FNMR (%)
32x32	90, 135	2.46	2.53	2.54
32x32	0, 45, 90	1.41	1.56	0.85
32x32	0, 45, 135	1.69	1.72	0.85
32x32	0, 90, 135	1.41	1.51	1.13
32x32	45, 90, 135	2.02	2.08	1.69
32x32	0, 45, 90, 135	1.43	1.55	0.85
64x64	0	5.20	5.41	5.37
64x64	45	4.24	4.55	4.24
64x64	90	3.53	3.80	4.24
64x64	135	4.91	5.22	5.37
64x64	0, 45	3.67	3.95	3.39
64x64	0, 90	3.11	3.30	3.67
64x64	0, 135	3.67	3.83	3.67
64x64	45, 90	3.11	3.38	2.82
64x64	45, 135	3.19	3.34	2.26
64x64	90, 135	2.82	3.08	3.11
64x64	0, 45, 90	3.11	3.38	2.82
64x64	0, 45, 135	3.22	3.40	2.54
64x64	0, 90, 135	3.30	3.49	2.54
64x64	45, 90, 135	2.83	3.01	1.98
64x64	0, 45, 90, 135	2.97	3.16	3.11
128x128	0	9.35	9.59	9.32
128x128	45	9.13	9.32	7.63
128x128	90	9.01	8.99	11.58
128x128	135	9.13	9.65	10.45
128x128	0, 45	7.86	8.28	6.50
128x128	0, 90	6.24	6.61	6.78
128x128	0, 135	6.37	6.55	7.34
128x128	45, 90	7.06	7.26	7.06
128x128	45, 135	5.93	6.03	6.21
128x128	90, 135	5.75	5.98	9.04
128x128	0, 45, 90	6.46	6.78	5.65
128x128	0, 45, 135	5.68	5.94	6.21
128x128	0, 90, 135	5.37	5.66	6.50
128x128	45, 90, 135	5.42	5.57	6.78
128x128	0, 45, 90, 135	5.33	5.52	6.21

Table 114.: Palmprint Results using Local Derivative Pattern to extract features and Chi-Square distance to compare.

B.4.4 *Local Derivative Pattern and Histogram Intersection*

Algorithm Parameters		Results		
		Validation	Test	
Region Size	Directions	EER (%)	FMR (%)	FNMR (%)
8x8	0	4.31	3.98	4.52
8x8	45	3.39	3.38	5.08
8x8	90	6.71	6.72	8.19
8x8	135	8.22	8.33	7.91
8x8	0, 45	2.25	2.24	3.67
8x8	0, 90	2.26	2.20	4.24
8x8	0, 135	2.45	2.40	3.39
8x8	45, 90	4.52	4.45	4.80
8x8	45, 135	3.44	3.36	5.08
8x8	90, 135	6.50	6.46	7.06
8x8	0, 45, 90	2.82	2.74	3.67
8x8	0, 45, 135	2.09	2.02	3.39
8x8	0, 90, 135	2.91	2.78	4.24
8x8	45, 90, 135	4.50	4.39	5.37
8x8	0, 45, 90, 135	2.54	2.43	4.24
16x16	0	1.24	1.23	1.98
16x16	45	1.41	1.42	1.13
16x16	90	2.26	2.13	2.54
16x16	135	1.69	1.61	3.95
16x16	0, 45	1.17	1.22	0.85
16x16	0, 90	1.13	1.17	0.85
16x16	0, 135	0.63	0.62	1.13
16x16	45, 90	1.41	1.41	1.13
16x16	45, 135	1.34	1.27	1.13
16x16	90, 135	1.69	1.60	3.11
16x16	0, 45, 90	1.41	1.41	0.85
16x16	0, 45, 135	0.80	0.80	1.13
16x16	0, 90, 135	0.85	0.85	1.13
16x16	45, 90, 135	1.69	1.58	0.85
16x16	0, 45, 90, 135	1.16	1.15	0.85
32x32	0	2.26	2.39	1.69
32x32	45	2.26	2.37	1.41
32x32	90	1.98	1.92	1.98
32x32	135	2.54	2.64	2.26
32x32	0, 45	1.54	1.58	1.13
32x32	0, 90	1.41	1.42	0.85
32x32	0, 135	0.86	0.89	1.69
32x32	45, 90	1.98	2.00	1.13
32x32	45, 135	1.41	1.42	1.41

Algorithm Parameters		Results		
		Validation	Test	
Region Size	Directions	EER (%)	FMR (%)	FNMR (%)
32x32	90, 135	1.52	1.57	1.69
32x32	0, 45, 90	1.48	1.47	1.13
32x32	0, 45, 135	1.18	1.16	1.13
32x32	0, 90, 135	1.13	1.18	1.13
32x32	45, 90, 135	1.69	1.74	1.13
32x32	0, 45, 90, 135	1.32	1.35	1.13
64x64	0	5.65	5.66	4.52
64x64	45	4.24	4.42	4.24
64x64	90	4.70	4.96	4.24
64x64	135	4.42	4.69	5.37
64x64	0, 45	3.70	3.81	3.95
64x64	0, 90	3.45	3.66	3.11
64x64	0, 135	3.39	3.54	2.54
64x64	45, 90	3.93	4.07	2.54
64x64	45, 135	3.11	3.21	1.98
64x64	90, 135	3.12	3.41	3.95
64x64	0, 45, 90	2.82	2.97	3.11
64x64	0, 45, 135	3.00	3.17	2.54
64x64	0, 90, 135	2.88	3.07	2.54
64x64	45, 90, 135	2.78	2.96	2.82
64x64	0, 45, 90, 135	3.03	3.21	2.26
128x128	0	10.55	10.38	11.58
128x128	45	10.08	10.26	9.04
128x128	90	10.51	10.65	9.32
128x128	135	8.53	9.03	11.86
128x128	0, 45	7.06	7.25	6.78
128x128	0, 90	6.62	7.03	7.06
128x128	0, 135	6.13	6.16	6.50
128x128	45, 90	8.31	8.53	5.93
128x128	45, 135	6.19	6.44	5.37
128x128	90, 135	6.83	6.92	5.93
128x128	0, 45, 90	6.29	6.61	6.50
128x128	0, 45, 135	5.37	5.54	4.80
128x128	0, 90, 135	5.28	5.43	5.08
128x128	45, 90, 135	6.04	6.26	5.08
128x128	0, 45, 90, 135	5.16	5.28	5.65

Table 115.: Palmprint Results using Local Derivative Pattern to extract features and Histogram Intersection to compare.

B.4.5 *Local Derivative Pattern and Support Vector Machines*

Algorithm Parameters		Results		
		Validation	Test	
Region Size	Directions	EER (%)	FMR (%)	FNMR (%)
8x8	0	0.87	0.96	1.13
8x8	45	1.13	1.29	0.28
8x8	90	0.56	0.63	0.56
8x8	135	0.28	0.30	1.41
8x8	0, 45	0.58	0.68	0.56
8x8	0, 90	0.071	0.077	0
8x8	0, 135	0.0095	0.0096	0.85
8x8	45, 90	0.79	0.92	0.28
8x8	45, 135	0.10	0.12	0.28
8x8	90, 135	0.17	0.22	0.28
8x8	0, 45, 90	0.28	0.30	0
8x8	0, 45, 135	0.088	0.099	0.28
8x8	0, 90, 135	0.0079	0.013	0.85
8x8	45, 90, 135	0.089	0.10	0
8x8	0, 45, 90, 135	0.059	0.056	0
16x16	0	0.57	0.70	0
16x16	45	0.25	0.34	0.56
16x16	90	0.56	0.62	0.56
16x16	135	0.28	0.38	0
16x16	0, 45	0.10	0.13	0.56
16x16	0, 90	0.019	0.022	0.56
16x16	0, 135	0.016	0.0096	0.85
16x16	45, 90	0.16	0.18	0.56
16x16	45, 135	0.16	0.20	0.28
16x16	90, 135	0.28	0.32	0
16x16	0, 45, 90	0.035	0.048	0.56
16x16	0, 45, 135	0.0096	0.011	0.28
16x16	0, 90, 135	0.025	0.021	0.28
16x16	45, 90, 135	0.13	0.19	0.28
16x16	0, 45, 90, 135	0.019	0.024	0.28
32x32	0	0.56	0.56	0.56
32x32	45	1.11	1.15	1.13
32x32	90	0.97	1.00	0.85
32x32	135	0.82	0.82	1.98
32x32	0, 45	0.12	0.18	1.69
32x32	0, 90	0.13	0.15	01.69
32x32	0, 135	0.027	0.0096	1.41
32x32	45, 90	0.28	0.36	1.69
32x32	45, 135	0.032	0.026	1.13

Algorithm Parameters		Results		
		Validation	Test	
Region Size	Directions	EER (%)	FMR (%)	FNMR (%)
32x32	90, 135	0.28	0.28	0.28
32x32	0, 45, 90	0.066	0.080	1.69
32x32	0, 45, 135	0.0064	0.0032	2.26
32x32	0, 90, 135	0.014	0.0064	1.98
32x32	45, 90, 135	0.074	0.077	0.56
32x32	0, 45, 90, 135	0.013	0.0080	2.26
64x64	0	3.74	3.62	3.11
64x64	45	2.49	2.42	2.82
64x64	90	3.16	3.01	1.98
64x64	135	3.48	3.37	5.65
64x64	0, 45	1.69	1.67	1.98
64x64	0, 90	2.26	2.09	1.98
64x64	0, 135	1.98	1.78	2.54
64x64	45, 90	1.65	1.67	2.54
64x64	45, 135	1.98	1.94	3.11
64x64	90, 135	1.41	1.38	3.67
64x64	0, 45, 90	1.55	1.52	1.69
64x64	0, 45, 135	1.27	1.24	2.26
64x64	0, 90, 135	1.13	1.04	3.39
64x64	45, 90, 135	1.38	1.36	2.82
64x64	0, 45, 90, 135	1.13	1.14	1.98
128x128	0	10.89	11.17	11.02
128x128	45	10.39	10.35	13.28
128x128	90	11.60	11.33	13.28
128x128	135	13.29	13.32	13.84
128x128	0, 45	5.97	5.86	5.93
128x128	0, 90	5.59	5.45	6.21
128x128	0, 135	5.54	5.45	7.91
128x128	45, 90	6.14	5.91	4.80
128x128	45, 135	5.24	5.10	5.65
128x128	90, 135	5.90	5.78	7.34
128x128	0, 45, 90	4.50	4.20	4.52
128x128	0, 45, 135	3.36	3.19	5.65
128x128	0, 90, 135	4.09	3.86	5.65
128x128	45, 90, 135	4.21	4.03	5.37
128x128	0, 45, 90, 135	3.29	3.07	4.80

Table 116.: Palmprint Results using Local Derivative Pattern to extract features and SVMs to compare.

B.4.6 *Local Derivative Pattern, PCA and Support Vector Machines*

Algorithm Parameters		Results		
		Validation	Test	
Region Size	Directions	EER (%)	FMR (%)	FNMR (%)
8x8	0	0.85	0.94	1.13
8x8	45	1.13	1.36	0.56
8x8	90	0.56	0.59	0.56
8x8	135	0.28	0.31	1.41
8x8	0, 45	0.56	0.66	0.56
8x8	0, 90	0.079	0.10	0
8x8	0, 135	0.019	0.019	0.85
8x8	45, 90	0.78	0.85	0.28
8x8	45, 135	0.093	0.11	0
8x8	90, 135	0.12	0.14	0.28
8x8	0, 45, 90	0.39	0.40	0
8x8	0, 45, 135	0.12	0.16	0
8x8	0, 90, 135	0.0080	0.018	0
8x8	45, 90, 135	0.12	0.14	0
8x8	0, 45, 90, 135	0.076	0.095	0
16x16	0	0.56	0.69	0
16x16	45	0.28	0.36	0.56
16x16	90	0.50	0.57	0.56
16x16	135	0.28	0.37	0.28
16x16	0, 45	0.18	0.22	0.56
16x16	0, 90	0.027	0.035	0.56
16x16	0, 135	0.013	0.013	0.85
16x16	45, 90	0.16	0.19	0.56
16x16	45, 135	0.19	0.22	0.28
16x16	90, 135	0.28	0.34	0
16x16	0, 45, 90	0.057	0.066	0.56
16x16	0, 45, 135	0.011	0.0096	0.28
16x16	0, 90, 135	0.033	0.030	0.28
16x16	45, 90, 135	0.20	0.27	0.28
16x16	0, 45, 90, 135	0.027	0.032	0.28
32x32	0	0.56	0.56	3.39
32x32	45	1.13	1.20	1.13
32x32	90	1.00	1.04	1.13
32x32	135	0.88	0.88	1.98
32x32	0, 45	0.19	0.26	1.41
32x32	0, 90	0.28	0.34	0.85
32x32	0, 135	0.060	0.049	0.85
32x32	45, 90	0.50	0.56	1.13
32x32	45, 135	0.037	0.037	0.85

Algorithm Parameters		Results		
		Validation	Test	
Region Size	Directions	EER (%)	FMR (%)	FNMR (%)
32x32	90, 135	0.28	0.29	0.28
32x32	0, 45, 90	0.14	0.19	1.13
32x32	0, 45, 135	0.0048	0.0048	1.98
32x32	0, 90, 135	0.033	0.029	1.13
32x32	45, 90, 135	0.14	0.17	0.28
32x32	0, 45, 90, 135	0.022	0.013	1.69
64x64	0	3.90	3.82	2.82
64x64	45	2.52	2.47	2.82
64x64	90	3.25	3.10	2.26
64x64	135	3.68	3.54	5.65
64x64	0, 45	1.98	1.96	1.98
64x64	0, 90	2.28	2.15	1.98
64x64	0, 135	1.98	1.80	2.82
64x64	45, 90	1.72	1.74	2.54
64x64	45, 135	2.17	2.15	3.11
64x64	90, 135	1.56	1.51	3.67
64x64	0, 45, 90	1.69	1.62	1.98
64x64	0, 45, 135	1.51	1.46	2.26
64x64	0, 90, 135	1.41	1.34	3.11
64x64	45, 90, 135	1.41	1.39	2.82
64x64	0, 45, 90, 135	1.34	1.33	2.82
128x128	0	10.88	11.16	11.02
128x128	45	10.39	10.34	13.28
128x128	90	11.60	11.33	13.28
128x128	135	13.30	13.34	13.84
128x128	0, 45	6.03	5.91	5.65
128x128	0, 90	5.50	5.38	7.68
128x128	0, 135	5.54	5.45	7.91
128x128	45, 90	6.14	5.92	4.80
128x128	45, 135	5.06	4.96	6.21
128x128	90, 135	5.90	5.79	7.34
128x128	0, 45, 90	4.29	4.04	4.52
128x128	0, 45, 135	3.40	3.26	5.65
128x128	0, 90, 135	4.40	4.18	5.37
128x128	45, 90, 135	4.18	4.00	5.37
128x128	0, 45, 90, 135	3.58	3.33	4.24

Table 117.: Palmprint Results using Local Derivative Pattern and PCA to extract features and SVMs to compare.

BIBLIOGRAPHY

[1] M. Abernethy. *User Authentication Incorporating Feature Level Data Fusion of Multiple Biometric Characteristics*. PhD thesis, Murdoch University, 2011.

[2] M.A.M. Abukmeil, H. Elaydi, and M. Alhanjouri. Palmprint Recognition via Bandlet, Ridgelet, Wavelet and Neural Network. *Journal of Computer Sciences and Applications*, 3(2):23–28, 2015.

[3] B. Aghili and H. Sadjedi. Personal Authentication Using Hand Geometry. In *2009 International Conference on Computational Intelligence and Software Engineering*, pages 1–4, Dec 2009.

[4] M. Akimoto, Y. Koshiishi, H. Ikeda, K. Maeda, and M. Hata. Skin Color Measurements: Usefulness of the Metric Hue Angle of Uniform Color Spaces for Dermatological Treatment. In *Progress In Electromagnetics Research Symposium Proceedings*, Aug. 2014.

[5] G. Amayeh, G. Bebis, A. Erol, and M. Nicolescu. Peg-Free Hand Shape Verification Using High Order Zernike Moments. In *2006 Conference on Computer Vision and Pattern Recognition Workshop (CVPRW'06)*, pages 40–47, June 2006.

[6] S. A. Angadi and S. M. Hatture. User identification using wavelet features of hand geometry graph. In *2015 SAI Intelligent Systems Conference (IntelliSys)*, pages 828–835, Nov 2015.

[7] M. Arif, T. Brouard, and N. Vincent. Personal Identification and Verification by Hand Recognition. In *2006 IEEE International Conference on Engineering of Intelligent Systems*, pages 1–6, 2006.

[8] G.S. Badrinath and P. Gupta. Palmprint Verification using SIFT features. In *First Workshops on Image Processing Theory, Tools and Applications*, pages 1–8, Nov 2008.

[9] A. Besbes, N. Komodakis, G. Langs, and N. Paragios. Shape priors and discrete MRFs for knowledge-based segmentation. In *2009 IEEE Conference on Computer Vision and Pattern Recognition*, pages 1295–1302, June 2009.

[10] S. Beucher. The Watershed Transformation Applied To Image Segmentation. In *Scanning Microscopy International*, pages 299–314, 1991.

[11] G. Boreki and A. Zimmer. Hand Geometry: A New Approach for Feature Extraction. In *Proceedings of the 4th IEEE Workshop on Automatic Identification Advanced Technologies*, AUTOID '05, pages 149–154, Washington, DC, USA, 2005. IEEE Computer Society.

[12] Y. Boykov and M.-P. Jolly. Interactive Graph Cuts for Optimal Boundary & Region Segmentation of Objects in N-D Images. In *Proceedings of the Eighth IEEE International Conference on Computer Vision (ICCV 2001)*, volume 1, pages 105–112 vol.1, 2001.

[13] Y. Boykov and V. Kolmogorov. An Experimental Comparison of Min-Cut/Max-Flow Algorithms for Energy Minimization in Vision. *IEEE Transactions on Pattern Analysis and Machine Intelligence*, 26(9):1124–1137, Sept 2004.

[14] W. Bu, Q. Zhao, X. Wu, Y. Tang, and K. Wang. A Novel Contactless Multimodal Biometric System Based on Multiple Hand Features. In *2011 International Conference on Hand-Based Biometrics*, pages 1–6, Nov 2011.

[15] E. Candes, L. Demanet, D. Donoho, and L. Ying. Fast discrete curvelet transforms. *Multiscale Modeling & Simulation*, 5(3):861–899, 2006.

[16] E.J. Candes and D.L. Donoho. Curvelets: A Surprisingly Effective Nonadaptive Representation for Objects with Edges. Technical report. Department of Statistics, Stanford University, 1999.

[17] J. Canny. A Computational Approach to Edge Detection. *IEEE Trans. Pattern Analysis and Machine Intelligence*, 8(6):679–698, June 1986.

[18] R. Cappelli, M. Ferrara, and D. Maio. A Fast and Accurate Palmprint Recognition System Based on Minutiae. *IEEE Transactions on Systems, Man, and Cybernetics, Part B (Cybernetics)*, 42(3):956–962, June 2012.

[19] Y.-L. Chang and X. Li. Adaptive image region-growing. *IEEE Transactions on Image Processing*, 3(6):868–872, Nov 1994.

[20] N. Charfi, H. Trichili, A.M. Alimi, and B. Solaiman. Bimodal biometric system based on SIFT descriptors of hand images. In *2014 IEEE International Conference on Systems, Man, and Cybernetics, SMC 2014, San Diego, CA, USA, October 5-8, 2014*, pages 4141 – 4145, Oct 2014.

[21] J. Chen and Y.-S. Moon. Using SIFT features in palmprint authentication. In *19th International Conference on Pattern Recognition (ICPR 2008)*, pages 1–4, Dec 2008.

[22] J.-S. Chen, Y.-S. Moon, and H.-W. Yeung. Palmprint Authentication Using Time Series. In *Audio- and Video-Based Biometric Person Authentication*, volume 3546 of *Lecture Notes in Computer Science*, pages 376–385. Springer Berlin Heidelberg, 2005.

[23] W. S. Chen, Y. S. Chiang, and Y. H. Chiu. Biometric Verification by Fusing Hand Geometry and Palmprint. In *Third International Conference on Intelligent Information Hiding and Multimedia Signal Processing (IIH-MSP 2007)*, volume 2, pages 403–406, Nov 2007.

[24] X. Chen, J.K. Udupa, A. Alavi, and D.A. Torigian. GC-ASM: Synergistic Integration of Graph-Cut and Active Shape Model Strategies for Medical Image Segmentation. *Computer Vision and Image Understanding*, 117(5):513–524, 2013.

[25] R. S. Choras and M. Choras. Hand Shape Geometry and Palmprint Features for the Personal Identification. In *Sixth International Conference on Intelligent Systems Design and Applications*, volume 2, pages 1085–1090, Oct 2006.

[26] K.C. Ciesielski, P.A.V. Miranda, A.X. Falco, and J.K. Udupa. Joint graph cut and relative fuzzy connectedness image segmentation algorithm. *Medical Image Analysis*, 17(8):10461057, 2013.

[27] T. Connie, A. T. B. Jin, M. G. K. Ong, and D. N. C. Ling. An automated palmprint recognition system . *Image and Vision Computing*, 23(5):501 – 515, 2005.

[28] T.F. Cootes, G.J. Edwards, and C.J. Taylor. Active Appearance Models. In *Proceedings of the 5th European Conference on Computer Vision (ECCV'98)*, volume II, pages 484–498, Berlin, Heidelberg, 1998. Springer Berlin Heidelberg.

[29] T.F. Cootes, G.J. Edwards, and C.J. Taylor. Active Appearance Models. *IEEE Trans. Pattern Anal. Mach. Intell.*, 23(6):681–685, June 2001.

[30] T.F. Cootes, C.J. Taylor, D.H. Cooper, and J. Graham. Active Shape Models: Their Training and Application. *Computer Vision and Image Understanding*, 61(1):38–59, January 1995.

[31] D. Cremers, M. Rousson, and R. Deriche. A Review of Statistical Approaches to Level Set Segmentation: Integrating Color, Texture, Motion and Shape. *International Journal of Computer Vision*, 72(2):195–215, 2007.

[32] Commission Internationale de L'Eclairage. Colorimetry (Second Edition)- Publication CIE 15.2. Technical report, Central Bureau of CIE, Viena, Austria, 1986.

[33] Commission Internationale de L'Eclairage. A colour appearance model for colour management systems: CIECAM02. Technical Report CIE 159:2004. Technical report, Central Bureau of CIE, Viena, Austria, 2004.

[34] A. de Santos-Sierra. *Design, Implementation and Evaluation of an Unconstrained and Contactless Biometric System based on Geometry and Stress Detection*. PhD thesis, Escuela Técnica Superior de Ingenieros de Telecomunicación, Universidad Politécnica de Madrid, 2012.

[35] A. de Santos-Sierra, J. Guerra-Casanova, C. Sánchez-Ávila, and G. Bailador. A Comparative Study on Unconstrained Hand Biometrics. In *2011 International Conference on Hand-Based Biometrics*, pages 1–6, Nov 2011.

[36] A. de Santos-Sierra, J. Guerra-Casanova, C. Sánchez-Ávila, and V. Jara-Vera. Silhouette-based Hand Recognition on Mobile Devices. In *43rd Annual 2009 International Carnahan Conference on Security Technology*, pages 160–166, Oct 2009.

[37] A. de Santos-Sierra, C. Sánchez-Ávila, G. Bailador, and J. Guerra-Casanova. Gaussian Multiscale Aggregation oriented to Hand Biometric Segmentation in Mobile Devices. In *2011 Third World Congress on Nature and Biologically Inspired Computing*, pages 237–242, Oct 2011.

[38] A. de Santos-Sierra, C. Sánchez-Ávila, J. Guerra-Casanova, and G. Bailador. Hand image segmentation by means of Gaussian multiscale aggregation for biometric applications. In *Proceedings of the International Conference on Signal Processing and Multimedia Applications*, pages 1–7, July 2011.

[39] A. de Santos-Sierra, C. Sánchez-Ávila, J. Guerra-Casanova, and G. Bailador. Invariant Hand Biometrics Feature Extraction. In *Proceedings of the 6th Chinese Conference on Biometric Recognition (CCBR 2011)*, pages 108–115. Springer Berlin Heidelberg, Dec. 2011.

[40] A. de Santos-Sierra, C. Sánchez-Ávila, J. Guerra-Casanova, and A. Mendaza-Ormaza. Hand Biometrics in Mobile Devices. In *Advanced Biometric Technologies*. InTech, 2011.

[41] A. de Santos-Sierra, C. Sánchez-Ávila, A. Mendaza-Ormaza, and J. Guerra-Casanova. An approach to hand biometrics in mobile devices. *Signal, Image and Video Processing*, 5(4):469, 2011.

[42] D. de Santos-Sierra, M.F. Arriaga-Gomez, G. Bailador, and C. Sánchez-Ávila. Low Computational Cost Multilayer Graph-based Segmentation Algorithms for Hand Recognition on Mobile Phones. In *2014 International Carnahan Conference on Security Technology (ICCST)*, pages 1–5, Oct 2014.

[43] K. Dong, G. Feng, and D. Hu. Digital Curvelet Transform for Palmprint Recognition. In *Proceedings of the 5th Chinese Conference on Advances in Biometric Person Authentication: Biometric Recognition (SINOBIOMETRICS 2004)*, pages 639–645. Springer Berlin Heidelberg, Dec. 2004.

[44] J. Doublet, O. Lepetit, and M. Revenu. Contact less Hand Recognition using shape and texture features. In *8th International Conference on Signal Processing*, volume 3, pages –, 2006.

[45] J. Doublet, O. Lepetit, and M. Revenu. Contactless Hand Recognition Based on Distribution Estimation. In *Biometrics Symposium, 2007*, pages 1–6, Sept 2007.

[46] J. Doublet, M. Revenu, and O. Lepetit. Robust GrayScale Distribution Estimation for Contactless Palmprint Recognition. In *Biometrics: Theory, Applications, and Systems, 2007. BTAS 2007. First IEEE International Conference on*, pages 1–6, Sept 2007.

[47] N. Duta. A survey of biometric technology based on hand shape . *Pattern Recognition*, 42(11):2797 – 2806, 2009.

[48] E.S.M. El-Alfy. Automatic Identification Based on Hand Geometry and Probabilistic Neural Networks. In *5th International Conference on New Technologies, Mobility and Security (NTMS)*, pages 1–5, May 2012.

[49] A.X. Falcão, J.K. Udupa, S. Samarasekera, S. Sharma, B.E. Hirsch, and R. de Alencar Lotufo. User-Steered Image Segmentation Paradigms: Live Wire and Live Lane. *Graphical Models and Image Processing*, 60(4):233–260, 1998.

[50] X. Fan, J. Yang, and L. Cheng. A Novel Segmentation Method for MR Brain Images Based on Fuzzy Connectedness and FCM. In *Proceedings of the 2nd International Conference on Fuzzy Systems and Knowledge Discovery (FSKD 2005), Part I*, pages 27–29. Springer Berlin Heidelberg, Aug. 2005.

[51] M. Faundez-Zanuy. Biometric verification of humans by means of hand geometry. In *Proceedings 39th Annual International Carnahan Conference on Security Technology*, pages 61–67, Oct 2005.

[52] M. Faundez-Zanuy. Data Fusion in Biometrics. *IEEE Aerospace and Electronic Systems Magazine*, 20:34–38, Jan 2005.

[53] M.A. Ferrer, A.Morales, C.M. Travieso, and J.B. Alonso. Low Cost Multimodal Biometric identification System Based on Hand Geometry, Palm and Finger Print Texture. In *2007 41st Annual IEEE International Carnahan Conference on Security Technology*, pages 52–58, Oct 2007.

[54] M.A. Ferrer, J. Fabregas, M. Faundez, J.B. Alonso, and C. Travieso. Hand Geometry Identification System Performance. In *43rd Annual 2009 International Carnahan Conference on Security Technology*, pages 167–171, Oct 2009.

[55] M.A. Ferrer, A. Morales, C.M. Travieso, and J.B. Alonso. Influence of the pegs number and distribution on a biometric device based on hand geometry. In *2008 42nd Annual IEEE International Carnahan Conference on Security Technology*, pages 221–225, Oct 2008.

[56] M.A. Ferrer, C.M. Travieso, and J.B. Alonso. Multimodal Biometric System based on Hand Geometry and Palm Print Texture. In *Proceedings 40th Annual 2006 International Carnahan Conference on Security Technology*, pages 92–97, Oct 2006.

[57] L.R. Ford and D.R. Fulkerson. Flows in Networks. pages xii, 194 p. Princetown University Press, 1962.

[58] G. Fouquier, L. Likforman, J. Darbon, and B. Sankur. The Biosecure Geometry-Based System for Hand Modality. In *2007 IEEE International Conference on Acoustics, Speech and Signal Processing - ICASSP '07*, volume 1, pages I–801–I–804, April 2007.

[59] R. Fuksis, A. Kadikis, and M. Greitans. Biohashing and Fusion of Palmprint and Palm Vein Biometric Data. In *2011 International Conference on Hand-Based Biometrics*, pages 1–6, Nov 2011.

[60] A. García-Casarrubios Muñoz, A. de Santos-Sierra, C. Sánchez-Ávila, J. Guerra-Casanova, G. Bailador, and V. Jara-vera. Hand Biometric Segmentation by

Means of Fuzzy Multiscale Aggregation for Mobile Devices. In *2010 International Workshop on Emerging Techniques and Challenges for Hand-Based Biometrics*, pages 1–6, Aug 2010.

[61] A. García-Casarrubios Muñoz, C. Sánchez-Ávila, A. de Santos-Sierra, and J. Guerra-Casanova. A Mobile-Oriented Hand Segmentation Algorithm Based on Fuzzy Multiscale Aggregation. In *Advances in Visual Computing: 6th International Symposium, ISVC 2010, Las Vegas, NV, USA, November 29-December 1, 2010. Proceedings, Part I*, pages 479–488. Springer Berlin Heidelberg, Berlin, Heidelberg, 2010.

[62] A. Ghandehari and R. Safabakhsh. Palmprint Verification Using Circular Gabor Filter. In *ICB*, volume 5558 of *Lecture Notes in Computer Science*, pages 675–684. Springer, 2009.

[63] E. Gonzalez, A. Morales, M.A. Ferrer, and C.M. Travieso. Looking for Hand Biometrics Interoperability. In *2011 International Conference on Hand-Based Biometrics*, pages 1–6, Nov 2011.

[64] R.C. Gonzalez and R.E. Woods. *Digital Image Processing*. Addison-Wesley Longman Publishing Co., Inc., 2nd edition, 2001.

[65] S. Gonzalez, C.M. Travieso, J.B. Alonso, and M.A. Ferrer. Automatic biometric identification system by hand geometry. In *Proceedings of the IEEE 37th Annual International Carnahan Conference onSecurity Technology*, pages 281–284, Oct 2003.

[66] P. Gopisivaraman and G. Udhayakumar. Palmprint Recognition Using Adaptive Histogram Equalization and Discrete Curvelet Transform. *International Journal of Innovative Research in Computer and Communication Engineering*, 2:50–55, March 2014. Special Issue 1.

[67] J. Guerra-Casanova, B. Ríos-Sánchez, M. Viana-Matesanz, G. Bailador, C. Sánchez-Ávila, and M. J. M. D. Giles. Comfort and Security Perception of Biometrics in Mobile Phones with Widespread Sensors. In *2016 IEEE 35th Symposium on Reliable Distributed Systems Workshops (SRDSW)*, pages 13–18, Sept 2016.

[68] Z. Guo, D. Zhang, L. Zhang, and W. Zuo. Palmprint verification using binary orientation co-occurrence vector. *Pattern Recognition Letters*, 30(13):1219 – 1227, 2009.

[69] Z. Guo, L. Zhang, D. Zhang, and X. Mou. Hierarchical multiscale LBP for face and palmprint recognition. In *2010 IEEE International Conference on Image Processing*, pages 4521–4524, Sept 2010.

[70] C.-C. Han, H.-L. Cheng, C.-L. Lin, and K.-C. Fan. Personal authentication using palm-print features. *Pattern Recognition*, 36:371–381, 2003.

[71] M. Hanmandlu, J. Grover, V. K. Madasu, and S. Vasirkala. Score level fusion of hand based biometrics using t-norms. In *2010 IEEE International Conference on Technologies for Homeland Security (HST)*, pages 70–76, Nov 2010.

[72] J. Hashemi and E. Fatemizadeh. Biometric Identification through Hand Geometry. In *EUROCON 2005 - The International Conference on "Computer as a Tool"*, volume 2, pages 1011–1014, Nov 2005.

[73] M. He, S.-J. Horng, P.i Fan, R.-S. Run, R.-J. Chen, J.-L. Lai, M.K. Khan, and K.O. Sentosa. Performance Evaluation of Score Level Fusion in Multimodal Biometric Systems. *Pattern Recognition*, 43(5):1789–1800, May 2010.

[74] Q. Huang and B. Dom. Quantitative methods of evaluating image segmentation. In *Proceedings of the International Conference on Image Processing*, volume 3, pages 53–56 vol.3, Oct 1995.

[75] International Organization for Standardization (ISO). *ISO/IEC 19795-1:2007: Information technology - Biometric performance testing and reporting - Part 1: Principles and framework*, 2007.

[76] International Organization for Standardization (ISO). *ISO/IEC 19795-2:2007: Information technology - Biometric performance testing and reporting - Part 2: Testing methodologies for technology and scenario evaluation*, 2007.

[77] A.K. Jain and R.C. Dubes. Algorithms for Clustering Data. Prentice-Hall, Inc., Upper Saddle River, NJ, USA, 1988.

[78] A.K. Jain and N. Duta. Deformable matching of hand shapes for user verification. In *Proceedings of the International Conference on Image Processing*, volume 2, pages 857–861 vol.2, Oct 1999.

[79] A.K. Jain, K. Nandakumar, and A. Ross. Score Normalization in Multimodal Biometric Systems. *Pattern Recognition*, 38(12):2270 – 2285, 2005.

[80] A.K. Jain, A. Ross, and S. Pankanti. A Prototype Hand Geometry-based Verification System. In *Proceedings of 2nd International Conference on Audio- and Video-based Biometric Person Authentication (AVBPA)*, pages 166–171, March 1999.

[81] W. Jia, D.-S. Huang, and D. Zhang. Palmprint verification based on robust line orientation code. *Pattern Recognition*, 41(5):1504 – 1513, 2008.

[82] X. Jiang, W. Xu, L. Sweeney, Y. Li, R. Gross, and D. Yurovsky. New Directions in Contact Free Hand Recognition. In *2007 IEEE International Conference on Image Processing*, volume 2, pages 389 – 392, Sept 2007.

[83] X.-Y. Jing, Y.-F. Yao, D. Zhang, J.-Y. Yang, and M. Li. Face and palmprint pixel level fusion and Kernel DCV-RBF classifier for small sample biometric recognition. *Pattern Recognition*, 40(11):3209 – 3224, 2007.

[84] A.A. Joshi, P. Deshpande, and A.S. Tavildar. Enhancing accuracy for personal identification usinghierarchical based fusion of finger geometry and palm print modalities. In *2014 International Conference on Electronics and Communication Systems (ICECS)*, pages 1–4, Feb 2014.

[85] S.-W. Zheng K.-W. Chuang, C.-C. Liu. A Region-of-Interest Segmentation Algorithm for Palmprint Images. In *The 29th Workshop on Combinatorial Mathematics and Computation Theory*, pages 96–102, 2012.

[86] B.J. Kang and K.R. Park. A new multi-unit iris authentication based on quality assessment and score level fusion for mobile phones. *Machine Vision and Applications*, 21(4):541–553, 2010.

[87] W. Kang and Q. Wu. Pose-Invariant Hand Shape Recognition Based on Finger Geometry. *IEEE Transactions on Systems, Man, and Cybernetics: Systems*, 44(11):1510–1521, Nov 2014.

[88] V. Kanhangad, A. Kumar, and D. Zhang. Combining 2D and 3D hand geometry features for biometric verification. In *2009 IEEE Computer Society Conference on Computer Vision and Pattern Recognition Workshops*, pages 39–44, June 2009.

[89] V. Kanhangad, A. Kumar, and D. Zhang. A Unified Framework for Contactless Hand Verification. *IEEE Transactions on Information Forensics and Security*, 6(3):1014–1027, Sept 2011.

[90] V. Kanhangad, A. Kumar, and D. Zhang. Contactless and Pose Invariant Biometric Identification Using Hand Surface. *IEEE Transactions on Image Processing*, 20(5):1415–1424, May 2011.

[91] M. Kass, A. Witkin, and D. Terzopoulos. Snakes: Active contour models. *International Journal of Computer Vision*, 1(4):321–331, 1988.

[92] A. Kaur and B.v Kranthi. Comparison between YCbCr Color Space and CIELab Color Space for Skin Color Segmentation. *International Journal of Applied Information Systems*, 3(4):30–33, July 2012.

[93] D. J. Kim, K. W. Chung, and K. S. Hong. Person authentication using face, teeth and voice modalities for mobile device security. *IEEE Transactions on Consumer Electronics*, 56(4):2678–2685, 2010.

[94] V. Kolmogorov and R. Zabin. What energy functions can be minimized via graph cuts? *IEEE Transactions on Pattern Analysis and Machine Intelligence*, 26(2):147–159, 2004.

[95] A.W.-K. Kong and D. Zhang. Competitive coding scheme for palmprint verification. In *Proceedings of the 17th International Conference on Pattern Recognition*, volume 1, pages 520–523 Vol.1, Aug 2004.

[96] A.W.-K. Kong, D. Zhang, and M. Kamel. Palmprint identification using feature-level fusion. *Pattern Recognition*, 39(3):478 – 487, 2006.

[97] A.W.-K. Kong, D. Zhang, and M. Kamel. A Survey of Palmprint Recognition. *Pattern Recogn.*, 42(7):1408–1418, July 2009.

[98] A.W.-K. Kong, D. Zhang, and W. Li. Palmprint feature extraction using 2-D Gabor filters. *Pattern Recognition*, 36:2339–2347, 2003.

[99] A.W.-K. Kong, D. Zhang, and G. Lu. A study of identical twins' palmprints for personal verification. *Pattern Recognition*, 39(11):2149 – 2156, 2006.

[100] J. Kong, H. Li, Y. Lu, M. Qi, and S. Wang. Hand-Based Personal Identification Using K-Means Clustering and Modified Zernike Moments. In *Third International Conference on Natural Computation (ICNC 2007)*, volume 2, pages 651–655, Aug 2007.

[101] A. Kumar. Incorporating Cohort Information for Reliable Palmprint Authentication. In *2008 Sixth Indian Conference on Computer Vision, Graphics Image Processing*, pages 583–590, Dec 2008.

[102] A. Kumar and H.C. Shen. Palmprint identification using palmcodes. In *Proceedings of the Third International Conference on Image and Graphics*, pages 258–261, Los Alamitos, CA, USA, 2004. IEEE Computer Society.

[103] A. Kumar, D.C.M. Wong, H.C. Shen, and A.K. Jain. Personal Verification Using Palmprint and Hand Geometry Biometric. In *4th International Conference on Audio- and Video-Based Biometric Person Authentication (AVBPA 2003)*, pages 668–678. Springer Berlin Heidelberg, June 2003.

[104] A. Kumar and D. Zhang. Personal recognition using hand shape and texture. *IEEE Transactions on Image Processing*, 15(8):2454–2461, Aug 2006.

[105] A. Kumar and D. Zhang. Hand-Geometry Recognition Using Entropy-Based Discretization. *IEEE Transactions on Information Forensics and Security*, 2(2):181–187, June 2007.

[106] J.-C. Lee. A novel biometric system based on palm vein image. *Pattern Recognition Letters*, 33(12):1520 – 1528, 2012.

[107] S.Z. Li. *Markov Random Field Modeling in Computer Vision*. Springer-Verlag New York, Inc., Secaucus, NJ, USA, 1995.

[108] W. Li, B. Zhang, L. Zhang, and J. Yan. Principal Line-Based Alignment Refinement for Palmprint Recognition. *IEEE Transactions on Systems, Man, and Cybernetics, Part C*, 42(6):1491–1499, 2012.

[109] W. Li, D. Zhang, and Z. Xu. Palmprint identification by fourier transform. *International Journal of Pattern Recognition and Artificial Intelligence*, 16(04):417–432, 2002.

[110] D.Y. Liliana and E.T. Utaminingsih. The combination of palm print and hand geometry for biometrics palm recognition. *International Journal of Video & Image Processing and Network Security*, 12(01), february 2012.

[111] C.-L. Lin, T.C. Chuang, and K.-C. Fan. Palmprint verification using hierarchical decomposition. *Pattern Recognition*, 38(12):2639–2652, 2005.

[112] E. Liu, A.K. Jain, and J. Tian. A Coarse to Fine Minutiae-Based Latent Palmprint Matching. *IEEE Transactions on Pattern Analysis Maching Intelligence*, 35(10):2307–2322, 2013.

[113] F. Liu, L. Zhou, Z.-M. Lu, and T. Nie. Palmprint Feature Extraction Based on Curvelet Transform. *Journal of Information Hiding and Multimedia Signal Processing*, 6(1):131–139, January 2015.

[114] J. Liu and J. K. Udupa. Oriented Active Shape Models. *IEEE Transactions on Medical Imaging*, 28(4):571–584, April 2009.

[115] N. Liu and B.C. Lovell. Hand Gesture Extraction by Active Shape Models. In *Digital Image Computing: Techniques and Applications (DICTA'05)*, pages 59–64, Dec 2005.

[116] G. Lu, D. Zhang, and K. Wang. Palmprint recognition using eigenpalms features . *Pattern Recognition Letters*, 24(910):1463 – 1467, 2003.

[117] B. Ma and F. Yang. A New Mixed-Mode Biometrics Information Fusion Based-on Fingerprint, Hand-geometry and Palm-print. pages 689–693, Los Alamitos, CA, USA, 2007. IEEE Computer Society.

[118] Y.L. Ma, F. Pollick, and W.T. Hewitt. Using B-spline curves for hand recognition. In *Proceedings of the 17th International Conference on Pattern Recognition (ICPR 2004)*, volume 3, pages 274–277 Vol.3, Aug 2004.

[119] Ravikanth Malladi, James A. Sethian, and Baba C. Vemuri. Shape modeling with front propagation: A level set approach. *IEEE Transactions on Pattern Analysis and Machine Intelligence*, 17:158–175, 1995.

[120] A. Meraoumia, S. Chitroub, and A. Bouridane. Multimodal biometric systems by fusion of palmprint and Finger-Knuckle-Print using Hidden Markov Model. In *2013 IEEE 20th International Conference on Electronics, Circuits, and Systems (ICECS)*, pages 421–424, Dec 2013.

[121] C. Methani and A.M. Namboodiri. Pose Invariant Palmprint Recognition. In *Advances in Biometrics: Third International Conference, ICB 2009, Alghero, Italy, June 2-5, 2009. Proceedings*, pages 577–586. Springer Berlin Heidelberg, 2009.

[122] F.C. Monteiro and A.C. Campilho. Performance Evaluation of Image Segmentation. In *Image Analysis and Recognition: Third International Conference, ICIAR 2006, Póvoa de Varzim, Portugal, September 18-20, 2006, Proceedings, Part I*, pages 248–259. Springer Berlin Heidelberg, 2006.

[123] A. Morales, M.A. Ferrer, J.B. Alonso, and C.M. Travieso. Comparing infrared and visible illumination for contactless hand based biometric scheme. In *2008 42nd Annual IEEE International Carnahan Conference on Security Technology*, pages 191–197, Oct 2008.

[124] A. Morales, M.A. Ferrer, F. Daz, J.B. Alonso, and C.M. Travieso. Contact-free hand biometric system for real environments. In *2008 16th European Signal Processing Conference*, pages 1–5, Aug 2008.

[125] A. Morales, M.A. Ferrer, and A. Kumar. Improved palmprint authentication using contactless imaging. In *4th IEEE International Conference on Biometrics: Theory, Applications and Systems (BTAS)*, pages 1–6, Sept 2010.

[126] A. Morales, M.A. Ferrer, and A. Kumar. Towards contactless palmprint authentication. *IET Computer Vision*, 5(6):407–416, November 2011.

[127] A. Morales, E. Gonzlez, and M.A. Ferrer. On the Feasibility of Interoperable Schemes in Hand Biometrics. *Sensors*, 12(2):1352–1382, 2012.

[128] A. Mostayed, M.E. Kabir, S.Z. Khan, and M.M.G. Mazumder. Biometric authentication from low resolution hand images using radon transform. In *12th International Conference on Computers and Information Technology*, pages 587–592, Dec 2009.

[129] H.T. Nguyen, M. Worring, and R. van den Boomgaard. Watersnakes: energy-driven watershed segmentation. *IEEE Transactions on Pattern Analysis and Machine Intelligence*, 25(3):330–342, March 2003.

[130] A. Nigam and P. Gupta. Designing an accurate hand biometric based authentication system fusing finger knuckleprint and palmprint. *Neurocomputing*, 151, Part 3:1120 – 1132, 2015.

[131] T. Ojala, M. Pietikäinen, and D. Harwood. A comparative study of texture measures with classification based on featured distributions. *Pattern Recognition*, 29(1):51–59, Jan 1996.

[132] T. Ojala, M. Pietikainen, and T. Maenpaa. Multiresolution gray-scale and rotation invariant texture classification with local binary patterns. *IEEE Transactions on Pattern Analysis and Machine Intelligence*, 24(7):971–987, July 2002.

[133] M.G.K. Ong, T. Connie, and A.T.B. Jin. Touch-less Palm Print Biometrics: Novel Design and Implementation. *Image and Vision Computing*, 26(12):1551–1560, Dec 2008.

[134] M.G.K. Ong, T. Connie, and A.T.B. Jin. A Contactless Biometric System Using Palm Print and Palm Vein Features. In *Advanced Biometric Technologies*. 2011.

[135] M.G.K. Ong, T. Connie, and A.T.B. Jin. A contactless biometric system using multiple hand features . *Journal of Visual Communication and Image Representation*, 23(7):1068 – 1084, 2012.

[136] M.G.K. Ong, T. Connie, A.T.B. Jin, and A.T.B. Jin. Design and implementation of a contactless palm print and palm vein sensor. In *2010 11th International Conference on Control Automation Robotics Vision*, pages 1268–1273, Dec 2010.

[137] M.G.K. Ong, T. Connie, A.T.B. Jin, and D.N.C. Ling. A Single-sensor Hand Geometry and Palmprint Verification System. In *Proceedings of the 2003 ACM SIGMM Workshop on Biometrics Methods and Applications*, WBMA '03, pages 100–106, New York, NY, USA, 2003. ACM.

[138] N. Otsu. A Threshold Selection Method from Gray-level Histograms. *IEEE Transactions on Systems, Man and Cybernetics*, 9(1):62–66, 1979.

[139] A.S. Parihar, A. Kumar, O.P. Verma, A. Gupta, P. Mukherjee, and D. Vatsa. Point based features for contact-less palmprint images. In *IEEE International Conference on Technologies for Homeland Security (HST)*, pages 165–170, Nov 2013.

[140] G. Park and S. Kim. Hand Biometric Recognition Based on Fused Hand Geometry and Vascular Patterns. *Sensors*, 13(3):2895–2910, 2013.

[141] N. Pavešić, S. Ribarić, and D. Ribarić. Personal authentication using hand-geometry and palmprint features - the state of the art. In *Proceedings of the Workshop Biometrics - Challenges Arising from Theory to Practice*, pages 17 – 26, Cambridge, 2004.

[142] D. Petrovska-Delacrétaz, G. Chollet, and B. Dorizzi, editors. *Guide to Biometric Reference Systems and Performance Evaluation*. Springer-Verlag London, 1 edition, 2009.

[143] D.L. Pham. Spatial Models for Fuzzy Clustering. *Computer Vision and Image Understanding*, 84(2):285–297, November 2001.

[144] S.M. Pizer, G. Gerig, S. Joshi, and S.R. Aylward. Multiscale medial shape-based analysis of image objects. *Proceedings of the IEEE*, 91(10):1670–1679, Oct 2003.

[145] N. Poh and S. Bengio. Database, protocols and tools for evaluating score-level fusion algorithms in biometric authentication. *Pattern Recognition*, 39(2):223–233, 2006.

[146] C. Poon, D.C.M. Wong, and H.C. Shen. A new method in locating and segmenting palmprint into region-of-interest. In *Proceedings of the 17th International Conference on Pattern Recognition (ICPR 2004)*, volume 4, pages 533–536 Vol.4, Aug 2004.

[147] S.M. Prasad, V.K. Govindan, and P.S. Sathidevi. Bimodal Personal Recognition Using Hand Images. In *Proceedings of the International Conference on Advances in Computing, Communication and Control*, ICAC3 '09, pages 403–409, New York, NY, USA, 2009.

[148] Promila and V. Laxmi. Palmprint Matching Using LBP. In *2012 International Conference on Computing Sciences*, pages 110–115. Sept 2012.

[149] I K.G.D. Putra. High Performance Palmprint Identification system based on two dimensional gabor. *TELKOMINIKA*, 8(3):309–318, 2010.

[150] M.B. Ramalho, P.L. Correia, and L.D. Soares. Hand-based multimodal identification system with secure biometric template storage. *IET Computer Vision*, 6(3):165–173, May 2012.

[151] C.R. Rao and H. Toutenburg. *Linear Models: Least Squares and Alternatives*. Springer series in statistics. Springer, 1999.

[152] K.B. Ray and R. Misra. Extracting Region of Interest for Palm Print Authentication. *IJASCSE*, 2, December 2013.

[153] S. Ribarić, Ribarić D., and N. Pavešić. A Biometric Identification System Based on the Fusion of Hand and Palm Features. In *Workshop COST-275*, pages 79–82, 2002.

[154] S. Ribarić and I. Fratrić. A biometric identification system based on eigenpalm and eigenfinger features. *IEEE Transactions on Pattern Analysis and Machine Intelligence*, 27(11):1698–1709, Nov 2005.

[155] S. Ribarić and I. Fratri'c. An online biometric authentication system based on eigenfingers and finger-geometry. In *13th European Signal Processing Conference*, pages 1–4, Sept 2005.

[156] S. Ribaric, D. Ribaric, and N. Pavesic. Multimodal biometric user-identification system for network-based applications. *IEEE Proceedings on Vision, Image and Signal Processing*, 150(6):409–416, Dec 2003.

[157] B. Ríos-Sánchez, M.F. Arriaga-Gómez, J. Guerra-Casanova, D. de Santos-Sierra, I. de Mendizábal-Vázquez, G. Bailador, and C. Sánchez-Ávila. gb2sμMOD: A MUltiMODal biometric video database using visible and IR light. *Information Fusion*, 32, Part B:64 – 79, 2016. SI Information Fusion in Biometrics.

[158] B. Ríos-Sánchez, M. Viana-Matesanz, and C. Sánchez-Ávila. Multibiometría de huella palmar y geometría de mano para un sistema sin contacto orientado a dispositivos móviles. In *XXXI Simposium Nacional de la Unión Científica Internacional de Radio*, Sept 2016.

[159] J.B.T.M. Roerdink and A. Meijster. The Watershed Transform: Definitions, Algorithms and Parallelization Strategies. *Fundama Informaticae*, 41(1,2):187–228, April 2000.

[160] A. Ross. A Prototype Hand Geometry-based Verification System. pages 166–171, 1999.

[161] A.A. Ross, K. Nandakumar, and A.K. Jain. *Handbook of Multibiometrics (International Series on Biometrics)*. Springer-Verlag New York, Inc., Secaucus, NJ, USA, 2006.

[162] M. Rousson and Nikos Paragios. Prior Knowledge, Level Set Representations & Visual Grouping. *International Journal of Computer Vision*, 76(3):231–243, 2008.

[163] R. Sanchez-Reillo and A. Gonzalez-Marcos. Access control system with hand geometry verification and smart cards. In *Proceedings of the IEEE 33rd Annual International Carnahan Conference on Security Technology*, pages 485–487, 1999.

[164] R. Sanchez-Reillo, C. Sánchez-Avila, and A. Gonzalez-Marcos. Biometric identification through hand geometry measurements. *IEEE Transactions on Pattern Analysis and Machine Intelligence*, 22(10):1168–1171, Oct 2000.

[165] H. Sang, Y. Ma, and J. Huang. Robust Palmprint Recognition Base on Touch-Less Color Palmprint Images Acquired. *Signal and Information Processing*, 4(2):134–139, 2013.

[166] S. Selvarajan, V. Palanisamy, and B. Mathivanan. Human identification and recognition system using more significant hand attributes. In *2008 International Conference on Computer and Communication Engineering*, pages 1211–1216, May 2008.

[167] M. Sezgin and B. Sankur. Survey over image thresholding techniques and quantitative performance evaluation. *Journal of Electronic Imaging*, 13(1):146–168, 2004.

[168] M.K. Shahin, A.M. Badawi, and M.E. Rasmy. A Multimodal Hand Vein, Hand Geometry, and Fingerprint Prototype Design for High Security Biometrics. In *2008 Cairo International Biomedical Engineering Conference*, pages 1–6, Dec 2008.

[169] L. Shang, J. Chen, P.-G. Su, and Y. Zhou. ROI Extraction of Palmprint Images Using Modified Harris Corner Point Detection Algorithm. In *Proceedings of the 8th International Conference on Intelligent Computing Theories and Applications (ICIC 2012)*, volume 7390 of *Lecture Notes in Computer Science*, pages 479–486. Springer Berlin Heidelberg, July 2012.

[170] F. Shojaiee and F. Hajati. Local composition derivative pattern for palmprint recognition. In *22nd Iranian Conference on Electrical Engineering (ICEE)*, pages 965–970, May 2014.

[171] I. Sobel and G. Feldman. A 3x3 isotropic gradient operator for image processing, presented at a talk at the Stanford Artificial Project. In *Pattern Classification and Scene Analysis*, pages 271 – 272. John Wiley & Sons, 1968.

[172] V. Spruyt, A. Ledda, and S. Geerts. Real-time multi-colourspace hand segmentation. In *2010 IEEE International Conference on Image Processing*, pages 3117–3120, Sept 2010.

[173] C. Sui, N.M. Kwok, and T. Ren. A Restricted Coulomb Energy (RCE) Neural Network System for Hand Image Segmentation. In *2011 Canadian Conference on Computer and Robot Vision*, pages 270–277, May 2011.

[174] Z. Sun, T. Tan, Y. Wang, and S.Z. Li. Ordinal palmprint represention for personal identification. In *IEEE Computer Society Conference on Computer Vision and Pattern Recognition*, volume 1, pages 279–284 vol. 1, June 2005.

[175] J. Svoboda, M.M. Bronstein, and M. Drahansky. Contactless biometric hand geometry recognition using a low-cost 3D camera. In *2015 International Conference on Biometrics (ICB)*, pages 452–457, May 2015.

[176] Z. Tan, J. Yang, Z. Shang, G. Shi, and S. Chang. Minutiae-Based Offline Palmprint Identification System. In *2009 WRI Global Congress on Intelligent Systems*, volume 4, pages 466–471, May 2009.

[177] S. Tantachun, C. Pintavirooj, P. Lertprasart, and S. Bunluechokchai. Biometrics with Eigen-Hand. In *2006 1st IEEE Conference on Industrial Electronics and Applications*, pages 1–4, 2006.

[178] J.K. Udupa and S. Samarasekera. Fuzzy Connectedness and Object Definition: Theory, Algorithms, and Applications in Image Segmentation. *Graphical Models and Image Processing*, 58(3):246 – 261, 1996.

[179] A. Uhl and P. Wild. Comparing verification performance of kids and adults for Fingerprint, Palmprint, Hand-geometry and Digitprint biometrics. In *3rd IEEE International Conference on Biometrics: Theory, Applications, and Systems*, pages 1–6, Sept 2009.

[180] R. Unnikrishnan, C. Pantofaru, and M. Hebert. Toward Objective Evaluation of Image Segmentation Algorithms. *IEEE Transactions on Pattern Analysis and Maching Intelligence*, 29(6):929–944, June 2007.

[181] A. Utsumi and J. Oyha. Hand image segmentation using sequential-image-based hierarchical adaptation. In *Proceedings of International Conference on Image Processing*, volume 1, pages 208–211, Oct 1997.

[182] D. Vaidya, S. Pawar, M.A. Joshi, A.M. Sapkal, and S. Kar. Feature-level Fusion of Palm Print and Palm Vein for Person Authentication Based on Entropy Technique. *International Journal of Electronics & Communication Technology*, 5, Jan 2014.

[183] P. Varchol, D. Levicky, and J. Juhar. Multimodal biometric authentication using speech and hand geometry fusion. In *15th International Conference on Systems, Signals and Image Processing*, pages 57–60, June 2008.

[184] E. Vildjiounaite, S.M. Makela, M. Lindholm, V. Kyllonen, and H. Ailisto. Increasing Security of Mobile Devices by Decreasing User Effort in Verification. In *2nd International Conference on Systems and Networks Communications (ICSNC 2007)*, pages 80–80, 2007.

[185] J.-G. Wang, W.-Y. Yau, A. Suwandy, and E. Sung. Person recognition by fusing palmprint and palm vein images based on Laplacianpalm representation . *Pattern Recognition*, 41(5):1514 – 1527, 2008.

[186] W.-C. Wang, W.S. Chen, and S.W. Shih. Biometric recognition by fusing palmprint and hand-geometry based on morphology. In *IEEE International Conference on Acoustics, Speech and Signal Processing*, pages 893–896, April 2009.

[187] I.L. Weatherall and B.D. Coombs. Skin color measurements in terms of CIELAB color space values. *The Journal of Investigative Dermatology*, 99(4):468–473, 1992.

[188] T.A. Budi Wirayuda, D.H. Kuswanto, H.A. Adhi, and R.N. Dayawati. Implementation of feature extraction based hand geometry in biometric identification system. In *2013 International Conference of Information and Communication Technology (ICoICT)*, pages 259–263, March 2013.

[189] R.L.N. Wong and P. Shi. Peg-free hand geometry recognition using hierarchical geometry and shape matching. In *IAPR Workshop on Machine Vision Applications*, pages 281–284, 2002.

[190] J. Wu and Z. Qiu. A Hierarchical Palmprint Identification Method Using Hand Geometry and Grayscale Distribution Features. In *18th International Conference on Pattern Recognition (ICPR'06)*, volume 4, pages 409–412, 2006.

[191] K.-S. Wu, J.-C. Lee, T.-M. Lo, K.-C. Chang, and C.-P. Chang. A secure palm vein recognition system . *Journal of Systems and Software*, 86(11):2870 – 2876, 2013.

[192] C. Xin, X. Wu, Z. Qiushi, and T. Youbao. A contactless hand shape identification system. In *3rd International Conference on Advanced Computer Control*, pages 561–565, Jan 2011.

[193] W. Xinchun, Y. Kaihua, L. Yuming, and Y. Qing. Palmprint Recognition Based on Curvelet Transform Decision Fusion. *Procedia Engineering*, 23:303 – 309, 2011.

[194] W. Xiong, K.-A. Toh, W.-Y. Yau, and X. Jiang. Model-guided deformable hand shape recognition without positioning aids . *Pattern Recognition*, 38(10):1651 – 1664, 2005.

[195] W. Xiong, C. Xu, and S.H. Ong. Peg-free Human Hand Shape Analysis and Recognition. In *Proceedings of the IEEE International Conference on Acoustics, Speech, and Signal Processing (ICASSP '05)*, volume 2, pages 77–80, March 2005.

[196] H. Yan and D. Long. A Novel Bimodal Identification Approach Based on Hand-Print. In *2008 Congress on Image and Signal Processing*, volume 4, pages 506–510, May 2008.

[197] F. Yang, B. Ma, Q.X. Wang, D. Yao, C. Fang, S. Zhao, and X. Zhou. Information Fusion of Biometrics Based-on Fingerprint, Hand-geometry and Palm-print. In *2007 IEEE Workshop on Automatic Identification Advanced Technologies*, pages 247–252, June 2007.

[198] Y.-F. Yao, X.-Y. Jing, and H.-S. Wong. Face and palmprint feature level fusion for single sample biometrics recognition. *Neurocomputing*, 70(79):1582 – 1586, 2007.

[199] X. Yin, D. Guo, and M. Xie. Hand image segmentation using color and RCE neural network . *Robotics and Autonomous Systems*, 34(4):235 – 250, 2001.

[200] E. Yoruk, E. Konukoglu, B. Sankur, and J. Darbon. Shape-based hand recognition. *IEEE Transactions on Image Processing*, 15(7):1803–1815, July 2006.

[201] B. Zhang, Y. Gao, S. Zhao, and J. Liu. Local Derivative Pattern Versus Local Binary Pattern: Face Recognition With High-Order Local Pattern Descriptor. *IEEE Transactions on Image Processing*, 19(2):533–544, Feb 2010.

[202] D. Zhang, W.-K Kong, J. You, and M. Wong. Online palmprint identification. *IEEE Transactions on Pattern Analysis and Machine Intelligence*, 25(9):1041–1050, Sept 2003.

[203] H. Zhang, J.E. Fritts, and S.A. Goldman. Image segmentation evaluation: A survey of unsupervised methods . *Computer Vision and Image Understanding*, 110(2):260 – 280, 2008.

[204] J. Zhang, T. Tan, and L. Ma. Invariant texture segmentation via circular Gabor filters. In *Proceedings of 16th International Conference on Pattern Recognition*, volume 2, pages 901–904 vol.2, Aug 2002.

[205] Q. Zhao, X. Wu, and W. Bu. Contactless palmprint verification based on SIFT and iterative RANSAC. In *20th IEEE International Conference on Image Processing (ICIP)*, pages 4186–4189, Sept 2013.

[206] Y. Zhao, W. Jia, R. Hu, and J. Gui. Palmprint Identification Using LBP and Different Representations. In *2011 International Conference on Hand-Based Biometrics*, pages 1–5, Nov 2011.

[207] Y. Zheng, Y. Liu, G. Shi, J. Li, and Q. Wang. Segmentation of Offline Palmprint. In *3rd International IEEE Conference on Signal-Image Technologies and Internet-Based System*, pages 804–811, Dec 2007.

[208] Y. Zhou and A. Kumar. Human Identification Using Palm-Vein Images. *IEEE Transactions on Information Forensics and Security*, 6(4):1259–1274, Dec 2011.

[209] W. Zuo, Z. Lin, Z. Guo, and D. Zhang. The multiscale competitive code via sparse representation for palmprint verification. In *2010 IEEE Computer Society Conference on Computer Vision and Pattern Recognition*, pages 2265–2272, June 2010.